



Tesis Doctoral

Complejos de metales de transición
conteniendo ligandos de tipo carbeno N-
heterocíclico de 5 y 6 miembros. Síntesis y
estudios de reactividad.

Marta Roselló Merino

Sevilla, 2013

UNIVERSIDAD DE SEVILLA

CONSEJO SUPERIOR DE INVESTIGACIONES CIENTÍFICAS

Departamento de Química Inorgánica

Instituto de Investigaciones Químicas



**Complejos de metales de transición conteniendo
ligandos de tipo carbeno N-heterocíclico de 5 y 6
miembros. Síntesis y estudios de reactividad.**

**Transition metal complexes bearing 5- and 6-membered
N-heterocyclic carbene ligands. Synthesis and reactivity
studies**

Marta Roselló Merino

Sevilla, 2013

**Complejos de metales de transición conteniendo
ligandos de tipo carbeno N-heterocíclico de 5 y 6
miembros. Síntesis y estudios de reactividad.**

por

Marta Roselló Merino

Tutor:

**Trabajo presentado para aspirar al
Título de Doctor en Química
Sevilla, 2013**

Ernesto Carmona Guzmán

Catedrático,

Universidad de Sevilla

Marta Roselló Merino

Director:

Salvador Conejero Iglesias

Científico Titular

(CSIC)

TABLE OF CONTENTS

ABBREVIATIONS	13
GENERAL INTRODUCTION	19
“N-heterocyclic carbenes: An established ligand class for transition metal complexes”	
CHAPTER 1	35
“Reactivity of electron deficient biscarbene platinum (II) complexes with halogens”	
INTRODUCTION.....	37
“Overview of oxidative addition/reductive elimination in Pt(II)/Pt(IV) unsaturated species”	
<i>1.1. Oxidative addition of halogens to Pt(II) species</i>	38
<i>1.2. Reductive elimination from Pt(IV) species</i>	40
<i>1.3. Oxidative addition and reductive elimination reactions of unsaturated Pt(II) and Pt(IV) species</i>	42
RESULTS AND DISCUSSION	47
<i>1.1. Preparation of new T-shaped platinum biscarbene complexes</i>	47
<i>1.2. Reactivity with halogens</i>	72
1.2.1. Summary of the reactivity of Pt(II) 14-electron species with halogens previously reported by our group. Formation of Pt(IV) species and their reductive C–X coupling products.....	73

1.2.2. Reactivity with halogens of Pt complexes bearing less bulky NHCs.....	77
1.2.2.1. Formation of Pt(IV) complexes	77
1.2.2.2. The search for Pt(III) complexes	82
CHAPTER 2	89
“Reactivity of 14 electron T-shaped Pt(II) complexes with amine boranes”	
INTRODUCTION	91
“The mechanism of transition metal catalyzed dehydrogenation of amineboranes”	
<i>II.1. Initial activation of DMAB by transition metal complexes</i>	<i>93</i>
<i>II.2. Towards the formation of the final dehydrogenation products</i>	<i>98</i>
RESULTS AND DISCUSSION	107
2.1. <i>Catalytic reactions</i>	<i>107</i>
2.1.1. <i>Catalytic reactions in open systems</i>	<i>108</i>
2.1.2. <i>Catalytic reactions in closed systems</i>	<i>112</i>
2.1.3. <i>Catalytic reactions for other amineboranes</i>	<i>115</i>
2.2. <i>Coordination modes of borane-Lewis base adducts to transition metal complexes. The first step towards dehydrogenation.....</i>	<i>117</i>
2.3. <i>σ-borane adducts of $BH_3 \cdot NR_3$ and electron deficient Pt(II) complexes</i>	<i>117</i>
2.4. <i>Dehydrogenation of amine boranes by electron deficient Pt(II) complexes: insights into the mechanism using 1 and DMAB as a model system.....</i>	<i>124</i>
2.5. <i>DFT studies</i>	<i>133</i>
2.6. <i>Mechanistic proposal</i>	<i>138</i>
2.7. <i>Comparison of our system to related mechanistic scenarios</i>	<i>141</i>

2.8. Dehydrogenation of amine boranes by electron deficient Pt(II) complexes: Reactivity with other metal complexes and amineboranes	143
2.8.1. Dehydrogenation of other amineboranes with complex 1	143
2.8.2. Dehydrogenation of amineboranes by complex 2b	147
2.8.3. Dehydrogenation of amineboranes with complexes 15 and 16	152
2.9. Hydrolysis of ammonia borane	153
2.10. Synthesis of diaminoboranes	156
CHAPTER 3	161
“A general route to 2-pyridylidene transition metal complexes”	
INTRODUCTION	163
“Pyridylidenes: a family of non-conventional NHCs”	
III.1 General properties	163
III.2. Current methods for the preparation of 2-pyridylidene transition metal complexes	165
III.2.1. Oxidative addition methods	166
III.2.2. N-functionalisation of metallated pyridyl ligands	168
III.2.3. C–H bond activation with pyridium cations	170
III.2.4. Metal mediated tautomerization of pyridines	172
III.2.5. Deprotonation of pyridinium salts / transmetalation ...	173
III.3. Towards decarboxylation as a useful synthetic procedure for 2- pyridylidene complexes	173
RESULTS AND DISCUSSION	177
3.1 Preparation of pyridinium carboxylates	177

3.2. Preparation of 2-pyridylidene rhodium and iridium complexes	182
3.3. Synthesis of iridium carbonyl derivatives for the study of the electron donor properties of 2-pyridylidene ligands	186
3.4. Synthesis of a bis-pyridylidene transition metal complex	187
3.5. Synthesis of platinum and gold 2-pyridylidene complexes	191
3.6. Attempts to prepare transition metal complexes bearing N,C-coordinating bidentate ligands using betaines as precursors	196
3.7. Attempted preparation of 3- and 4-pyridylidene transition metal complexes	199
3.8. 2-pyridylidene gold complexes as catalysts for the cycloaddition of allenes to dienes	205
CHAPTER 4	211
“Synthesis of transition metal complexes bearing bis and tris(imidazole-2-ylidene)borate ligands”	
INTRODUCTION	213
“Tris(imidazole-2-ylidene)borate ligands: An alternative to some common 6 electron donor ligands with <i>fac</i> - coordination”	
IV.1. Preparation of Tc and Bc ligands.....	216
IV.2. Synthesis of transition metal complexes bearing Tc and Bc ligands.....	217
RESULTS AND DISCUSSION	221
4.1. Preparation of iridium complexes bearing tris(imidazole-2-ylidene)borate ligands	221
4.2. Preparation of iridium complexes bearing bis(imidazole-2-ylidene)borate ligands.....	233

EXPERIMENTAL PART	235
CHAPTER 1	237
CHAPTER 2	261
CHAPTER 3	279
CHAPTER 4	305
CONCLUSSIONS	317

ABBREVIATIONS

NHC	N-heterocyclic carbene
<i>t</i> Bu	1,3-bis- <i>tert</i> -butylimidazol-2-ylidene
IPr	1,3-bis-(2,6-diisopropylphenyl)-imidazol-2-ylidene
IMe	1,3-dimethyl-imidazol-2-ylidene
IMes	1,3-bis-(2,4,6-trimethylphenyl)imidazol-2-ylidene
IMes*	4,5-dimethyl-1,3-bis-(2,4,6-trimethylphenyl)-imidazol-2-ylidene
<i>i</i> Pr ₂	1,3-bis-(2,6-diisopropyl)-imidazol-2-ylidene
<i>i</i> Pr ₂ Me ₂	4,5-dimethyl-1,3-bis-(2,6-diisopropyl)-imidazol-2-ylidene
ICy	1,3-bis-(2,6-dicyclohexyl)-imidazol-2-ylidene
Me	methyl, -CH ₃
Et	ethyl, -CH ₂ CH ₃
Pr	propyl, -CH ₂ CH ₂ CH ₃
<i>i</i> Pr	isopropyl, -CH(CH ₃) ₂
Ar	aryl
Ph	phenyl, -C ₆ H ₅
<i>p</i> -tol	<i>para</i> -tolyl, 4-methyl-phenyl, -(C ₆ H ₄)CH ₃
xyl	xylyl, 2,6-dimethyl-phenyl, -(C ₆ H ₃)(CH ₃) ₂
mes	mesityl, 2,4,6-trimethyl-phenyl, -(C ₆ H ₂)(CH ₃) ₃
diip	2,6-diisopropylphenyl

^t Bu	<i>tert</i> -butyl, CMe ₃
py	pyridine
pyr	pyridylidene
Tp	tris(pyrazolyl) borate
Cp	cyclopentadienyl
Tc ^R	tris(carbene) borate, carbene = 3-R-imidazol-2-ylidene, with R = alkyl, aryl
Bc ^R	bis(carbene) borate, carbene = 3-R-imidazol-2-ylidene, with R = alkyl, aryl
^R Im	N-substituted imidazole, with R = alkyl, aryl
LDA	lithium diisopropyl amine
THF	tetrahydrofuran, C ₄ H ₈ O
Et ₂ O	diethyl ether, CH ₃ CH ₂ OCH ₂ CH ₃
DCM	methylene chloride
cod	cycloocta-1,5-diene
acac	acetyl acetonate
dppe	1,2-Bis(diphenylphosphino)ethane
AB	ammonia borane
MAB	methylamine borane
DMAB	dimethylamine borane
TBAB	<i>tert</i> -butylamine borane
TMAB	trimethylamine borane
L	2 electron donor ligand
η	number of atoms of a ligand directly bound to a metal center

μ	bridging ligand
κ	hapticity, number of atoms in a multidentate ligand that are directly bound to the metal center
IR	infrared
ν	infrared vibrational frequency (cm^{-1})
h	hours
equiv.	equivalents
atm	atmospheres
Anal. Calc.	analysis calculated
Exp.	experimental
g	grams
mmol	millimol
mL	milliliter
cm	centimeter
Å	Angstrom
°	degree
C	Celsius
K	Kelvin
vol	volume
P	pressure
T	temperature
n	number of moles

R	Ideal Gas Constant
ORTEP	crystallographic representation (Oak Ridge Thermal Ellipsoid Program)
DFT	Density Functional Theory
HOMO	Highest Occupied Molecular Orbital
LUMO	Lowest Unoccupied Molecular Orbital
TEP	Tolman Electronic Parameter
% V _{bur}	percent buried volume
e-	electron
HRMS	high resolution mass spectroscopy
NMR	Nuclear Magnetic Resonance
δ	chemical shift in ppm
ppm	parts per million
NOESY	Nuclear Overhauser Enhancement Spectroscopy
COSY ¹ H- ¹ H	correlation spectroscopy
HSQC ¹ H- ¹³ C	correlation spectroscopy (Heteronuclear Single Quantum Coherence)
HMBC ¹ H- ¹³ C	correlation spectroscopy (Heteronuclear Multiple Bond Correlation)
s	singlet
d	doublet
t	triplet

q	quartet
p	pentet
sext	sextet
sept	septet
m	multiplet
br.	broad
${}^nJ_{AB}$	coupling constant (Hz) between A and B nuclei separated by n bonds
Hz	Hertz
THF-d ₈	deuterated tetrahydrofuran
dmsO-d ₆	deuterated dimethyl sulfoxide
MeOD-d ₄	deuterated methanol

GENERAL INTRODUCTION

GENERAL INTRODUCTION

N-heterocyclic carbenes:

An established ligand class for transition metal complexes

Carbenes are species containing a divalent carbon atom bearing only 6 electrons and as such were traditionally considered to be too unstable to be isolated. Even though the first works about transition metal complexes bearing carbene ligands by Öfele¹ and Wanzlick² date from the late 1960s, the isolation of the first stable free carbene was achieved in 1988 by Bertrand³, although this finding was surrounded by some controversy.⁴ It was not until 1991 when Arduengo⁵ synthesized and characterized crystallographically the first stable N-heterocyclic carbene (NHC) (Scheme 1) when the field took off. It is not surprising that these first isolated species were based on N-heterocycles, more specifically imidazol-2-ylidenes, as this type of carbenes is stabilized by the presence of two nitrogen atoms in the positions adjacent to the carbon atom with carbenic character. Bulky substituents in these positions provide these species with additional kinetic stability towards dimerization, although it was proved later that these kinds of species are even stable when smaller methyl substituents are at nitrogen atom of the N-heterocycle.⁶

¹ Öfele, K. *J. Organomet. Chem.* **1968**, *12*, 42

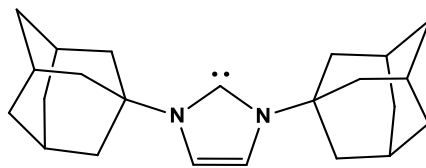
² Wanzlick, H. W.; Schonher, H. *Angew. Chem. Int. Ed. Engl.* **1968**, *7*, 141

³ Igau, A.; Grutzmacher, H.; Baceiredo, A.; Bertrand, G. *J. Am. Chem. Soc.*, **1988**, *110*, 6463

⁴ Martin, D.; Melaimi, M.; Soleilhavoup, M.; Bertrand, G. *Organometallics*, **2011**, *30*, 5304

⁵ Arduengo, A. J.; Harlow, R. L.; Kline, M. *J. Am. Chem. Soc.* **1991**, *113*, 361

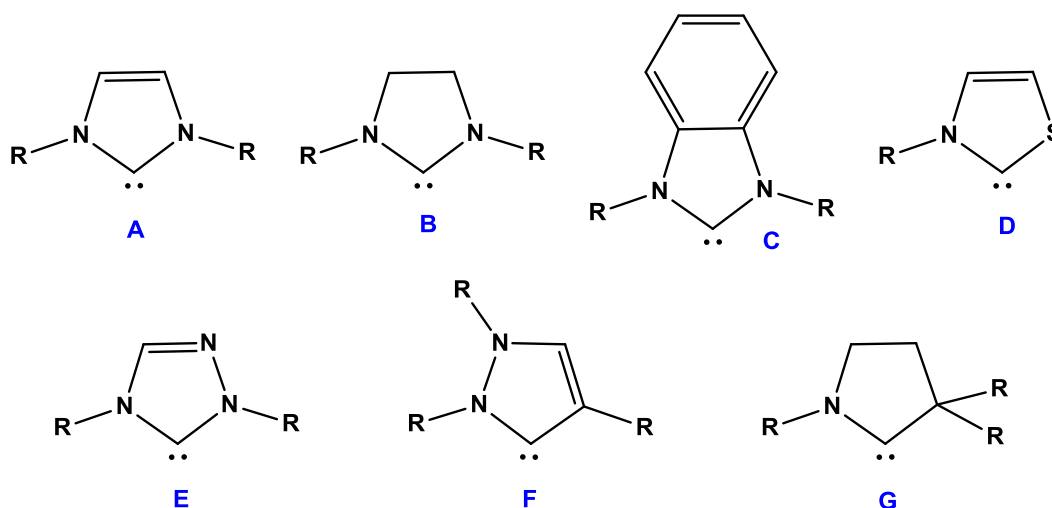
⁶ Arduengo, A. J.; Dias, H. V. R.; Harlow, R. L.; Kline, M. *J. Am. Chem. Soc.*, **1992**, *114*, 5530



Scheme 1. First stable carbene isolated by Arduengo.

Since Arduengo's benchmark work a great variety of NHC ligands have been reported, many of them isolable in their free form and others directly prepared as ligands for transition metal complexes. Thus NHCs have earned their position as one of the most widely used spectator ligands of general applicability in organometallic catalysis, along with phosphine and cyclopentadienyl ligands.⁷

Scheme 2 shows some of the more common NHC ligands based on 5-membered rings. Carbene type **A** (imidazol-2-ylidene) is probably the most widely used NHC ligand type and was also the first reported to be stable by Arduengo. Consequently, imidazol-2-ylidenes are frequently referred to as classical carbenes.



Scheme 2. Some common five-membered ring NHCs: Imidazolylidenes (**A**), imidazolilylidenes (**B**), benzimidazolylidenes (**C**), thiazolylidenes (**D**), triazolylidenes (**E**), pyrazolylidenes (**F**), pyrrolidinylidene (**G**).

⁷ a) Bourissou, D.; Guerret, O.; Gabbai, F. P.; Bertrand, G. *Chem. Rev.* **2000**, *100*, 39; b) Hahn, F. E.; Jahnke, M. C.; *Angew. Chem. Int. Ed.* **2008**, *47*, 3122

The most common method for the preparation of NHCs is deprotonation of the corresponding azolium salt under anhydrous conditions. For the ubiquitous imidazolylidenes these precursors are readily available, as the synthesis of imidazolium salts by the one-pot reaction of glyoxal, formaldehyde and primary amine easily leads to a great variety of differently substituted imidazolium rings and can be easily modified to prepare asymmetric species.⁸ Other less used methods for the synthesis of NHCs include the reduction of thioureas with potassium,⁹ decarboxylation of NHC-CO₂ species,¹⁰ vacuum pyrolysis¹¹ leading to the removal of volatile species from the NHC precursor or reduction of chloroazolium salts with Hg(TMS)₂.¹² César presented a comprehensive review of synthetic routes to NHC precursors.¹³

The possibility to control the steric and electronic properties of such spectator ligands is crucial to fine tune the catalytic performance of the transition metal complexes that bear them. Unlike phosphine and cyclopentadienyl (Cp) ligands, where substituent modification induces both electronic and steric changes, in NHCs where substituents are placed further away from the atom that directly binds to the metal it is possible to modify the steric properties of a ligand without altering its electronic properties and viceversa¹⁴.

⁸ Arduengo, A. J., III. U.S. Patent 5077414, 1991; *Chem. Abstr.* **1992**, 116, 106289e

⁹ a) Hahn, F. E.; Wittenbecher, L.; Van, D. L.; Fröhlich, R. *Angew. Chem. Int. Ed.* **2000**, 39, 541; b) Hahn, F. E.; Wittenbecher, L.; Boese, P.; Bläser, D. *Chem. Eur. J.* **1999**, 5, 1931.

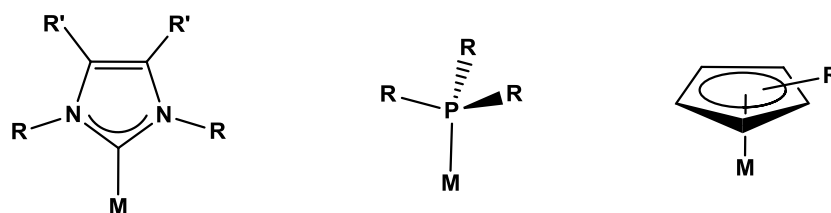
¹⁰ Voutchkova, A.M.; Appelhans, L.N.; Chianese, A.R.; Crabtree, R.H. *J. Am. Chem. Soc.* **2005**, 127, 17624

¹¹ Enders, D.; Breuer, K.; Raabe, G.; Runsink, J.; Teles, J. H.; Melder, J.-P.; Ebel, K.; Brode, S. *Angew. Chem. Int. Ed.* **1995**, 34, 1021

¹² Dröge, T.; Glorius, F. *Angew. Chem. Int. Ed.* **2010**, 49, 6940.

¹³ Benhamou, L.; Chardon, E.; Lavigne, G.; Bellemin-Laponnaz, S.; César, V. *Chem. Rev.* **2011**, 111, 2705.

¹⁴ Crabtree, R. H. *J. Organomet. Chem.* **2005**, 690, 5451.



Scheme 3. Model N-heterocyclic carbene, phosphine and cyclopentadienyl ligands.

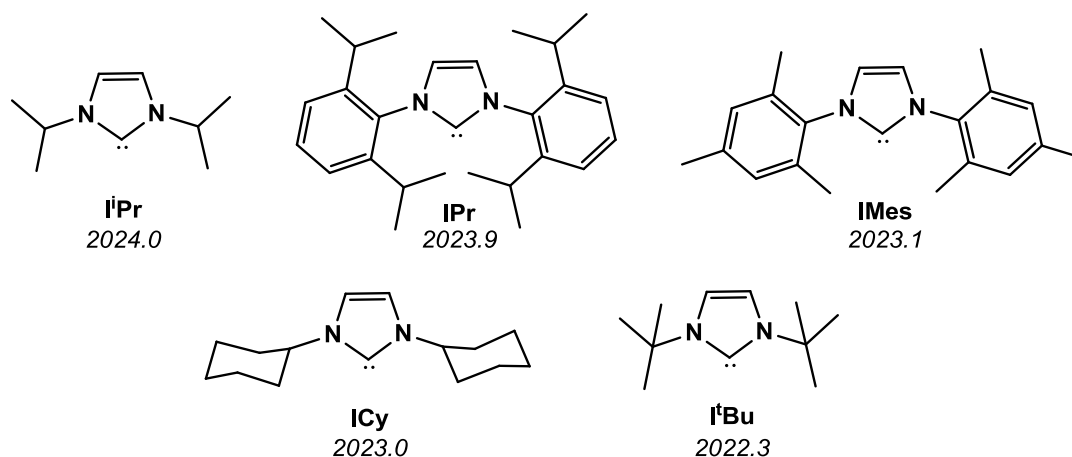
Evidence of this behavior is the fact that some of the most used NHCs, such as IMes, IPr, *i*Pr, *t*Bu or ICy, with N substituents with very different bulk actually have very similar electronic properties (according to CO IR stretching frequencies of carbonyl ligands on iridium complexes) (Scheme 4).

One of the most common parameters used to describe the electron donating capabilities of ligands is the so called Tolman electronic parameter (TEP), which corresponds to the A^1 stretching band for the carbonyl groups in the infrared spectra of the corresponding $[\text{Ni}(\text{CO})_3(\text{L})]$ complexes.¹⁵ The basis for this method is the fact that electron donation to the π^* orbital of CO from the metal is affected by electron donation of other ligands to said metal. Thus, the smaller the IR frequency for the carbonyl groups the better the donor properties of the ligand in consideration. However, nickel NHC complexes are in many cases toxic and not very stable, so the IR data of $[\text{Rh}(\text{CO})_2\text{Cl}]$ and $[\text{Ir}(\text{CO})_2\text{Cl}]$ have been studied instead. Comprehensive studies by Crabtree¹⁶ and Nolan¹⁷ have allowed for the correlation of these data and the TEP parameter.

¹⁵ Tolman, C. A.; *Chem. Rev.* **1977**, *77*, 313.

¹⁶ Chianese, A. R.; Li, X.; Janzen, M. C.; Faller, J.W.; Crabtree, R. H. *Organometallics* **2003**, *22*, 1663.

¹⁷ Kelly III, R. A.; Clavier, H.; Giudice, S.; Scott, N. M.; Stevens, E. D.; Bordner, J.; Samardjiev, I.; Hoff, C. D.; Cavallo, L.; Nolan, S. P. *Organometallics* **2008**, *27*, 202.



Scheme 4. Some common imidazol-2-ylidene carbenes and the average infrared CO stretching frequency for their $[\text{IrCl}(\text{CO})_2(\text{NHC})]$ complexes.^{17,18}

There are many ways in which the electronic properties of NHCs can be varied. The most straightforward would be the modification of the electronic properties of the substituents attached at the N atoms. For example, Plenio¹⁹ reported a series of aryl substituted imidazolylidenes where the substituents in the *para*-position of the ring were varied from electron donating to electron withdrawing (NEt_2 , Me, H, Br and $\text{SO}_2p\text{-Tol}$ among others). It was found that whereas the ligand with the most electron withdrawing group ($\text{SO}_2p\text{-Tol}$) had electronic properties similar to PCy_3 , the one with a NEt_2 group was far more electron donating.

Significant changes can also be induced by modifying the substitution pattern of the ring backbone. It was found that a variety of alkane substituents in the C4 and C5 positions of a IMes carbene resulted in very small changes of the electronic properties²⁰ and using more varied substituents (F, H, OMe) but in the carbon atoms furthest away from the carbene in benzimidazolylidene also resulted in small variation of the electronic properties.²¹ If equally varied substituents (CN, Cl,

¹⁸ Frey, G. D.; Rentsch, C. F.; von Preysing, D.; Scherg, T.; Mühlhofer, M.; Herdtweck, E.; Herrmann, W. A. *J. Organomet. Chem.* **2006**, *691*, 5725.

¹⁹ Leuthäuser, S.; Schwarz, D.; Plenio, H. *Chem. Eur. J.* **2007**, *13*, 7195.

²⁰ Urban, S.; Tursky, M.; Fröhlich, R.; Glorius, F. *Dalton Trans.* **2009**, 6934.

²¹ O'Brien, C. J.; Kantchev, E. A. B.; Chass, G. A.; Hadei, N.; Hopkinson, A. C.; Organ, M. G.; Setiadi, D. H.; Tang, T.-H.; Fang, D.-C. *Tetrahedron*, **2005**, *61*, 9723.

H) are placed in positions C4 and C5, much closer to the carbene, larger variations in electronic properties are in fact observed.²²

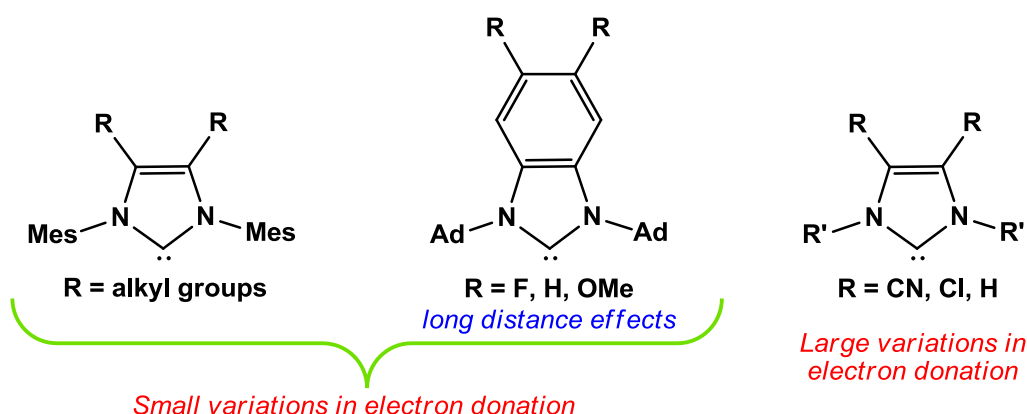
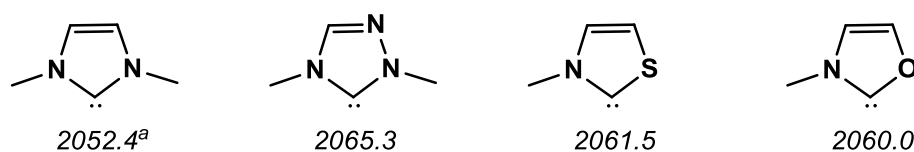


Figure 1. Effect in electron donating properties of introducing various substituents in the NHC backbone²⁰⁻²²

Another way of tuning the electronic properties is changing the heterocycle type, as the nature of the heteroatoms and their position in the ring has a great effect. Both introducing a third heteroatom (e.g. triazolylidenes) or swapping one nitrogen in the ubiquitous imidazolylidenes by oxygen or sulfur (e.g. oxazolylidene and thiazolylidene respectively) makes the resulting carbenes less electron rich (Scheme 5).

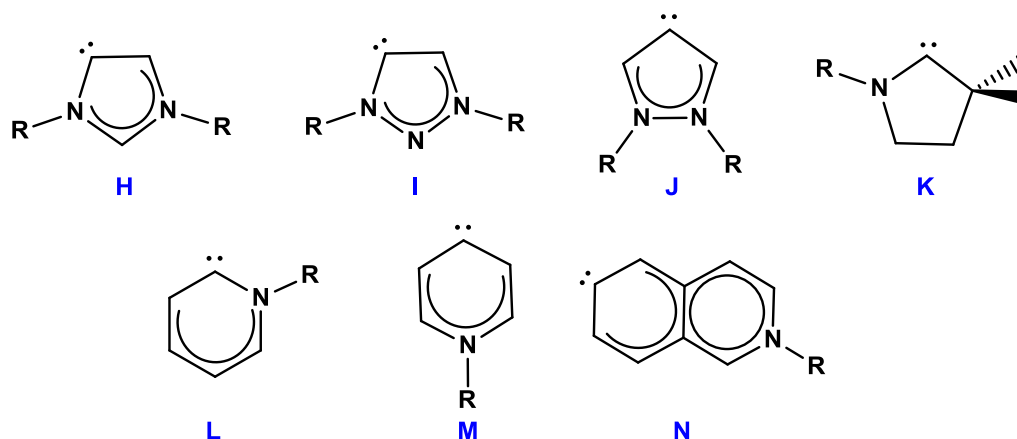


Scheme 5. DFT calculated TEP parameters for a variety of heterocycles. [a] Value obtained from experimental data.²³

On the other hand, removing one or both heteroatoms from the vicinity of the carbene (e.g. remote carbenes) increases the σ -donor properties of the ligands.

²² a) Khramov, D. M.; Lynch, V. M.; Bielawski, C. W. *Organometallics*, **2007**, *26*, 6042; b) Bittermann, A.; Härter, P.; Herdtweck, E.; Hoffmann, S. D.; Herrmann, W. A. *J. Organomet. Chem.* **2008**, *693*, 2079.

²³ Gusev, D. G.; *Organometallics* **2009**, *28*, 6458



Scheme 6. Some examples of NHCs with reduced heteroatom stabilization.

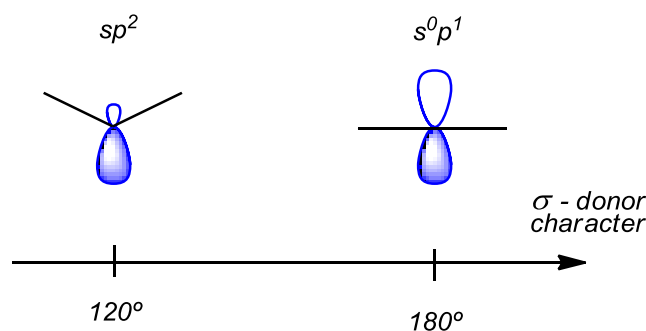
Some examples of this kind of NHCs are depicted in Scheme 6. Carbenes such as **H**, imidazole-4-ylidenes, are called abnormal carbenes because they coordinate to the metal at the C4 position, as opposed to the far more frequent classic imidazole-2-ylidenes, **A**. Carbenes **J**, **M** and **N** are examples of remote carbenes. Albrecht reviewed the synthesis and preparation of metal complexes of these ligands²⁴ extensively, whereas more recently Crabtree reviewed the properties of abnormal and mesoionic carbenes.²⁵

Changing the ring size also has an important effect in the electronic properties. Electron donation increases from five to six to seven membered ring NHCs, as the NCN angle increases and the hybridization of the carbene atom is modified. When the NCN angle is 120° the in-plane lone pair of electrons of the carbene is essentially in a sp^2 orbital. Larger NCN angles increase the p character of this orbital, making the HOMO higher in energy and thus presenting better σ -donor capabilities²⁶.

²⁴ Schuster, O.; Yang, L.; Raubenheimer, H. G.; Albrecht, M. *Chem. Rev.* **2009**, *109*, 3445.

²⁵ Crabtree, R. H. *Coord. Chem. Rev.* **2013**, *257*, 755.

²⁶ Comas-Vives, A.; Harvey, J. N. *Eur. J. Inorg. Chem.* **2011**, 5025.



Scheme 7. A change in the carbene angle modifies hybridization

It must be noted that changing the ring size also changes the steric properties for identical N substituents, as increasing the NCN angle brings these groups closer to the metal center.²⁷

Other differences of NHCs when compared to phosphines and cyclopentadienyls, besides their higher electron donor capabilities, are related to the disposition of the R substituents (Scheme 3). On the one hand, whereas NHC substituents point towards the metal, causing higher steric hindrance in the vicinity of the metal center, substituents in phosphines and cyclopentadienyls point away from the metal and away from the Cp ring center, respectively. These steric considerations can be quantified by the “buried volume” method.²⁸

²⁷ (a) Iglesias, M.; Beetstra, D. J.; Knight, J. C.; Ooi, L.; Stasch, A.; Coles, S.; Male, L.; Hursthouse, M. B.; Cavell, K. J.; Dervisi, A.; Fallis, I. A. *Organometallics*, **2008**, *27*, 3279; (b) Lu, W. Y.; Cavell, K. J.; Wixey, J. S. Kariuki, B. *Organometallics*, **2011**, *30*, 5649.

²⁸ Poater, A.; Cosenza, B.; Correa, A.; Giudice, S.; Ragone, F.; Scarano, V.; Cavallo, L. *Eur. J. Inorg. Chem.* **2009**, 1759.

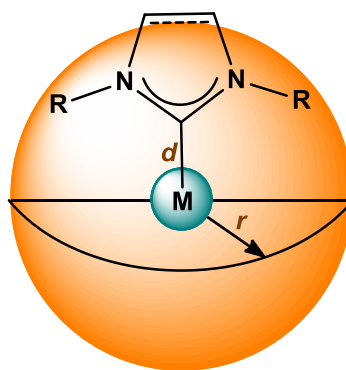


Figure 2. Parameters used in the calculation of buried volume data.

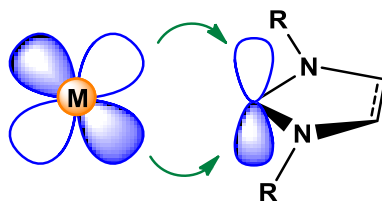
This concept is described as the percentage of the volume of a sphere of fixed radius that is occupied by the ligand, with the metal atom at its center, and is calculated with crystallographic or DFT calculated data. The values of % V_{bur} depend on the metal of choice. Complexes that present linear structures, such as $[(NHC)MCl]$ ($M = Au, Ag, Cu$) are preferred because they present less distortion in the NHC spatial properties by other ligands. If data are calculated for square-planar $[(NHC)Ir(CO)_2]$ complexes for example, the % V_{bur} decreases due to a more crowded environment around the metal center. A very detailed analysis of % V_{bur} values for a comprehensive variety of phosphine and NHC ligands was presented by Nolan and Clavier.²⁹

Another major difference between phosphines and Cp ligands and NHCs is that the first two have a cone geometry, which means that rotation around the metal-ligand axis does not essentially affect the steric or electronic properties of their transition metal complexes. However, the fan shape of NHC ligands confers anisotropy to their interaction with the metal and both steric hindrance and electronic properties depend on the orientation with which the carbene coordinates the metal.

An example of an electronic property that is affected by ligand orientation is π -back donation. Adequate full d orbitals at the metal must be available with the correct orientation to interact with the empty p orbital in the carbene (Scheme 8).

²⁹ Clavier, H.; Nolan, S. P. *Chem. Commun.* **2010**, 46, 841.

This is more restrictive than in the case of phosphines, where two orbitals on phosphorus are available for back donation from the metal.



Scheme 8. π -back bonding between a metal center and a diaminocarbene.

Even though π -back donation had been traditionally considered negligible for NHCs, with most works focusing on their excellent σ -donor abilities, many recent contributions have indicated that this is not the case. Computational studies by Meyer³⁰ for Cu, Ag, Au and Pd NHC complexes were among the first to indicate that π -back donation represented between 15 to 30 % of the bonding component. More interestingly, a study that tried to rationalize the activity of a series of Grubbs-type ruthenium catalysts for olefin metathesis indicated that π -back bonding was even more important for carbenes than for phosphines.³¹ A comprehensive study on the importance of π -back bonding in metal-NHC complexes was recently presented by Comas-Vives and Harvey.²⁶ They conclude that factors such as the electron-rich character of the metal center, the nature of the ancillary ligands, and the energy difference and overlap between the donor (metal) and acceptor (carbene) orbitals determine the strength of backbonding, which was found to be non-negligible in all cases. The π accepting properties of NHCs have been recently studied by measuring the ³¹P NMR chemical shifts of carbene-phosphinidene adducts.³²

The metal-NHC bonding picture is further complicated by the possibility of π -bonding from filled π -orbitals of the NHC to empty d orbitals of the metal, which is particularly important for electron deficient metal centers. An interesting example that demonstrates this behavior are the doubly cyclometallated iridium

³⁰ a) Hu, X. L.; Tang, Y. J.; Gantzel, P.; Meyer, K. *Organometallics*, **2003**, *22*, 612; b) Hu, X. L.; Castro-Rodriguez, I.; Olsen, K.; Meyer, K. *Organometallics* **2004**, *23*, 755

³¹ Occhipinti, G.; Bjorsvik, H. R.; Jensen, V. R. *J. Am. Chem. Soc.* **2006**, *128*, 6952

³² Back, O.; Henry-Ellinger, M.; Martin, C. D.; Martin, D.; Bertrand, G. *Angew. Chem. Int. Ed.* **2013**, *52*, 2939.

complexes **I** and **II** (Figure 3), which are remarkably stable despite being electron deficient 16 and 14 e^- species respectively.³³ Interestingly, X-ray data showed no evidence of stabilization via agostic interactions with the σ C-H bonds of the *tert*-butyl substituents.

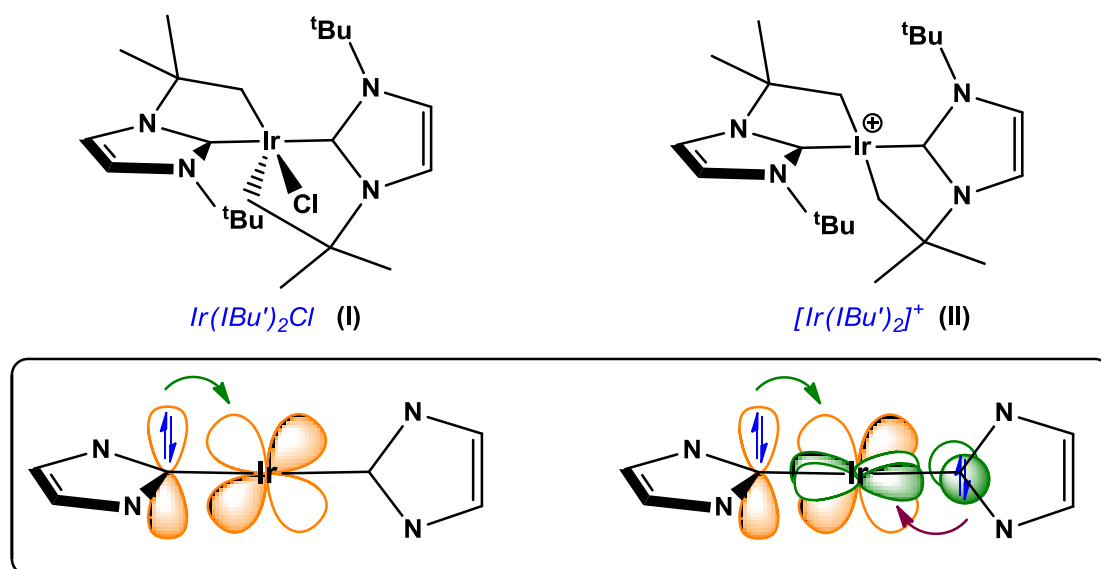


Figure 3. Simplified molecular orbitals indicating stabilization of 16 e^- complex **I** and 14 e^- complex **II** by π -donation from filled NHC π -orbitals. Complete structure of the ligands omitted for clarity on the bottom schemes.

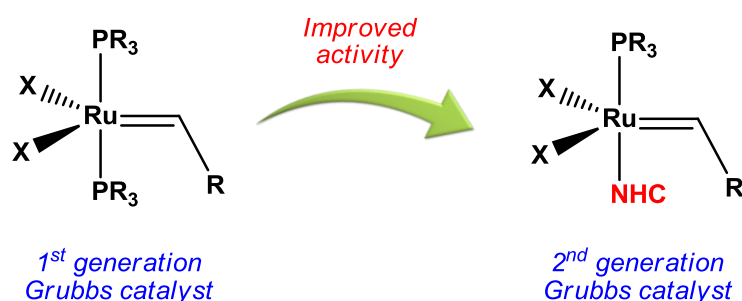
Calculations showed that for these species electronic stabilization by π -donation from the ligand was more favorable than by agostic interactions. For 16 e^- complex **I**, only one of the carbenes is engaged in this kind of interactions, as evidenced by experimental data that show that one of the Ir–C bonds is significantly shorter than the other. On the contrary complex **II**, where stabilization by π -donation from both ligands is needed, is totally symmetric.

Since the first reports of the ease of preparation of NHC ligands, they have been extensively used in catalysis. One of the first reports in this field used palladium bis-NHC complexes for the Heck reaction, in which aryl halides are coupled to

³³ N.M. Scott, R. Dorta, E.D. Stevens, A. Correa, L. Cavallo, S.P. Nolan, J. Am. Chem. Soc. 127 (2005) 3516

alkenes, and achieved good results with surprisingly low catalyst loadings.³⁴ This result was explained by the observed strong metal-NHC bond, which led to minimal decomposition and also removed the need to add an excess of ligand, as was the case with phosphine complexes. Moreover, the preformed Pd-NHC complexes proved to have high thermal and hydrolytic stability when compared to their phosphine counterparts.

Another well known example of catalysts where replacement of a phosphine ligand by an NHC brought about a markedly improved performance is the ruthenium-NHC catalysts for olefin metathesis. The initial phosphine based complex reported by Grubbs was improved by NHC variants that were reported at roughly the same time by Herrmann³⁵, Grubbs³⁶ and Nolan³⁷ (Scheme 9).



Scheme 9. General formula of first and second generation Grubbs catalysts.

It was found that even if phosphine dissociation was easier in the first generation catalysts, olefin coordination was favored for the resulting 14 electron intermediate bearing a NHC ligand.³⁸

A comprehensive review of the early use of NHC-metal complexes in a variety of catalytic organic transformations was presented by Herrmann³⁹, whereas more

³⁴ Herrmann, W. A.; Elison, M.; Fischer, J.; Köcher, C.; Artus, G. R. J. *Angew. Chem. Int. Ed.* **1995**, *34*, 2371.

³⁵ Weskamp, T.; Kohl, F. J.; Hieringer, W.; Gleich, D.; Herrmann, W. A. *Angew. Chem. Int. Ed.* **1999**, *38*, 2416.

³⁶ Scholl, M.; Trnka, T. M.; Morgan, J. P.; Grubbs, R. H. *Tetrahedron Lett.* **1999**, *40*, 2247.

³⁷ Huang, J.; Schanz, H. Z.; Stevens, E. D.; Nolan, S. P. *Organometallics* **1999**, *18*, 5375.

³⁸ Sanford, M. S.; Ulman, M.; Grubbs, R. H. *J. Am. Chem. Soc.* **2001**, *123*, 749.

³⁹ Herrmann, W. A. *Angew. Chem. Int. Ed.* **2002**, *41*, 1290.

recent reports on catalysis by late transition metals bearing NHC ligands have been reported.⁴⁰ The special properties of NHCs have also led to their use in organocatalysis,⁴¹ and more and more frequently are being utilized to isolate unusual structures in main group chemistry⁴² and in the activation of small molecules.⁴³

In summary, a wide variety of applications has been found for NHC ligands, and the more common imidazolylidene carbenes are now on par with phosphines as the ligands of choice for organometallic chemistry. However, less explored NHC types are available with yet different electronic and steric properties and it is expected to find new reactivities of organometallic molecules bearing this useful type of ligands.

⁴⁰ a) Díez-González, S.; Marion, N.; Nolan, S. P. *Chem. Rev.* **2009**, *109*, 3612; b) Heterocyclic carbenes, from laboratory curiosities to efficient synthetic tools (Ed.: S. Díez-González), Royal Society of Chemistry Publishing, Cambridge, **2011**

⁴¹ a) Enders, D.; Niemeier, O.; Henseler, A.. *Chem. Rev.* **2007**, *107*, 5606; b) Bugaut, X.; Glorius, F.; *Chem. Soc. Rev.* **2012**, *41*, 3511.

⁴² a) Wang, Y.; Robinson, G. H. *Dalton Trans.* **2012**, *41*, 337; b) Wang, Y.; Robinson, G. H. *Inorg. Chem.* **2011**, *50*, 12326; c) Martin, C. D.; Soleilhavoup, M.; Bertrand, G. *Chem. Sci.* **2013**, DOI: 10.1039/C3SC51174J

⁴³ Martin, C. D.; Soleilhavoup, M.; Bertrand, G. *Chem. Sci.* **2011**, *2*, 389

CHAPTER 1

Reactivity of electron deficient biscarbene
platinum (II) complexes with halogens

CHAPTER 1. INTRODUCTION

Overview of oxidative addition/reductive
elimination in Pt(II)/Pt(IV) unsaturated species

Oxidative addition and reductive elimination reactions are among the most important in organometallic chemistry¹ and in the particular case of reactions between Pt(II) species and halogens (X_2) they have been well studied due to their importance in key transformations involving the activation and functionalization of C–H bonds.² In a potential route for the production of alkyl or aryl halides from alkanes/arenes, a Pt(II) complex with alkyl or aryl ligands, ideally formed by C–H activation of alkanes or arenes, would initially be oxidized to a Pt(IV) species by X_2 . Reductive elimination could then produce alkyl or aryl halides and a new Pt(II) complex that would undergo C–H activation to make the process catalytic.³ Alkyl and aryl halides are widely used as starting materials in a plethora of metal-catalyzed organic transformations. However, it should be noted that whereas oxidative addition of alkyl and aryl halides to transition metal complexes is a well established process that takes place in a large amount of chemical transformations, the reverse reaction, reductive elimination of alkyl or aryl halides

¹ J. F. Hartwig, *Organotransition Metal Chemistry: From Bonding to Catalysis*, University Science Books, Sausalito, **2009**.

² a) Lersch, M.; Tilset, M. *Chem. Rev.* **2005**, *105*, 2471; b) Rendina, L. M.; Puddephatt, R. J. *Chem. Rev.* **1997**, *97*, 1735

³ Horváth, I. T.; Cook, R. A.; Millar, J. M.; Kiss, G.; *Organometallics* **1993**, *12*, 8.

is much less common.⁴ In the last few years this latter process has been particularly relevant to the formation of carbon-fluorine bonds.⁵

In this section mechanistic aspects of oxidative addition and reductive elimination in Pt(II) and Pt(IV) species will be discussed, with a focus on the reactivity with halogens. Examples of such reactivity for unsaturated Pt(II)/Pt(IV) species will be mentioned due to their relevance to the work with biscarbene unsaturated platinum complexes in our group. The interest in such species stems from the fact that coordinatively unsaturated, 16-electron Pt(IV) complexes have proved to be key intermediates in both oxidative addition and reductive elimination processes.

1.1. Oxidative addition of halogens to Pt(II) species

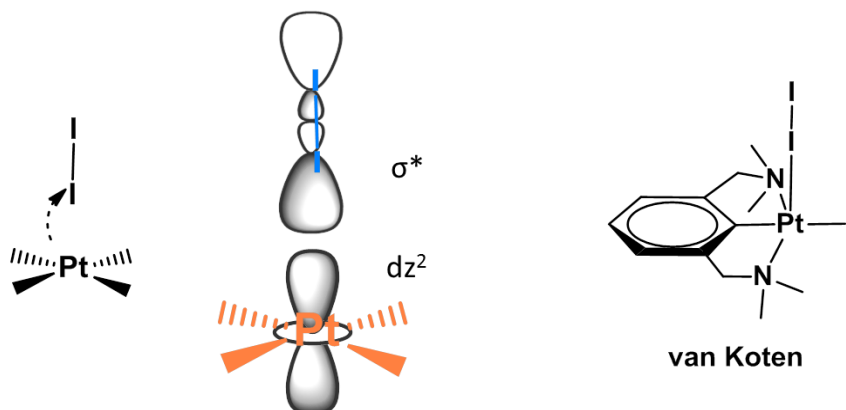
Many mechanisms are possible for the oxidative addition of X₂ to a square-planar Pt(II) complex but the initial step appears to be a head-on interaction of the halogen molecule with the dz² orbital of the metal. This interaction weakens the X–X bond and makes the metal center more electropositive. A side-on halogen coordination, which would lead to a *cis* oxidative addition product, is unfavorable due to the repulsive interactions between the platinum dz² orbital and the filled p orbitals on the halogen.⁶ Head-on halogen complexes of Pt have been experimentally observed and crystallographically characterized in some cases.⁷

⁴ Vigalok, A. *Chem. Eur. J.* **2008**, *14*, 5102

⁵ a) Grushin, V. V. *Acc. Chem. Res.* **2010**, *43*, 160; b) Vigalok, A. *Organometallics*, **2011**, *30*, 4802; c) Furuya, T.; Kamlet, A. S.; Ritter, T. *Nature*, **2011**, *473*, 470; d) Hollingworth, C.; Gouverneur, V. *Chem. Commun.* **2012**, *48*, 2929.

⁶ Bickelhaupt, F. M.; Baerends, E. J.; Ravenek, W. *Inorg. Chem.* **1990**, *29*, 350-354.

⁷ a) van Beek, J. A. M.; van Koten, G.; Smeets, W. J. J.; Spek, A.L. *J. Am. Chem. Soc.* **1986**, *108*, 5010-5011, b) J. A. M. van Beek, G. van Koten, G. P. C. M. Dekker, E. Wissing, M. C. Zontberg and C. H. Stam, *J. Organomet. Chem.*, 1990, **394**, 659; c) Makiura, R.; Nagasawa, I.; Kimura, N.; Ishimaru, S.; Kitagawa, H.; Ikeda, R. *Chem. Commun.* **2001**, 1642-1643.



As for how the oxidative addition reaction proceeds after halogen coordination, there are early examples that indicate a free radical mechanism being in operation to yield the product of *trans* oxidative addition, as in the case of $\text{Pt}(\text{acac})_2$.⁸ However it is much more common for the reaction to proceed in a two-electron oxidation stepwise process in which the initial halogen charge transfer complex yields a cationic pentacoordinated Pt(IV) species by halide dissociation. Nucleophilic attack of the halide produces the oxidative addition Pt(IV) product with *trans* selectivity.⁹ However, the flexibility of the unsaturated pentacoordinate intermediate allows for ligand rearrangement so that *cis* products are observed when they are thermodynamically feasible.^{9a,d}

Detection of the intermediate Pt(IV) unsaturated species is sometimes facilitated by the coordination of a solvent molecule.¹⁰ More recently there has been evidence of unsaturated Pt(IV) species being stable enough to be observed and isolated without the need of solvent coordination.¹¹

⁸ Hopgood, D.; Jenkins, R.A.; *J. Am. Chem. Soc.* **1973**, *95*, 4461

⁹ a) van Koten, G.; Terheijden, J.; van Beek, J.A.M.; Wehman-Ooyevaar, I.C.M.; Muller, F.; Stam, C.H.; *Organometallics* **1990**, *9*, 903; b) Hughes, R.P.; Sweetser, J.T.; Tawa, M.D.; Williamson, A.; Incarvito, C.D.; Rhatigan, B.; Rheingold, A.L.; Rossi, G.; *Organometallics*, **2001**, *20*, 3800; c) Tamasi, G.; Cini, R.; Intini, F.P.; Sivo, M.F.; Natile, G.; *Angew. Chem. Int. Ed.*, **2004**, *43*, 5081; d) Yahav, A.; Goldberg, I.; Vigalok, A.; *Organometallics*, **2005**, *24*, 5654; e) Westra, A.N.; Bourne, S.A.; Koch, K.R.; *Dalton Trans.* **2005**, 2916; f) Werner, M.; Wagner, C.; Steinborn, D.; *J. Organomet. Chem.* **2009**, *694*, 190; g) Serra, D.; Cao, P.; Cabrera, J.; Padilla, R.; Rominger, F.; Limbach, M.; *Organometallics*, **2011**, *30*, 1885.

¹⁰ Margiotta, N.; Rinaldo, R.; Intini, F.P.; Natile, G.; *Dalton Trans.*, **2011**, *40*, 12877.

¹¹ Grice, K.A.; Scheuermann, M.L.; Goldberg, K.I.; *Top. Organomet. Chem.* **2011**, *35*, 1.

I.2. Reductive elimination from Pt(IV) species

Examples of reductive elimination from Pt(IV) species are less frequent than those of its microscopic reverse, oxidative addition to a Pt(II) species. Octahedral Pt(IV) complexes have proved to be rather stable towards reductive elimination and in fact most examples of the reaction have been shown to proceed through unsaturated five-coordinate Pt(IV) species analogous to those involved in oxidative addition processes. Some examples of concerted elimination from octahedral Pt(IV) species have nonetheless been reported.¹²

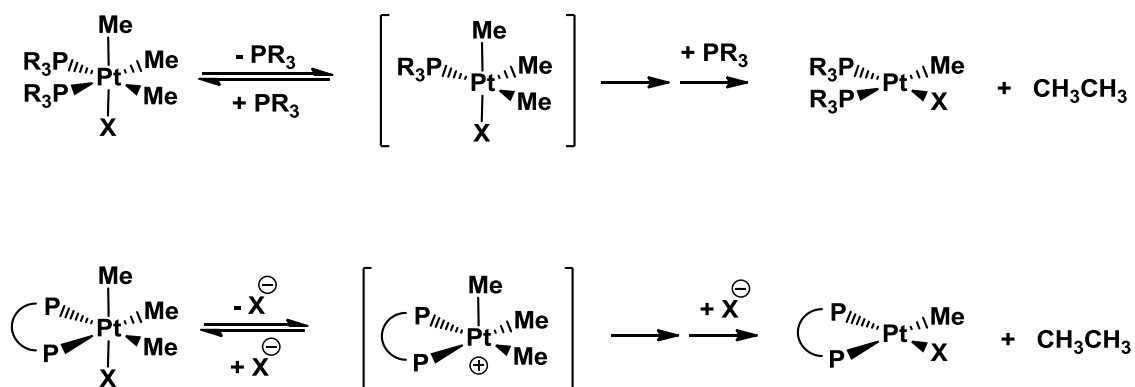
There are several possibilities to form five-coordinate Pt(IV) species from their saturated counterparts. Depending on the substituents present, ligand or halide dissociation takes place first to form the unsaturated species at which reductive elimination can occur. This behavior was first reported for the reductive elimination of phenyl iodide from $L_2PtPh_2I_2$ ($L = PEt_3$) by Ettorre¹³, who noted that added iodide slowed down the reaction in consistency with a dissociative mechanism. A few years later Puddephatt et al.¹⁴ reported that ethane reductive elimination from L_2PtMe_3X was slower upon phosphine addition when $L = PR_3$ and even more so when the chelating phosphine dppe was used, as in this case dissociation is not favored. Later studies showed that in the cases where chelating ligands were present dissociation of an halide was the most favorable way to form an unsaturated species.¹⁵

¹² a) Crumpton-Bregel, D.M.; Goldberg, K.I.; *J. Am. Chem. Soc.*, **2003**, *125*, 9442; b) Khusnutdinova, J.R.; Newman, L.L.; Zavalij, P.Y.; Lam, Y.-F.; Vedernikov, A.N.; *J. Am. Chem. Soc.*, **2008**, *130*, 2174

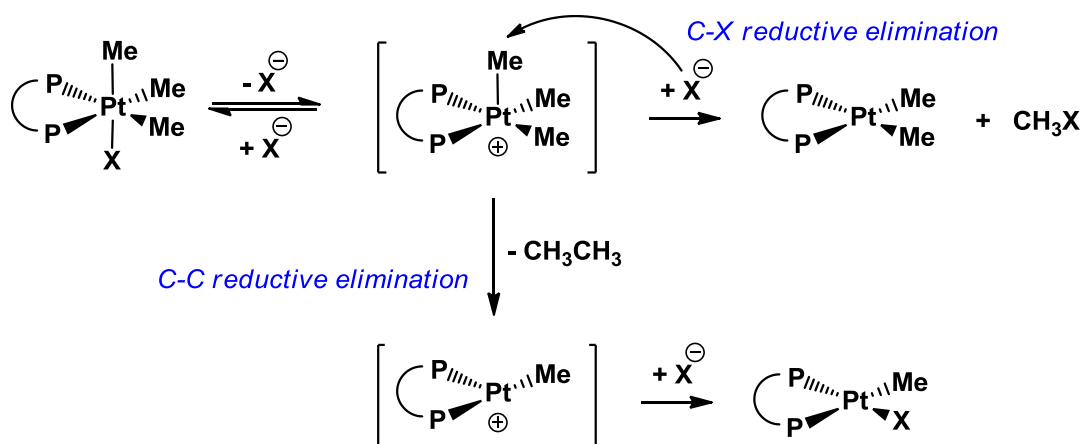
¹³ Ettore, R.; *Inorg. Nucl. Chem. Lett.*, **1969**, *5*, 45

¹⁴ Brown, M.P.; Puddephatt, R.J.; Upton, C.E.E.; *J. Chem. Soc. Dalton Trans.*, **1974**, 2457

¹⁵ Goldberg, K.I.; Yan, J.Y.; Winter, E.L.; *J. Am. Chem. Soc.*, **1994**, *116*, 1573



In Pt(IV) complexes with both alkyl and halide ligands competing pathways for both C–C or C–X reductive elimination can take place, but an understanding of the mechanism allows for selective formation of either product. A pentacoordinate intermediate as described above is common to both pathways. Addition of external halide suppresses C–C coupling, but even though it slows down the formation of the unsaturated intermediate, it increases the velocity of the nucleophilic attack of the halide to release the C–X coupling product. On the other hand, increasing the solvent polarity or adding appropriate Lewis acids favors C–C coupling as it decreases the nucleophilicity of X^- .



In some cases, bulky ligands such as N-heterocyclic carbenes induce fast reductive elimination process of methyl iodide in the reactions of the NHCs with the platinum complex $[PtMe_3]_4$. Even the smallest NHC IMe (IMe = 1,3-

dimethylimidazol-2-ylidene) produces the reductive elimination reaction without observing any transient Pt(IV) intermediate,¹⁶ indicating that sterics constrains, as expected, favor this C–X coupling reactions.

It is expected that Pt(IV) complexes that are already coordinatively unsaturated are more prone towards reductive elimination than octahedral Pt(IV) complexes. They also facilitate the kinetic study of the key C–C or C–X coupling step, as there is no interference from a previous ligand dissociation step. Nevertheless, the number of low electron count Pt(IV) complexes that have been isolated and characterized until present is very limited.¹¹ Due to the nature these pentacoordinate Pt(IV) complexes, which mostly possess methyl, hydride and silyl groups besides the spectator ligands, only C–C, C–H and C–Si coupling reactions from these species have been studied so far.

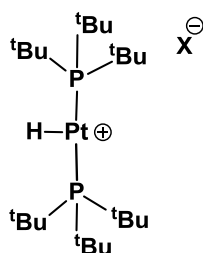
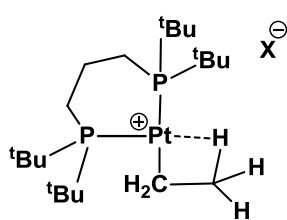
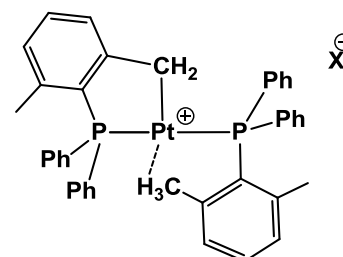
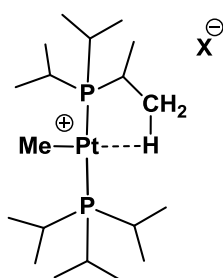
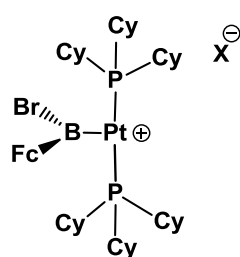
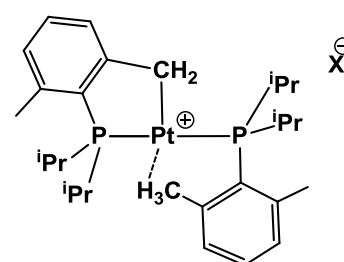
I.3. Oxidative addition and reductive elimination reactions of unsaturated Pt(II) and Pt(IV) species

It is interesting to consider how oxidative addition proceeds and whether unsaturated Pt(IV) complexes are obtained when suitable Pt(II) unsaturated species are oxidized. There are few examples in the literature of coordinatively unsaturated Pt(II) species. The first example dates back to 1983 and is a phosphine hydride reported by Srivatava¹⁷ that was synthesized by chloride abstraction with a variety of silver salts. Then Spencer and Orpen¹⁸ prepared a T-shaped Pt(II) alkyl complex with a chelating phosphine, stabilized by an agostic interaction, according with spectroscopic (NMR) and crystallographic studies.

¹⁶ a) Lindner, R.; Wagner, C.; Steinborn, D. *J. Am. Chem. Soc.* **2009**, *131*, 8861; b) Rivada-Wheelaughan, O.; Donnadiou, B.; Maya, C.; Conejero S. *Chem. Eur. J.* **2010**, *16*, 10323

¹⁷ Goel, R. G.; Srivastava, R. C.; *Can. J. Chem.* **1983**, *61*, 1352

¹⁸ Mole, L.; Spencer, J. L.; Carr, N.; Orpen, G.; *Organometallics* **1991**, *10*, 49.

Srivatava
1983Spencer & Orpen
1991Baratta
2003Weller
2004Braunschweig
2005Carmona
2012

More recent examples were presented by Weller¹⁹, with a bisphosphine complex that underwent intramolecular C–H activation to yield a cyclometallated species, Baratta²⁰ and Carmona²¹ again with bulky xylyl phosphines that underwent cyclometallation and Braunschweig²², with a bisphosphine complex where the presence of a boryl ligand, with a large *trans* influence, was key to isolating a true T-shaped 14-electron species without stabilization with agostic interactions. However, no oxidative addition products have been reported for these species, even though they may be intermediates in the reactivity they present (e.g. intramolecular C–H activation, reaction with H₂). In the case of a T-shaped Pt(II) complex reported by Rourke²³, with a cyclometallated phenyl pyridine ligand,

¹⁹ Ingleson, M. J.; Mahon, M. F.; Weller, A. S.; *Chem. Commun.* **2004**, 2398.

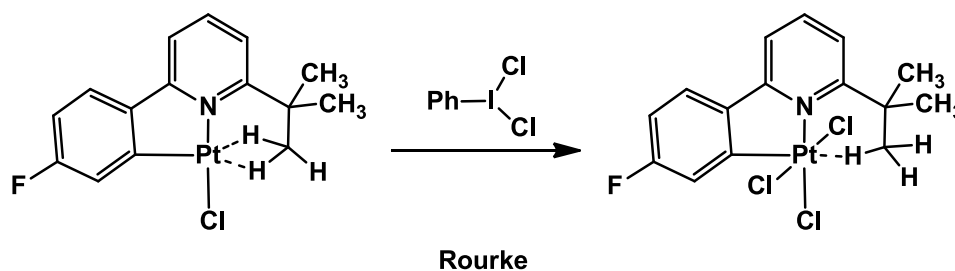
²⁰ Baratta, W.; Stoccoro, S.; Doppio, A.; Herdtweck, E.; Zucca, A.; Rigo, P.; *Angew. Chem. Int. Ed.* **2003**, *42*, 105.

²¹ Campos, J.; Peloso, R.; Carmona, E.; *Angew. Chem. Int. Ed.* **2012**, *51*, 8255.

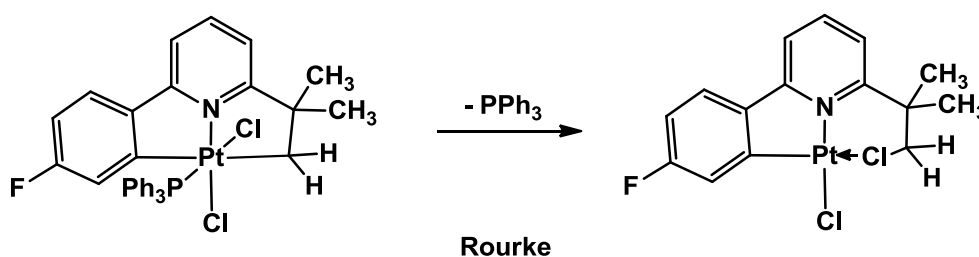
²² Braunschweig, H.; Radacki, K.; Rais, D.; Scheschkewitz, D.; *Angew. Chem. Int. Ed.* **2005**, *44*, 5651.

²³ Crosby, S. H.; Clarkson, G. J.; Rourke, J. P.; *J. Am. Chem. Soc.* **2009**, *131*, 14142.

oxidative addition led to the unsaturated Pt(IV) species,²⁴ stabilized by an agostic interaction as was the case of the starting material.



No reductive elimination reaction was reported for this new Pt(IV) species, but a closely related saturated complex bearing a phosphine ligand underwent intramolecular C–Cl reductive coupling.²⁵



Interestingly, out of the two possible isomers of the starting material, with the chloride substituents in *cis* and *trans* dispositions, only the *cis* species can yield the C–Cl coupling product whereas the *trans* species is unreactive.

Pt(III) species as intermediates in oxidative addition/reductive elimination processes

Mononuclear platinum complexes in oxidation states 0,+2 and +4 are much more common than species in a +3 oxidation state, as the great majority of platinum redox chemistry is based on two electron processes. There are only a few examples of mononuclear Pt(III) complexes, mainly reported in the 1980s²⁶ and in

²⁴ Crosby, S. H.; Clarkson, G. J.; Deeth, R. J.; Rourke, J. P.; *Dalton Trans.*, **2011**, 40, 1227.

²⁵ Crosby, S. H.; Clarkson, G. J.; Rourke, J. P.; *Organometallics* **2012**, 31, 7256.

²⁶ a) Usón, R.; Forniés, J.; Tomás, M.; Menjón, B.; Sünkel, K.; Bau, R.; *J. Chem. Soc., Chem. Commun.* **1984**, 751, b) Blake, A. J.; Gould, R. O.; Holder, A. J.; Hyde, T. I.; Lavery, A. J.; Odulate, M. O.; Schröder, M.; *J. Chem. Soc., Chem. Commun.* **1987**, 118, c) Bontchev, P. R.; Mitewa, M.; Gentcheva, G.; *Pure Appl. Chem.* **1989**, 61, 897, d) Stephen, E.; Blake, A. J.; Davies, E. S.; McMaster, J.; Schröder,

fact the first example of an alkyl Pt(III) complex, reported by our group,²⁷ was only published last year. The scarcity of these mononuclear d^7 compounds may be caused by the high reactivity of the unpaired electron, located in the dz^2 orbital perpendicular to the coordination plane. Dimeric Pt(III) complexes are actually much more common and many species are known.^{28,29}

Platinum (III) species have in some occasions been invoked as intermediates in the oxidation of Pt(II) species to Pt(IV). This is the case for the oxidation of Pt(II) species with Cu(II) salts, which was applied in an extension of the Shilov system reported by Sen that used O_2 as the ultimate oxidant.³⁰ Van Koten suggested the participation of Pt(III) in the oxidation of Pt(II) complexes with CuX_2 ³¹ and Lippert reported that a stable Pt(III) dimer is actually obtained from O_2 oxidation of a Pt(II)-Cu(II) species in which the presence of copper was proved to be vital for the redox process to proceed.³² Platinum (III) species also appeared to participate in the reverse reaction, Pt(IV) reduction with $CuCl$,³³ to account for the observed kinetic data.

In other cases oxidation reactions seem to lead to transient Pt(III) species that are unstable towards disproportionation to yield new Pt(II) and Pt(IV) species. Tilset presented a thorough study on the redox chemistry of platinum dialkyl diimine complexes which demonstrated the intermediacy of Pt(III) species and revealed a mechanism in which such species undergo an intermolecular methyl transfer to

M. *Chem. Commun.* **2008**, 5707; e) Bélombé, M. M.; Nenwa, J.; Hey-Hawkins, E.; Lönnecke, P.; Strauch, P.; Koch, K. R. *Polyhedron*, **2008**, 27, 3688; f) Bois, H.; Connelly, N. G.; Crossley, J. G.; Guillorit, J. C.; Lewis, G. R.; Orpen, A. G.; Thornton, P. *Dalton Trans.* **1998**, 2833; g) Alves, H.; Simão, D.; Cordeiro Santos, I.; Gama, V.; Teives Henriques, R.; Novais, H.; Almeida, M. *Eur. J. Inorg. Chem.* **2004**, 1318.

²⁷ Rivada-Wheelaghan, O.; Ortuño, M.A.; Díez, J.; García-Garrido, S.E.; Maya, C.; Lledós, A.; Conejero, S.; *J. Am. Chem. Soc.* **2012**, 134, 15261.

²⁸ Woollins, J. D.; Kelly, P. F. *Coord. Chem. Rev.* **1985**, 65, 115.

²⁹ If more Pt(III) dimers references are needed, this paper has plenty: *Inorganic Chemistry Communications* 12 (2009) 1061–1063.

³⁰ Lin, M.; Shen, C.; García-Zayas, E. A.; Sen, A. *J. Am. Chem. Soc.* **2001**, 123, 1000.

³¹ Van Beek, J.A.M.; van Koten, G.; Wehman-Ooyevaar, I.C.M.; Smeets, W.J.J.; van der Sluis, P.; Spek,

A.L. *J. Chem. Soc. Dalton Trans.*, **1991**, 883.

³² Müller, J.; Freisinger, E.; Sanz Miguel, P.J.; Lippert, B. *Inorg. Chem.* **2003**, 42, 5117.

³³ Moodley, K. G.; Nicole, M. J. *J. Chem. Soc., Dalton Trans.* **1977**, 239.

produce the new Pt(II) and Pt(IV) species.³⁴ This disproportionation reaction has been invoked in related oxidation reactions of platinum species with N-donor ligands, such as those reported by Sanford³⁵ or Chen.³⁶ Further evidence of the presence of transient Pt(III) species was presented by Labinger, Bercaw and Goldberg³⁷ who described the observation of blue coloration in the oxidation of Pt complexes with O₂, indicative of the presence of mixed-valence paramagnetic platinum species, often called platinum blues.³⁸ However, whether oxidation reactions always proceed via Pt(III) is unclear and in fact Bercaw and Labinger reported that even though the addition of radical scavengers stops the formation of blue colored solutions in their system the rate of oxidation to Pt(IV) is not affected.³⁹

In the following chapter we will describe previous work from our group with Pt(II) electron deficient complexes bearing bulky NHC ligands and will expand it to species containing smaller NHC ligands with the objective of studying their reactivity with halogens.

³⁴ Johansson, L.; Ryan, O.B.; Rømming, C.; Tilset, M. *Organometallics* **1998**, *17*, 3957.

³⁵ Lanci, M.P.; Remy, M.S.; Lao, D.B.; Sanford, M.S.; Mayer, J.M. *Organometallics* **2011**, *30*, 3704.

³⁶ Moret, M.-E.; Chen, P. *J. Am. Chem. Soc.* **2009**, *131*, 5675.

³⁷ Rostovtsev, V.V.; Labinger, J.A.; Bercaw, J.E.; Lasseter, T.M.; Goldberg, K.I. *Organometallics* **1998**, *17*, 4530.

³⁸ Lippert, B. *Chimia*, **2007**, *61*, 732

³⁹ Rostovtsev, V.V.; Henling, M.L.; Labinger, J.A.; Bercaw, J. E. *Inorg. Chem.* **2002**, *41*, 3608.

CHAPTER 1. RESULTS AND DISCUSSION

Reactivity of electron deficient biscarbene platinum (II) complexes with halogens

1.1. Preparation of new T-shaped platinum biscarbene complexes

The synthesis of electron deficient platinum (II) species bearing bulky N-heterocyclic (NHC) carbenes has previously been reported by our group.¹ The reactivity of these complexes towards C–H bond activation of arenes,² halogens and hydrogen has been studied so far. Taking into consideration that this reactivity is highly dependent on the nature of the NHCs, we considered the preparation of related species with less bulky carbenes and to extend the study of the reactivity of this family of compounds to amine boranes for comparative purposes.

Figure 1 shows some of the previously prepared species $[\text{Pt}(\text{I}^t\text{Bu}')(\text{I}^t\text{Bu})][\text{B}(\text{Ar}^F)_4]$ (**1**), $[\text{Pt}(\text{CH}_3)(\text{IPr})_2][\text{B}(\text{Ar}^F)_4]$ (**2a**), $[\text{Pt}(\text{IPr}')(\text{IPr})][\text{B}(\text{Ar}^F)_4]$ (**2b**), $[\text{Pt}(\text{CH}_3)(\text{IMes}^*)_2][\text{B}(\text{Ar}^F)_4]$ (**3a**) and $[\text{Pt}(\text{IMes}^*)(\text{IMes}^*)][\text{B}(\text{Ar}^F)_4]$ (**3b**), that were used in this work ($\text{I}^t\text{Bu}' = 1,3\text{-bis-}tert\text{-butylimidazol-2-ylidene}$, $\text{IMes}^* = 4,5\text{-dimethyl-1,3-bis(2,4,6-trimethylphenyl)-imidazol-2-ylidene}$, $\text{IPr} = 1,3\text{-bis-(2,6-diisopropylphenyl)-imidazol-2-ylidene}$, NHC' and NHC denotes a cyclometalated and a non cyclometalated carbene, respectively).

¹ Rivada-Wheelaghan, O.; Donnadieu, B.; Maya, C.; Conejero, S. *Chem. Eur. J.* **2010**, *16*, 10323.

² Rivada-Wheelaghan, O.; Ortuño, M. A.; Díez, J.; Lledós, A.; Conejero, S. *Angew. Chem. Int. Ed.* **2012**, *51*, 3936.

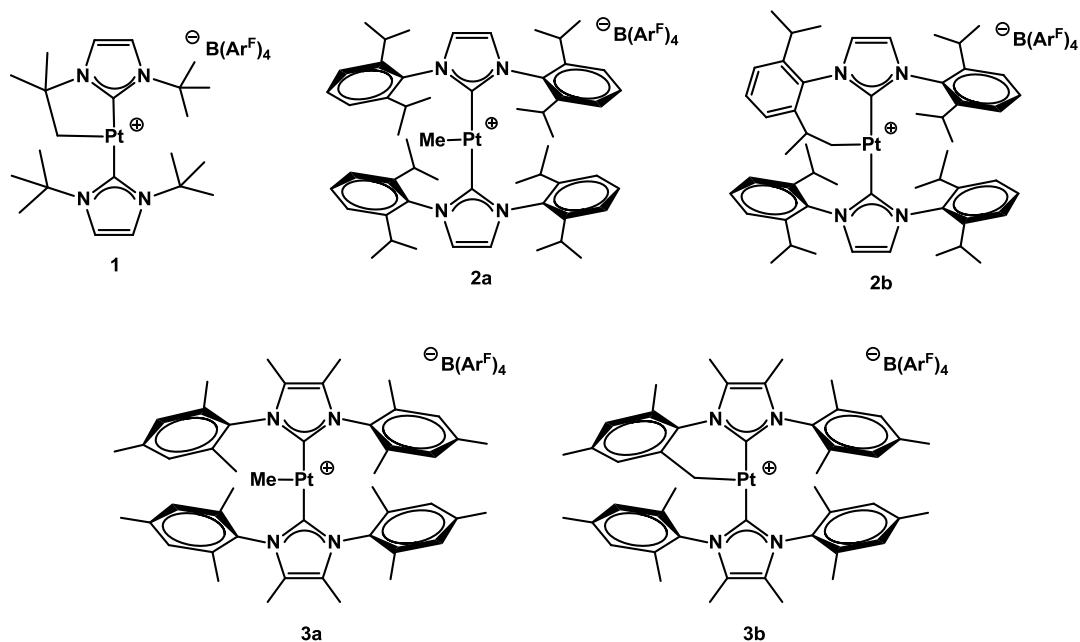


Figure 1. Some electron deficient platinum biscarbene complexes previously described by our group.

We set upon the preparation of analogous species containing the less bulky carbenes $i\text{Pr}_2$ (1,3-bis-isopropylimidazol-2-ylidene) and $i\text{Pr}_2\text{Me}_2$ (4,5-dimethyl-1,3-bis-isopropylimidazol-2-ylidene) (Figure 2) that can be easily prepared by the methods reported in the literature.³ The buried volume percentage for these isopropyl substituted carbenes (e.g. $\%V_{\text{bur}} = 27.9$ for $i\text{Pr}_2\text{Me}_2$) is markedly smaller than for the previously employed carbenes [$\%V_{\text{bur}} = 34.2$ (IMes), 35.8 (IPr), 37.0 ($i^t\text{Bu}$)].⁴

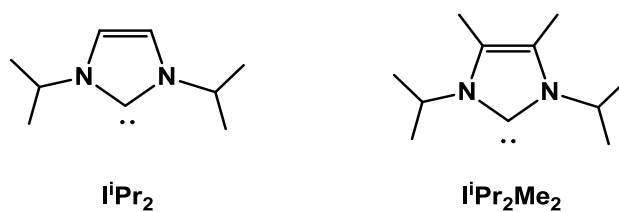
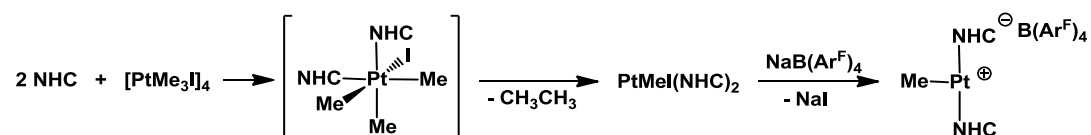


Figure 2. Less bulky NHC ligands used in this work

³ For $i\text{Pr}_2$: Schaub, T.; Radius, U. *Chem. Eur. J.* **2005**, *11*, 5024. For $i\text{Pr}_2\text{Me}_2$: Kuhn, N.; Kratz, T. *Synthesis*, **1993**, *6*, 561.

The previously described electron deficient platinum species **1**, **2a** and **3a** were synthesized in high yields by halide abstraction with $\text{NaB}(\text{Ar}^{\text{F}})_4$ from the corresponding neutral $\text{PtMe}(\text{NHC})_2$ complexes. It was found the most straightforward and clean synthesis of the latter compounds is by reacting, in THF at room temperature, two equivalents of the free carbene with the Pt(IV) precursor $[\text{PtMe}_3\text{I}]_4$ that is readily prone to undergo reductive elimination reactions of ethane (Scheme 1).



Scheme 1. General synthetic procedure for complexes **1**, **2** and **3**.

The cyclometallated derivatives **2b** and **3b** have been obtained by mild heating of complexes **2a** and **3a** respectively.

However, when the same reaction conditions were used to obtain $\text{PtMe}(\text{I}^i\text{Pr}_2\text{Me}_2)_2$ from $[\text{PtMe}_3\text{I}]_4$ and $\text{I}^i\text{Pr}_2\text{Me}_2$, a complex mixture of species in varying proportions was always obtained depending on the reaction time, temperature, concentration or whether an excess of carbene was used. Unlike the reaction with bulkier carbenes, in this case *cis*- $\text{PtMe}_2(\text{I}^i\text{Pr}_2\text{Me}_2)_2$ (**4**), a species previously reported by Nolan,⁴ was the main product.

⁴ Fortman, G.C.; Scott, N.M.; Linden, A.; Stevens, E. D.; Dorta, R.; Nolan, S.P. *Chem. Commun.* **2010**, 46, 1050.

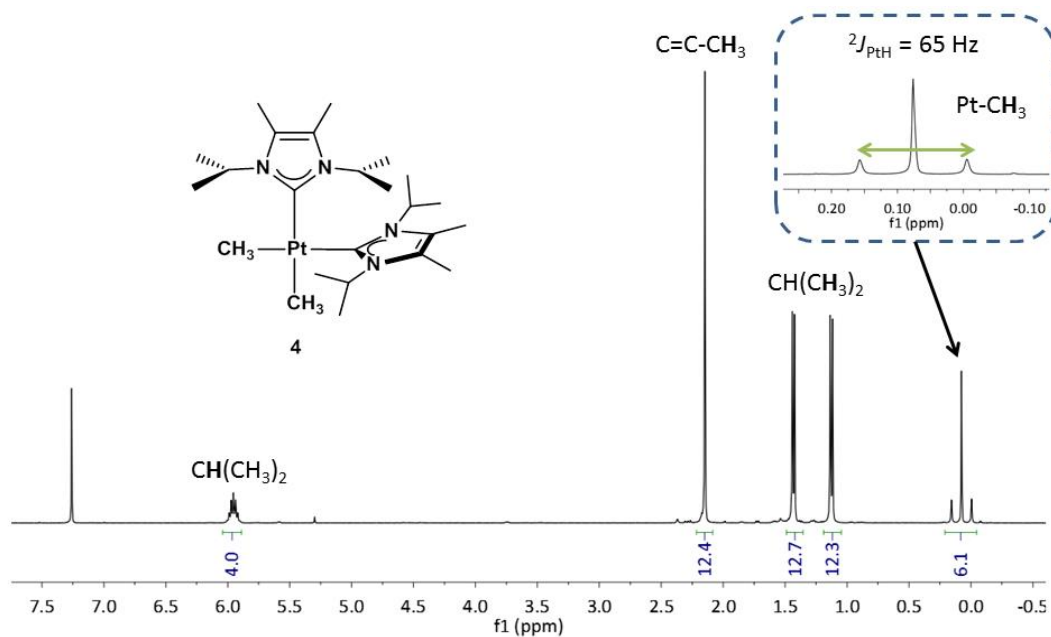
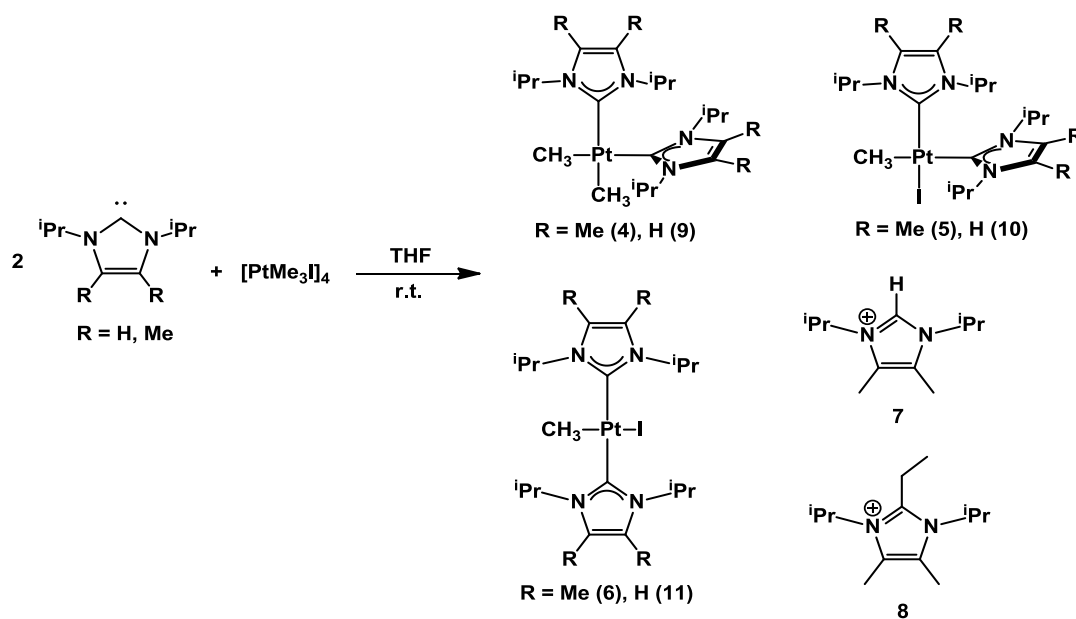


Figure 3. ^1H NMR in CDCl_3 of $\text{PtMe}_2(\text{I}'\text{Pr}_2\text{Me}_2)_2$ (**4**)

The *cis* isomer should be the most stable for this dimethyl species and this disposition of the carbene ligands was confirmed by the X-ray structure reported by Nolan.

In addition, both *cis*- and *trans*- $\text{PtMe}(\text{I}'\text{Pr}_2\text{Me}_2)_2$ (**5** and **6**) were formed as minor species along with two organic species identified as the protonated carbene, 1,3-bis-isopropylimidazolium iodide (**7**), and 1,3-bis-isopropyl-2-ethyl-imidazolium iodide (**8**) (Scheme 2).



Scheme 2. Products obtained in the reaction of iPr_2Me_2 and iPr_2 with platinum tetramer $[PtMe_3I]_4$

It was observed that cis -PtMeI(iPr_2Me_2)₂ was initially formed and isomerized over time to its $trans$ isomer **6**. The structure of this complex was elucidated by x-ray diffraction studies and is shown in Figure 4.

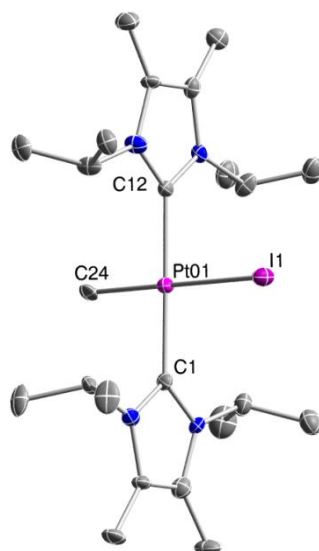


Figure 4. X-ray structure of complex **6**. Selected bond distances (Å) and angles (°): Pt01–C12, 2.016(7); Pt01–I1, 2.693(2); Pt01–C24 2.016(7). C1–Pt01–C12, 179.4(3); C24–Pt01–I1, 179.0(5).

In this molecule the imidazolylidene rings lie perpendicular to the metal coordination plane. The Pt–C_{carbene} bond distances have a value of 2.016(7) Å, which is slightly shorter than that reported for PtMeI(*t*Bu)₂ (2.06 Å). Even though a shorter Pt–C_{carbene} distance would be expected for a slightly more basic carbene, in this case the larger steric hindrance of the *tert*-butyl groups compared to the isopropyl groups may have a larger influence in lengthening the Pt–C_{carbene} distance. Another interesting feature of this structure is the fact that the CH groups of the isopropyl substituents are actually quite close to the platinum center, as the methyl groups of the isopropyl units point away from the metal center. The Pt–H distance has value of 2.697(1) Å, whereas the Pt–C distance is 3.362(8) Å, with a Pt–H–C angle of 125.5(5)°. This suggests the existence of anagostic interactions.⁵ This is a type of 3-center-4-electron interaction, mainly electrostatic, in which the metal acts as a hydrogen bond acceptor and is typical of square planar d⁸ metal complexes.

Figure 5 and Figure 6 depict the ¹H NMR spectra of *cis*- and *trans*-PtMeI(*i*Pr₂Me₂)₂ respectively. The *cis* isomer presents three different signals for the methyl groups

⁵ Brookhart, M.; Green, M. L. H.; Parkin, G. *Proc. Natl. Acad. Sci. U. S. A.* **2007**, *104*, 6908.

of the isopropyl substituents, accounting for the less symmetric disposition of the carbene ligands and the presence of two different additional substituents. Only two signals are observed for the *trans* isomer due to higher symmetry. Moreover, the $^2J_{\text{PtH}}$ constant for the platinum bound methyl group is 57 Hz for the *cis* isomer and 95 Hz for the *trans* species, reflecting the different *trans* influence of the carbene and the iodide ligands, respectively.

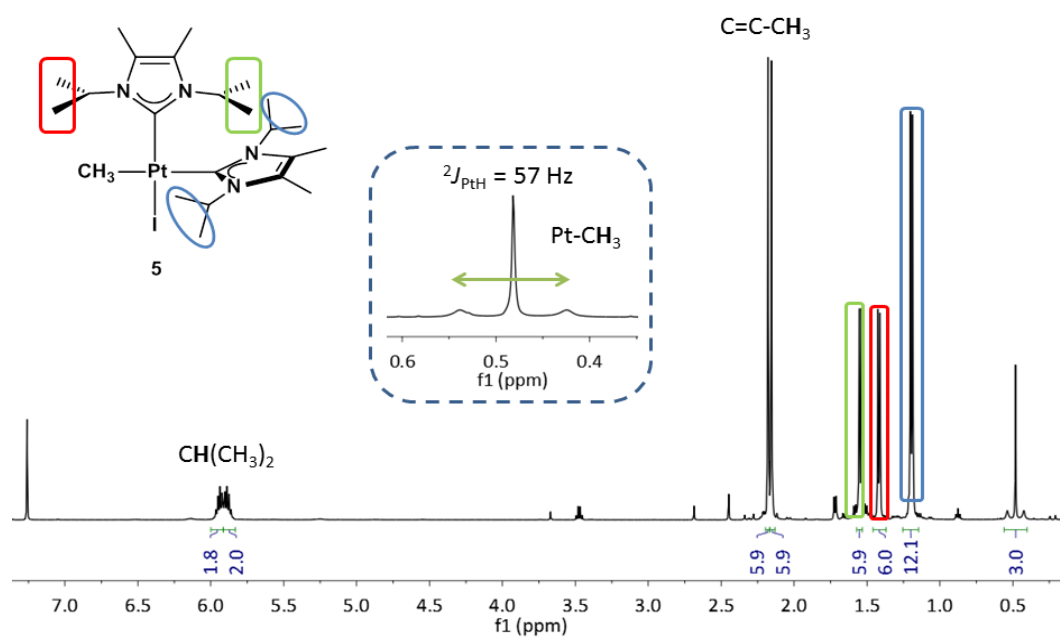


Figure 5. ¹H NMR in CDCl₃ of *cis*-PtMeI(iPr₂Me₂)₂ (5).

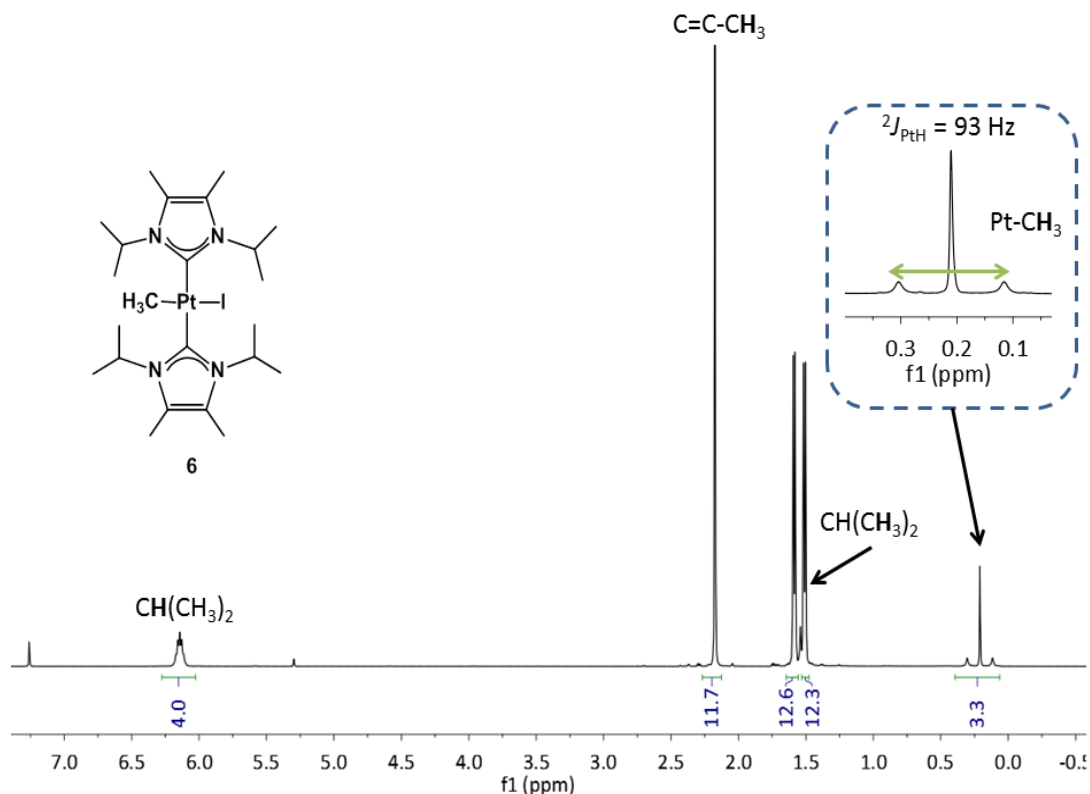
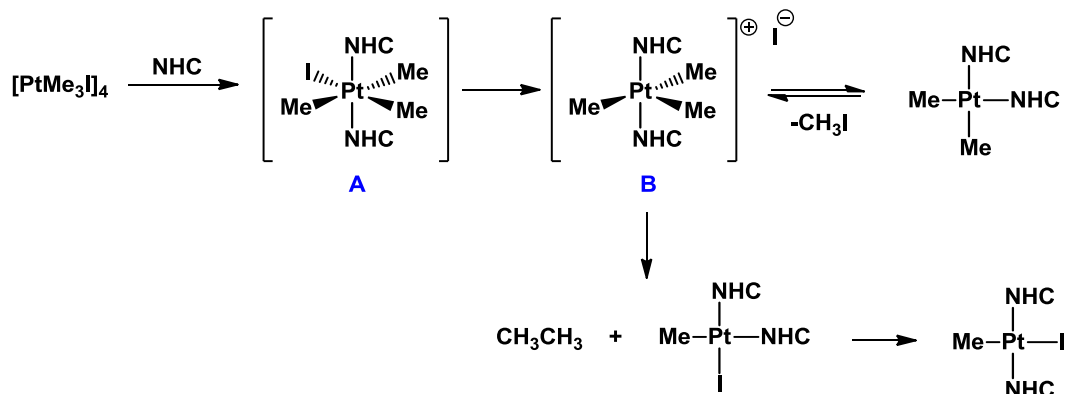


Figure 6. ^1H NMR in CDCl_3 of $\text{trans-PtMeI}(\text{I}^i\text{Pr}_2\text{Me}_2)_2$ (**6**).

As proposed for the formation of the $\text{PtMeI}(\text{NHC})_2$ species **1-3** with bulkier carbenes, the reaction between carbenes $\text{I}^i\text{Pr}_2\text{Me}_2$ or I^iPr_2 , and complex $[\text{PtMe}_3\text{I}]_4$ might proceed via an undetected Pt(IV) species that can undergo either ethane or methyl iodide reductive elimination to yield $\text{PtMeI}(\text{NCH})_2$ or $\text{PtMe}_2(\text{NCH})_2$ respectively, as seen in Scheme 3. This process was studied in depth for phosphine ligands by Goldberg et al., concluding that reductive elimination of methyl iodide is kinetically preferred, albeit the product formed by ethane elimination is thermodynamically favoured.⁶ Even though the Pt(IV) intermediates could be observed for phosphine ligands and have also been isolated for related reactions with smaller carbenes, such as 1-methyl-oxazol-2-ylidenes, reductive elimination was favoured even for slightly larger carbenes such as 1,3-dimethyl-imidazol-2-ylidenes.⁷

⁶ Goldberg, K. I.; Yan, J.Y.; Breitung, E. M. *J. Am. Chem. Soc.* **1995**, *117*, 6889.

⁷ Lindner, R.; Wagner, C.; Steinborn, D. *J. Am. Chem. Soc.* **2009**, *131*, 8861.



Scheme 3. Proposed mechanism for the formation of $\text{PtMeI}(\text{NHC})_2$ and $\text{PtMe}_2(\text{NHC})_2$ species.

That dimethyl species analogous to **4** are not observed for IMes^* or IPr carbenes might indicate that the reaction of iodomethane with the dimethyl derivatives is fast, so that these species are not detected even at short reaction times. The fact that reductive elimination of iodomethane is reversible, whereas reductive elimination of ethane is not would lead to the dimethylplatinum derivatives being eventually consumed, even in the case of the isopropyl substituted carbenes. Therefore there must be a side reaction in which iodomethane is depleted, which might also be related to the formation of the observed organic products. It seems conceivable to think that iodomethane is reacting with the highly nucleophilic $i\text{Pr}_2\text{Me}_2$ ligand. In fact, it was found that when the free carbene $i\text{Pr}_2\text{Me}_2$ is reacted with an excess of methyl iodide, a 1:1 mixture of **7** and **8** is produced (Figure 7).

Therefore, during the reaction of $i\text{Pr}_2\text{Me}_2$ with $[\text{PtMe}_3\text{I}]_4$, the liberated methyl iodide reacts in the same manner generating derivatives **7** and **8** and at the same time consuming part of the CH_3I . The lack of this reagent in the reaction medium makes it possible to observe the dimethyl $\text{Pt}(\text{II})$ species $[\text{PtMe}_2(\text{NHC})_2]$, **4**.

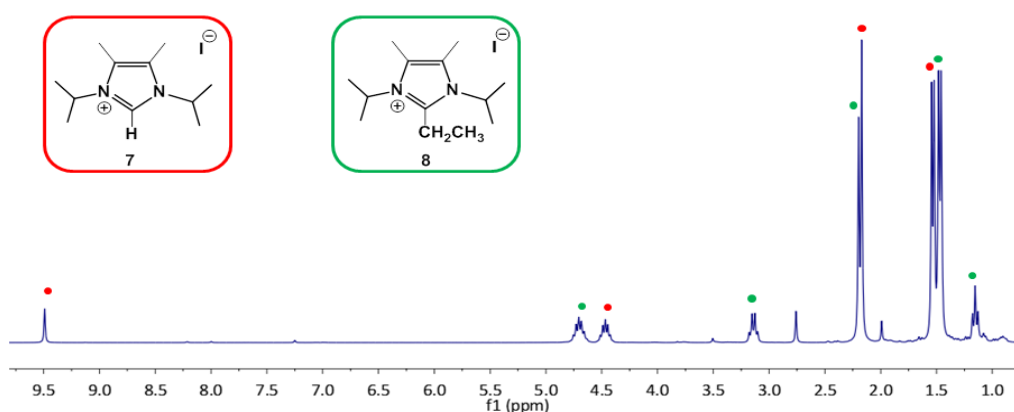
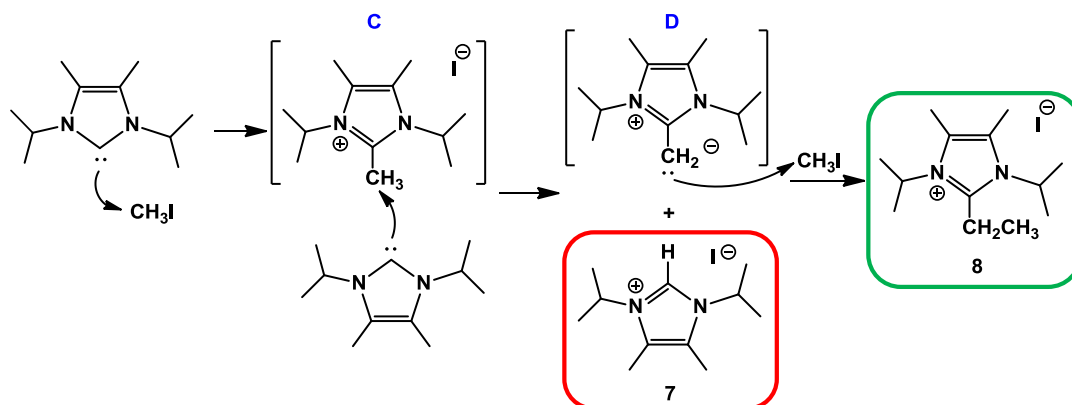


Figure 7. ^1H NMR in CDCl_3 of the reaction of $\text{I}^i\text{Pr}_2\text{Me}_2$ with an excess of MeI.

To explain the formation of the cationic species **7** and **8** we propose a mechanism as depicted in

Scheme 4. First, MeI undergoes a nucleophilic substitution by the free $\text{I}^i\text{Pr}_2\text{Me}_2$ to yield 1,3-bis-isopropyl-2-methyl-imidazolium iodide (**C**) which is not detected. Then, the methyl group at C1 is acidic enough to be deprotonated by another $\text{I}^i\text{Pr}_2\text{Me}_2$ unit,⁸ yielding the imidazolium salt **7** and the ylidic intermediate **D**, which can act as a nucleophile reacting with a second molecule of MeI to produce the ethyl derivative **8**.

⁸ 2-methyl imidazolium cations are known to be deprotonated by bases. See: (a) Hollóczki, O.; Nyulászai, L. *Org. Biomol. Chem.* **2011**, *9*, 2634; (b) Fürstner, A.; Alcarazo, M.; Goddard, R.; Lehmann, C. *Angew. Chem. Int. Ed.* **2010**, *47*, 3210.

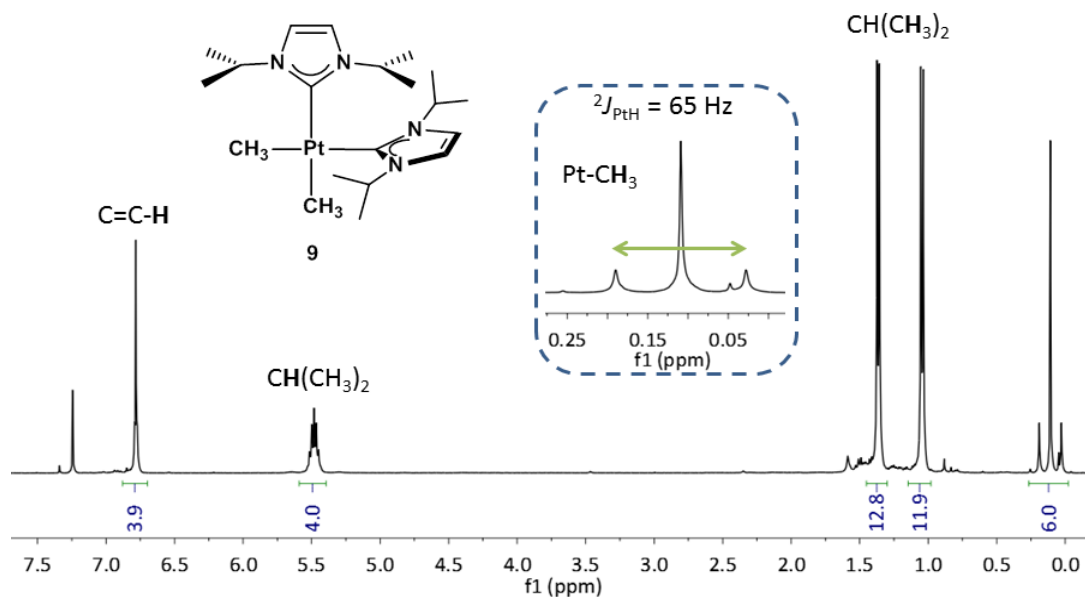


Scheme 4. Proposed mechanism for the formation of **7** and **8**.

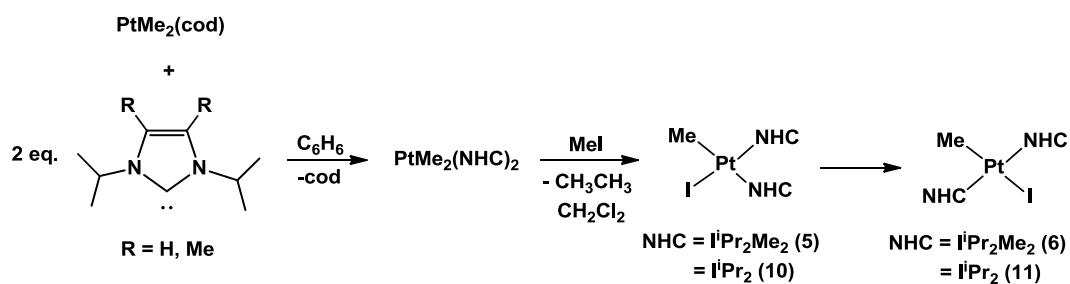
It is not completely understood why carbenes such as IPr, $I^t\text{Bu}$ and IMes* do not exhibit a similar reactivity, but it seems reasonable to think that the bulkier nature of these carbenes compared to $I^i\text{Pr}_2\text{Me}_2$ makes them be less reactive towards MeI by an S_N2 type process.

It was therefore concluded that $[\text{PtMe}_3\text{I}]_4$ was not a suitable precursor for the $\text{PtMe}(\text{NHC})_2$ species we were seeking to obtain and an alternative route was devised.

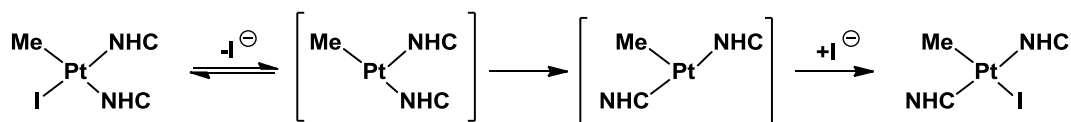
Having in mind, as shown in the previous pages, that complex $\text{trans-}[\text{PtMe}(\text{I}^i\text{Pr}_2\text{Me}_2)_2]$ is formed by reaction of $\text{cis-}[\text{PrMe}_2(\text{I}^i\text{Pr}_2\text{Me}_2)_2]$ with MeI we set out to synthesise complex $\text{cis-}[\text{PrMe}_2(\text{I}^i\text{Pr}_2\text{Me}_2)_2]$ following the procedure previously reported by Nolan, and to apply it for the preparation of the analogous derivative $\text{cis-}[\text{PrMe}_2(\text{I}^i\text{Pr}_2)]$.

Figure 8. ^1H NMR in CDCl_3 of $\text{PtMe}_2(\text{iPr}_2)_2$ (9).

The reaction of two equivalents of either iPr_2Me_2 or iPr_2 with $\text{PtMe}_2(\text{cod})$ ($\text{cod} = 1,5\text{-cyclooctadiene}$) in benzene resulted in the clean formation of the previously reported $\text{PtMe}_2(\text{iPr}_2\text{Me}_2)_2$ (4) and the new $\text{PtMe}_2(\text{iPr}_2)_2$ (9), respectively. The ^1H and $^{13}\text{C}\{^1\text{H}\}$ NMR data of the latter are very similar to those of derivative 4 and deserve no further discussion. Addition of an excess of methyl iodide to dichloromethane solutions of these species resulted in the immediate formation of the $\text{PtMeI}(\text{NHC})_2$ species in the form of the *cis* isomers, with concomitant elimination of ethane. Further stirring at room temperature led to the isomerisation to the desired *trans* complexes. This synthetic procedure is summarized in Scheme 5.

Scheme 5. Alternative synthesis for $\text{PtMeI}(\text{NCH})_2$ species.

The isomerisation process for complex **5** bearing $i\text{Pr}_2\text{Me}_2$ carbenes was found to be rather slow, being complete in over 12 hours at room temperature, and it was even slower for the species with $i\text{Pr}_2$ ligands which took 2 days to completely isomerize. This difference in isomerization rate is related to the difference in electron σ -donor properties of the carbene ligands.⁹ The isomerization process occurs via an initial halide dissociation to yield a 14 electron T-shaped species where the ligand distribution is rearranged,¹⁰ as depicted in Scheme 6.



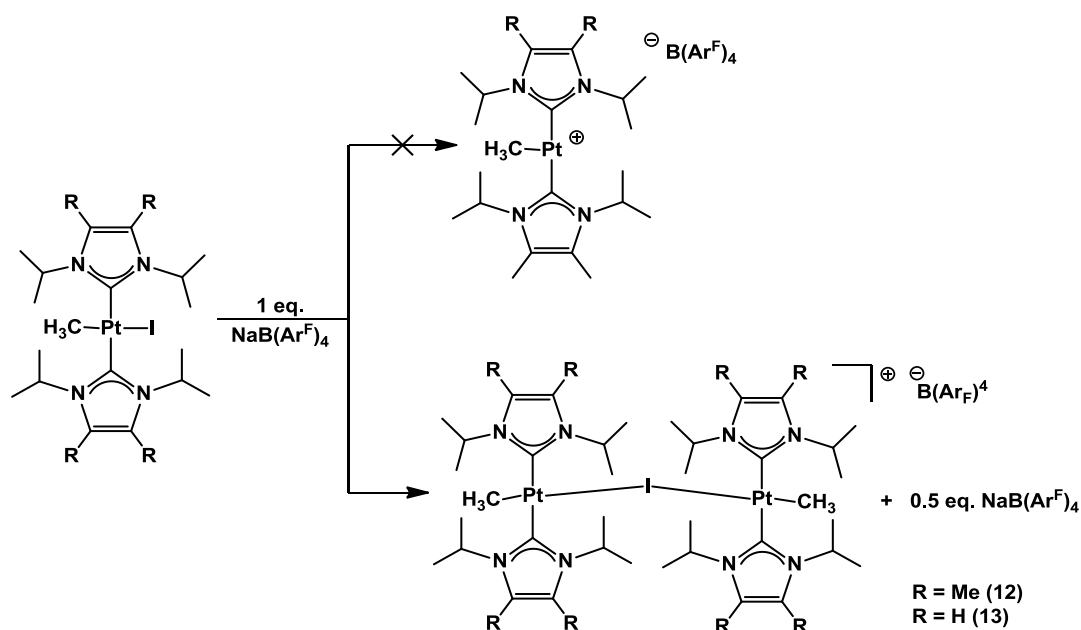
Scheme 6. Proposed mechanism for the *cis/trans* isomerization of $\text{PtMeI}(\text{NHC})_2$ species.

The $i\text{Pr}_2\text{Me}_2$ ligand, with two methyl groups in the imidazol backbone, is a better σ donor than $i\text{Pr}_2$ and therefore provides a better stabilization for the 14 electron species. It also exerts a greater *trans* influence, facilitating iodide dissociation. The combination of these two effects makes the isomerization process faster for $i\text{Pr}_2\text{Me}_2$ containing species compared to $i\text{Pr}_2$.

Once we had obtained the *trans*- $\text{PtMeI}(\text{NHC})_2$ species **6** and **11**, analogous to those used for bulkier carbenes as precursors for 14 electron species, we proceeded to use the same methodology for the compounds bearing smaller carbenes. However, when **6** or **11** were reacted with 1 equivalent of $\text{NaB}(\text{Ar}^{\text{F}})_4$ in anhydrous dichloromethane the expected unsaturated T-shaped species were not formed. Instead, dinuclear platinum derivatives with a bridging iodide ligand were obtained, as indicated in Scheme 7.

⁹ Gusev, D. G. *Organometallics* **2009**, *28*, 6458.

¹⁰ (a) G. Alibrandi, L. Monsù Scolaro, R. Romeo, *Inorg. Chem.* **1991**, *30*, 4007; (b) R. Romeo, G. Alibrandi, *Inorg. Chem.* **1997**, *36*, 4822.



Scheme 7. Reaction of *trans*-PtMeI(NCH)₂ complexes with NaB(Ar^F)₄.

The ¹H NMR spectra of **12** and **13** indicated a highly symmetric environment for the carbene ligands, with only two signals for the methyl groups of the isopropyl substituents. However, the fact that the initially expected unsaturated T-shaped species were not formed was evident by the value of the coupling to ¹⁹⁵Pt of the directly bound methyl groups, which at 98 and 96 Hz indicated that the position *trans* to these groups was occupied.

The structure of these dimeric species was determined by X-ray diffraction studies for complex **12**, as seen in Figure 9.

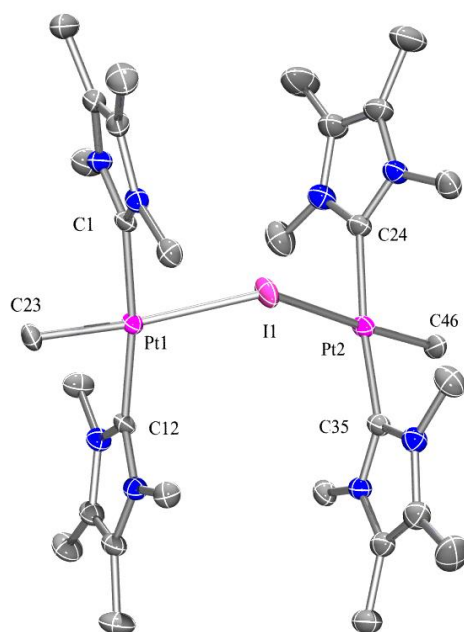
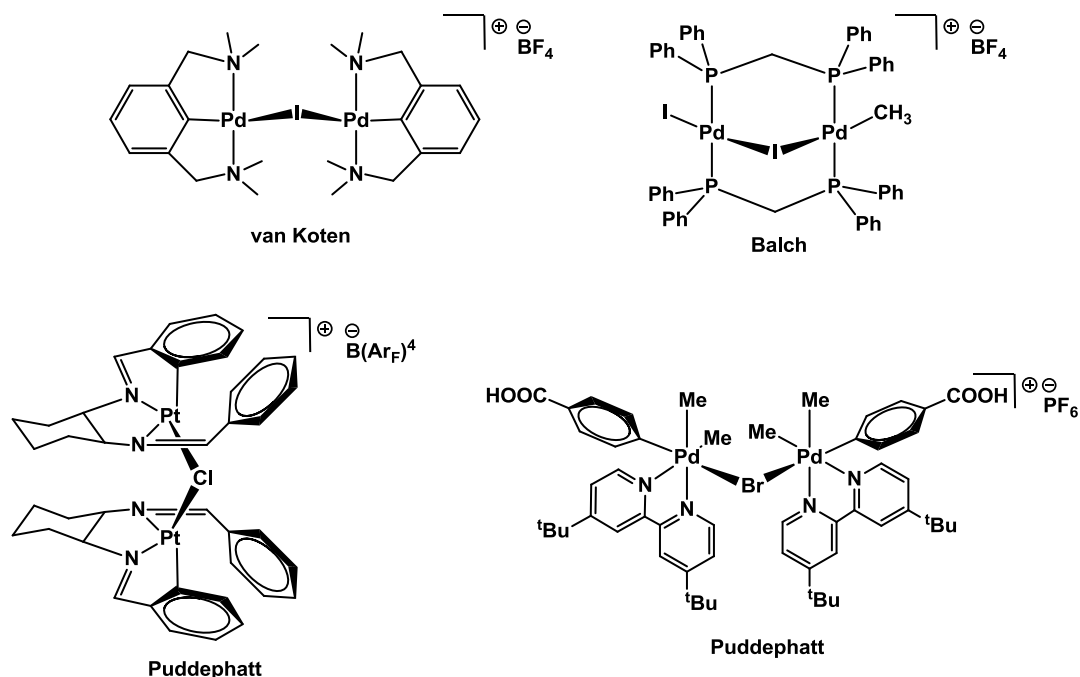


Figure 9. Molecular representation of the cation of complex **12** ($B(Ar^F)_4$ anion and methyls of the *iso*-propyl groups are not shown for clarity). Selected bond distances (\AA) and angles ($^\circ$): Pt1–I1 2.733; Pt1–Pt2 5.148; C1–Pt1 2.0264; C12–Pt1 2.0261; C24–Pt2 2.0367; C35–Pt2 2.0352; C23–Pt1 2.0409; C46–Pt2 2.0949; Pt1–I1–Pt2 140.7

There are not many examples in the literature of metal dimers with a single halide atom as a bridging group. Some examples are depicted in Scheme 8.



Scheme 8. Some palladium and platinum species containing a single halide bridging group.¹¹

In bimetallic complexes with a single halide atom as a bridge, a 90° angle is expected for the MXM unit, as this optimizes the interactions of the metals with the p orbitals of the halide atom. Steric constraints may force deviations from this value, resulting in complexes with a larger MXM angle. This is the case for complex **12**, that presents a Pt–I–Pt angle of 140.7° and also for the complexes reported by van Koten (134.8°) and Puddephatt (127.9°, bottom right in Scheme 8). On the other hand, MXM angles smaller than 90° are observed in species where there is some degree of MM bonding, as in the examples by Balch (67.0°) and Puddephatt (77.5°, bottom left in Scheme 8). In these latter examples, the MM distance is 2.98 and 2.97 Å respectively, which closely resembles that of species with a clear Pd–Pd bond.^{11b} In contrast, complex **12** presents a Pt–Pt distance of 5.15 Å, which indicates that there is no bonding between the metal atoms.

¹¹ (a) Terheijden, J.; van Koten, G.; Grove, D. M.; Vrieze, K.; Spek, A. L. *J. Chem. Soc., Dalton Trans.* **1987**, 1359; (b) Olmstead, M. M.; Farr, J. P.; Balch, A. L. *Inorg. Chim. Acta* **1981**, *52*, 47; (c) Baar, C.R.; Jenkins, H.A.; Jennings, M.C.; Yap, G.P.A.; Puddephatt, R.J.; *Organometallics* **2000**, *19*, 4870; (d) C.S.A. Fraser, D.J. Eisler, R.J. Puddephatt, *Polyhedron* **2006**, *25*, 2660.

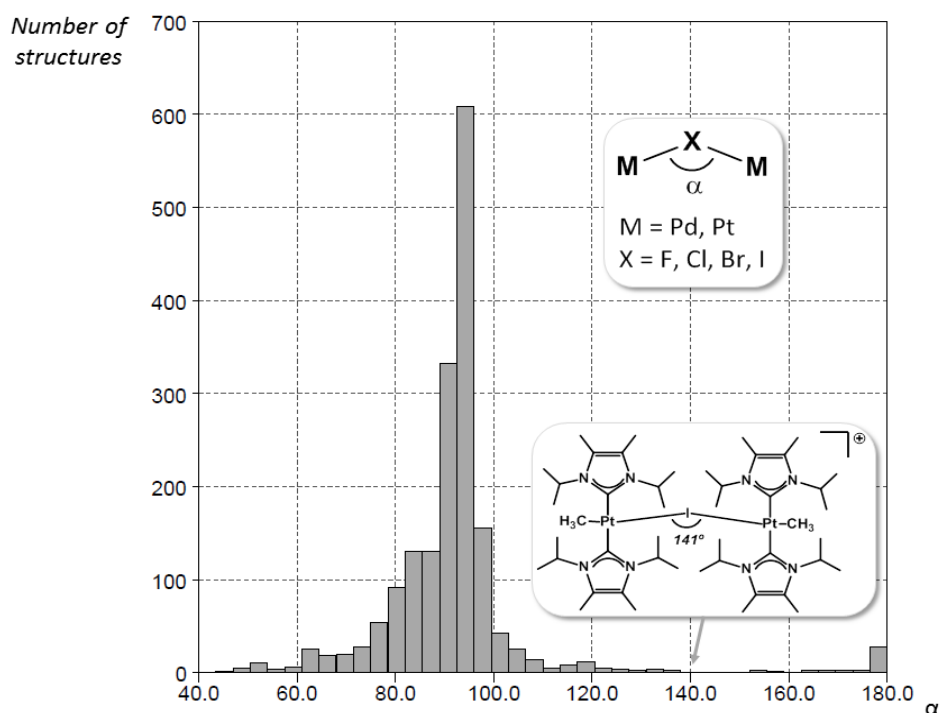
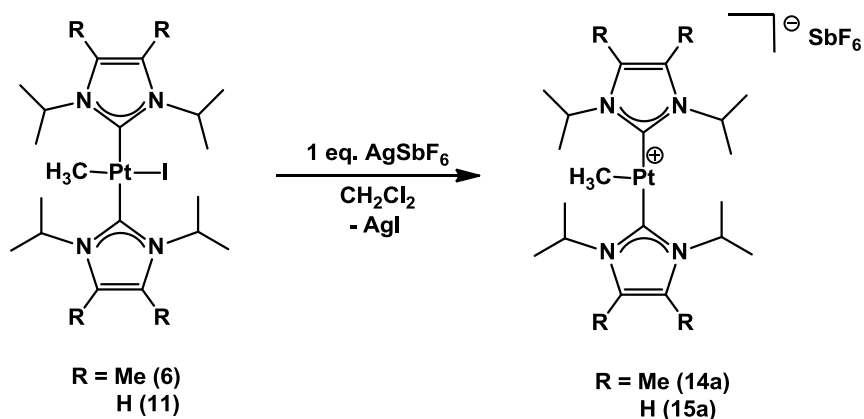


Figure 10. Histogram representing the number of reported crystal structures of complexes containing a Pt–X–Pt unit against the angle between said atoms.

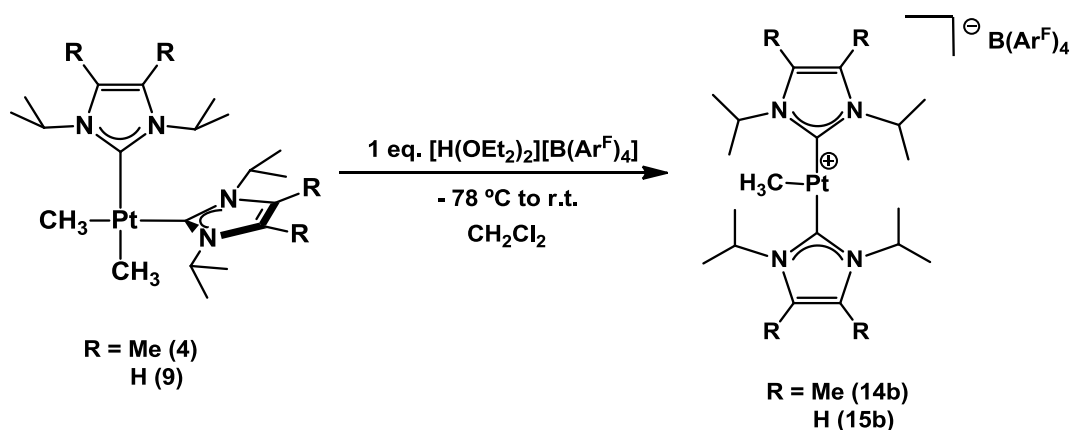
In general though, for polynuclear platinum species containing any number of bridging halide atoms, the great majority of reported structures present a Pt–X–Pt angle of 90° , as can be seen in Figure 10.

To obtain the desired monomeric T-shaped complexes from the *trans*-PtMeI(NCH)₂ species **6** and **11** the use of a silver salt was required to completely removed the coordinate iodide ligand. When one equivalent of AgSbF₆ was added to solutions of **6** and **11** in dry dichloromethane the desired species **14a** and **15a** were obtained, as depicted in Scheme 9. The initial pale yellow solution turned to bright yellow upon silver addition, along with the precipitation of AgI, as is characteristic for the formation of these coordinatively unsaturated species.¹



Scheme 9. Preparation of T-shaped species with smaller NHCs from PtMeI(NCH)₂ precursors and a silver salt.

An alternative synthetic method was devised to obtain the related species with a B(Ar^F)₄ anion using PtMe₂(NHC)₂ complexes **4** and **9** as precursors. These species reacted with the acid [H(OEt₂)₂][B(Ar^F)₄] in dichloromethane at low temperature with loss of CH₄ to yield the T-shaped complexes **14b** and **15b** (Scheme 10).



Scheme 10. Preparation of T-shaped species with smaller NHCs from PtMe₂(NHC)₂ precursors and Brookhart's acid.

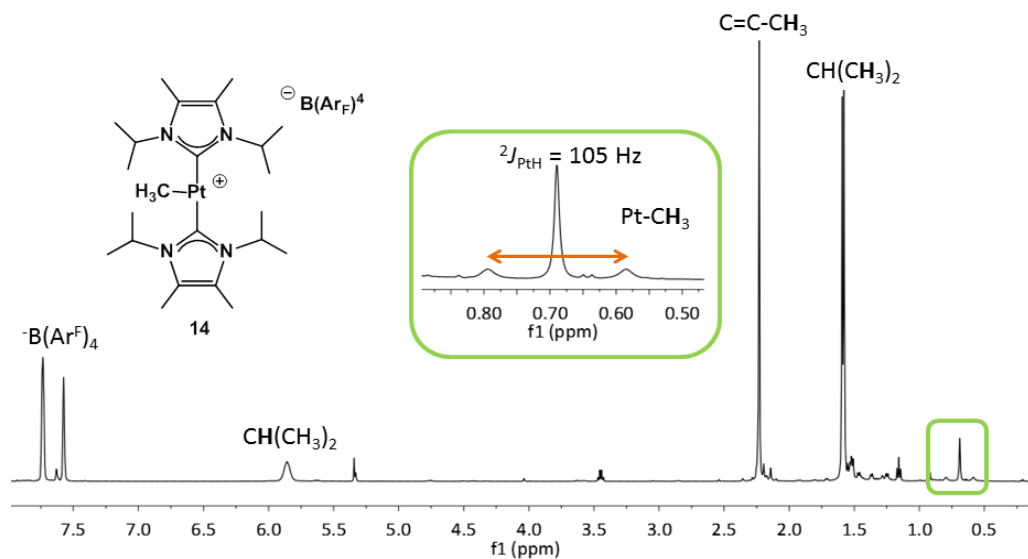
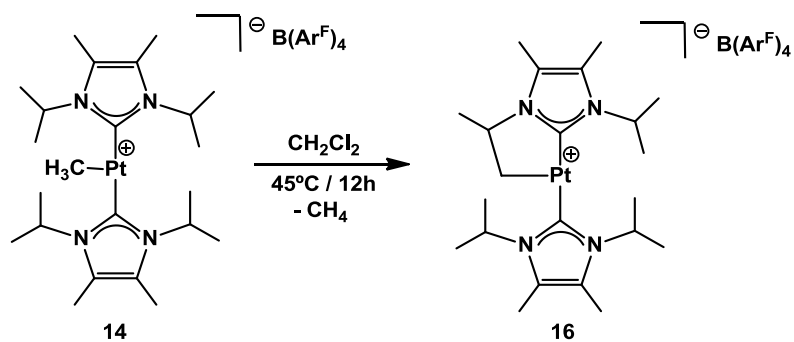
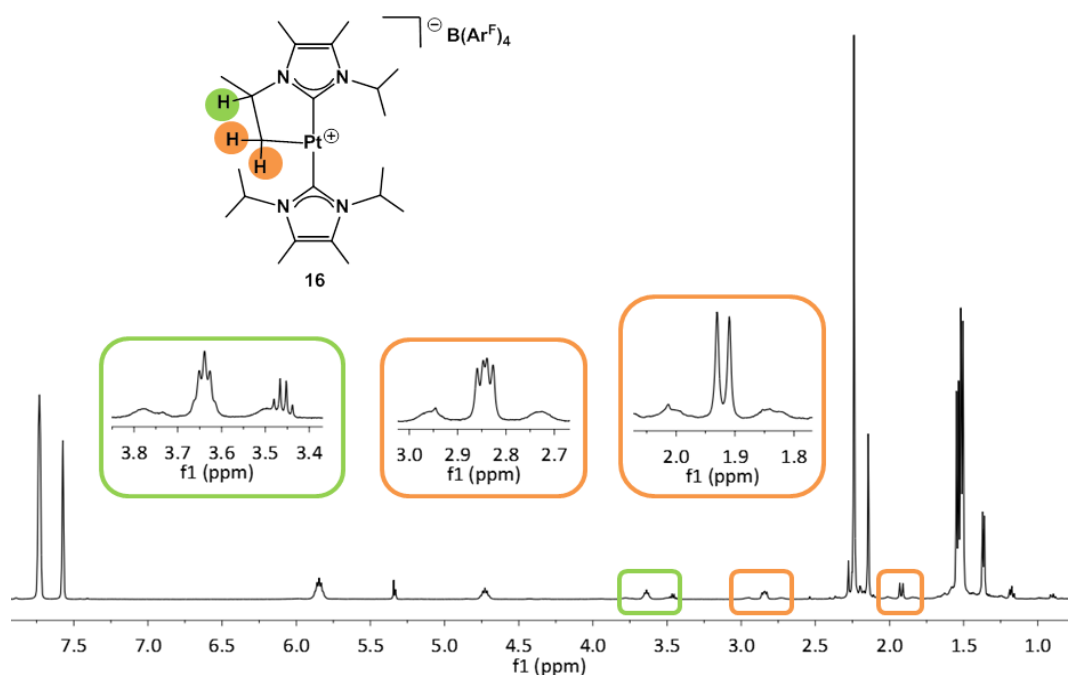


Figure 11. ^1H NMR in CD_2Cl_2 of complex **14b**.

The main feature of the ^1H NMR spectra of species **14** and **15** is the increase of the $^2J_{\text{PtH}}$ coupling constant of the $\text{Pt}-\text{CH}_3$ group from 65 Hz in **4** and **9** to 105 and 103 Hz respectively in the new unsaturated species. This indicates the absence of a coordinated ligand *trans* to this $\text{Pt}-\text{CH}_3$ group, even though the solvent may be interacting in solution. Moreover, the species with SbF_6^- and $\text{B}(\text{Ar}^{\text{F}})_4^-$ anions showed, in addition to identical ^1H and ^{13}C NMR chemical shifts, exactly the same value of coupling constant, indicating that these groups do not interact with the metal center. Unfortunately, all attempts to obtain crystals suitable for an X-ray diffraction study to ascertain whether and solvent molecule or an agostic interaction is occupying the vacant site met with failure.

Complex **14** undergoes cyclometallation of one of the isopropyl arms with loss of CH_4 to produce species **16**. Methane is indeed detected as a singlet at 0.21 ppm in the ^1H NMR spectrum when the reaction is carried out in a closed NMR tube in a deuterated solvent. This process occurs quite slowly at room temperature but is complete overnight if dichloromethane solutions of **14** are heated at 45°C (Scheme 11).

Scheme 11. Formation of cyclometallated species **16**.Figure 12. ^1H NMR in CD_2Cl_2 of complex **16**.

The formation of a cyclometallated species is evident in the ^1H NMR spectrum of **16** (Figure 12), as the symmetry of both $i\text{Pr}_2\text{Me}_2$ ligands, which appeared as a single set of signals in the parent complex **14**, is lost. As seen in Figure 12, the CH protons from the isopropyl groups appear as 3 different signals, one at 5.85 ppm integrating two protons for the isopropyl groups of the non-cyclometallated ligand, and two at 4.73 and 3.64 ppm for the now inequivalent CH protons of the

cyclometallated carbene. Moreover, the protons of the cyclometallated arm (marked in color in Figure 12) show coupling to ^{195}Pt . The diastereotopic protons of the Pt-CH₂ exhibit, as expected, two distinct $^2J_{\text{PtH}}$ values of 115 and 88 Hz.

In contrast, it was found that complex **15** does not undergo cyclometallation under the same reaction conditions as complex **14**. In fact, heating **15** in a variety of solvents such as hexafluorobenzene, 1,2-dichloroethane or toluene at higher temperatures resulted in either no reaction or decomposition of the starting material.

It is therefore interesting to compare the lesser tendency towards cyclometallation of species **14** and **15** with respect to the previously reported complex **1**, bearing *tert*-butyl substituted NHCs. This cyclometallated species is immediately observed after reaction of PtMe(I*t*Bu)₂ with NaB(Ar^F)₄, and even at -70 °C no [PtMe(I*t*Bu)₂]⁺ is observed when the reaction is monitored by ¹H NMR. In this case, the nature of the *tert*-butyl substituents means that there is always a CH₃ group in the vicinity of the Pt atom available for cyclometallation. With regard to the isopropyl substituted carbenes both methyl groups point away from the metal center so that a rotation of the isopropyl unit is necessary for cyclometallation to take place, thus being less favoured than for the complex containing I*t*Bu ligands. As for the differences between I*i*Pr₂ and I*i*Pr₂Me₂ containing species, the methyl groups in the imidazol backbone push the isopropyl substituents closer to the metal center (Figure 13) making them more available for cyclometallation. This effect is clearly observed by the angle α defined by the CH group of the *iso*-proyl fragment, the nitrogen atom and the carbon atom of the C=C bond (Figure 13).

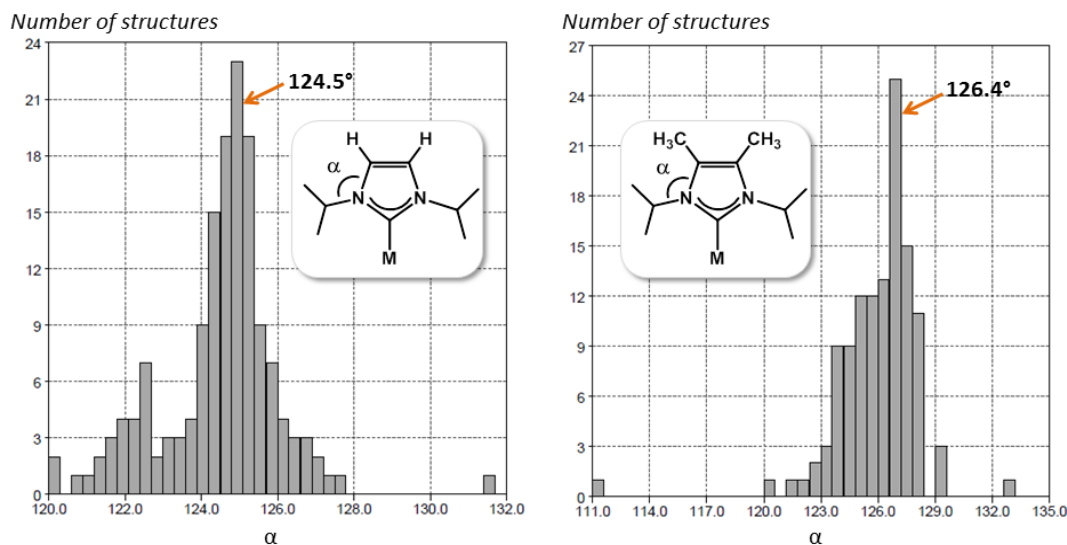
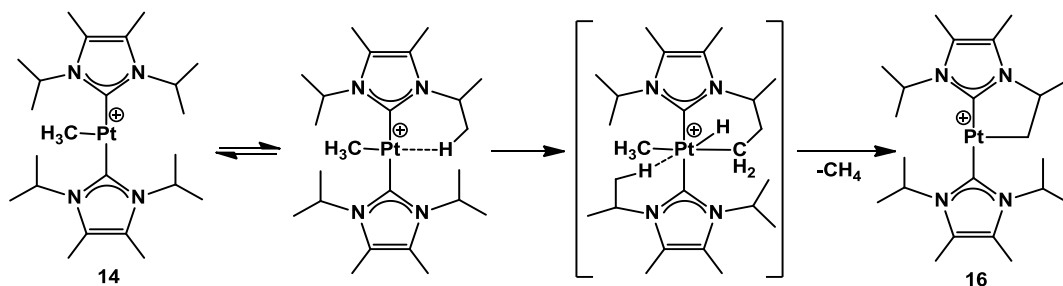


Figure 13. Histograms representing the number of reported X-ray structures of transition metal (M) complexes bearing $1'\text{Pr}_2$ and $1'\text{Pr}_2\text{Me}_2$ ligands. On average, angle α is larger for the latter, bringing the isopropyl groups closer to the metal center.

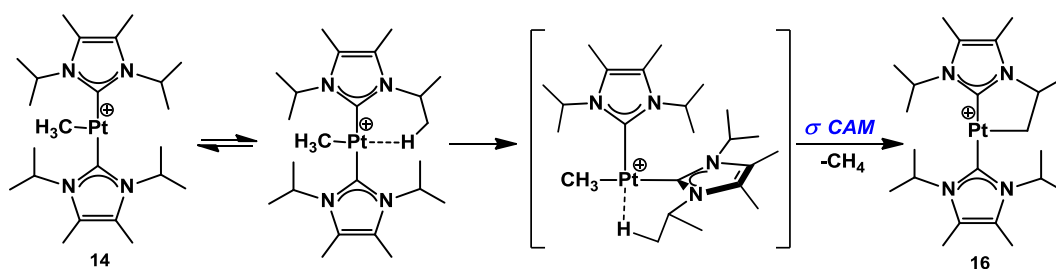
In addition, these methyl substituents also increase the electron donating properties of $1'\text{Pr}_2\text{Me}_2$ with respect to $1'\text{Pr}_2$ and therefore stabilization of a possible Pt(IV) intermediate in the cyclometallation process would be more favorable (Scheme 12). The combination of both these steric and electronic factors results in cyclometallation not being favoured for **15**.



Scheme 12. Proposed oxidative addition mechanism for the cyclometallation of **14**

An alternative mechanism to the oxidative addition route depicted in Scheme 12 for the cyclometallation process would be the route depicted in Scheme 13, in which the T-shaped complex would initially isomerise to the *cis* species, from

which C-H activation can occur through a σ -CAM process to liberate methane and generate the cyclometallated complex **16**. These two mechanisms were calculated for the formation of complex **1**, bearing t Bu substituents and were found to have similar energy barriers.¹² In the case of complex **14**, the smaller size of the carbene ligands would result in lower barriers for the *trans/cis* isomerization, making the route in Scheme 13 more feasible for this system.



Scheme 13. Alternative *cis/trans* isomerisation, followed by σ CAM C-H activation mechanism for the cyclometallation of **14**.

Another difference between t Bu complex **1** and species **16** is the presence of agostic interactions. Whereas **1** presents an agostic interaction between the metal center and the cyclometalated t Bu group, as evidenced by the coupling to ^{195}Pt seen the ^{13}C NMR signal of one of the t Bu groups, no such interaction has been detected for the species with isopropyl groups by NMR spectroscopy at room temperature. This again could be due to the spatial disposition of the t Bu groups that always present a CH_3 unit close to the metal center. At this point, coordination of a solvent molecule (CH_2Cl_2) to complex **16** cannot be completely ruled out and might be responsible for the unobserved agostic interaction (see below). Nevertheless, elemental analysis of pure samples of this complex matches well for a T-shaped, 14-electron species without a coordinated methylene chloride molecule.

To ascertain whether agostic interactions were present at lower temperature, the non-cyclometallated complexes **14** and **15** were analyzed by ^1H NMR, in CD_2Cl_2 as solvent, at different temperatures from 25 to -70 °C. No changes besides a slight

¹² "Síntesis de complejos coordinativamente insaturados de Pt(II) estabilizados por ligandos carbeno N-heterocíclicos. Activación y funcionalización de enlaces C-H". Rivada-Wheelaghan, O.; Tesis Doctoral, 2013.

broadening of the signals were observed for complex **15**. On the other hand, upon cooling dichloromethane solutions of **14** under $-60\text{ }^{\circ}\text{C}$ two species are discernible by ^1H NMR in ca. 1:1 ratio. One of them seems to be the same complex than that observed at room temperature, whereas in the other product the symmetry of the ligands was lost and more than one set of signals appeared, indicating a possible equilibrium between species with and without agostic interactions (Figure 14).

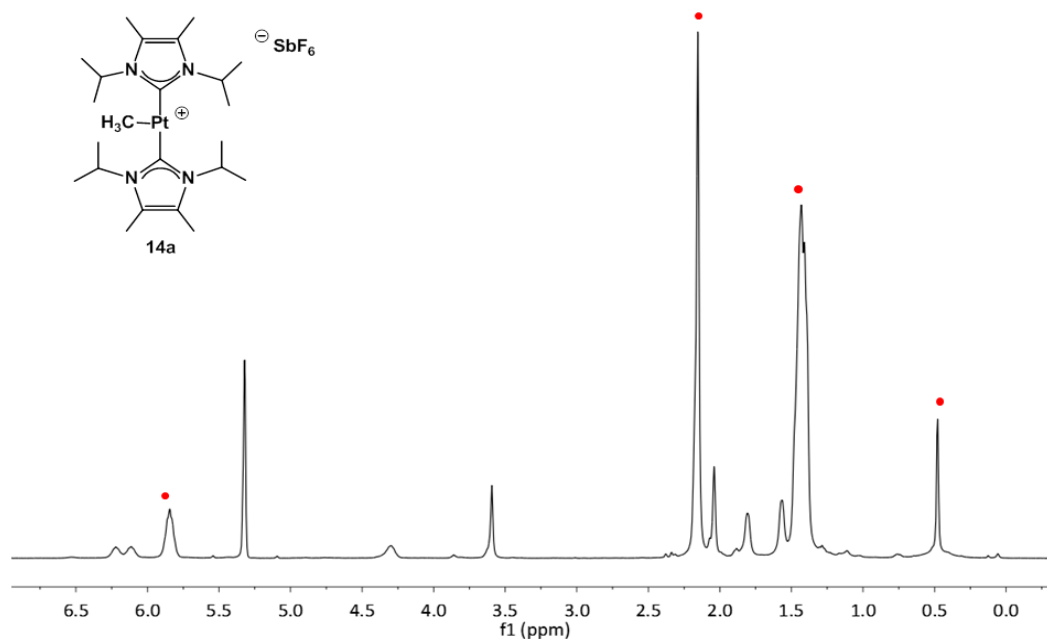


Figure 14. ^1H NMR in CD_2Cl_2 at $-80\text{ }^{\circ}\text{C}$ of complex **14a**. Signals of the symmetric product with no agostic interactions are marked with red dots. Note that some signals (e.g. the $\text{Pt}-\text{CH}_3$) overlap with those of the species with agostic interactions, present in equilibrium.

One of the CH signals of the lower symmetry species experiences a marked upfield chemical shift to 4.3 ppm, which could be indicative of the presence of an agostic interaction between the corresponding isopropyl substituent and the metal center. A similar shift (3.71 ppm) is observed by Whittlesey¹³ for the ruthenium complex $[\text{Ru}(\text{I}^i\text{Pr}_2\text{Me}_2')(\text{I}^i\text{Pr}_2\text{Me}_2)_2\text{Cl}]$ for which the presence of an

¹³ Bramananthan, N.; Mas-Marzá, E.; Fernández, F. E.; Ellul, C. E.; Mahon, M. F.; Whittlesey, M. K. *Eur. J. Inorg. Chem.* **2012**, 2213.

agostic interaction was confirmed by X-ray diffraction studies. However, in this case the corresponding CH₃ group also experiences a marked shift to 0.08 ppm, which we do not observe for **14a**. Therefore, NMR data are not conclusive to ascertain the presence of an agostic interaction in this species.

As stated above, another possibility for explaining the presence of more than one species upon cooling would be solvent coordination (CD₂Cl₂), which would lead to the observation of an equilibrium between species with and without bound dichloromethane. However, such a species would still be quite symmetric, exhibiting only two different kinds of isopropyl groups, which is in contrast to an even larger decrease in symmetry observed for **14a** at low temperature. The fact that no similar behavior is occurring for complex **15**, which owing to its slightly less basic carbene ligands should favor solvent coordination even more than **14**, led us to propose that agostic interactions are appearing at low temperature.

Two different CH groups present the right disposition to participate in agostic interactions (Figure 15). However, considering that the related complex **1** presented an interaction with the methyl groups similar to **B**, which was identified via the ¹⁹⁵Pt coupling that the interacting CH₃ group presented in the ¹³C NMR spectrum (²J_{PtC} = 25 Hz), and the fact that coordinatively unsaturated ruthenium(II) complexes¹⁴ stabilized by ⁱPr₂Me₂ exhibit agostic interactions with the methyl groups and not with the CH units, led us to suggest that a structure such as **B** in Figure 15 is most likely present.

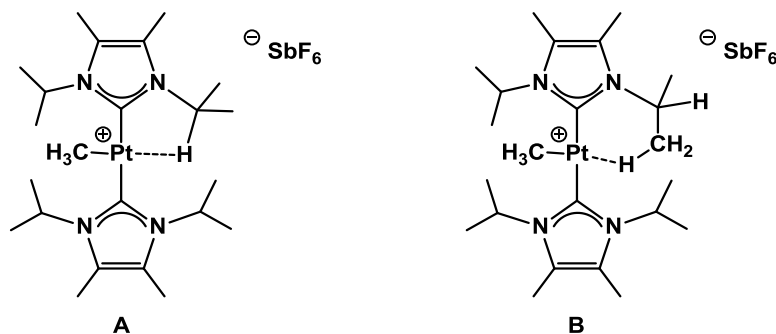


Figure 15. Possible agostic interactions for complex **14**.

¹⁴ Haller, L. J. L.; Page, M. J.; Macgregor, S. A.; Mahon, M. F.; Whittlesey, M. K. *J. Am. Chem. Soc.* **2009**, *131*, 4604.

For complex **14** however, the broadening of the signals, of the range of this coupling to ^{195}Pt did not allow us to extract the related information from the ^{13}C NMR spectrum and no conclusions can be drawn from spectroscopic data.

As a final note, it was found that species **15** and **16** were unstable over time, even when stored under inert atmosphere. For example, complex **16** decomposed to a mixture of unidentified products over the course of a few months in the glove box.

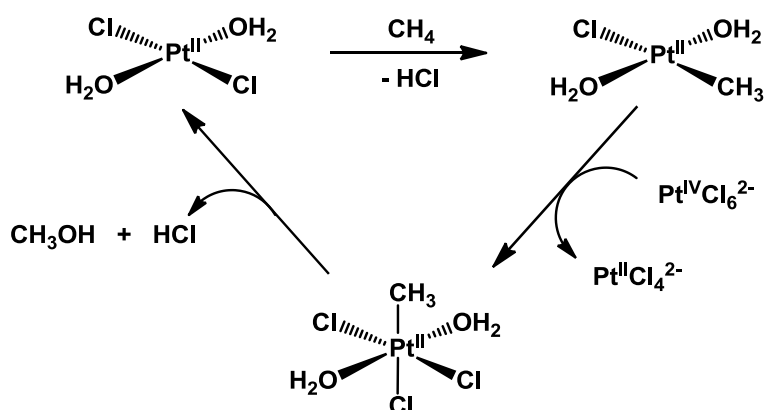
1.2. Reactivity with halogens

This section will describe the reactivity of complexes **15** and **16** with halogens (I_2 and Br_2). The reactivity of bulkier NHC complexes **1**, **2** and **3** has already been described by our group^{12,15} with the initial aim of assessing the effect of NHC ligands in carbon-halogen coupling reactions mediated by platinum and of isolating intermediate species involved in these transformations.

Initial indication that these platinum species could promote fast C–X coupling was found in the formation of a small amount of a iodomethane elimination product in the reaction of I^tBu with platinum tetramer $[\text{PtMe}_3\text{I}]_4$.¹ This behavior was even more evident for the smaller I^iPr_2 and $\text{I}^i\text{Pr}_2\text{Me}_2$ carbenes, as discussed in section 1.1., for which the product resulting from iodomethane elimination was the major species in both cases. For all of these reactions, transient Pt(IV) intermediates were not detected, probably due to the bulk of the NHC ligands favouring reductive elimination in these coordinatively saturated species. However, we envisaged that our cationic 14-electron Pt(II) species could be good candidates to prepare coordinatively unsaturated 16-electron Pt(IV) complexes via oxidative addition reactions and to explore the reactivity and stability of these unusual compounds. Pt(IV) alkyl-halide species of this nature had not been reported before when we started these investigations but they presented great interest

¹⁵ Rivada-Wheelaghan, O.; Ortuño, M.A.; Díez, J.; García-Garrido, S.E.; Maya, C.; Lledós, A.; Conejero, S. *J. Am. Chem. Soc.* **2012**, *134*, 15261.

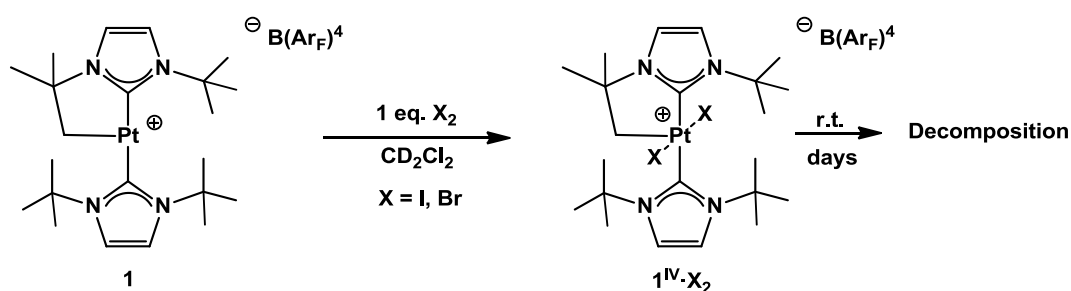
because they had been postulated as key intermediates in the conversion of methane to methanol and chloroform as described by Shilov (Scheme 14).¹⁶



Scheme 14. Shilov system

1.2.1. Summary of the reactivity of Pt(II) 14-electron species with halogens previously reported by our group. Formation of Pt(IV) species and their reductive C–X coupling products.

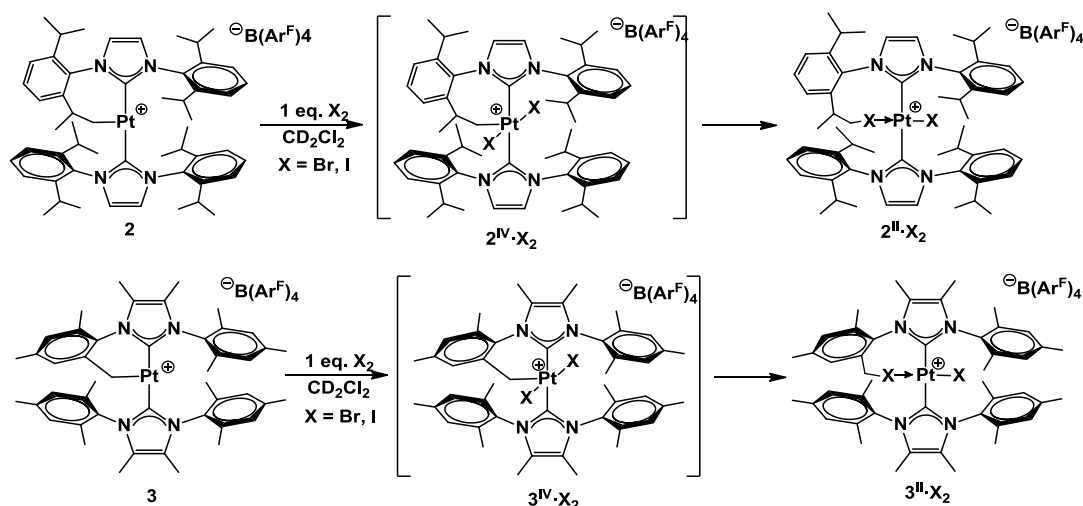
Reaction of complex **1** with one equivalent of I₂ or Br₂ in CH₂Cl₂ led to the formation of the expected coordinatively unsaturated Pt(IV) species¹² (**1**^{IV}·X₂, where the superscript values indicate the oxidation state, Scheme 15). These species bearing the ^tBu ligand could be observed at room temperature and were stable in the solid state, but decomposed after a few hours in solution to yield a mixture of unidentified compounds.



Scheme 15. Oxidative addition of X₂ to complex **1**.

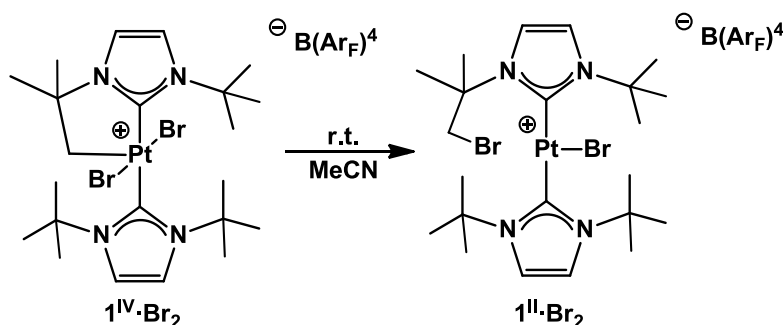
¹⁶ Shilov, A. E.; Shteinman, A. A. *Coord. Chem. Rev.* **1977**, *24*, 97.

Reaction of complexes **2** and **3** with Br_2 led to analogous species, but in this case the Pt(IV) complexes could only be observed at low temperature (Scheme 16). However, whereas the IPr derivative $\mathbf{2}^{\text{IV}}\cdot\text{Br}_2$ was stable in solution at temperatures below $-15\text{ }^\circ\text{C}$, the analogous IMes* species $\mathbf{3}^{\text{IV}}\cdot\text{Br}_2$ could only be detected at $-78\text{ }^\circ\text{C}$ and never in its pure form. No analogous Pt(IV) species $\mathbf{2}^{\text{IV}}\cdot\text{I}_2$ or $\mathbf{3}^{\text{IV}}\cdot\text{I}_2$ were detected in reactions with I_2 . In all cases, for reactions with I_2 and Br_2 , upon warming to room temperature, the observed final products were the cationic Pt(II) derivatives arising from reductive carbon-halogen bond coupling reactions $\mathbf{2}^{\text{II}}\cdot\text{I}_2$ and $\mathbf{3}^{\text{II}}\cdot\text{I}_2$. An interaction of the new formed CH_2X group with the platinum center is established, as evidenced by the observation of coupling to ^{195}Pt in the signals of the CH_2X protons, to stabilize this highly electrophilic Pt(II) complexes.



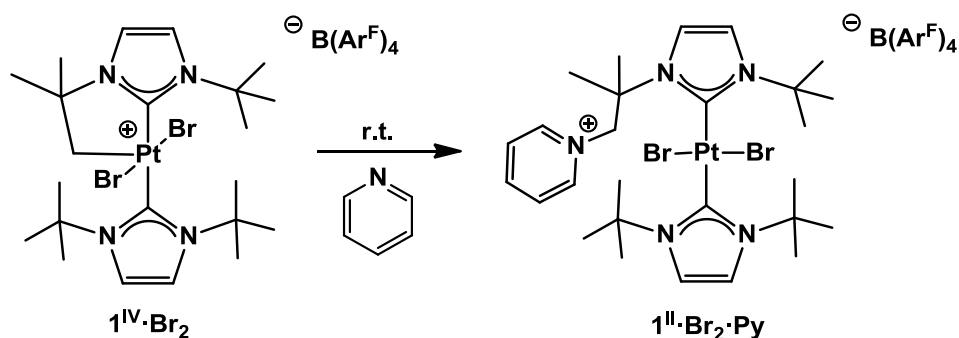
Scheme 16. Reactivity of complexes **2** and **3** with halogens.

It must be noted that a related Pt(II) species can be obtained when $[\text{PtBr}_2(\text{I}^t\text{Bu}')(\text{I}^t\text{Bu})][\text{B}(\text{Ar}^{\text{F}})_4]$ is left to evolve at room temperature in a more polar solvent such as acetonitrile or methanol (Scheme 17) as opposed to the behavior in CH_2Cl_2 , used in the synthesis of the Pt(IV) complexes.



Scheme 17. Reductive elimination of $[PtBr_2(I^tBu')(I^tBu)][B(Ar^F)_4]$ ($1^{IV}\cdot Br_2$) in a more polar solvent.

Another interesting reaction of this Pt(IV) species $1^{IV}\cdot Br_2$ was observed upon addition of pyridine. A nucleophilic addition took place in which pyridine was not bound to the metal center but to the cyclometallated CH_2 group (Scheme 18). This result could be rationalized if the electrophilic nature of $Pt^{IV}-C$ bonds as opposed to the nucleophilic character of $Pt^{II}-C$ bonds, is considered.¹⁷ In fact this is actually what one should expect since nucleophilic addition of H_2O or Cl^- to coordinatively unsaturated $Pt^{IV}-CH_3$ intermediates were believed to take place in the Shilov chemistry for the conversion of methane into methanol or chloroform.¹⁸



Scheme 18. Reactivity of $[PtBr_2(I^tBu')(I^tBu)][B(Ar^F)_4]$ ($1^{IV}\cdot Br_2$) with pyridine.

The Pt(IV) species described in this section are the first examples of crystallographically characterized alkyl-halide Pt(IV) complexes stabilized by an agostic interaction. A report published by Rourke¹⁹ during the course of our work

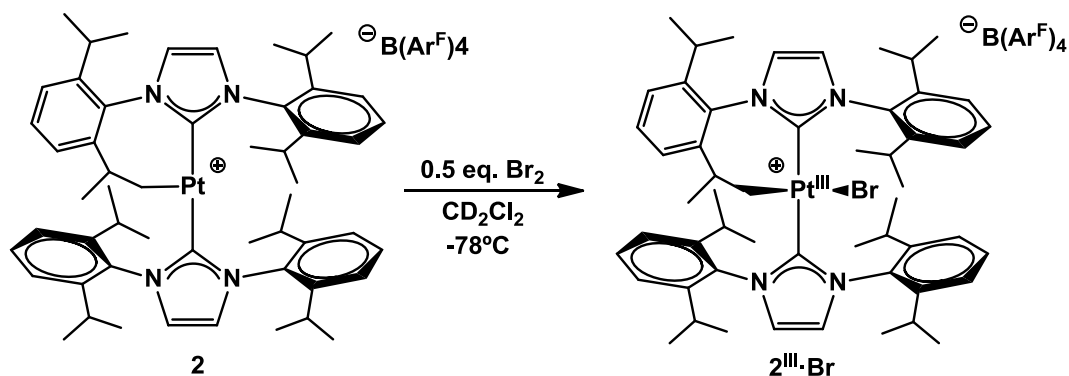
¹⁷ Labinger, J. A.; Bercaw, J. E. *Top. Organomet. Chem.* **2011**, 35, 29.

¹⁸ Grice, K. A.; Scheuermann, M. L.; Goldberg, K. I. *Top. Organomet. Chem.* **2011**, 35, 1.

¹⁹ Crosby, S.H.; Deeth, R.J.; Clarkson, G.J.; Rourke, J.P., *Dalton Trans.* **2011**, 40, 1227

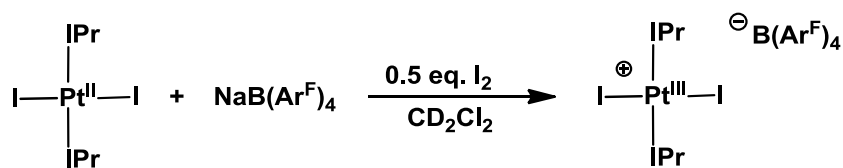
presented the formation of both alkyl-halide and aryl-halide Pt(IV) species, but crystallographic data were only reported for the latter.

Remarkably, during mechanistic studies on the oxidation reaction of complex **2** with Br_2 a mononuclear, paramagnetic Pt(III)-alkyl intermediate $\mathbf{2}^{\text{III}}\cdot\text{Br}$ was detected. This unique compound could be isolated (and crystallographically characterized) when the reaction was carried out by addition of only 0.5 equivalents of Br_2 , as depicted in Scheme 19.¹⁵



Scheme 19. Formation of paramagnetic Pt(III) species with seesaw structure.

It presented an interesting seesaw structure which was in accordance with DFT calculations. Moreover, this DFT study demonstrated that the Br-Pt-L angle for Pt(III) biscarbene complexes was dependent on the ligand in the *trans* position, with strong σ -donors favouring the seesaw structure and square planar geometries being predicted for *trans*-bihalide Pt(III) species. This latter hypothesis was supported by the X-ray structure of the related Pt(III) derivative $[\text{Pt}(\text{I})_2(\text{IPr})_2][\text{B}(\text{Ar}^{\text{F}})_4]$, synthesized as depicted in Scheme 20, that exhibits a square planar geometry.



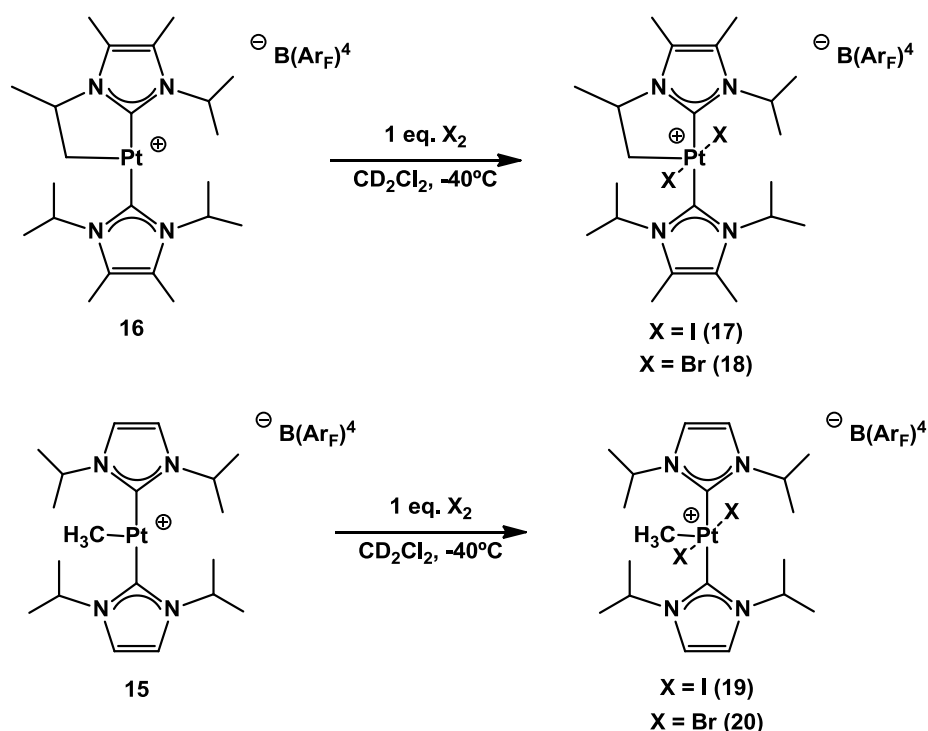
Scheme 20. Formation of square planar Pt(III) complexes.

1.2.2. Reactivity with halogens of Pt complexes bearing less bulky NHCs.

Encouraged by the interesting results obtained for the reactivity of T-shaped platinum complexes bearing bulky NHCs ($i^t\text{Bu}$, IPr, IMes*) described in the previous section, we decided to expand these investigations to analogous platinum complexes bearing less bulky NHCs, namely $i^i\text{Pr}_2$ and $i^i\text{Pr}_2\text{Me}_2$.

1.2.2.1. Formation of Pt(IV) complexes

Complexes **15** and **16** react with 1 equivalent of I_2 or Br_2 at low temperature to yield the expected Pt(IV) products. The deep yellow solutions of **15** and **16** turned deep red upon formation of the new species.



Scheme 21. Reaction of complexes **15** and **16** with halogens.

Complexes **17** and **18** (Scheme 21) derived from the cyclometallated T-shaped platinum (II) complex bearing $i^i\text{Pr}_2\text{Me}_2$ ligands **15**, were only stable at low temperature and could be characterized by NMR spectroscopy at -40°C . As seen in Figure 16, the most characteristic feature of the ^1H NMR spectrum of complex **17** is the presence of two peaks at 5.41 and 5.08 ppm corresponding to the

inequivalent protons of the cyclometallated CH₂ unit. Both peaks present coupling to ¹⁹⁵Pt with a ²J_{PtH} of 80 Hz. This value, smaller than the ²J_{PtH} of the analogous signals in the Pt(II) starting species (**16**), is indicative of a higher oxidation state at the metal centre.²⁰

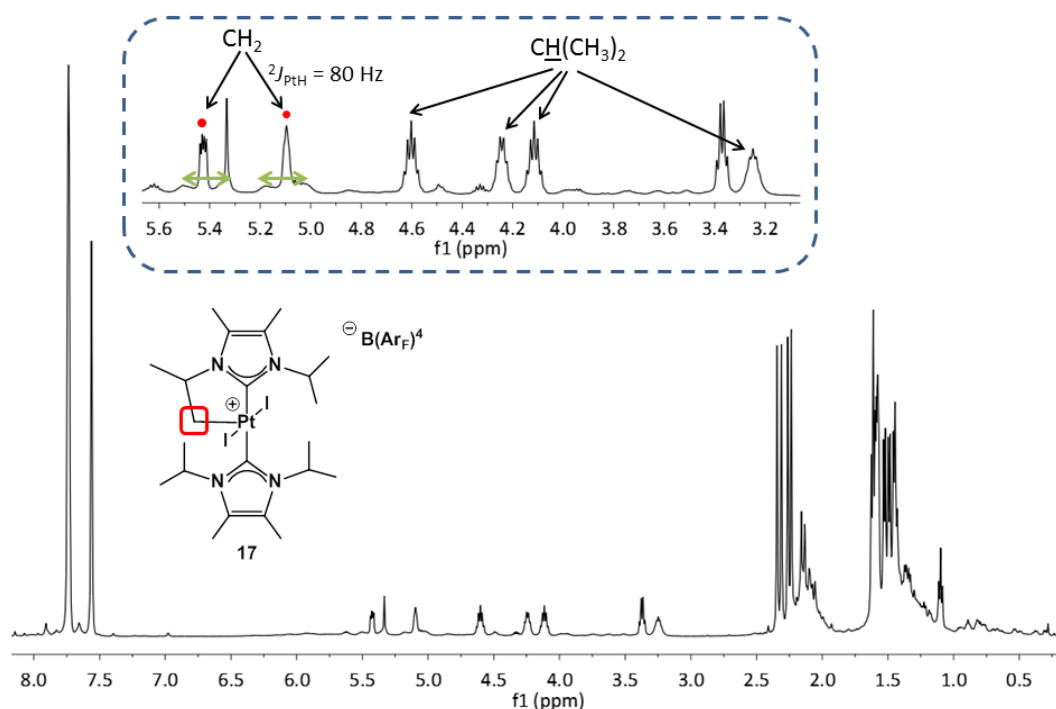


Figure 16. ¹H NMR in CD₂Cl₂ at -40 °C of complex **17**.

The chemical shift of the carbenic carbon atom, resonating at 161.6 ppm in the ¹³C NMR spectrum, is shifted up-field almost 9 ppm compared to complex **16**, again in agreement with a change in oxidation state from Pt(II) to Pt(IV). The cyclometallated methylene carbon appears at 44.5 ppm with ¹J_{CH} = 153 Hz and in this case the coupling to ¹⁹⁵Pt could not be detected.

Complex **18** shows similar spectra, as depicted in Figure 17. In this case the ²J_{PtH} value of the diastereotopic CH₂ protons is slightly larger at 86 Hz, but the resonance of the carbenic carbon at 162.1 ppm is very similar. For this species the cyclometallated CH₂ carbon resonates at 49.3 ppm with ¹J_{CH} = 154 Hz. For this species it was possible to observe the coupling to ¹⁹⁵Pt which presented a value of

$^1J_{PtC} = 483$ Hz. This is within the range of typical Pt(IV)-C(sp³) $^1J_{PtC}$ values (400-500 Hz), whereas Pt(II)-C(sp³) $^1J_{PtC}$ values are higher at 800-900 Hz.²⁰

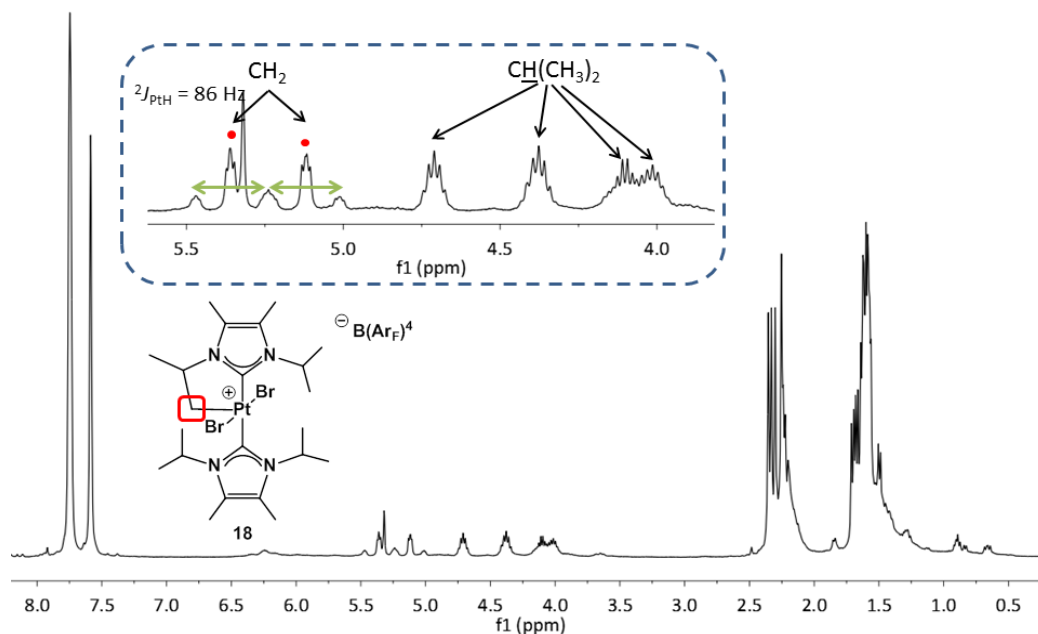


Figure 17. ^1H NMR in CD_2Cl_2 at -40 °C of complex **18**.

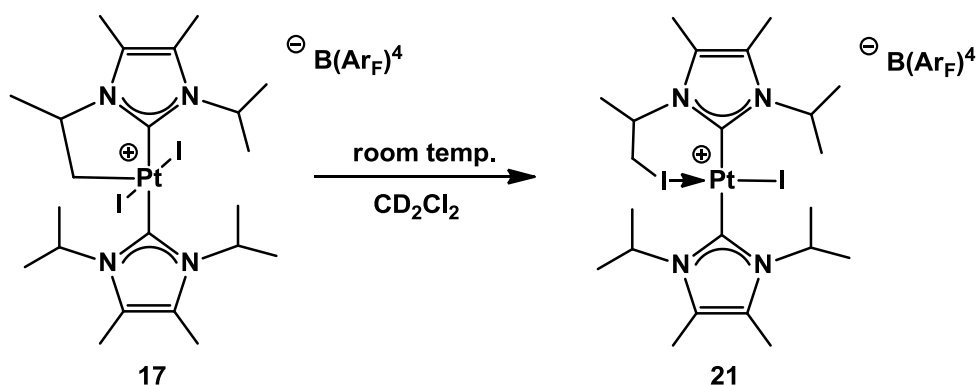
The ^1H NMR spectra of complexes **17** and **18** suggest that agostic interactions may be stabilizing these unsaturated species, as the non-cyclometallated iPr_2Me_2 ligands present different signals for the methyl groups in the imidazolylidene ring and for the CH groups of the isopropyl substituents. This is at variance with the highly symmetric spectra of the Pt(II) species (c.f. complexes **14** and **15**) and suggests that free rotation around the Pt–C axis is hindered, probably by the existence of agostic interactions between the platinum center and the protons of the isopropyl CH_3 groups. A similar behavior was observed for the related $\text{PtI}_2(\text{i}^t\text{Bu}')(\text{i}^t\text{Bu})\text{B}(\text{Ar}^F)_4$ complex **1^{IV}·I₂** where agostic interactions were detected both in the solid state structure and in solution.

Upon raising the temperature to 0 °C new Pt(II) complexes resulting from reducing C–X coupling are formed, the reaction being complete after a few hours

²⁰ a) Felk, U.; Kaminsky, W.; Goldberg, K. I. *J. Am. Chem. Soc.* **2001**, *123*, 6423; b) Pregosin, P. S. *NMR in Organometallic Chemistry*, Chapter 7, p. 212.

at room temperature. This result is in contrast with the higher thermal stability of the related Pt(IV) complexes containing the $t\text{Bu}$ ligand and their reluctance to undergo C–X coupling in dichloromethane. The cleanest reaction is observed for complex **17**, which produces new Pt(II) complex **21** (Scheme 22).

This species has two characteristic signals at 3.91 and 3.55 ppm corresponding to the diastereotopic CH_2 protons. Even though no coupling to ^{195}Pt could be observed, probably due to its small value, it is quite possible that the CH_2I moiety is interacting with the platinum center to stabilize the unsaturated species. Similar behavior was observed for the related species with the $t\text{Bu}$ ligand, where coupling to ^{195}Pt could only be seen in spectra recorded in the 300 MHz spectrometer (due to broadening of satellites by Chemical Shift Anisotropy relaxation effects).



Scheme 22. Reductive C–I coupling to yield Pt(II) complex **21**.

On the other hand, evolution of the brominated complex **18** at room temperature resulted in a mixture of unidentified products, in analogy with the results observed for derivative $[\text{Pt}(\text{Br}_2)(t\text{Bu}')(t\text{Bu})][\text{B}(\text{Ar}^F)_4] \mathbf{1}^{\text{IV}} \cdot \text{Br}_2$.

On a similar note, when complex **15** reacts with one equivalent of I_2 or Br_2 at low temperature ($-40\text{ }^\circ\text{C}$) analogous Pt(IV) complexes **19** and **20** are formed (Scheme 21).

The most interesting feature of the ^1H NMR spectra of these species is the shift to lower field of the Pt–Me resonance to 2.09 and 2.61 ppm respectively (compared to derivative **15**) and a $^2J_{\text{PtH}}$ of 30 Hz and 32 Hz, as seen in Figure 18.

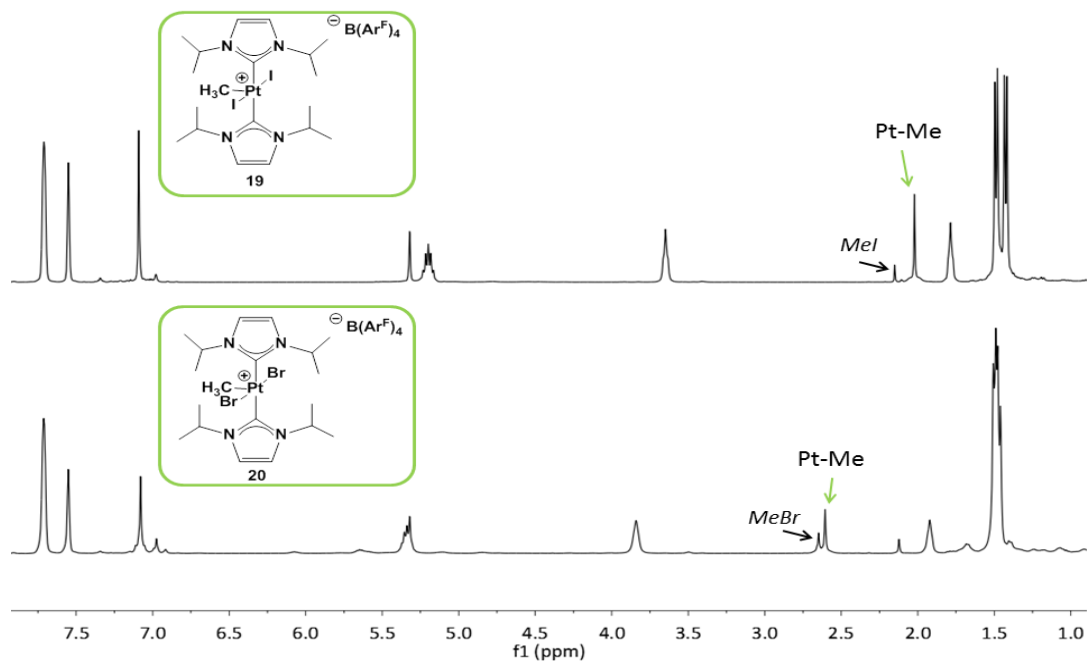
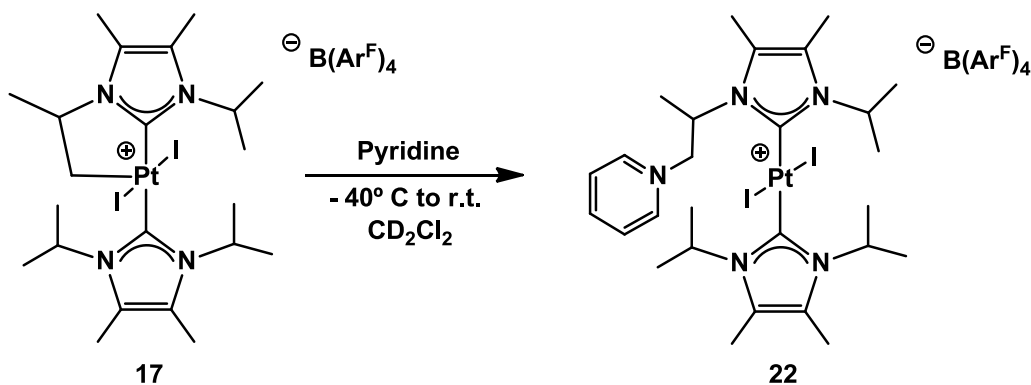


Figure 18. ^1H NMR in CD_2Cl_2 at $-30\text{ }^\circ\text{C}$ of complexes **19** and **20**.

Iodine complex **19** is relatively stable at room temperature, but slowly decomposes in solution with loss of iodomethane. This reaction is slow, taking days to consume all starting material and yields a mixture of as of yet unidentified species. In contrast, decomposition of **20**, with loss of bromomethane is fast, taking place in only a few minutes at room temperature. Indeed, even at $-30\text{ }^\circ\text{C}$, decomposition is evident right after Br_2 addition, as depicted in Figure 18 where bromomethane is clearly detected in the ^1H NMR spectrum. However, for this species the final product mixture is far more complex than for complex **19** and no species could be identified either.

The reactivity of Pt(IV) species with pyridine, observed for the complexes with $t\text{Bu}$ ligands (Scheme 18), was also tested for complexes **17** and **18**. Again, only complex **17** reacted cleanly to produce the expected product, where a nucleophilic attack on the cyclometallated CH_2 carbon has taken place to yield the carbon-nitrogen coupling product **22**, as shown in Scheme 23.

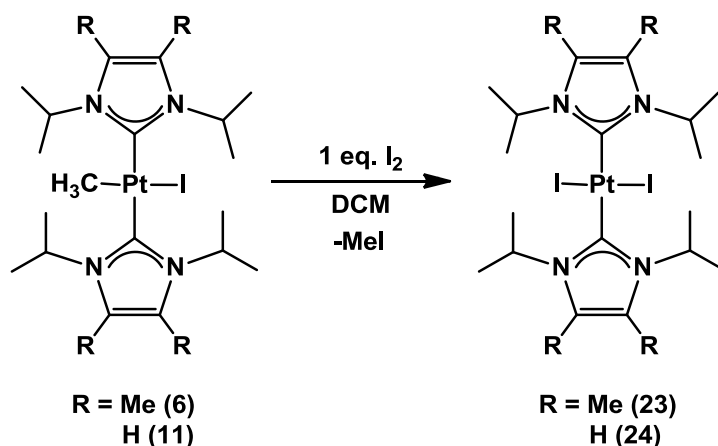
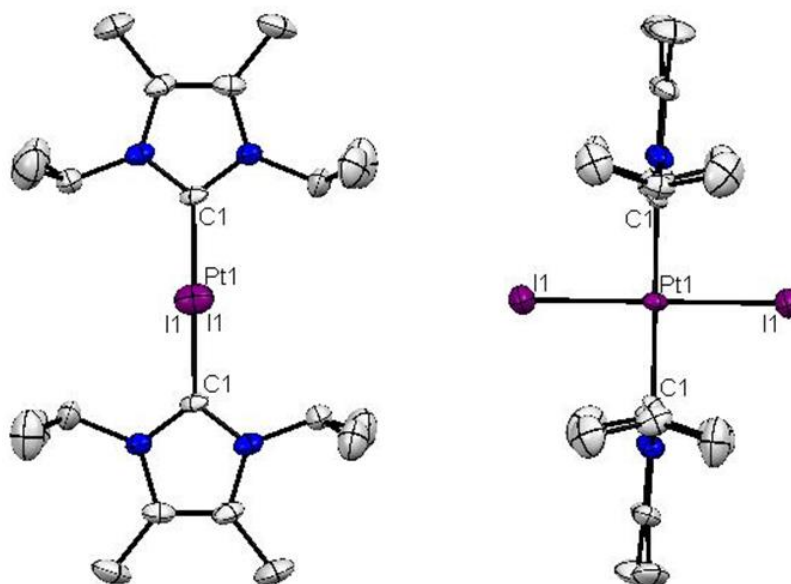
Scheme 23. Reactivity of Pt(IV) complex **17** with pyridine.

The fact that the reaction of complex **17** with pyridine leading to **22** occurs within seconds rules out the possibility of formation of complex **22** by nucleophilic substitution of the iodine atom of the CH_2I moiety in the platinum (II) complex **21**, which takes hours to form. Therefore, the results shown here are clearly relevant and related to the Shilov chemistry, confirming that coordinatively unsaturated Pt(IV) alkyl complexes can react with nucleophiles such as pyridine to promote C–N coupling reactions.

1.2.2.2. The search for Pt(III) complexes

As we have previously discussed, addition of 0.5 equivalents of Br_2 to complex IPr $[\text{Pt}(\text{IPr}')(\text{IPr})][\text{B}(\text{Ar}^{\text{F}})_4]$, **2**, at low temperature allowed for the observation of an unusual mononuclear, paramagnetic Pt(III) complex with an interesting seesaw structure. Similar reactions were tested for complexes **15** and **16**, but slow addition of a bromine solution at low temperature did not lead to the observation of the blue coloration that is to be expected for a Pt(III) species. Instead, only 0.5 equivalents of **15** and **16** reacted to yield complexes **18** and **20**, with the rest remaining unreacted.

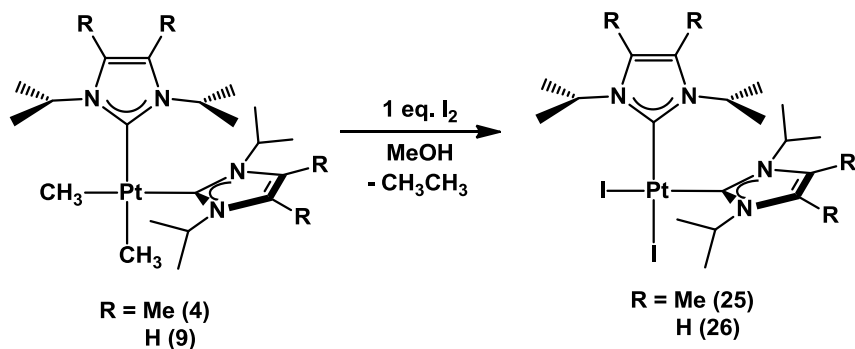
We then attempted the preparation of square planar Pt(III) species using $\text{PtI}_2(\text{NHC})_2$ as starting species, since the corresponding IPr derivative $[\text{Pt}(\text{I}_2)(\text{IPr})_2][\text{B}(\text{Ar}^{\text{F}})_4]$ resulted to be much more stable than the alkyl derivative. These complexes were prepared by iodine addition to the corresponding *trans*- $\text{PtMe}(\text{NHC})_2$ complexes, as shown in Scheme 24.

Scheme 24. Synthesis of *trans*-PtI₂(NHC)₂ complexes.Figure 19. ORTEP diagrams of complex **23**. Diagram on the left is rotated 90 °C around the vertical axis.

X-ray quality crystals of complex **23** were obtained by slow diffusion of pentane into a dichloromethane solution and the elucidated structure is shown in Figure 19. The structure is similar to the PtMeI(NHC)₂ species (**6**) in the sense that the carbene rings lie perpendicular to coordination plane around the platinum atom. In this case the Pt–I distance is over 0.084 Å shorter (2.6084(6) Å) compared to complex **6** due to the higher *trans* influence of the methyl ligand. In contrast, the

Pt–C_{carbene} bond is slightly longer in complex **23** (2.023(6) Å) with respect to complex **6** (2.016(7) Å).

The synthesis of *trans*-PtI₂(NHC)₂ was also attempted from *cis*-PtMe₂(NHC)₂ which would avoid the additional step of forming *trans*-PtMeI(NHC)₂ by reaction of MeI with the dimethyl complex and subsequent isomerization. When *cis*-PtMe₂(NHC)₂ was treated with I₂ in methanol as solvent, the *cis*-PtI₂(NHC)₂ isomer was obtained, as depicted in Scheme 25.



Scheme 25. Formation of *cis*-PtI₂(NHC)₂ species.

However, isomerization to form the more stable *trans* isomers proved to be much more difficult than in the case of the isomerization of *cis*-PtMeI(NHC)₂ to *trans*-PtMeI(NHC)₂. Whereas for the latter case heating in dichloromethane overnight leads to complete isomerization to the *trans* species, the same treatment led to no isomerization for the former. When a mixture of dichloromethane and methanol was used as the solvent for the isomerization, some transformation was observed, but several days were needed for reaction completion. This challenging isomerization step, which lengthened the reaction time considerably led us to finally settle on *trans*-PtMeI(NHC)₂ as the most convenient precursor for the preparation of *trans*-PtI₂(NHC)₂.

Analysis of the NMR spectra of the *cis* and *trans* PtI₂(NHC)₂ complexes indicated a major difference between these species in the ¹³C NMR signal of the carbenic carbon atom.

	<i>cis</i> isomer		<i>trans</i> isomer	
	25	26	23	24
δ_C (ppm)	148.0	148.8	161.4	163.1
$^1J_{PtC}$ (Hz)	1525	1463		893

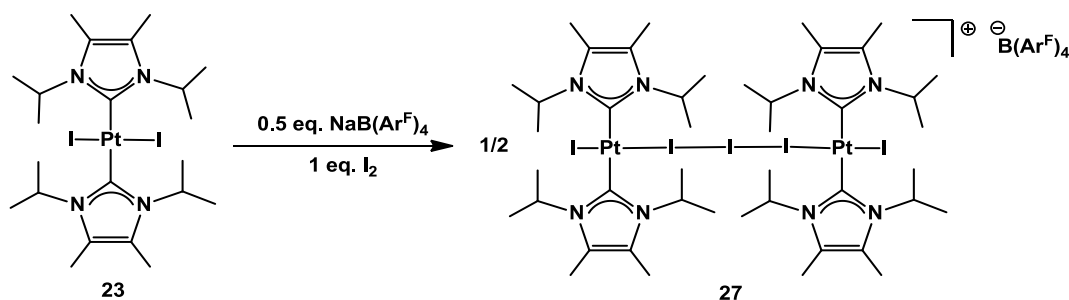
Table 1. ^{13}C chemical shifts and $^1J_{PtC}$ values in CD_2Cl_2 for the carbenic carbon atom in a series of *cis/trans* $\text{PtI}_2(\text{NHC})_2$ complexes.

As indicated in Table 1, both *cis* isomers presented a much larger coupling constant of the carbenic carbon atom to ^{195}Pt in the $^{13}\text{C}\{^1\text{H}\}$ NMR and a lower chemical shift. Similar effects have been observed for ^{31}P signals of *cis/trans*- $\text{PtX}_2(\text{PR}_3)_2$ complexes²¹ and were attributed to the larger extent of π back-donation from Pt that is possible for the *cis* isomers with respect to the *trans*. In the case of the *cis* isomer, both d_{xz} and d_{yz} orbitals in the Pt atom are available for back donation into the carbene ligand. For the *trans* isomer however, only the d_{xz} orbital is available. This larger back-donation means that the carbenic atoms in the *cis* isomers have higher electron density and thus resonate at higher field and present a larger coupling constant to ^{195}Pt .

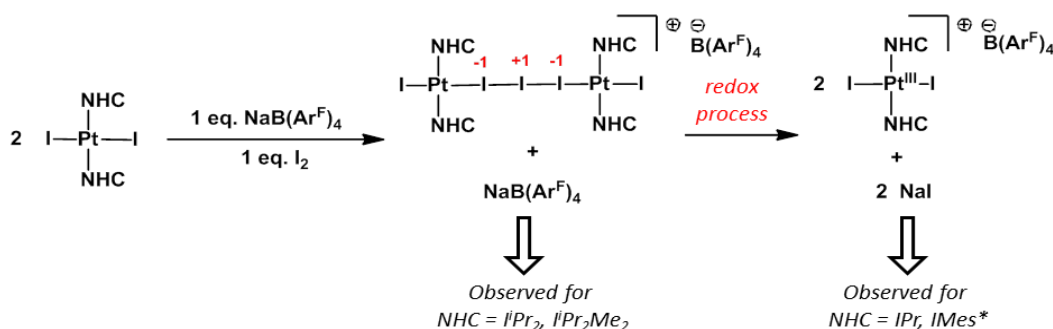
In an attempt to reproduce the synthetic procedure for the formation of Pt(III) species employed for IPr complex **2** (Scheme 20), the new $\text{PtI}_2(\text{NHC})_2$ species were initially reacted with $\text{NaB}(\text{Ar}^F)_4$ and further addition of I_2 was tested in some cases, as discussed below.

When one equivalent of $\text{NaB}(\text{Ar}^F)_4$ was added to a dichloromethane solution of complex *trans*- $[\text{Pt}(\text{I})_2(\text{I}^i\text{Pr}_2\text{Me}_2)_2]$ **23**, no apparent reaction took place. This was also observed for the analogous complexes bearing IPr and IMes* ligands. Addition of one equivalent of I_2 to this mixture of reagents led to the formation of square planar Pt(III) blue paramagnetic species $[\text{Pt}(\text{I}_2)(\text{NHC})_2][\text{B}(\text{Ar}^F)_4]$. In the case of complex **23** however, I_2 addition did not lead to a color change to blue but to dark red. ^1H NMR analysis of the reaction indicated that a new diamagnetic species had formed. X-ray diffraction studies on crystals of this new species indicated the formation of a Pt(II) dimer with a bridging I_3 ligand, as shown in Scheme 26.

²¹ Grim, S.O.; Keiter, R.L.; McFarlane, W.; *Inorg. Chem.* **1967**, *6*, 1133.

Scheme 26. Synthesis of Pt(II) dimer **27**.

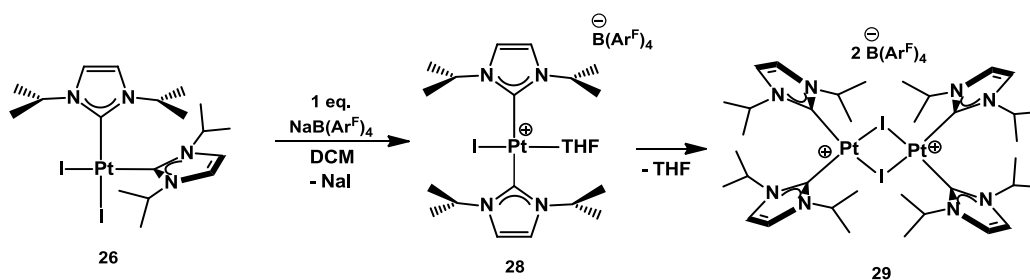
There are only a few reports on complexes bearing triiodide as a ligand²² and this is the first example in which it acts as a bridging ligand. This species may actually be an intermediate in the formation of Pt(III) species that are observed when IPr and IMes* are used as ligands. A greater steric bulk in those cases may hinder the observation of the dimer and allow for the reaction to proceed to the oxidized Pt(III) species, along with triiodide reduction (Scheme 27). In any case, this latter process was not observed for derivative **27**, even when solutions of this compound were stirred at r. t. for prolonged periods of time.

Scheme 27. Reactions of $\text{PtI}_2(\text{NHC})_2$ with I_2 and $\text{NaB}(\text{Ar}^{\text{F}})_4$ resulting in Pt(II) or Pt(III) species, depending on the ligand bulk.

In the case of the *cis*- $\text{PtI}_2(\text{NHC})_2$ species **26** reactivity with $\text{NaB}(\text{Ar}^{\text{F}})_4$ is different than for the *trans* isomers, as will be show below. When a solution of **26** was treated with one equivalent of $\text{NaB}(\text{Ar}^{\text{F}})_4$ in DCM a new unsaturated species is

²² a) Gossage, R. A.; Ryabov, A. D.; Spek, A. L.; Stufkens, D. J.; van Beek, J. A. M.; van Eldik, R.; van Koten, G. *J. Am. Chem. Soc.* **1999**, *121*, 2488; b) Zhao, S.-B.; Wang, R.-Y.; Wang, S. *Organometallics* **2009**, *28*, 2572

initially formed that is stabilized by THF coordination (Scheme 33).²³ The carbenic carbon atoms in complex **28** resonate at 144 ppm in the ¹³C NMR spectrum, at a lower chemical shift than the parent compound **26** (Table 1). A similar shift was observed upon formation of the cationic T-shaped species from parent PtMeI(NHC)₂ compounds. The simplicity of the ¹H and ¹³C NMR spectra of this species, suggests a highly symmetric environment for the carbene ligands, indicating that they have probably isomerized to a *trans* disposition in this unsaturated species.



Scheme 28. Reaction of *cis*-PtI₂(NHC)₂ complexes with NaB(Ar^F)₄

Over time, complex **28** evolves to form a new species that does not present coordination of THF. ¹H NMR spectra of this new compound (**29**) is very similar to that of its parent complexes, but a shift of about 5 ppm can now be observed in the carbenic carbon signal in the ¹³C NMR spectrum, resonating at 139 ppm.

Crystals suitable for X-ray diffraction studies could be grown for **29**, revealing the formation of a dicationic platinum dimer with two bridging iodide ligands and each platinum center supporting two NHC ligands in a *cis* disposition (Figure 20). No analogous structures have been reported for platinum complexes bearing NHC ligands, although there are some examples of related species bearing phosphine ligands and bridging halides.²⁴ Among the latter, there is only one example of a crystallographically characterized complex with bridging iodides, [Pt₂(μ-

²³ Traces of THF were present in the batch of NaB(Ar^F)₄ and were found to be key to stabilizing the unsaturated species **28**.

²⁴ Some recent examples : a) Ingleson, M.J.; Kociok-Köhn, G.; Weller, A.S. *Inorg. Chim. Acta*, **2005**, 358, 1571; b) Schott, D.; Pregosin, P.S.; Albinati, A. Rizzato, S. *Inorg. Chim. Acta*, **2007**, 360, 3203 c) Achard, T.; Giordano, L.; Tenaglia, A.; Gimbert, Y.; Buono, G. *Organometallics*, **2010**, 29, 3936

$I)_2(dppm)_2][BF_4]_2$ (dppm = bis(diphenylphosphino)methane).²⁵ Its values for the Pt-I distance and the I-Pt-I angle, at 2.662(1) Å and 86.6(1)° respectively are comparable to those for complex **29**, at 2.6443(2) Å and 85.09(1)°.

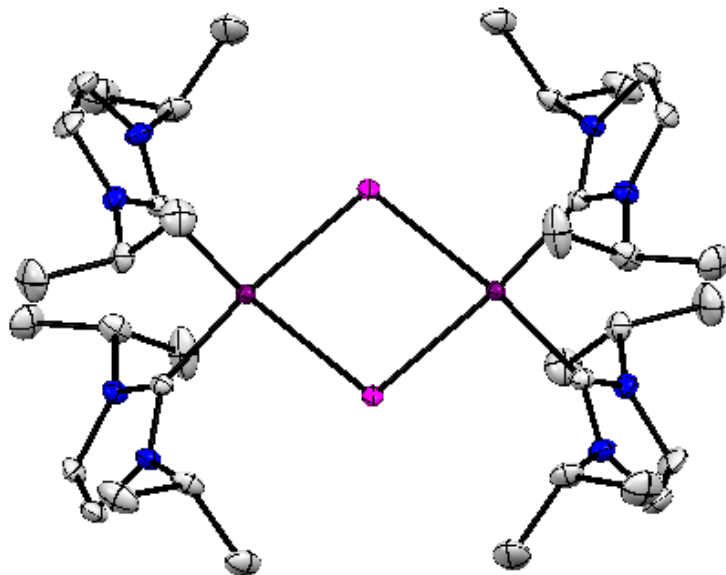


Figure 20. X-ray structure of complex **29**. Anions omitted for clarity.

²⁵ Neve, F.; Crispini, A.; Ghedini, M.; De Munno, G. *Inorg. Chim. Acta*, **1990**, *176*, 23

CHAPTER 2

Reactivity of 14 electron T-shaped Pt(II)
complexes with amine boranes

CHAPTER 2. INTRODUCTION

The mechanism of transition metal catalyzed dehydrogenation of amineboranes

The catalytic dehydrogenation of ammonia borane ($\text{NH}_3\cdot\text{BH}_3$) and related species has been a field of active research for the past decade.¹ Initial interest in this family of compounds arose from their potential application as hydrogen storage materials for transportation use. Materials to be used for such purposes need to meet high volumetric and gravimetric storage capacity, and ammonia borane, BH_3NH_3 , with 19.6 wt% appeared as one of the most promising chemicals, fulfilling the requirements established by the US Department of Energy.² Research in this area has also increased the interest in amineboranes ($\text{NHR}_2\cdot\text{BH}_3$) for other applications, such as transfer hydrogenation³ or the synthesis of BN polymeric materials.⁴

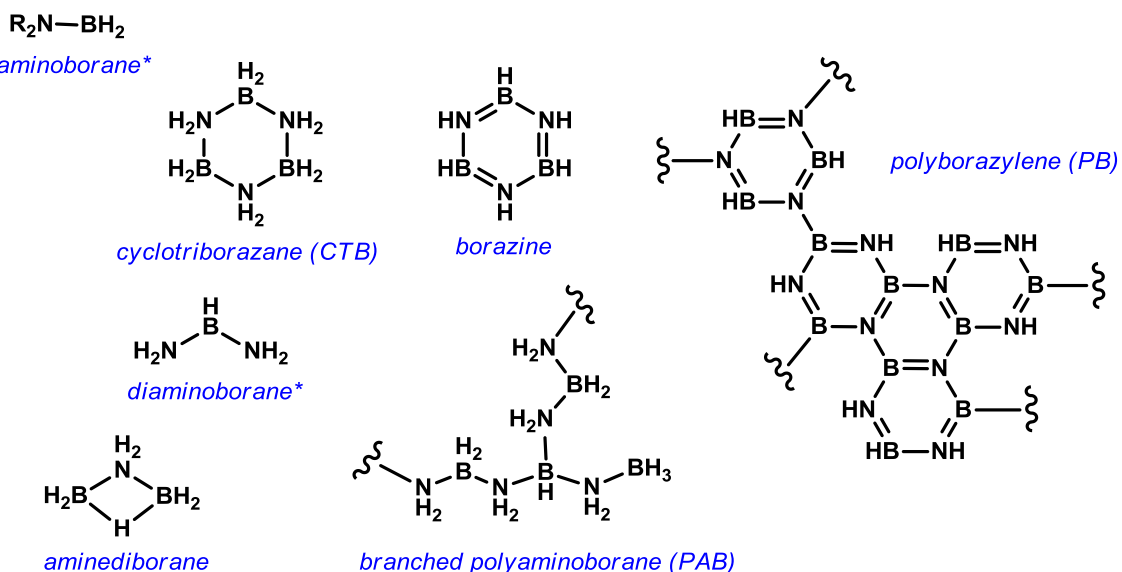
Mechanistic information about the interaction and reactivity of amineboranes with metal centers is essential to optimize further applications of these materials as a means to control the outcome of the reaction (Scheme 1).

¹ a) Staubitz, A.; Robertson, A. P. M.; Sloan, M. E.; Manners, I. *Chem. Rev.* **2010**, *110*, 4079. b) Alcaraz, G.; Sabo-Etienne, S. *Angew. Chem. Int. Ed.* **2010**, *49*, 7170. c) Hamilton, C. W.; Baker, R. T.; Staubitz, A.; Manners, I. *Chem. Soc. Rev.* **2009**, *38*, 279. d) Stephens, F. H.; Pons, V.; Baker, R. T. *Dalton Trans.* **2007**, 2613.

² Satyapal, S.; Petrovic, J.; Read, C.; Thomas, G.; Ordaz, G. *Catal. Today*, **2007**, *120*, 246.

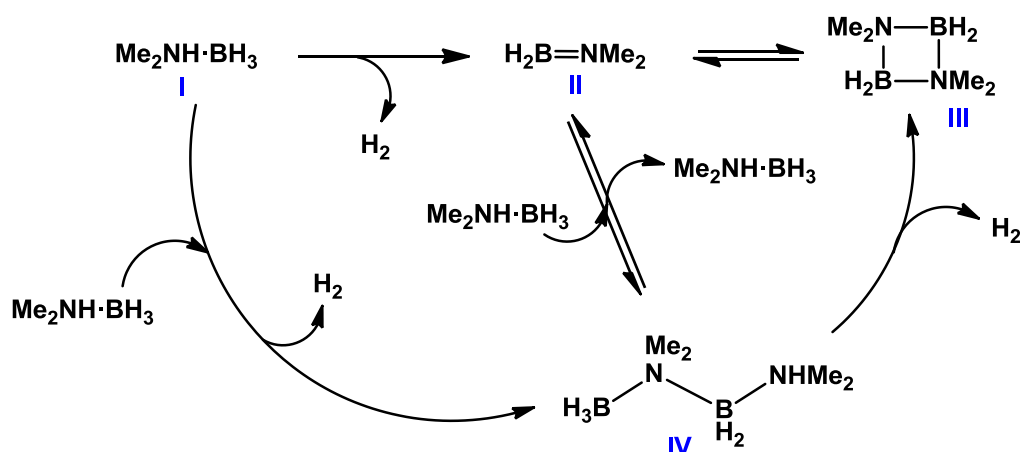
³ Huang, Z.; Autrey, T. *Energy Environ. Sci.*, **2012**, *5*, 9257.

⁴ Staubitz, A.; Sloan, M. E.; Robertson, A. P. M.; Friedrich, A.; Schneider, S.; Gates, P. J.; Guànné, J. S. A. D.; Manners, I. *J. Am. Chem. Soc.* **2010**, *132*, 13332.



Scheme 1. Most common dehydrogenation products of ammonia borane, including polymeric species and products arising from B–N cleavage. Species marked with * are unstable.

This is particularly crucial in the fields of hydrogen storage and polymer synthesis to obtain specific dehydrogenated products that facilitate spent fuel recovery and to prepare polymers with well defined characteristics respectively. Even though it neither possesses the greater hydrogen gravimetric capacity nor does it yield polymeric materials, dimethylamine borane ($NHMe_2 \cdot BH_3$) (I) is usually chosen for mechanistic studies, due to its good solubility and that of the intermediate products that can be detected during the dehydrogenation process (Scheme 2). Moreover, it yields a single final dehydrogenation product, the aminoborane dimer $[BH_2NMe_2]_2$ (III) which simplifies the mechanistic picture with respect to ammonia borane and primary amine boranes where several dehydrogenation products are possible.



Scheme 2. Main intermediates observed in the dehydrogenation of DMAB catalyzed by transition metal complexes.

Aminoborane monomer **II** is usually detected in the course of the dehydrogenation reactions of **I** and in many cases the linear dimer **IV** is also seen.⁵ Diaminoborane $\text{BH}(\text{NMe}_2)_2$ (**V**) is occasionally detected as a minor side product, but no attempts have been made to understand the origin of this by-product, even though an early report suggests that it forms by reaction of aminoborane (BH_2NMe_2) and free amine.⁶

The majority of mechanistic studies so far reported focus on the way metal centers activate the amine borane and the steps that lead to the release of the first equivalent of H_2 . Fewer studies tackle the formation of the cyclic dimer **III** and the role that intermediates such as **IV** play in the process.⁵

II.1. Initial activation of DMAB by transition metal complexes

There are several proposed mechanisms, supported by experimental evidence and/or DFT calculations, for the way in which amineboranes are activated by the metal and dehydrogenation proceeds, and they vary depending not only on the metal of choice but on the ligands. Usually the process is considered to involve a σ bound amine borane that undergoes B–H oxidative addition and N–H transfer, either in a concerted fashion or in sequential steps, where either process can

⁵ Sewell, L. J.; Lloyd-Jones, G. C.; Weller, A. S. *J. Am. Chem. Soc.* **2012**, *134*, 3598.

⁶ Burg, A. B.; Randolph, C. L. *J. Am. Chem. Soc.* **1951**, *73*, 953.

occur first depending on the system. This activation is referred to as an *inner sphere* (Scheme 3) process if all of these steps take place at the metal. In some cases however the ligand assists in the dehydrogenation process in what is called an *outer sphere* mechanism.

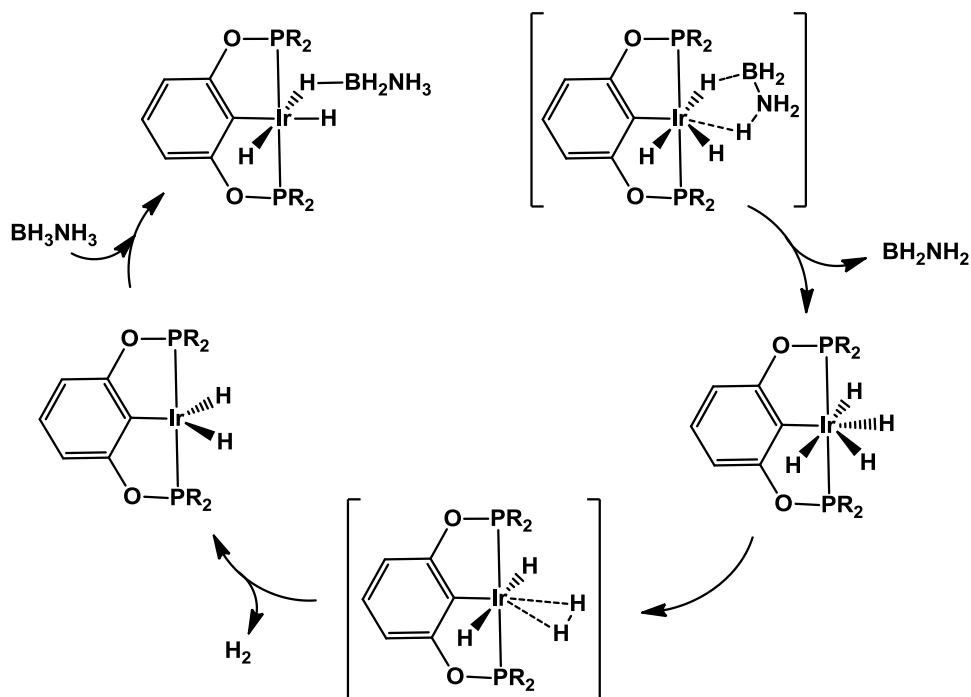


Scheme 3. a) Inner sphere mechanism, b) outer sphere mechanism. BH and NH activation can take place in a concerted manner or in sequential steps.

The iridium pincer complex Ir(H)₂(POCOP)⁷ was one of the first and more active catalysts reported for the dehydrogenation of ammonia borane. In this case a concerted BH/NH activation of the substrate was proposed based on DFT calculations⁸ (Scheme 4). This mechanism involved an iridium (V) tetrahydride intermediate that was experimentally observed by ¹H NMR in the early stages of the reaction.

⁷ M. C. Denney, V. Pons, T. J. Hebden, D. M. Heinekey, K. I. Goldberg, *J. Am. Chem. Soc.* **2006**, *128*, 12048.

⁸ A. Paul, C. B. Musgrave, *Angew. Chem. Int. Ed.* **2007**, *46*, 8153.



Scheme 4. Proposed mechanism for the dehydrogenation of ammonia borane catalysed by Ir(H)₂(POCOP).

Interestingly despite the fast dehydrogenation of ammonia borane induced by Ir(H)₂(POCOP), this iridium complex proved to catalyse the dehydrogenation of DMAB very slowly (less than 1 eq of H₂ after 48h).⁹ Faster catalysis was observed for the primary methylamine borane NH₂Me·BH₃ (MAB).

In contrast with this concerted BH/NH activation mechanism, DFT calculations for DMAB dehydrogenation catalysed by the [Ir(H)₂(PCy₃)₂]⁺ fragment suggested that B–H activation takes place first, followed by H₂ release and then NH activation, which was the rate determining step.¹⁰ The latter fact was experimentally ascertained carrying out a reaction with BH₃NMe₂, which turned out to be slower than with BH₃NHMe₂, in agreement with N–H breaking being the rate-limiting step. This mechanism has also been shown to be the more favourable by

⁹ Dietrich, B.L.; Goldberg, K.I.; Heinekey, D.M.; Autrey, T.; Linehan, J.C. *Inorg. Chem.*, **2008**, *47*, 8583.

¹⁰ Stevens, C. J.; Dallanegra, R.; Chaplin, A. B.; Weller, A. S.; Macgregor, S. A.; Ward, B.; McKay, D.; Alcaraz, G.; Sabo-Etienne, S. *Chem. Eur. J.* **2011**, *17*, 3011.

DFT calculations for ammonia borane dehydrogenation with $[\text{Ir}(\text{dppm})_2][\text{OTf}]$ (dppm = 1,1-bis(diphosphinomethane)), bearing a chelating phosphine.¹¹

A computational study for a similar phosphine complex, in this case with a rhodium center, $[\text{Rh}(\text{P}^i\text{Bu}_3)_2]^+$, showed that there were competitive pathways with either B–H activation or N–H activation taking place first.¹² Even though the intermediate of N–H activation was lower in energy, the barrier for this H transfer was higher. The second H transfer to produce BH_2NMe_2 had again a lower barrier when coming from a BH unit, so all in all both BH/NH and NH/BH activation pathways had NH hydrogen transfer as their limiting step with similar barriers and therefore were competitive. These examples of group 9 metals bearing phosphine ligands show how small variations in the metal and ligand alter the energetic preference for each of the activation pathways.

Moving to transition metal catalysts of other groups, DFT calculations have also been performed by Luo for complex $[\text{TiCp}_2]$, an early transition metal catalyst.¹³ This study suggests initial B–H activation followed by NH proton transfer and was inspired by the experimental work by Manners.¹⁴ Later Chirik reported the catalytic dehydrogenation of DMAB with differently substituted Ti and Zr Cp complexes¹⁵ and making use of deuteration labelling studies provided experimental evidence for an initial reversible B–H oxidative addition step, as indicated by the DFT study. Unlike the trend previously observed for $\text{Ir}(\text{H})_2(\text{POCOP})$, these titanocene catalysts were less active for primary amine boranes such as MAB and almost inactive for the catalytic dehydrogenation of ammonia borane. So far the reason of this trend remains unexplained. Within this family of compounds reduced catalytic activity was observed with bulkier substituents in the Cp rings and in going down the group from titanium to zirconium.

¹¹ Rossin, A.; Caporali, M.; Gonsalvi, L.; Guerri, A.; Lledos, A.; Peruzzini, M.; Zanobini, F. *Eur. J. Inorg. Chem.* **2009**, 3055.

¹² T. M. Douglas, A. B. Chaplin, A. S. Weller, X. Yang, M. B. Hall *J. Am. Chem. Soc.* **2009**, *131*, 15440.

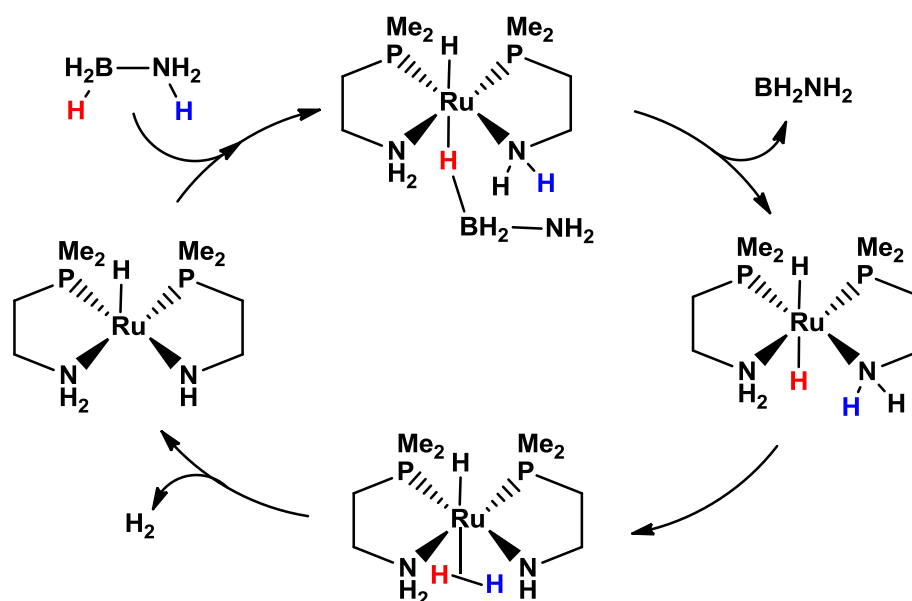
¹³ Luo, Y.; Ohno, K. *Organometallic*, **2007**, *26*, 3597.

¹⁴ Clark, T. J.; Russell, C. A.; Manners, I. *J. Am. Chem. Soc.* **2006**, *128*, 9582.

¹⁵ Pun, D.; Lobkovsky, E.; Chirik, P. J. *Chem. Commun.* **2007**, 3297.

In the case of main group elements, mechanistic proposals indicate that NH deprotonation is the first step as reported in the work with group 2 metals by Hill¹⁶ and for group 3 metals as reported by Wright.¹⁷

In contrast to these examples of *inner sphere* activation of the amine borane, there are instances where N–H transfer does not take place at the metal but is rather assisted by the ligands in an *outer sphere* process. This has been shown for a variety of ruthenium catalysts¹⁸ that had been previously used as alcohol dehydrogenation catalysts. The use of these species was inspired by the fact that even though ammonia borane is isoelectronic with ethane, its polarity is more similar to methanol. This hypothesis proved correct, as these ruthenium species are some of the more active catalysts for the dehydrogenation of amine boranes.



Scheme 5. Ligand assisted mechanism for a ruthenium complex reported by Fagnou.^{18a}

¹⁶ Hill, M. S.; Hodgson, M.; Liptrot, D. J.; Mahon, M. F. *Dalton Trans.* **2011**, *40*, 7783.

¹⁷ Cowley, H. J.; Holt, M. S.; Melen, R. L.; Rawson, J. M.; Wright, D. S. *Chem. Commun.* **2011**, *47*, 2682.

¹⁸ a) Blaquiere, N.; Diallo-Garcia, S.; Gorelsky, S. I.; Black, D. A.; Fagnou, K. *J. Am. Chem. Soc.* **2008**, *130*, 14034; b) Kass, M.; Friedrich, A.; Drees, M.; Schneider, S. *Angew. Chem. Int. Ed.* **2009**, *48*, 905; c) Boulho, C.; Djukic, J.-P. *Dalton Trans.* **2010**, *39*, 8893; d) MacInnis, M. C.; McDonald, R.; Ferguson, M. J.; Tobisch, S.; Turculet, L. *J. Am. Chem. Soc.* **2011**, *133*, 13622;

An outer sphere mechanism is also in operation for a nickel N-Heterocyclic carbene (NHC) complex¹⁹ that is actually one of the species that exerts the most extensive dehydrogenation of ammonia borane so far reported (up to 2.5 eq. of H₂). This system displays one of the more complex mechanisms so far described and in fact different computational studies were published. The first one by Hall²⁰ indicates initial BH activation, whereas a latter study by Paul and Musgrave²¹ suggests that NH coordination is favoured. In both cases, and this is the most interesting feature of this nickel system, one of the NHC ligands is involved in NH deprotonation.

II.2. Towards the formation of the final dehydrogenation products

Irrespective of how the amine borane is initially activated and aminoborane is produced, there are several mechanistic possibilities for the formation of the final dehydrogenation product, the cyclic dimer **III** (Scheme 2). Less information is available as to how this transformation proceeds.

Many groups assume an off-metal dimerization of aminoborane **II** to yield **III**, but only recently has the rate for this process been measured, using the cationic iridium complex [Ir(H₂)(PCy₃)₂(BH₂NMe₂)]⁺ as a latent source of **II**.¹⁰ Addition of an excess of MeCN displaces BH₂NMe₂ (**II**) and blocks further coordination to iridium, effectively leaving **II** to dimerize as if no metal were present. Kinetic data of this process yielded a second-order rate constant. Moreover, formation of linear dimer **IV** was not observed in this off-metal process.

Aminoborane can also coordinate to the metal, as exemplified for this iridium species and seen in many other instances, such as for analogous rhodium phosphine complexes,^{5,12,22} rhodium and iridium biscarbene complexes²³ and

¹⁹ a) Keaton, R.J.; Blacquiere, J.M.; Baker, R.T. *J. Am. Chem. Soc.* **2007**, *129*, 1844 b) Yang, X.; Hall, M. B. *J. Organomet. Chem.* **2009**, *694*, 2831

²⁰ Yang, X.; Hall, M. B. *J. Am. Chem. Soc.* **2008**, *130*, 1798

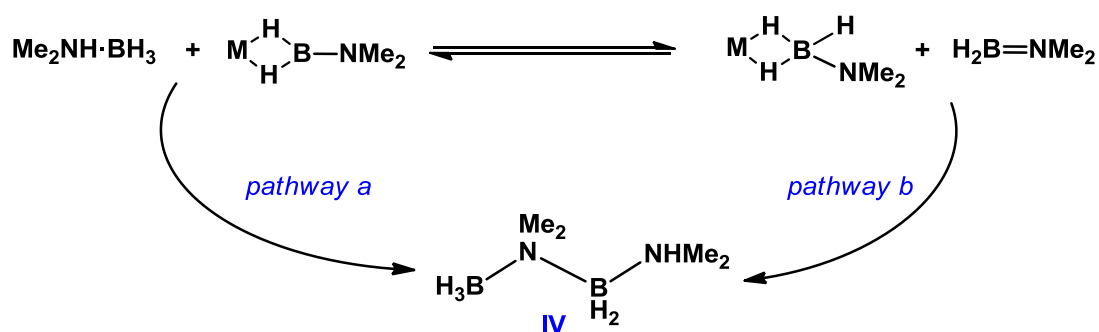
²¹ Zimmerman, P. M.; Paul, A.; Musgrave, C. B. *Inorg. Chem.* **2009**, *48*, 5418

²² Chaplin, A. B.; Weller, A. S. *Inorg. Chem.* **2010**, *49*, 1111.

²³ Tang, C. Y.; Thompson, A. L.; Aldridge, S. *J. Am. Chem. Soc.* **2010**, *132*, 10578.

ruthenium phosphine complexes^{18d,24}. These adducts can lead to further reactivity as described below.

There are many possibilities for the formation of the linear dimer **IV** which is frequently observed as an intermediate. An off-metal process was discarded by further tests using $[\text{Ir}(\text{H}_2)(\text{PCy}_3)_2(\text{BH}_2\text{NMe}_2)]^+$, as addition of MeCN to yield free aminoborane, followed by addition of DMAB only resulted in dimerization of **II** while DMAB remained unreacted, with no linear dimer being observed throughout the process.¹⁰ It is clear that the metal must be involved in the formation of **IV** and some possible pathways to this species are depicted in Scheme 6.



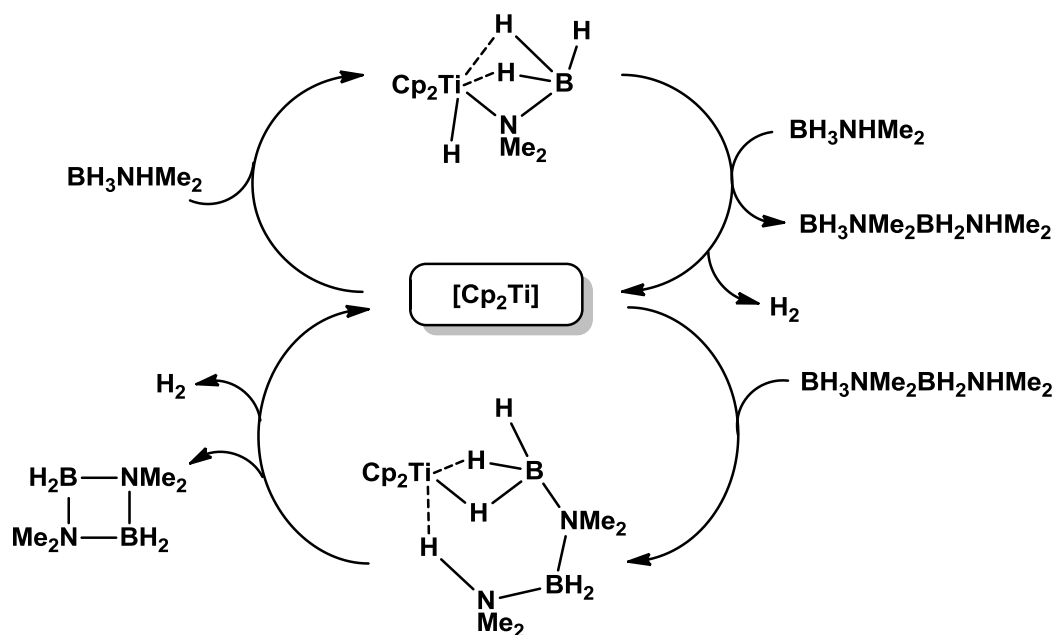
Scheme 6. Some possible pathways for the formation of linear dimer **IV**.

One possibility is the reaction of metal coordinated aminoborane with further amine borane to give rise to the linear dimer **IV** (pathway a). Alternatively the linear dimer can form from reaction of σ -bonded amine borane and the aminoborane present in the reaction medium (pathway b). This latter pathway involving an unsaturated monomer that inserts into a metal bound saturated unit is reminiscent of the polymerization of alkenes.

In contrast, other systems seem to favor the coupling of two molecules of amine borane in the metal center without prior hydrogen release. This has been proposed for the TiCp_2 system based on kinetic studies¹⁴ (Scheme 7) and it has also been suggested for a rhodium system where it was possible to obtain

²⁴ Alcaraz, G.; Vendier, L.; Clot, E.; Sabo-Etienne, S. *Angew. Chem. Int. Ed.* **2010**, *49*, 918.

crystallographic evidence of a metal center bearing two coordinated amine boranes.²⁵



Scheme 7. Proposed mechanism for the catalytic dehydrocoupling of DMAB by titanocene species.¹⁴ Some complexes analogous to the adduct on top have recently been isolated for zirconocene species.²⁶

Another example of this behavior was reported by Schneider for a ruthenium system²⁷ for which the linear dimer formed by metal assisted dehydrocoupling of two molecules of amineborane.

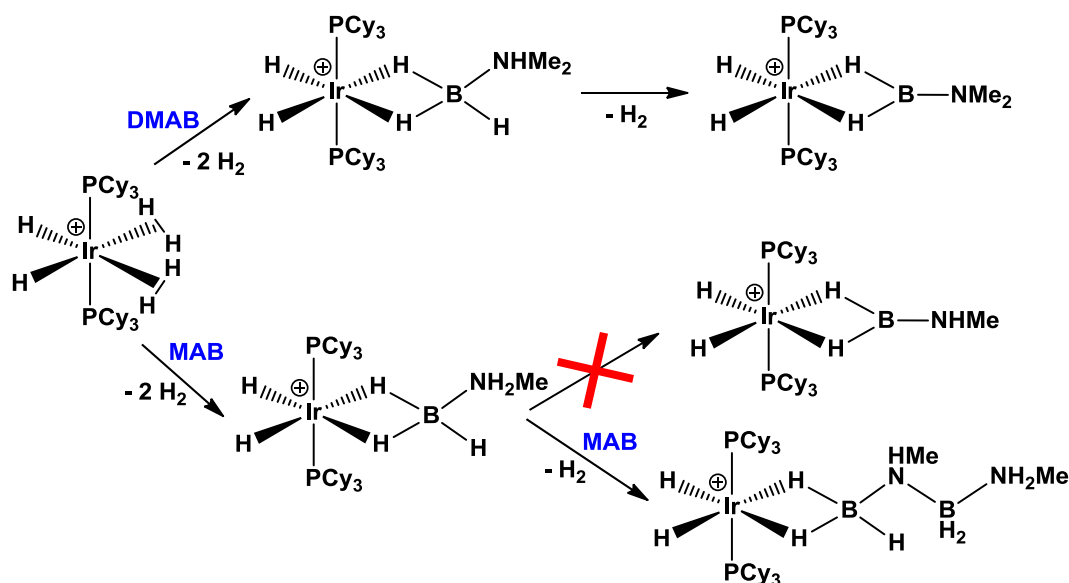
Methylamine borane $\text{NH}_2\text{Me}\cdot\text{BH}_3$ (MAB) polymerization studies by Manners⁴ with a variety of catalysts indicated that the metal center is involved both in an initial dehydrogenation of MAB to produce the aminoborane monomer and also in the chain growth by dehydrogenative coupling to additional MAB.

²⁵ Dallanegra, R.; Chaplin, A. B.; Weller, A. S. *Angew. Chem. Int. Ed.* **2009**, *48*, 6875.

²⁶ Helten, H.; Dutta, B.; Vance, J. R.; Sloan, M. E.; Haddow, M. F.; Sproules, S.; Collison, D.; Whittell, G. R.; Lloyd-Jones, G. C.; Manners, I. *Angew. Chem. Int. Ed.* **2013**, *52*, 437.

²⁷ Friedrich, A.; Drees, M.; Schneider, S. *Chem. Eur. J.* **2009**, *15*, 10339.

Interesting reactivity is observed for the $[\text{IrH}_2(\text{PCy}_3)_2]^+$ catalyst described above.¹⁰ Whereas the DMAB σ -complex can evolve to the aminoborane adduct in the absence of any excess of DMAB, the methylamine borane (MAB) adduct is stable unless further MAB is added. Addition of a second equivalent of MAB resulted in the formation of an Ir bound linear dimer complex (Scheme 8).²⁸ This indicates that in some cases the interaction with another molecule of amineborane is necessary to facilitate dehydrogenation and this is probably related to the observation of linear dimers.



Scheme 8. Complex $\text{IrH}_2(\text{H}_2)_2(\text{PCy}_3)_2^+$ presents different behavior for stoichiometric reactions with DMAB or MAB

Linear dimer adducts have also been isolated for Rh complexes bearing phosphine ligands^{12,5,29} and in all cases they were stable towards dehydrocoupling in the absence of excess of DMAB or further IV. This indicates that a simple intramolecular process is not occurring and points again towards the importance of intermolecular interactions and dihydrogen bonds³⁰ in lowering the barriers for

²⁸ Johnson, H. C.; Robertson, A. P. M.; Chaplin, A. B.; Sewell, L. J.; Thompson, A. L.; Haddow, M. F.; Manners, I.; Weller, A. S. *J. Am. Chem. Soc.* **2011**, *133*, 11076.

²⁹ Dallanegra, R.; Chaplin, A. B.; Tsim, J.; Weller, A. S. *Chem. Commun.* **2010**, *46*, 3092.

³⁰ a) Chen, X.; Bao, X.; Zhao, J.-C.; Shore, S. G. *J. Am. Chem. Soc.* **2011**, *133*, 14172; b) Li, J.; Kathmann, S. M.; Hu, H.-S.; Schenter, G. K.; Autrey, T.; Gutowski, M. *Inorg. Chem.* **2010**, *49*, 7710.

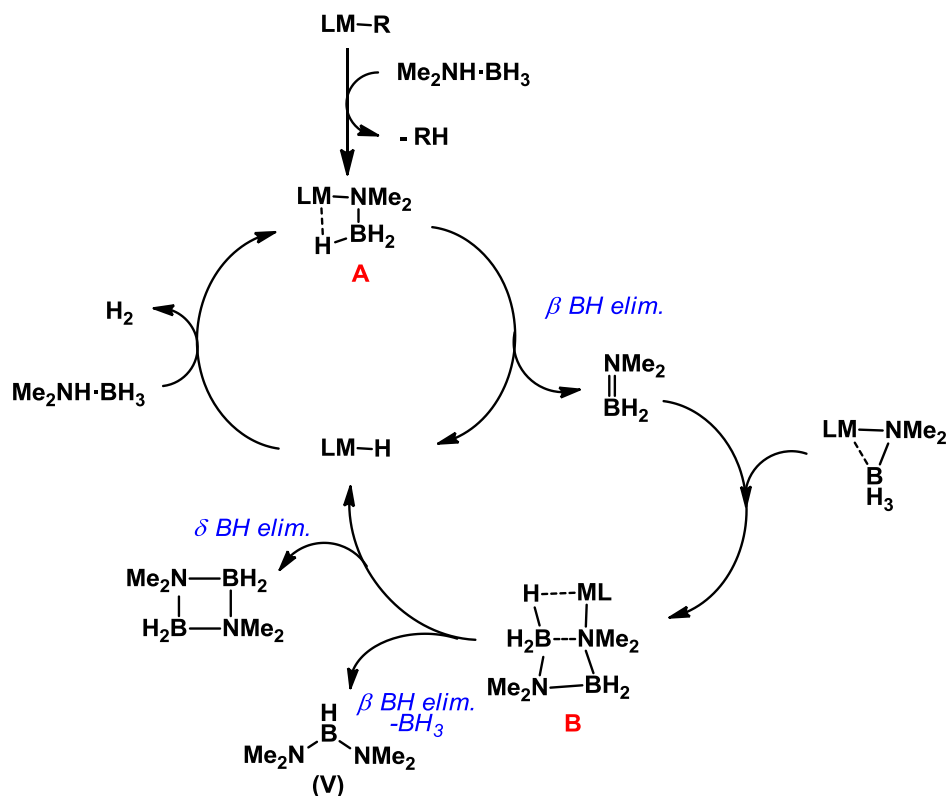
dehydrogenation, painting an even more complex picture of the mechanism of the overall reaction.

Thus it appears that unlike the coupling of aminoborane monomers to yield the cyclic dimer, which can happen off-metal, dehydrogenative cyclation of the linear dimer needs to be catalyzed by a metal. This was actually tested by Manners in one of the first reports about dehydrogenation of amino boranes.³¹ The linear dimer was independently synthesized but evolution to the cyclic dimer was only observed in the presence of the $[\text{RhCl}(\text{cod})]_2$ catalyst. Similar experiments were carried out by Schneider,²⁷ as calculations showed that the transformation of DMAB and linear dimer to the cyclic dimer was kinetically feasible but thermodynamically unfavored in the absence of catalyst. As predicted, mixtures of DMAB and linear dimer **IV** were stable if no ruthenium catalyst was added. Interestingly, in this system aminoborane was detected as an intermediate in the dehydrogenation of **IV** to yield **III**, which suggests that the metal is also involved in B–N cleavage processes.

As for the main group metals mentioned in the previous section, the mechanism of the dehydrogenation reaction appears to be quite similar in all cases³² and after initial NH activation the mechanism seems to proceed via intermediates in which species analogous to the linear dimer are coordinated to the metal center.

³¹ Jaska, C. A.; Temple, K.; Lough, A. J.; Manners, I. *J. Am. Chem. Soc.* **2003**, *125*, 9424.

³² Less, R. J.; Melen, R. L.; Wright, D. S. *RSC Advances* **2012**, *2*, 2191.



Scheme 9. Proposed mechanism for the dehydrogenation of DMAB catalyzed by group 2 metals.¹⁶

As seen in Scheme 9, after NH deprotonation of DMAB to form a $[M]-NMe_2BH_3$ species (**A**), β B–H elimination yields aminoborane and a metal hydride, both of which can be detected experimentally depending on the metal of choice. It is proposed that hydrogen is produced by deprotonation of a second molecule of DMAB by the metal hydride, thus regenerating $[M]-NMe_2BH_3$. Aminoborane can insert into this metal complex to yield a new species detected experimentally bearing a coordinated $[BH_3NMe_2BH_2NMe_2]^-$ ion (**B**). This anion is the NH deprotonated version of linear dimer $BH_3NMe_2BH_2NHMe_2$, which was never observed free in solution. The observed boron-containing reaction products are formed from the complex bearing the $[BH_3NMe_2BH_2NMe_2]^-$ ion. δ BH elimination results in the formation of the cyclic dimer $[BH_2NMe_2]_2$, whereas β BH elimination, followed by BH_3 loss releases diaminoborane $BH(NMe_2)_2$ (**V**), which is present in small amounts after reaction completion. Both reactions regenerate the metal hydride, thus closing the catalytic cycle.

Not all reported systems for the dehydrogenation of DMAB involve the participation of linear dimer **IV** or related species. As a way of an example, this species is not detected when the cationic rhodium complexes bearing chelating phosphines reported by Manners and Weller are used.³³ In these systems diamminoborane (**V**) was observed as an intermediate, along with an unidentified boron-containing species and both were consumed upon reaction completion. However, no further mechanistic information was provided in this case.

Another examples where the linear dimer is not observed are the photogenerated carbonyl species of group 6 metals prepared by Shimoi³⁴ from $[M(CO)_6]$ precursors ($M = Cr, Mo, W$) and that derived from $[FeCp(CO)_2]_2$ reported by Manners.³⁵ This latter species actually proved to be inactive in the dehydrocoupling of independently prepared **IV**. The rhenium nitrosyl complex reported by Berke³⁶ also appeared to proceed without the intermediacy of the linear dimer.

From all these examples it appears that in systems where aminoborane (NR_2BH_2) metal adducts or related species can be observed and even isolated, such as Weller's group 9 phosphine complexes or Manners' $TiCp_2$ system, the linear dimer **IV** is seen as an intermediate, whereas for systems that do not appear to coordinate **II** this species dimerizes in an off-metal process to yield **III** directly. A similar rationale was used by Baker to explain the different products obtained in ammonia borane dehydrogenation, suggesting that catalysts that were able to strongly bind BH_2NH_2 produced the insoluble cyclic pentamer $[BH_2NH_2]_5$ as the main product, whereas borazine and polyborazylene (PB) were observed for catalysts that released BH_2NH_2 in solution.³⁷ This hypothesis was experimentally tested by carrying out the catalytic dehydrogenation of AB in the presence of cyclohexane, which traps any free aminoborane by forming the hydroboration product Cy_2BNH_2 . When the catalyst was $[RhCl(cod)]_2$, which typically yields

³³ Dallanegra, R.; Robertson, A. P. M.; Chaplin, A. B.; Manners, I.; Weller, A. S. *Chem. Commun.* **2011**, 47, 3763.

³⁴ Kawano, Y.; Uruichi, M.; Shimoi, M.; Taki, S.; Kawaguchi, T.; Kakizawa, T.; Ogino, H. *J. Am. Chem. Soc.* **2009**, 131, 14946.

³⁵ Vance, J. R.; Robertson, A. P. M.; Lee, K.; Manners, I. *Chem. Eur. J.* **2011**, 17, 4099.

³⁶ Jiang, Y.; Berke, H. *Chem. Commun.* **2007**, 3571.

³⁷ Pons, V.; Baker, R. T.; Szymczak, N. K.; Heldebrant, D. J.; Linehan, J. C.; Matus, M. H.; Grant, D. J.; Dixon, D. A. *Chem. Commun.* **2008**, 6597.

borazine and PB, only Cy_2BNH_2 was observed. However, when $\text{Ir}(\text{H})_2(\text{POCOP})$ was used, which produces the cyclic pentamer as the AB dehydrogenation product, the outcome of the reaction was not altered. Heating this reaction, which would facilitate the dissociation of aminoborane from the iridium center did in fact lead to the partial conversion to Cy_2BNH_2 .

CHAPTER 2. RESULTS AND DISCUSSION

Reactivity of 14 electron T-shaped Pt(II) complexes with amine boranes

The reactivity of 14 electron T-shaped Pt(II) complexes with bulky carbene ligands towards arenes, halogens and hydrogen has already been studied by our group. Electron deficient transition metal complexes of the type $[M(PR_3)_2]^+$ ($M = Rh, Ir$) have been extensively studied for the dehydrogenation of ammonia borane and related amine boranes,¹ so we decided to test this reactivity with our platinum species. No catalytic studies with platinum complexes under homogeneous conditions have been reported for this transformation yet. As for other group 10 metals, a few very active palladium catalysts have been reported² and as for nickel, a NHC-Ni(0) complex by Baker et al. is in fact the catalyst that promotes the most extensive H_2 release from ammonia borane reported to date.³

2.1. Catalytic reactions

Several methods were used to monitor the progress of the catalytic reactions. Initially, the increasing gas pressure due to H_2 release was measured using a Man on the Moon series X102 kit, which monitors the variation of pressure and temperature of the gas phase inside a closed reaction flask.⁴ The reaction flask is connected to a switchable 3-way valve via a Thorion screw through polyamide

¹ (a) Stevens, C. J.; Dallanegra, R.; Chaplin, A. B.; Weller, A. S.; Macgregor, S. A.; Ward, B.; McKay, D.; Alcaraz, G.; Sabo-Etienne, S.; *Chem.—Eur. J.* **2011**, *17*, 3011; (b) Sewell, L. J.; Lloyd-Jones, G.C.; Weller, A.S. *J. Am. Chem. Soc.* **2012**, *134*, 3598–3610.

² (a) Kim, S.K.; Han, W. S.; Kim, T. J.; Kim, T. Y.; Nam, S. W.; Mitoraj, M.; Piekos, L.; Michalak, A.; Hwang, S. J.; Kang, S. O. *J. Am. Chem. Soc.* **2010**, *132*, 9954; (b) Vogt, M.; de Bruin, B.; Berke, H.; Trincado, M.; Grützmacher, H. *Chem. Sci.* **2011**, *2*, 723.

³ Keaton, R.J.; Blacquiere, J.M.; Baker, R.T. *J. Am. Chem. Soc.* **2007**, *129*, 1844.

⁴ www.manonthemoontech.com

tubing. The valve can be switched between two positions, one of them connecting the reactor vessel to the exterior so that it can be used like a conventional Schlenk flask. The other position connects the flask to the pressure transducer, thus closing the system. The assembled device is depicted in Figure 1.

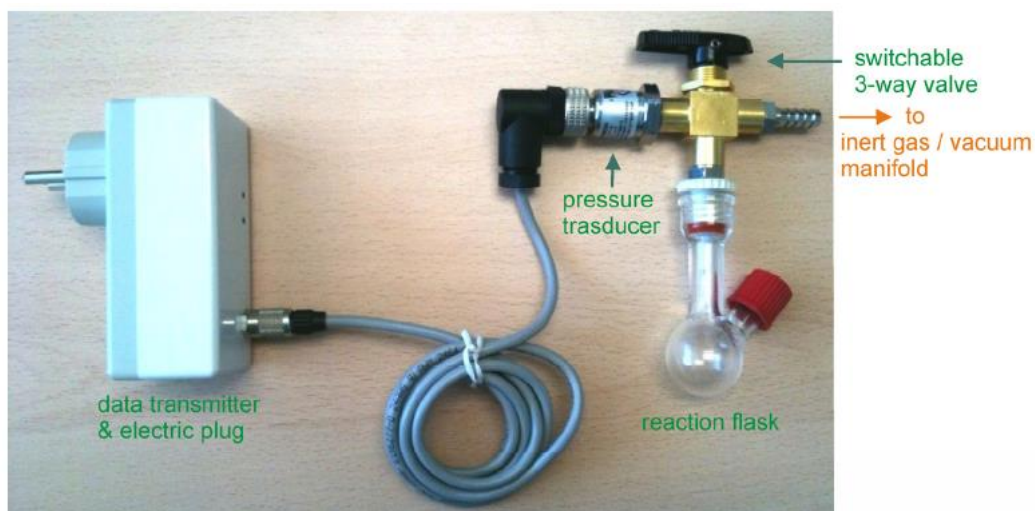
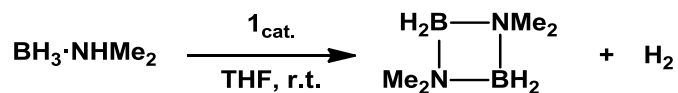


Figure 1. Man on the moon series X102 kit⁴

Reaction progress was also monitored by ¹¹B NMR spectroscopy, by recording the decreasing integral values of the amine borane peak over time.

2.1.1. Catalytic reactions in open systems

Initial screening of our family of platinum complexes indicated that complex [Pt(^tBu')(^tBu)][B(Ar^f)₄] **1** was the most efficient for the catalytic dehydrogenation of amine boranes, providing the shorter reaction times. Among the different substrates tested, DMAB appeared to dehydrogenate the fastest, requiring less than 15 min in THF at room temperature to be completely consumed (Scheme 1).



Scheme 1. Catalytic dehydrogenation of dimethylamine borane (DMAB)

The dimer $[\text{NMe}_2\text{BH}_2]_2$ is the only detectable product at the end of the reaction, whereas the catalyst is transformed into the T-shaped Pt(II) hydrido species $[\text{PtH}(\text{tBu})_2][\text{B}(\text{Ar}^f)_4]$, formed by hydrogenation of complex **1**. The simplicity of the ^1H NMR of complex **1** (compared with other cyclometallated derivatives such as **2** and **3**) along with the fact that the dehydrogenated products of DMAB and possible intermediates are usually very soluble in common organic solvents led us to study the catalytic dehydrogenation of DMAB under several substrate concentrations and catalysts loadings.

Even though we did not carry out an in-depth kinetic study for the dehydrogenation of DMAB, some information about the reaction kinetics was obtained by ^{11}B NMR monitoring of the catalytic DMAB dehydrogenation reactions in open systems.

Reactions performed in THF with a relative high catalyst loading (5 mol%) and varying concentrations of amineborane presented a first order dependency on the concentration of DMAB. For a first order reaction, the rate constant k depends only on the concentration of one of the reactants as in

$$r = -\frac{d[\text{DMAB}]}{dt} = k[\text{DMAB}]$$

which can be expressed as

$$\ln[\text{DMAB}] = -k \cdot t + \ln[\text{DMAB}]_0$$

Therefore, representing $\ln[\text{DMAB}]$ versus time should result in a linear profile if the reaction presents first order behavior.

Our experimental data, the integral values of the DMAB ^{11}B NMR signal, are directly related to the DMAB concentration and representation of $\ln[\text{DMAB integral}]$ over time shows a linear dependency (insets in Figure 2 and Figure 3), indicating first order kinetics for these reaction conditions.

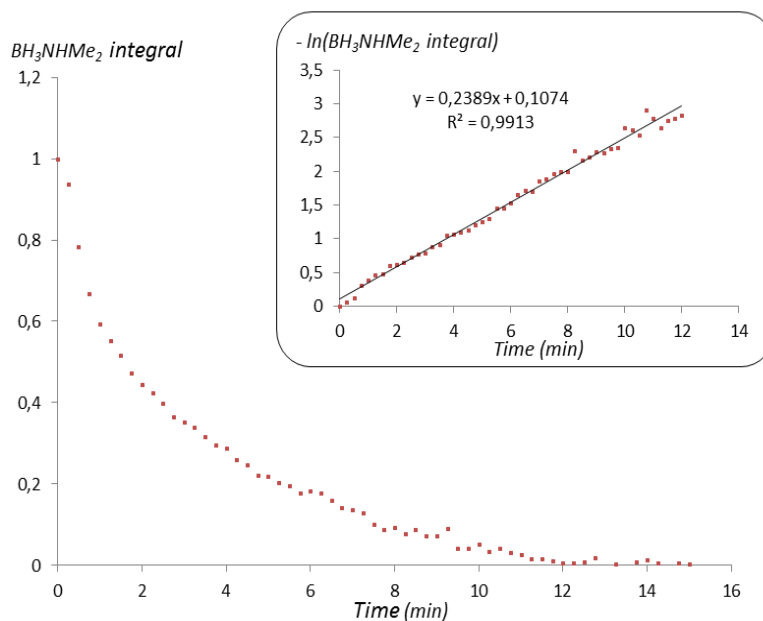


Figure 2. BH_3NHMe_2 normalized integral value plotted against time for the catalytic dehydrogenation of a 0.270M solution of BH_3NHMe_2 with 5 mol% of **1**.

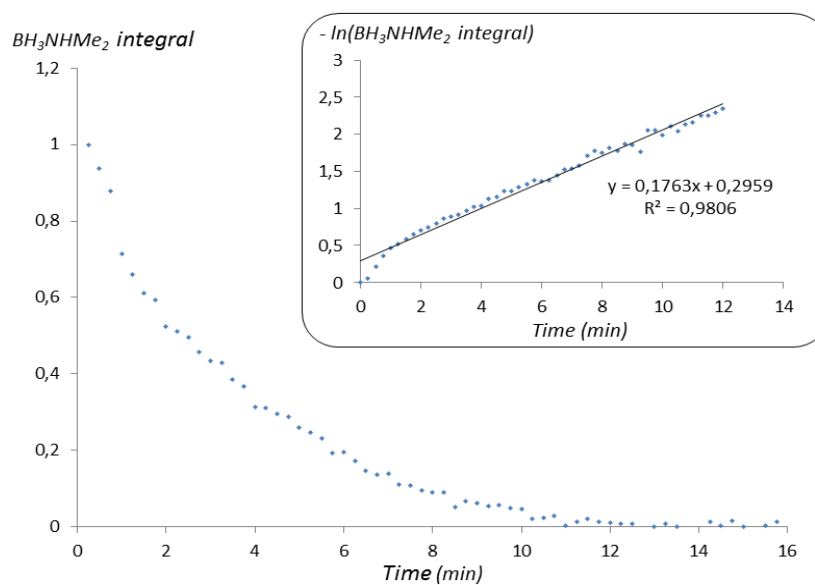


Figure 3. BH_3NHMe_2 normalized integral value plotted against time for the catalytic dehydrogenation of a 0.135M solution of BH_3NHMe_2 with 5 mol% of **1**.

As can be seen for the reaction profiles in Figure 2 and Figure 3, consumption of DMAB is complete after 12 minutes at room temperature.

For reactions with lower catalyst loadings (2.5 mol% and lower), a zero-order dependency is found, as can be seen in Figure 4. In this plot of the concentration of DMAB versus time, the presence of an induction period is observed.

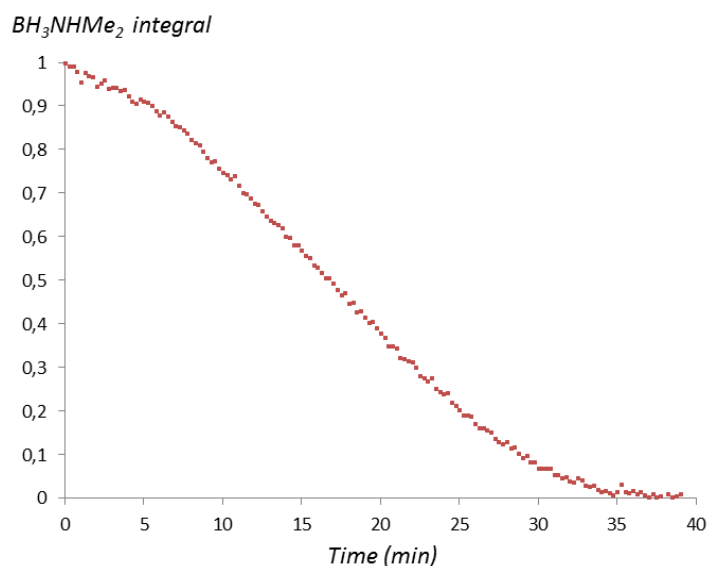


Figure 4. BH_3NHMe_2 normalized integral value plotted against time for the catalytic dehydrogenation of a 0.270M solution of BH_3NHMe_2 with 2.5 mol% of **1**.

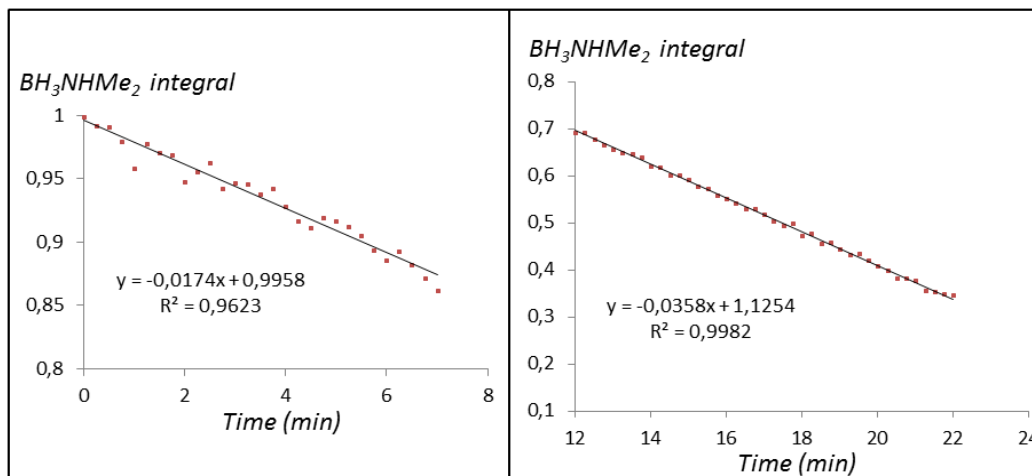


Figure 5. Linear fitting for the different slopes of the zero order dehydrogenation reaction (Figure 4) at the early stages (left) and after induction period (right).

Figure 5 shows the linear fitting for the two different regimes, during and after the induction period.

Closer inspection of Figure 2 and Figure 3 reveals that an induction period was also present in these first order reactions, albeit shorter than in reactions with lower catalysts loadings. This behavior will be discussed below when analyzing the mechanism of the platinum catalyzed dehydrogenation reaction, but it is anticipated that this induction period is not due to the formation of platinum colloids or nanoparticles, since poisoning experiments in the presence of elemental mercury seem to have no effect on the rate of the dehydrogenation reaction.

2.1.2. Catalytic reactions in closed systems

Reactions monitored in closed systems (NMR tubes or the X102 kit reaction vessel) revealed the influence of H_2 pressure build-up in the velocity of the reaction. It was found that H_2 competes with the amine borane for coordination to the platinum center and accordingly it was observed that the reaction slowed down as the concentration of H_2 increased. In some test experiments carried out with concentrated amine borane solutions in NMR tubes, which present a smaller

volume than the Man on the Moon reaction vessels, it was observed that the reaction did not reach completion even after long reaction times. For example, Figure 6 shows how after fast DMAB consumption for the first 30 minutes of the reaction, dehydrogenation slows down and 40% of DMAB was still unreacted after 15 hours at room temperature.

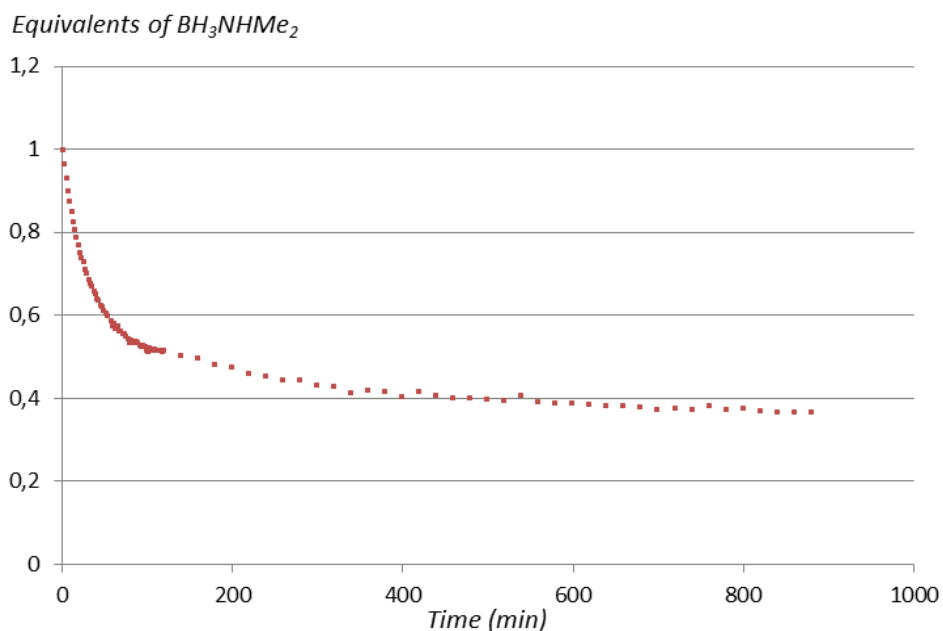


Figure 6. ^{11}B NMR monitoring of the catalytic dehydrogenation of a 0.135M solution of BH_3NHMe_2 in THF with 5 mol% of **1a** in a closed NMR tube. The plot of the normalized integral value of the BH_3NHMe_2 peak (δ_B 5.1) over time is depicted.

In contrast, Figure 7 shows the monitoring of a similar reaction with the same amount of catalyst but with twice the concentration of DMAB. In this case the experiment was run in the X102 kit reaction vessel with a much larger volume available for the released H_2 than an NMR tube. This reaction does reach completion, with the production of 1 equivalent of H_2 in 30 minutes. This is more than twice as slow as an equivalent reaction monitored in an open system.

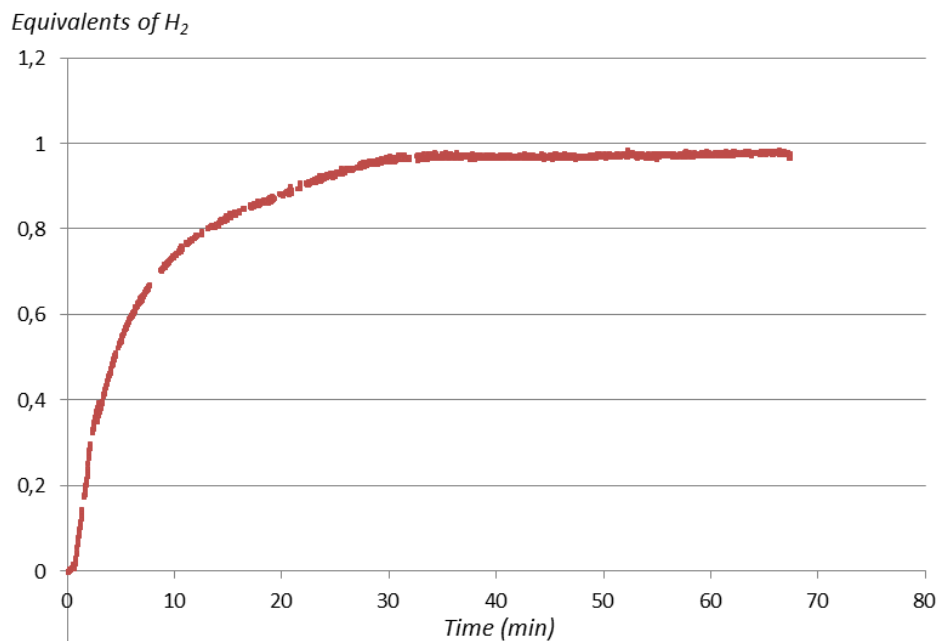


Figure 7. Monitoring of the amount of H₂ released in the catalytic dehydrogenation of a 0.270 M solution of BH₃NHMe₂ in THF with 5 mol% of **1a** in a closed reaction vessel.

To ascertain the velocity of the reaction without the influence of H₂ pressure build-up, the progress of the dehydrogenation was monitored with ¹¹B NMR in open tubes. Exposure to air and consequently moisture did not affect these tests as the reactions were faster than diffusion of air into the solution and indeed no hydrolysis products of DMAB were detected.

Figure 8 shows a comparison of the monitoring of the same catalytic reaction depicted in Figure 6, carried out in a closed NMR tube, and an identical reaction that was monitored in an open tube (Figure 3). The latter reached completion in around 12 minutes, whereas only 20 % of DMAB had reacted in a closed tube at the same reaction time.

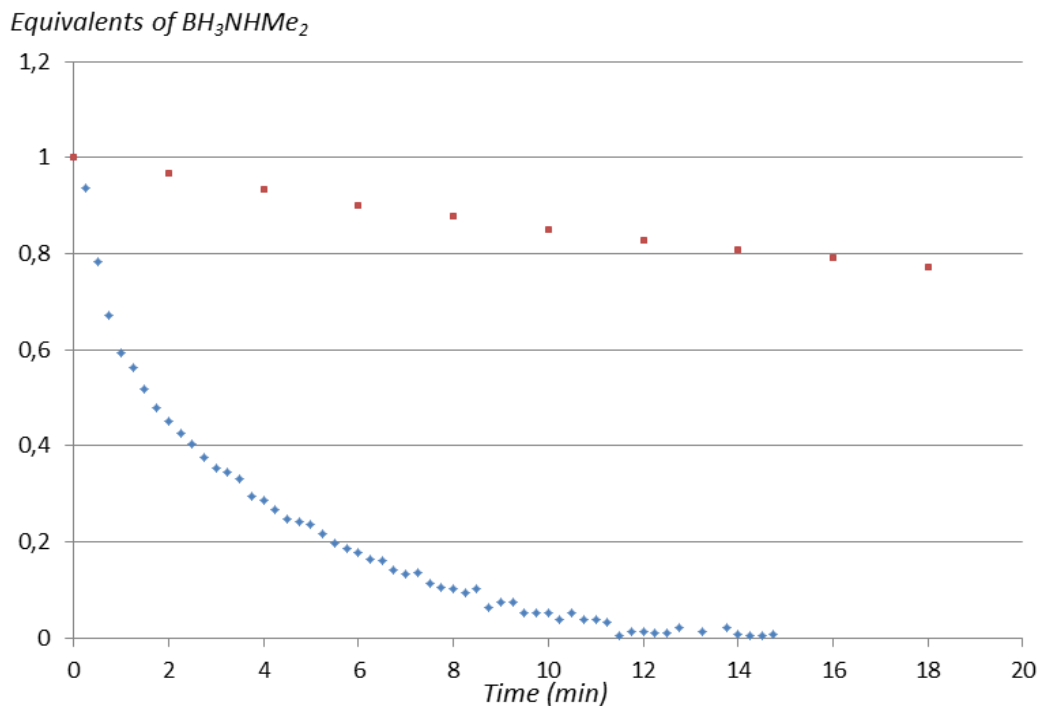
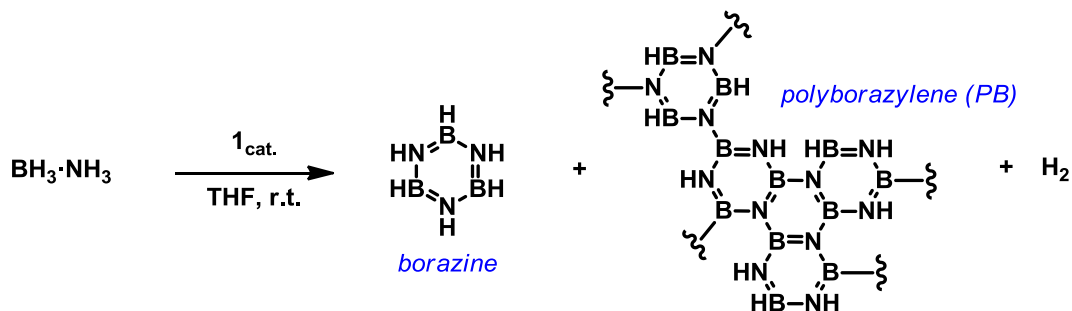


Figure 8. ^{11}B NMR monitoring of the catalytic dehydrogenation of a 0.135M solution of BH_3NHMe_2 in THF with 5 mol% of **1** in a closed NMR tube (red) and in an open tube (blue). The plot of the normalized integral value of the BH_3NHMe_2 peak ($\delta_{\text{B}} -13.6$) over time is depicted.

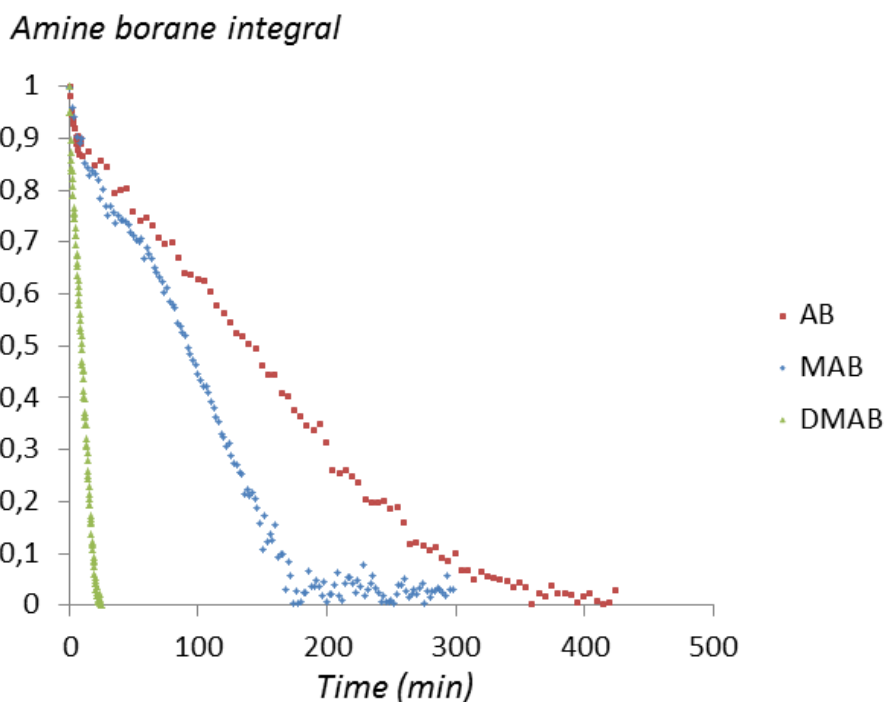
2.1.3. Catalytic reactions for other amineboranes

Before studying the mechanism of the reaction of complex **1** with **DMAB** we have tested other amine-boranes under similar reaction conditions. The catalytic dehydrogenation of ammonia-borane (AB, $\text{NH}_3\cdot\text{BH}_3$) was found to be much slower than that of DMAB. As depicted in Figure 9 consumption of ammonia borane was completed in over 6 hours, having released 1 equivalent of H_2 at this point. However, further dehydrogenation took place as the final reaction products were borazine and polyborazylene (Scheme 2).



Scheme 2. Final products of the catalytic dehydrogenation of AB.

Primary amine methylamine borane showed an intermediate behavior, and was consumed in 3 hours in the same reaction conditions, as can be seen in Figure 9. In this case polymeric species were formed. This reactivity trend indicates that for our system the more basic the amine, the faster the dehydrogenation proceeds.

Figure 9. ^{11}B NMR monitoring of the catalytic dehydrogenation of 0.270 M solutions of various amine boranes in THF with 5 mol% of **1** in an open NMR tube

2.2. Coordination modes of borane-Lewis base adducts to transition metal complexes. The first step towards dehydrogenation.

Shimoi et al. introduced the chemistry of borane-Lewis base adducts in 1999 with the study of a series of transition metal complexes of general formula $[L_nM(\eta^1\text{-H}_3\text{B}\cdot\text{A})]$, where A is a tertiary amine or phosphine.⁵ In these species, the borane interacts in an end-on η^1 fashion with the metal center (Figure 10, left). Calculations show that this bond involves mainly electron donation from the borane σ_{BH} orbital to the metal, with negligible back-donation into the σ^*_{BH} which lies high in energy.

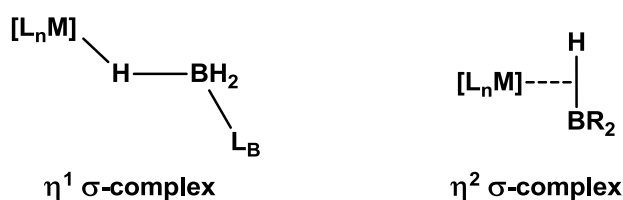


Figure 10. σ -borane complexes.

This bonding mode differs from that of tricoordinate borane species, which present a side-on η^2 coordination of the B–H bond to the metal. These compounds, known as true σ -borane complexes, present significant back-donation from the metal to an empty p orbital of the boron atom.⁶

In Shimoi-type complexes, the tetracoordinate borane adduct acts as a two electron donor and presents high affinity for electrophilic metal centers that offer no possibilities for back-donation.

2.3. σ -borane adducts of $\text{BH}_3\cdot\text{NR}_3$ and electron deficient Pt(II) complexes

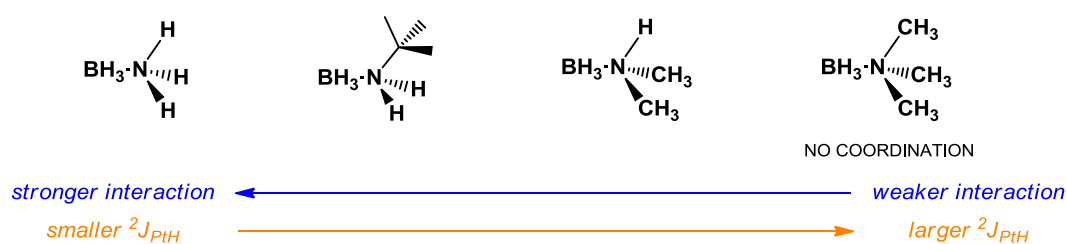
In an attempt to understand the possible interaction between amine borane adducts and the platinum center in our family of electron deficient complexes, we studied 1:1 mixtures of a variety of amine boranes (BH_3NH_3 , $\text{BH}_3\text{NH}_2^t\text{Bu}$,

⁵ Shimoi, M.; Nagai, S.; Ichikawa, M.; Kawano, Y.; Katoh, K.; Uruichi, M.; Ogino, H. *J. Am. Chem. Soc.* **1999**, *121*, 11704.

⁶ Alcaraz, G.; Sabo-Etienne, S. *Angew. Chem. Int. Ed.* **2010**, *49*, 7170.

BH₃NHMe₂ and BH₃NMe₃) and complexes **1-3**, **15** and **16** in both CD₂Cl₂ and d₈-THF. The most interesting feature of the ¹H NMR spectra of these samples was the appearance of a broad signal integrating 3H for the BH₃ unit with a chemical shift at a higher field than that of the free amine borane (Table 1). This signal appeared as a broad peak that sharpened upon ¹¹B decoupling. In some instances, satellites due to coupling to ¹⁹⁵Pt were observed in the ¹H{¹¹B} NMR spectra, clearly indicating that it is the BH hydrogens which are interacting with the platinum center and not the NH hydrogens. Coordination of the amine borane to the platinum center was also reflected in the diminished value of the ²J_{PtH} constant of the protons of the methyl or methylene unit *trans* to the coordination site.

As expected, sterically demanding groups at the nitrogen atoms of the NHCs makes coordination of amine-boranes more difficult, and on the other hand, bulkier NR₃ groups on the amine-borane exert a strong influence on its coordination. For example, when we studied the coordination of progressively larger ammonia borane (NH₃·BH₃), *t*-butylamine borane (N^{*t*}BuH₂·BH₃), dimethylamine borane (NMe₂H·BH₃) and trimethylamine borane (NMe₃·BH₃) to complex **1**, it was observed that whereas the first two species coordinated to the metal center, dimethylamine borane interacted much more weakly as evidenced by the fact that all DMAB signals broadened to the point of merging into the baseline. This suggests that a fast exchange between coordinated and non-coordinated DMAB is taking place. In this case the smaller value of the ²J_{PtH} constant of the Pt–CH₂ protons, at 103 Hz, was indicative of DMAB coordination (c.f. unsaturated complex **1**, with ²J_{PtH} = 120 Hz).



Scheme 3. Various amine boranes ordered in decreasing coordination capabilities to metal complex **1**.

Interestingly, trimethylamine borane was too bulky to interact at all with the platinum centre, and chemical shifts of both **1** and NMe₃·BH₃ appeared as those of

the free species in the 1:1 mixture. In contrast, complex **16**, which has isopropyl instead of *tert*-butyl groups and therefore presents less steric hindrance around the metal center,⁷ can form adducts detected by ¹H NMR with all of the above amine boranes. The chemical shifts and coupling constants for all these adducts are summarized in Table 1.

⁷ As discussed in the introduction to this chapter: %V_{bur} = 27.9 (IⁱPr₂Me₂), 34.2 (IMes), 35.8 (IPr), 37.0 (I^tBu).

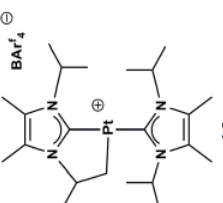
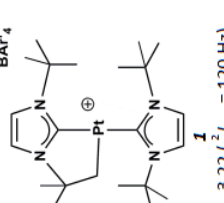
	BH ₃ NH ₃	BH ₃ NH ₂ tBu	BH ₃ NHMe ₂	BH ₃ NMe ₃
¹ H-NMR Free amine borane  16 3.64 (³ J _{FHH} = 144 Hz) 2.84 (² J _{FHH} = 115 Hz) 1.92 (¹ J _{FHH} = 88 Hz)	BH ₃ : 1.52 ppm NH ₃ : 3.38 ppm BH ₃ : -21.8 ppm At 0°C BH ₃ : 0.29 ppm, (¹ J _{FHH} = 117 Hz) 3.33 (NH ₃) 4.10 (³ J _{FHH} = 100 Hz) 2.43 (² J _{FHH} = 98 Hz) 1.68 (¹ J _{FHH} = 77 Hz)	BH ₃ : 1.36 ppm NH ₂ tBu: 1.27 ppm NH ₂ tBu: 3.45 ppm BH ₃ : -21.1 ppm At 0°C BH ₃ : -0.16 ppm (¹ J _{FHH} = 116 Hz) 3.17, 3.07 (NH ₂ tBu), 1.17 (NH ₂ tBu) 4.05 (³ J _{FHH} = 102 Hz) 2.43 (² J _{FHH} = 99 Hz) 1.68 (¹ J _{FHH} = 78 Hz)	BH ₃ : 1.53 ppm NHMe ₂ : 2.53 ppm NHMe ₂ : 3.68 ppm BH ₃ : -13.6 ppm At 0°C BH ₃ : 0.13 ppm (¹ J _{FHH} = 117 Hz) 2.96 (NHMe ₂), 2.52 (NHMe ₂) 4.05 (³ J _{FHH} = 101 Hz) 2.28 * 1.57 * * ² J _{FHH} could not be measured due to signal overlap	BH ₃ : 1.64 ppm NMe ₃ : 2.61 ppm BH ₃ : -8.5 ppm At 0°C BH ₃ : -0.10 ppm (No ¹ J _{FHH} observed) 2.52 (NMe ₃) 3.99 (³ J _{FHH} = 106 Hz) 2.44 (² J _{FHH} = 93 Hz) 1.63 (¹ J _{FHH} = 78 Hz)
¹¹ B-NMR  1 3.22 (² J _{FHH} = 120 Hz)	BH ₃ : 0.59 ppm 3.39 (NH ₃) ¹¹ B-NMR: -19.3 2.57 (² J _{FHH} = 97 Hz)	BH ₃ : 0.49 ppm (25°C) 3.21 (NH ₂ tBu) 1.23 (NH ₂ tBu) ¹¹ B-NMR: -18.3 2.60 (² J _{FHH} = 99 Hz)	No signals from BH ₃ NHMe ₂ are seen at 0°-25°C, but the CH ₂ peak shifts and changes its ² J _{FHH} depending on the temperature and [BH ₃ NHMe ₂] 3.01 (² J _{FHH} = 103 Hz) at 0° C	BH ₃ : 1.64 ppm 2.61 (NMe ₃) ¹¹ B-NMR: -8.56 3.22 (² J _{FHH} = 120 Hz) (No interaction)

Table 1

A value around 117 Hz for the $^1J_{\text{PtH}}$ constant of the BH_3 protons was found for all adducts in dichloromethane. There are few examples in the literature for species containing Pt-H-B interactions, mainly coordination compounds of boron clusters. We have found only one example of a BH unit directly bound to Pt for which a $^1J_{\text{PtH}}$ value was reported, the Pt(IV) complex in Figure 11. For this species, the BH atom interacting with the Pt center resonated at -3.2 ppm and had a $^1J_{\text{PtH}}$ of 330 Hz.⁸ However, it should be pointed out that this example cannot be considered strictly a $\sigma\text{-B-H}$ complex, presenting more of a borohydride character.

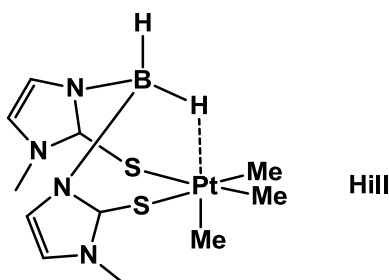


Figure 11. Pt(IV) complex with a reported $^1J_{\text{PtH}}$ value for a B-H bond interacting with a platinum center

Coupling to ^{195}Pt could not be observed in the BH_3 signal of the $^1\text{H}\{^{11}\text{B}\}$ NMR spectra of amine borane adducts of complex **1**. The signal appears as a broad peak upon decoupling, as seen on the inset in Figure 12.

⁸ Crossley, I.R.; Hill, A.F.; Willis, A.C.; *Organometallics* **2005**, *24*, 4889-4892.

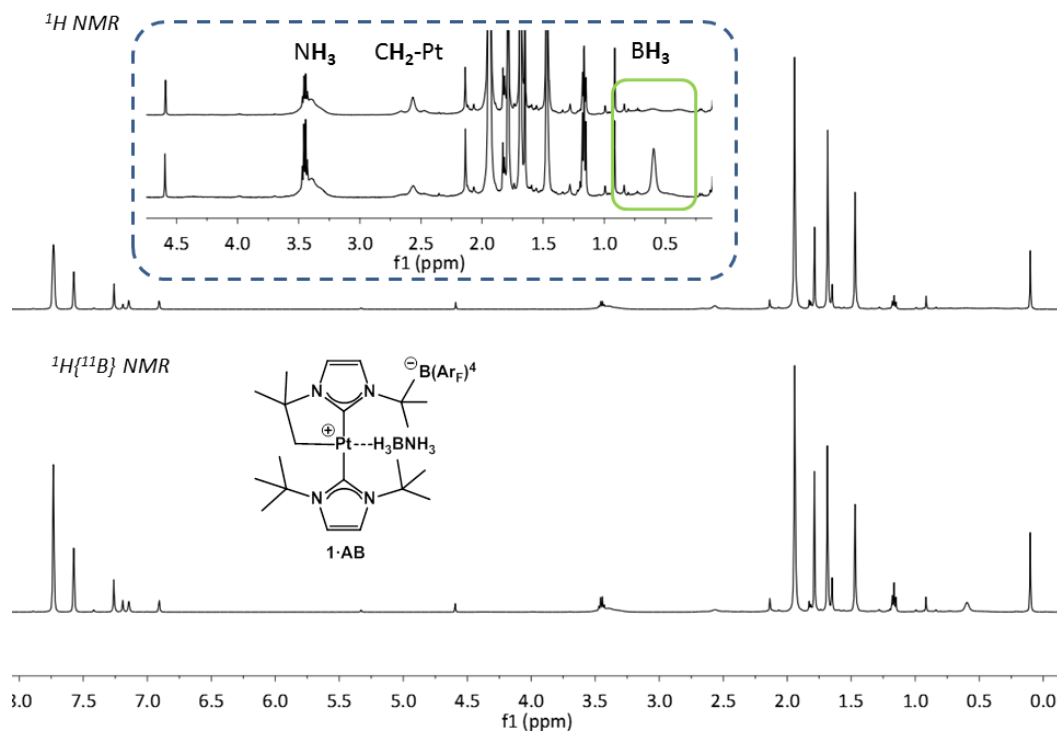


Figure 12. ^1H NMR of a 1:1 mixture of **1** and AB in CD_2Cl_2 at 0°C .

In contrast, adducts of complex **16** usually presented platinum satellites in their BH_3 signals upon ^{11}B decoupling. This indicates a stronger interaction, probably due to the smaller steric hindrance. In fact, the adduct of **16** and trimethylamine borane presents a BH_3 signal with no platinum satellites, similar to complex **1** adducts. Coupling to ^{195}Pt is also observed for complex **15** adducts, where the amine borane signals are clearly identified due to the greater simplicity of the ^1H NMR spectra of this non cyclometallated species (Figure 13).

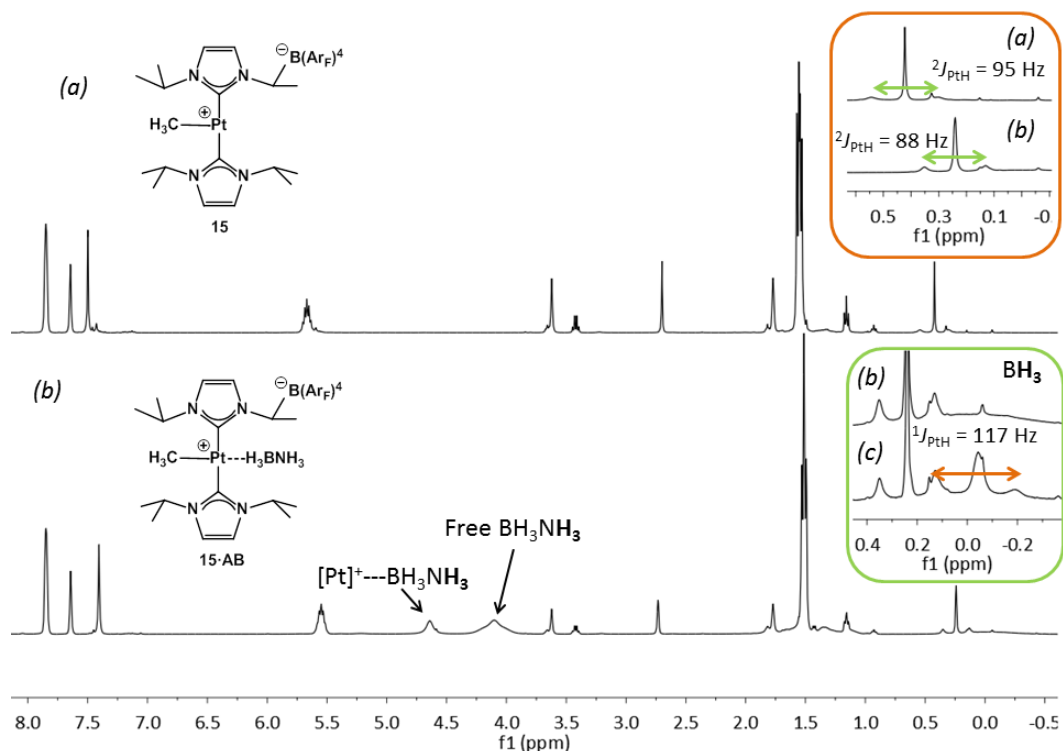


Figure 13. (a) ^1H NMR of complex **15** in d_8 -THF at 0°C ; (b) ^1H NMR of a 1:3 mixture of complex **15** and ammonia borane in d_8 -THF at 0°C ; (c, inset) $^1\text{H}\{^{11}\text{B}\}$ NMR of a 1:3 mixture of complex **15** and ammonia borane in d_8 -THF at 0°C .

An interesting feature that distinguishes amine borane adducts of complexes **1** and **15** is the fact that when an excess of the amine borane is added, in solutions of complex **1** an average signal for the free and coordinated amine borane is seen, whereas for solutions of complex **15** separate signals for the free and coordinated species are observed, as seen in Figure 13. Only one set of signals for the ligand backbone with chemical shifts that differ from those of the T-shaped species are seen in any case. This different behavior points again towards a weaker interaction of AB for adducts of **1**.

The same behavior is observed for adducts of complex **3b**, where signals for free and coordinated AB are clearly distinct. For adduct **3b-AB**, the BH_3 resonates at -1.70 ppm in the ^1H NMR in d_8 -THF at 0°C , with a $^1J_{\text{PtH}}$ of 130 Hz , clearly seen upon ^{11}B decoupling. The higher field chemical shift and larger coupling to ^{195}Pt

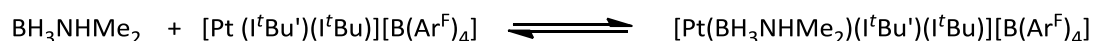
indicates a larger hydride character for the BH₃ hydrogen atoms in **3b·AB** as compared to **15·AB**.

As for IPr complex **2b**, its adduct with AB presents a BH₃ signal at -0.41 ppm in d₈-THF at 0 °C, with a ¹J_{PtH} of 100 Hz.

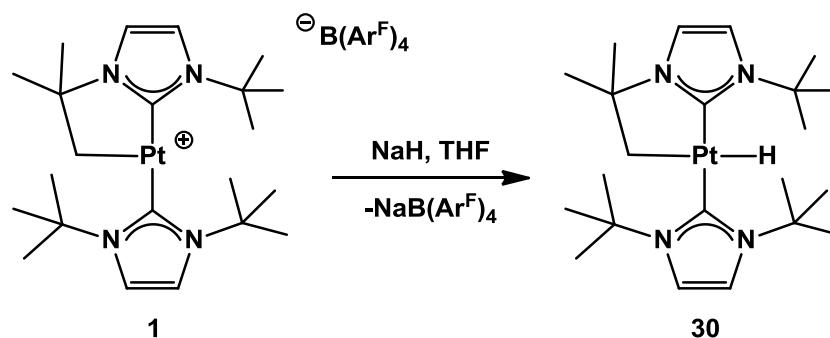
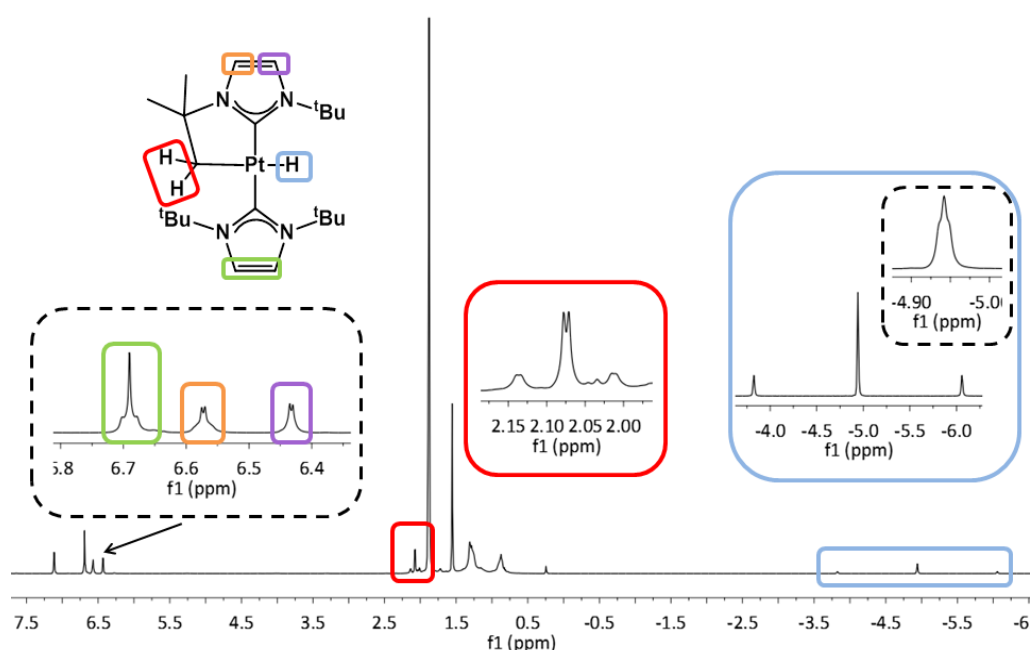
2.4. Dehydrogenation of amine boranes by electron deficient Pt(II) complexes: insights into the mechanism using **1** and DMAB as a model system.

After an initial screening, complex **1** proved to be the most active species towards the dehydrogenation of ammonia borane among our family of T-shaped platinum complexes. This fact coupled with the simplicity of its NMR spectra made us choose it for the study of the mechanism of the metal catalyzed dehydrogenation process. As for the substrate of choice, again for the sake of simplicity, dimethylamine borane (DMAB) was chosen. As opposed to ammonia borane it produces not only soluble dehydrogenation products but a single final dehydrogenated species, the cyclic dimer [BH₂NMe₂]₂.

When a stoichiometric mixture of DMAB and **1** in d₈-THF was analyzed by ¹H NMR spectroscopy at temperatures below 0 °C, the stable σ-B–H complex **1·DMAB** is observed. The signals for this adduct, particularly those of DMAB, shift depending on the temperature and concentration (table 1), indicating that an equilibrium exists between the free and coordinated species:



When the temperature is raised over 0 °C signals of a new platinum species start to appear. This new complex is a platinum hydride (δ_H -5.55, ¹J_{PtH} = 895 Hz) that was identified as the neutral Pt(II) species PtH(I^tBu')(I^tBu) (**30**) and was independently synthesized from **1** and excess NaH in THF (Scheme 4), and fully characterized by NMR and IR spectroscopy, and elemental analysis.

Scheme 4. Synthesis of neutral hydride **30**.Figure 14. ^1H NMR spectrum in C_6D_6 of $\text{PtH}(\text{IBu})'(\text{IBu})$ (**30**)

An interesting feature of the ^1H NMR spectrum of complex **30** (Figure 14) is the fact that the hydride signal is actually a triplet with $^3J_{\text{HH}}$ of 2.8 Hz, being coupled to the protons of the $\text{CH}_2\text{-Pt}$ unit. This latter signal, which resonates at 2.12 ppm also presents coupling to ^{195}Pt , with a $^2J_{\text{PtH}}$ of 894 Hz and appears as a doublet with $^3J_{\text{HH}}$ of 2.8 Hz. The magnitude of this coupling constant is consistent with the formulation of the hydride in *trans* to strong sigma donor ligand (alkyl in the

present case). Longer range couplings to ^{195}Pt are also observed in the signals for the protons in the imidazol backbone.

Very interestingly, the ^1H NMR spectrum of the reaction between **1** and a slight excess of DMAB (3 eq.) shows the formation of a new species derived from BH_3NHMe_2 that grows at the same rate as hydride **30** (Figure 15). This compound is characterized by a broad signal in the ^1H NMR at 6.44 ppm.

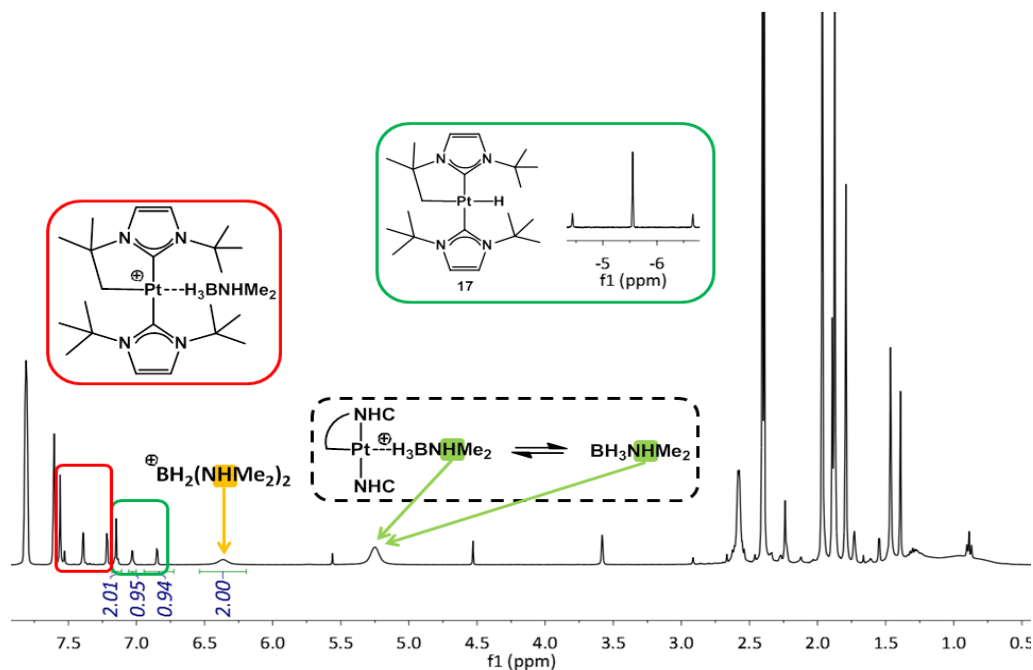
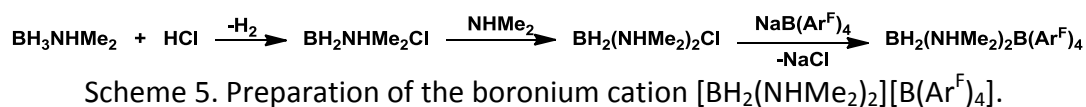


Figure 15. ^1H NMR in d_8 -THF spectrum of **1** with 3 equivalents of DMAB. 5 minutes at 10°C . Note a 1:1 proportion between **30** and the boronium cation $[\text{BH}_2(\text{NHMe}_2)_2]^+$ (**31·NHMe₂**).

This species was identified as the boronium cation $[\text{BH}_2(\text{NHMe}_2)_2]^+$ (**31·NHMe₂**) and its NMR chemical shifts (Figure 32) were confirmed by analyzing an independently synthesized sample that was prepared as shown in Scheme 5, following an adapted literature method.



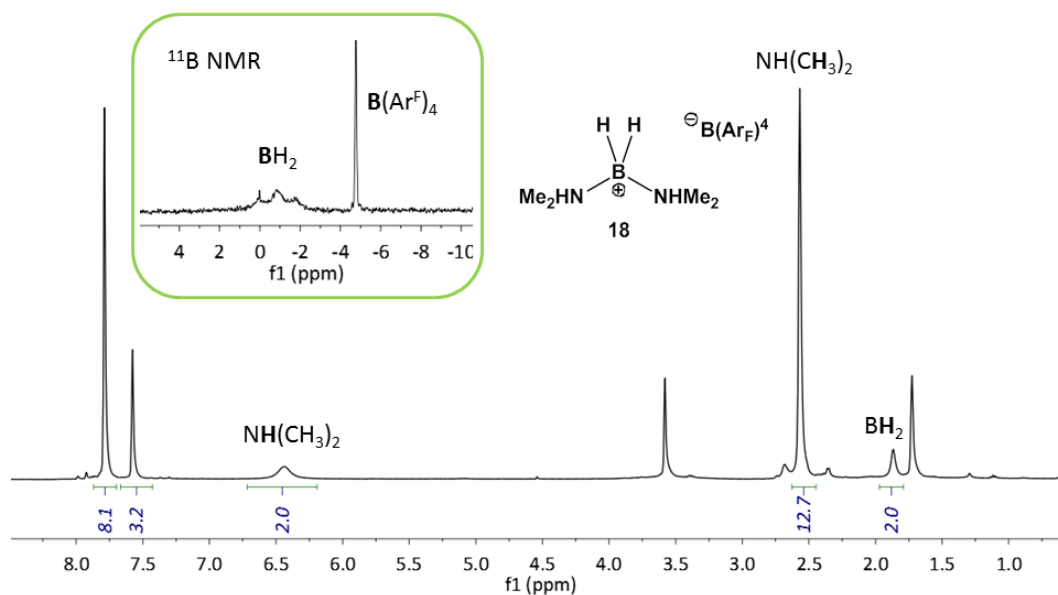


Figure 16. ${}^1\text{H}\{{}^{11}\text{B}\}$ NMR in d_8 -THF of $[\text{BH}_2(\text{NHMe}_2)_2]\text{B}(\text{Ar}^{\text{F}})_4$ (**31·NHMe₂**).

The ${}^1\text{H}$ NMR spectrum of this species confirms that **31·NHMe₂** does form in the reactions between DMAB and **1**. ${}^{11}\text{B}$ decoupling allows for the observation of its BH_2 protons that appear at 1.87 ppm, as depicted in Figure 16. The ${}^{11}\text{B}$ NMR spectrum of **31·NHMe₂** shows a characteristic broad triplet at -2.8 ppm with ${}^1J_{\text{BH}} = 113$ Hz, as well as a singlet signal for the $\text{B}(\text{Ar}^{\text{F}})_4$ anion at -6.7 ppm.

The broad signal of $[\text{BH}_2(\text{NHMe}_2)_2]^+$ is not easy to detect in the ${}^{11}\text{B}$ NMR spectra of reactions between DMAB and **1**, and disappears when the reaction is complete, making it easy to miss. Only the inspection of the ${}^1\text{H}$ NMR spectra of these reactions, where its characteristic NH proton signal at 6.44 ppm is very easy to spot, allowed us to confirm that both **31·NHMe₂** and platinum hydride **30** are present in solution as long as unreacted DMAB is still present.

As we continue to monitor the evolution of the dehydrogenation reaction, and roughly at the same time as the platinum hydride complex **30** and the boronium cation **31·NHMe₂** form, a signal for free H_2 is observed at 4.55 ppm in the ${}^1\text{H}$ NMR spectrum along with the detection of a small sharp peak for BH_2NMe_2 at δ_{B} 37.5 in the ${}^{11}\text{B}$ NMR spectrum, confirming that H_2 loss from BH_3NHMe_2 is taking place. Dimethylaminoborane monomer BH_2NMe_2 rapidly dimerizes to form the more stable $[\text{BH}_2\text{NMe}_2]_2$ dimer which appears in the ${}^{11}\text{B}$ NMR spectrum at 5.1 ppm and

is the final dehydrogenation product. Small amounts of $\text{BH}(\text{NMe}_2)_2$ (δ_{B} 28.7, d, $^1J_{\text{BH}} = 130$ Hz) are also observed at the end of the reaction. The formation of these species will be discussed in a forthcoming section.

As for the fate of the platinum catalyst, the H_2 generated in the reaction competes with DMAB for coordination to **1** and consequently as the H_2 concentration increases a new hydride species **32** starts to form. This complex has already been reported by our group and results from H_2 addition to cyclometallated species **1**. The ^1H NMR spectrum of **32** indicates a very symmetric environment for the $t\text{Bu}$ ligands pointing towards the fact that no cyclometallated *tert*-butyl groups are present in this species. The most striking feature of its ^1H NMR spectrum is the presence of a hydride signal at -25.6 ppm with a large $^1J_{\text{PtH}}$ coupling of 2491 Hz in d_8 -THF, indicative of a T-shaped 14 electron species. The formation of this hydride is reversible and H_2 loss under mild heating or just by subjecting complex **32** to vacuum yields complex **1** again

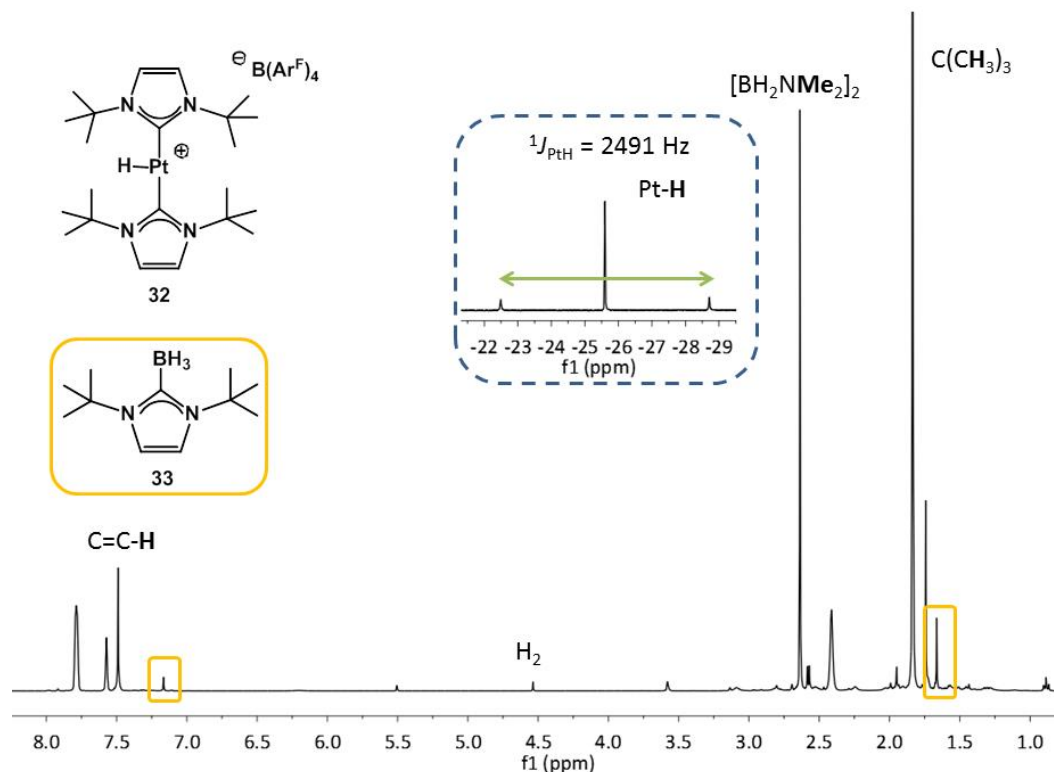


Figure 17. ^1H NMR in d_8 -THF spectrum of **1** with 3 equivalents of DMAB after 24h at room temperature.

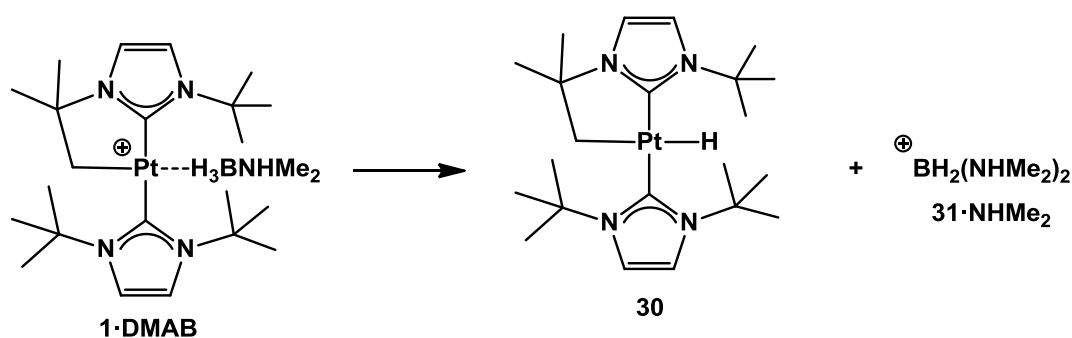
As observed in Figure 17 which shows a substoichiometric reaction mixture that has been left to evolve for one day, cationic hydride **32** and cyclic dimer $[\text{BH}_2\text{NMe}_2]_2$ are the mayor reaction products.

Carbene borane adduct $t\text{Bu}\cdot\text{BH}_3$, **33**,⁹ is also formed as a minor side product, as depicted in Figure 17. This species is easy to identify in the ^{11}B NMR spectrum, where it appears as a quartet at -31.6 ppm and was independently shown to arise from reaction of complex **1** with BH_3 . In fact when a bright yellow solution of **1** was mixed with 1 equivalent of $\text{BH}_3\cdot\text{THF}$, adduct **33** was the only clearly identified species after disappearance of complex **1**. The solution darkened but no other platinum species could be detected, possibly indicating the formation of platinum black. In reactions between DMAB and complex **1**, formation of boronium cation

⁹ This species has been previously synthesized, see: Brahmi, M. M.; Monot, J.; Desage-El Murr, M.; Curran, D. P.; Fensterbank, L.; Lacôte, E.; Malacria, M. *J. Org. Chem.* **2010**, *75*, 6983.

31·NHMe₂, bearing two amines, indicates that dissociation of NHMe₂·BH₃ into NHMe₂ and BH₃ is taking place, and therefore the free BH₃ present in the reaction media leads to the observed decomposition product, **33**. The formation of minor amounts of platinum black, together with the fact that a short induction period was observed at low concentrations of DMAB, lead us to consider the possibility of heterogeneous catalytic dehydrogenation of DMAB. However, reactions in the presence of Hg proceeded in the same manner as those without it, indicating that the observed dehydrogenation reactivity was not caused by platinum colloids or nanoparticles.

The observation of the formation of the platinum hydride **30** in the early stages of the reaction immediately after formation of σ -B-H complex points towards the first step in the mechanism of the reaction being the abstraction of a hydride atom from DMAB by the platinum center to yield the neutral platinum hydride complex and a borenium cation [BH₂(NHMe₂)]⁺ that is trapped in the form of the boronium cation [BH₂(NHMe₂)₂]⁺ (Scheme 6).¹⁰



Scheme 6. Hydride abstraction from DMAB by complex **1**.

Very likely, both the platinum hydride **30** and the boronium cation **31·NHMe₂** are formed in a single step, through a nucleophilic addition of free NHMe₂ to the boron atom in the σ -B-H complex, as depicted in Scheme 13. This assumption finds support by the fact that the Lewis acidity of the platinum atom would polarize more the B-H bond in the σ -complex **1·DMAB** increasing considerably

¹⁰ A borenium cation refers to a tricoordinated boron species and is highly unstable due to its electron deficiency. A boronium cation is a tetracoordinated boron species and consequently more stable.

the electrophilic character at the boron atom, making reasonable the nucleophilic addition of NHMe_2 (arising from dissociation of DMAB, as mentioned before).

To ascertain the role of complex **30** and the boronium cation $[\text{BH}_2(\text{NHMe}_2)_2]^+$ in the formation of the amino-borane $\text{Me}_2\text{N-BH}_2$ and dihydrogen, an equimolar mixture of these two species was reacted and studied by NMR spectroscopy at low temperature and then slowly heated to room temperature. At low temperature ($-30\text{ }^\circ\text{C}$) no reaction is observed, but as the temperature is raised, the proton NMR signals of the hydride **30** and $^+\text{BH}_2(\text{NHMe}_2)_2$ broaden, hinting at a possible interaction between the two species, and afterwards H_2 is slowly produced.¹¹ It takes several hours for the reaction to reach completion, the NHMe_2 adduct of cationic hydride $[\text{Pt}(\text{H})(\text{t}^i\text{Bu})_2(\text{NHMe}_2)][\text{B}(\text{Ar}^{\text{F}})_4]$ **32·NHMe₂** being the final platinum-containing species. Interestingly, no boron-containing species are detected in the ^{11}B NMR spectrum after $^+\text{BH}_2(\text{NHMe}_2)_2$ is consumed, suggesting the formation of insoluble, possibly polymeric species. Thus, a different mechanism should be operative to explain the fast dehydrogenation of DMAB by **1**.

Another test reaction was carried out to check whether hydride **30** could dehydrogenate DMAB, as both species are present at the same time in solution in the reactions between **1** and DMAB. Monitoring a 1:1 solution of these species in THF indicated that hydrogen is indeed released and aminoborane is formed, but no other platinum species besides hydride **30** could be detected throughout the process. As was seen for the hydrogen release from $^+\text{BH}_2(\text{NHMe}_2)_2$, it is possible that a different mechanism is in operation for this process and that its participation in the overall process is negligible, given that DMAB dehydrogenation using **30** as catalyst was observed to be much slower than with **1**, requiring *ca.* 90 min to achieve 45% conversion in an open system.

¹¹ Lowering the temperature again to $-30\text{ }^\circ\text{C}$ after sequential intervals at room temperature allows for the observation of well defined signals for the neutral hydride **30** and boronium cation **31·NHMe₂** at intermediate reaction times, along with increasing amounts of H_2 . The only new species detected in these spectra is the cationic hydride amine adduct $[\text{Pt}(\text{H})(\text{t}^i\text{Bu})_2(\text{NHMe}_2)][\text{B}(\text{Ar}^{\text{F}})_4]$.

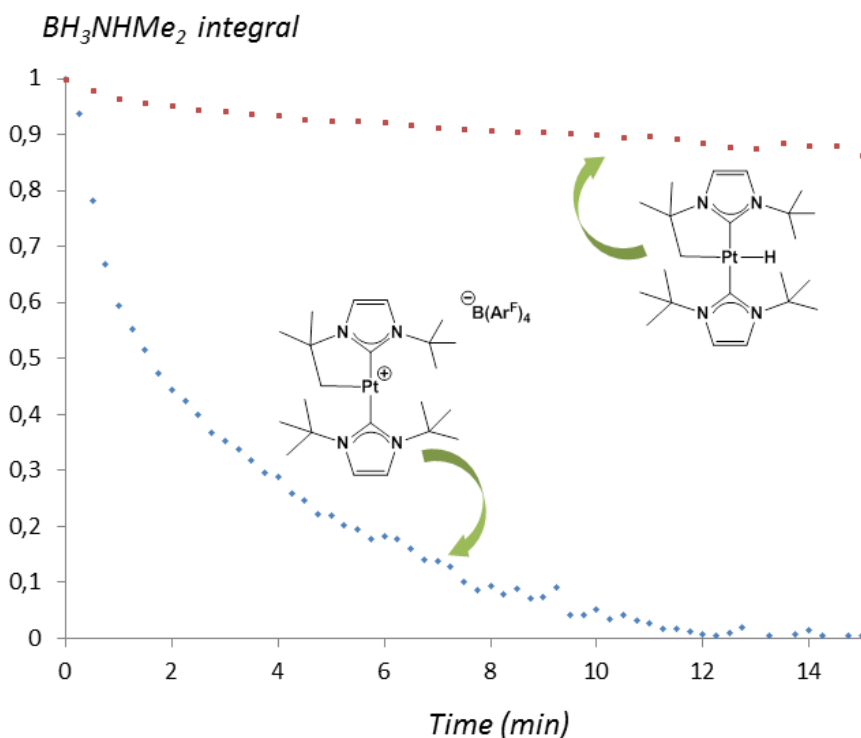
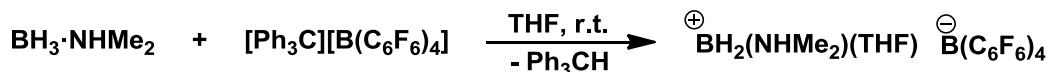


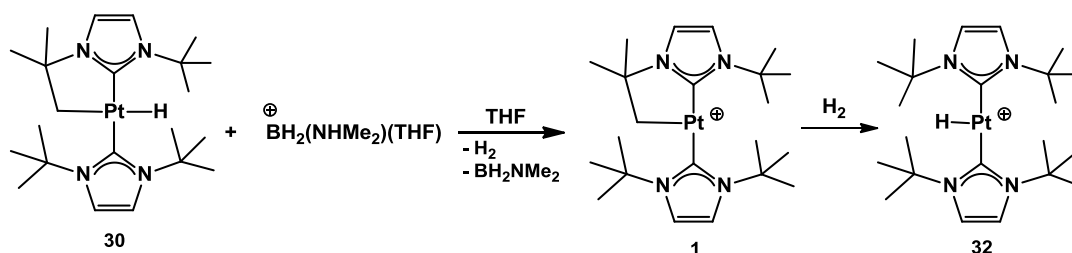
Figure 18. BH_3NHMe_2 normalized integral value plotted against time for the catalytic dehydrogenation of a 0.270M solution of BH_3NHMe_2 with 5 mol% of **30** (red) and 5 mol% of **1** (blue).

These puzzling results lead us to look for alternative reaction pathways involving the formation of transient, highly reactive species. We assumed that the THF stabilised boronium cation $[\text{H}_2\text{B}(\text{NHMe}_2)(\text{THF})]^+$ might be present at some point during catalysis. This boronium cation might be formed by dissociation of one NHMe_2 ligand from $[\text{H}_2\text{B}(\text{NHMe}_2)_2]^+$ and bears an acidic NH group and a better leaving group (THF). Nonetheless, it should be pointed out that the presence of $^+\text{BH}_2(\text{NHMe}_2)(\text{THF})$ was never observed while monitoring dehydrogenation reactions. To check this possibility the THF boronium cation $[\text{BH}_2(\text{NHMe}_2)(\text{THF})]^+$ was independently prepared by the reaction of DMAB with one equivalent of the hydride abstractor $[\text{Ph}_3\text{C}][\text{B}(\text{C}_6\text{F}_5)_4]$ in THF (Scheme 7). The reaction was clean and yielded a single boron-containing species that appeared as a broad triplet at 4.3 ppm in the ^{11}B NMR spectrum.



Scheme 7. Synthesis of THF stabilized borenium cation.

Gratifyingly, when a 1:1 mixture of $[\text{BH}_2(\text{NHMe}_2)(\text{THF})][\text{B}(\text{C}_6\text{F}_5)_4]$ and **30** was dissolved in d_8 -THF at low temperature (Scheme 8), complex **1** and BH_2NMe_2 were immediately formed as the only observable reaction products, with H_2 liberation, even at $-30\text{ }^\circ\text{C}$. Complex **1** partially transformed to hydride **32** due to reaction with the hydrogen released.

Scheme 8. Formation of hydrogen and aminoborane from hydride **30** and the boronium cation $^{\oplus}\text{BH}_2(\text{NHMe}_2)(\text{THF})$.

The fast reaction of the THF stabilised boronium cation to produce hydrogen and aminoborane explains why it is never observed in solution. However, the neutral platinum hydride **30** is regenerated under catalytic conditions when DMAB is present together with complex **1**, with concomitant formation of the bis(dimethylamino) boronium cation $[\text{H}_2\text{B}(\text{NHMe}_2)_2]^{\oplus}$. The latter species and complex **30** are thus resting states, and the rate of the dehydrogenation is probably determined by the dissociation of a NHMe_2 group to lead to the THF stabilised boronium cation $[\text{BH}_2(\text{NHMe}_2)(\text{THF})]^{\oplus}$.

2.5. DFT studies

A computational study was carried out by Dr López-Serrano to help us explain the experimental observations described in the previous section. Ammonia borane (AB) and OMe_2 were used as models for DMAB and the THF solvent respectively, whereas no simplifications were made for complex **1**.

Coordination of AB to **1** was found to be exothermic by $14.6 \text{ kcal}\cdot\text{mol}^{-1}$ in THF yielding a Shimoi-type adduct that maps onto the experimentally observed **1**·DMAB. When activation routes of the B–H bond at the platinum center were considered, it was found that AB dehydrogenation could take place through concerted BH/NH activation to yield transient **1**·H₂ and aminoborane, as shown in Figure 19.

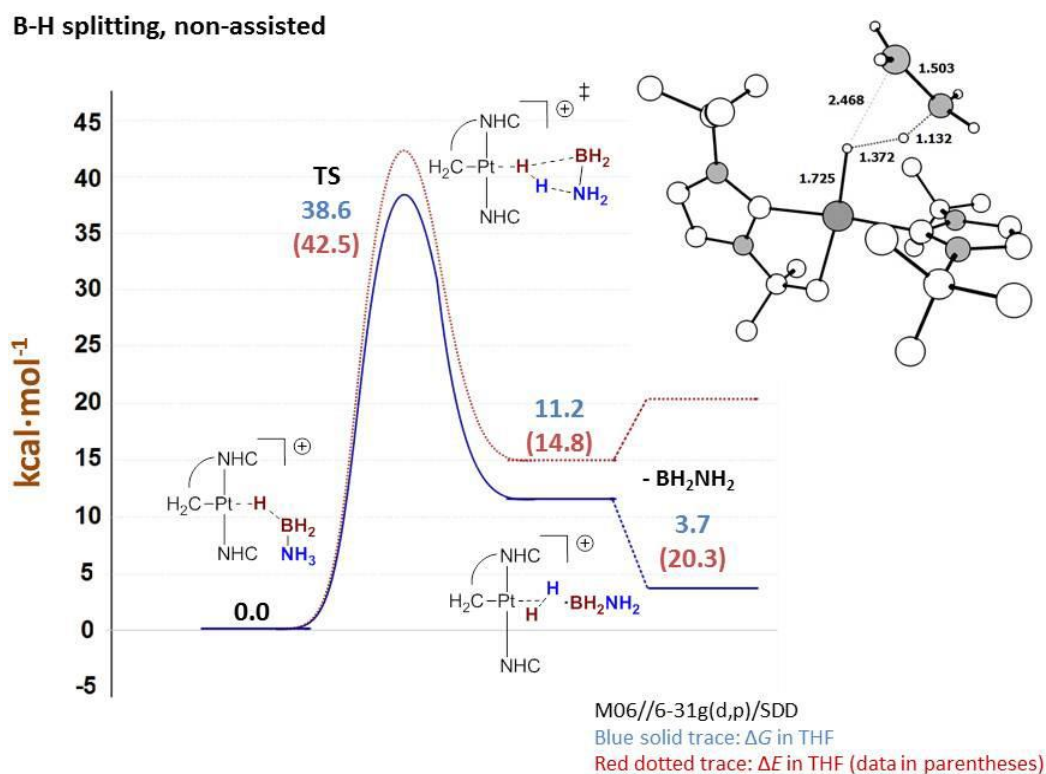


Figure 19. Energy profile for the unassisted AB dehydrogenation at **1** and optimized geometry of the transition state (most H atoms have been omitted for clarity).

However, the energy barrier for this step, at $42.5 \text{ kcal}\cdot\text{mol}^{-1}$, is too high to explain the observed reactivity, where B–H activation takes place at temperatures over $0 \text{ }^\circ\text{C}$. Alternative possibilities in which a Lewis base (L_B), such as OMe_2 or NH_3 , was included to assist the B–H activation step resulted in this barrier being lowered by more than $18 \text{ kcal}\cdot\text{mol}^{-1}$ ($\Delta E_{\text{THF}}^\ddagger = 24.1$ and $24.3 \text{ kcal}\cdot\text{mol}^{-1}$ for the Me_2O - and the NH_3 - assisted reactions respectively, Figure 35). Moreover, the presence of these Lewis bases stabilizes the resulting boronium cations adducts. Minima were

obtained for the corresponding adducts of neutral hydride **30** and the L_B stabilized boronium cations. The Me_2O adduct is $13.1 \text{ kcal}\cdot\text{mol}^{-1}$ above $\mathbf{1}\cdot\mathbf{AB}\cdot\mathbf{OMe}_2$, whereas the NH_3 adduct has nearly the same energy as $\mathbf{1}\cdot\mathbf{AB}\cdot\mathbf{NH}_3$. This means that ammonia is much better at stabilizing the boronium cation, making it a better leaving group than in the ether stabilized adduct. The overall process to produce **30** and $[\text{NH}_3\text{BH}_2\cdot L_B]^+$ is thermoneutral when $L_B = \text{NH}_3$, whereas even after fragment separation the energy of the products is around $15 \text{ kcal}\cdot\text{mol}^{-1}$ higher for $L_B = \text{OMe}_2$. This explains why $[\text{NH}_3\text{BH}_2\cdot \text{NH}_3]^+$ and not the ether adduct is observed in our system, indicating that participation of external amine is a key feature of the mechanism. These thermodynamic observations are summarized on the energy profiles on Figure 20.

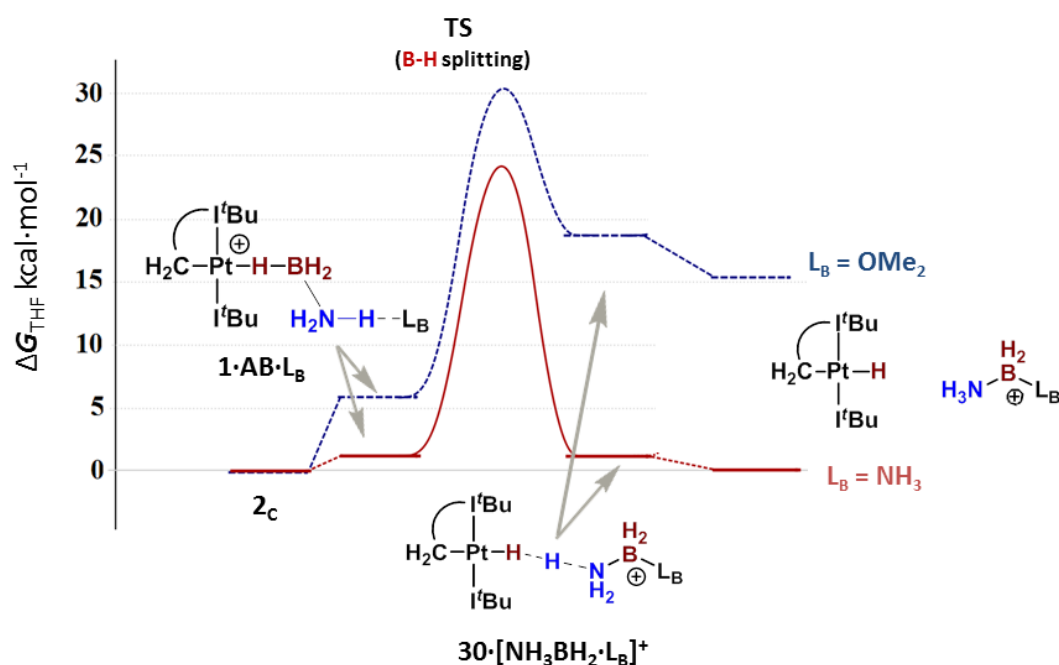


Figure 20. Simplified DFT-optimized geometries of key species and calculated free energy profile in THF of the AB B–H activation and neutral hydride formation assisted by NH_3 (red solid trace) and Me_2O (blue dashed trace).

Hydrogen release from these species was subsequently calculated to shed some light into the experimental observation that H_2 liberation from protonation of

hydride **30** was extremely facile for $[\text{NH}_3\text{BH}_2\cdot\text{THF}]^+$ but slow for boronium **31**·**NHMe**₂.

Besides the fragment separation pathway (leading to complex **30** and the boronium cation) depicted in Figure 20 for adducts $\mathbf{30}\cdot[\text{NH}_3\text{BH}_2\cdot\text{L}_\text{B}]^+$ an alternative possibility exists in which these species evolve via N–H splitting effectively protonating the neutral hydride. This pathway results in aminoborane and eventually H₂ release. When L_B = NH₃, fragment separation is favored over hydride protonation ($\Delta G_{\text{THF}} = -1.3$ vs. 2.5 kcal·mol⁻¹), whereas for the ether adduct (L_B = OMe₂) hydride protonation is greatly favored ($\Delta G_{\text{THF}} = -3.7$ vs. -15.1 kcal·mol⁻¹). This indicates that whenever $[\text{NH}_3\text{BH}_2\cdot(\text{OMe}_2)]^+$ is formed, its interaction with neutral hydride **30** will lead to aminoborane and H₂ release, in accordance with the experimental observation. For L_B = NH₃, hydride protonation is less favourable and this explains why we can see the platinum hydride **30** and the boronium cation **31**·**NHMe**₂ in our reaction crudes. These thermodynamic observations are shown in Figure 21.

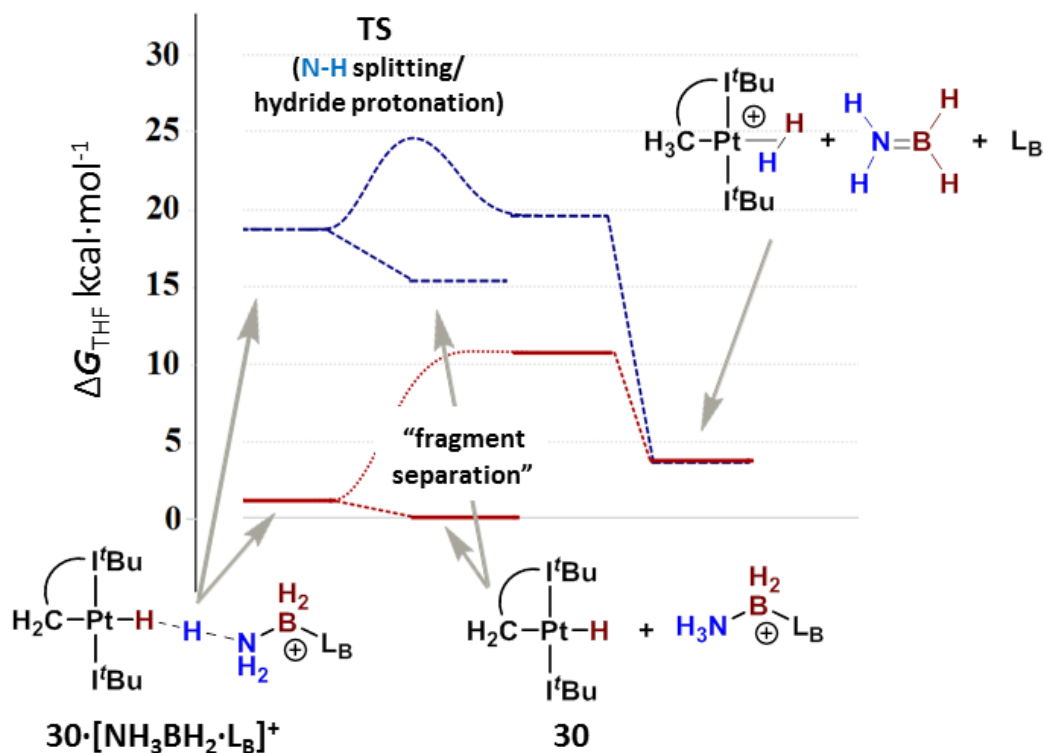


Figure 21. Simplified DFT-optimized geometries of key species and calculated free energy profile in THF of the AB dehydrogenation assisted by NH_3 (red solid trace) and Me_2O (blue dashed trace).

Kinetic preference for fragment separation versus hydride protonation in the case of the $30\cdot[\text{NH}_3\text{BH}_2\cdot\text{NH}_3]^+$ system can be deduced from the energy profiles in Figure 22, where it can be seen that the ΔE_{THF} values for the separated fragments (dashed lines) is lower for $\text{L}_\text{B} = \text{NH}_3$, indicating a faster reaction.

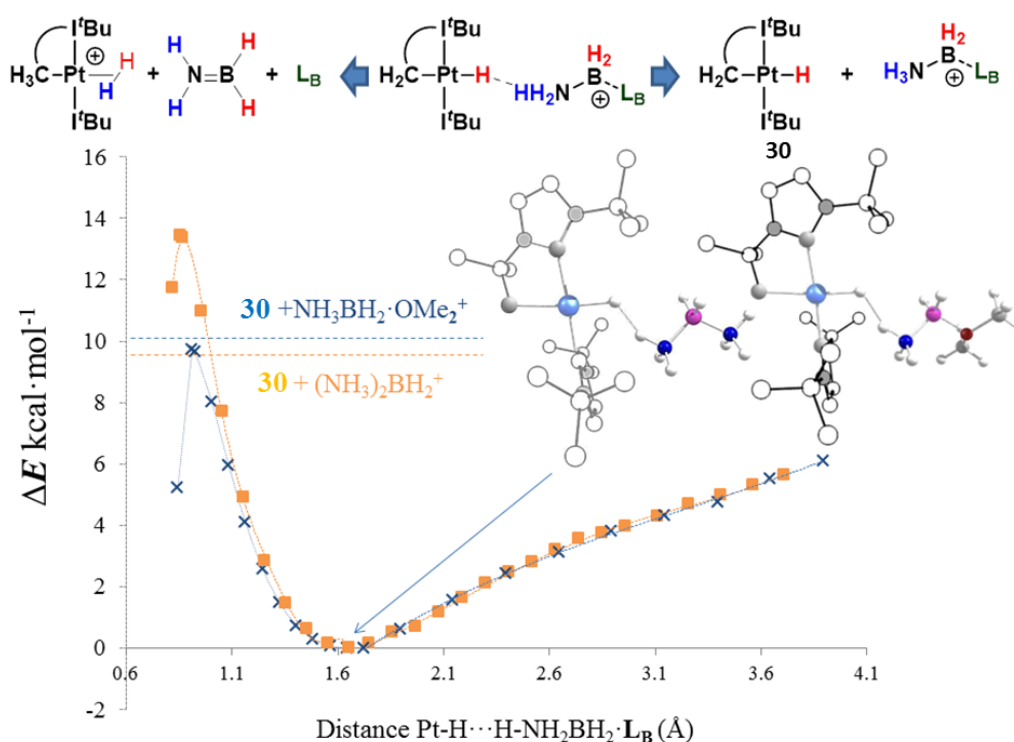
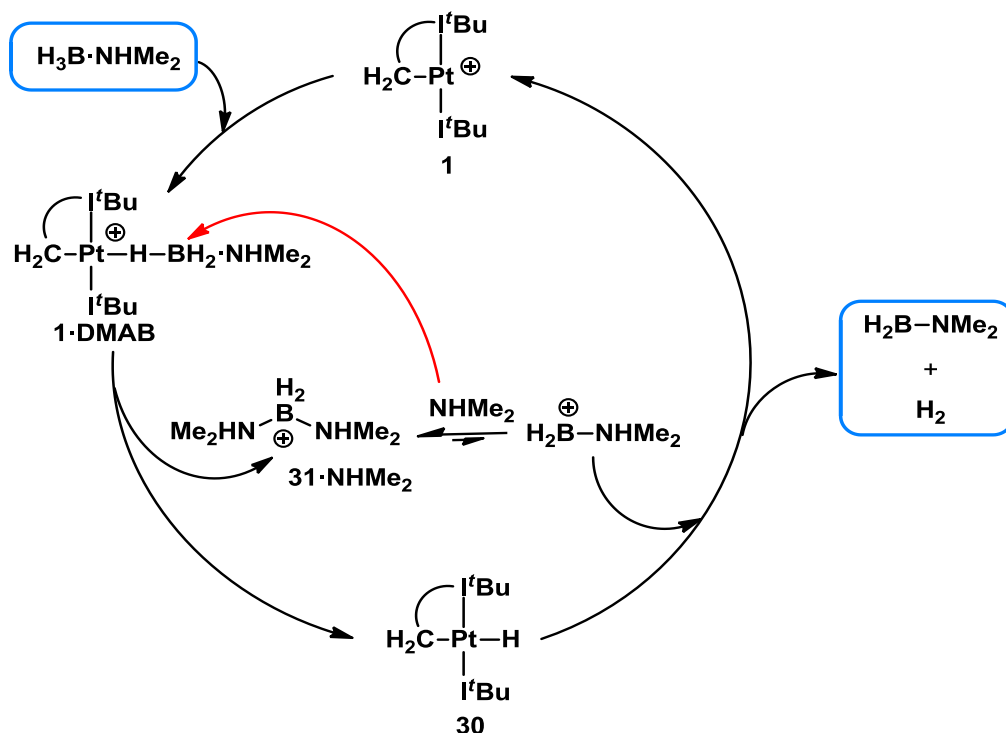


Figure 22. Relaxed Potential Energy Scan (optimizations in THF) showing the dissociation of the **30** and $[\text{NH}_3\text{BH}_2\cdot\text{L}_\text{B}]^+$ fragments (optimized geometries also shown) vs. metal-hydride protonation ($\text{L}_\text{B} = \text{OMe}_2$ –blue Xs-, NH_3 –orange squares). The horizontal dashed lines represent the energy of the separated fragments when the $\text{Pt-H}\cdots\text{H-NH}_2\text{BH}_2\cdot\text{L}_\text{B}$ distances are set to 10 Å.

2.6. Mechanistic proposal

All the above experimental observations along with the parallel computational study led us to propose the mechanism summarized in Scheme 9 for the catalytic dehydrogenation of DMAB.



Scheme 9. Proposed catalytic cycle for the dehydrogenation of DMAB with complex **1**.

In brief, complex **1** can interact with a molecule of DMAB to form a Shimoi-type adduct, **1·DMAB**. B-H splitting from this adduct is assisted by external amine, leading to the formation of neutral hydride **30** and boronium cation **31·NHMe₂**. This boronium cation is in equilibrium with the THF stabilized borenium cation, which does in turn readily react with hydride **30** to release aminoborane and H_2 , regenerating the starting cationic complex **1**.

As for the source of free amine, it is evident that it must come from a metal assisted B-N cleavage of the amine borane, as metal-free DMAB solutions are stable over time. Experimental evidence of this behavior is the observation of a short induction period in which the reaction rate is initially slower when the progress of the catalytic reaction is monitored over time (see Figure 19). Such induction periods are typical of heterogeneous reactions and account for the time in which nanoparticles are formed, but as explained above, mercury poisoning experiments did not affect the kinetic profile of the reaction. An initial period of

time during which some of the amine borane dissociates could also explain the slower initial rate, and once a sufficient amount of free amine is present in solution the reaction proceeds faster. Only a catalytic amount of amine is needed to assist the B–H splitting step, as can be deduced by the catalytic cycle on Scheme 9. The concomitant liberation of BH_3 explains the formation of small amounts of the decomposition product **33**, in a process not included in the cycle. With the aim of validating the key role of free amine in the mechanism a catalytic reaction was carried out with the addition of a catalytic amount of dimethylamine (Figure 23). In this case the induction period was not observed, with the reaction being slightly faster, and most interestingly, the carbene borane adduct ${}^t\text{Bu}\cdot\text{BH}_3$ **20** was not observed. This indicated that no DMAB dissociation was necessary in these conditions for the dehydrogenation reaction to proceed.

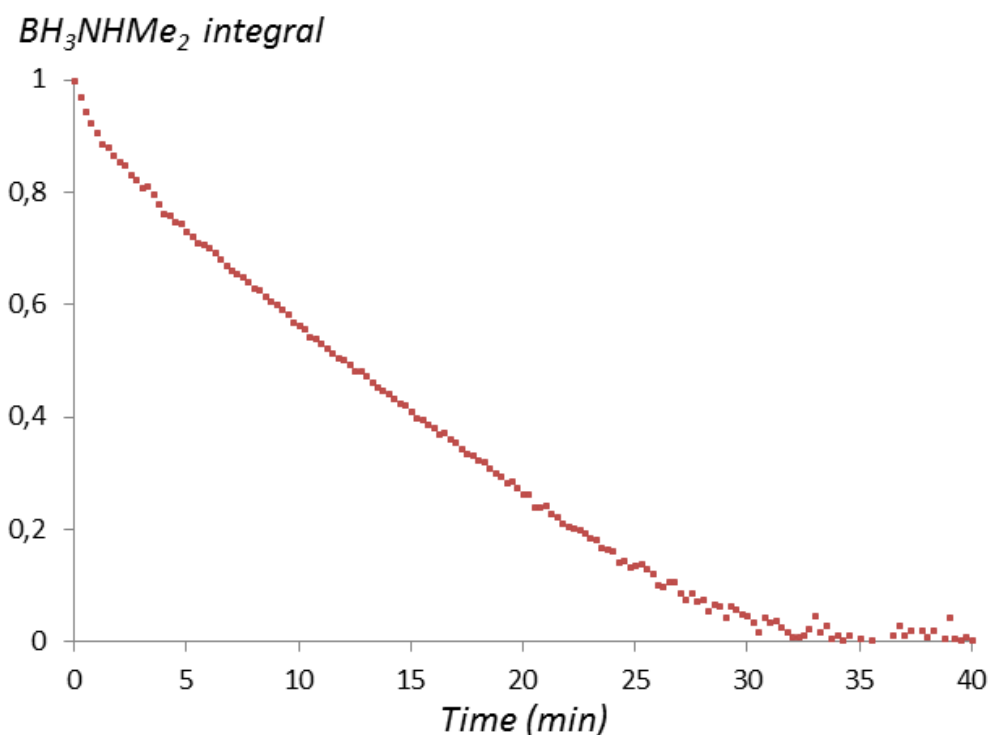
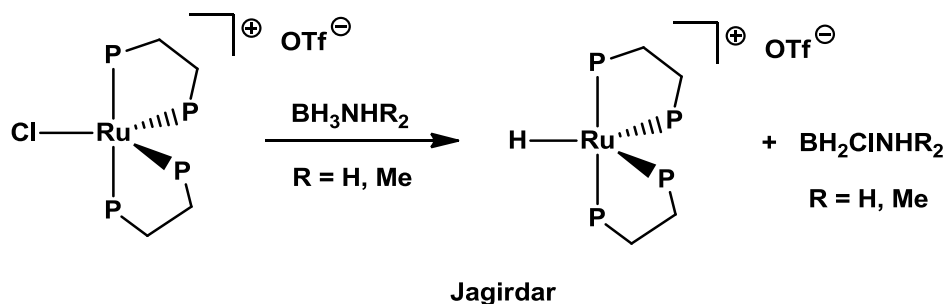


Figure 23. BH_3NHMe_2 normalized integral value plotted against time for the catalytic dehydrogenation of a 0.270M solution of BH_3NHMe_2 with 2.5 mol% of **1** and NHMe_2 . Note the absence of induction period (c.f. Figure 4).

2.7. Comparison of our system to related mechanistic scenarios

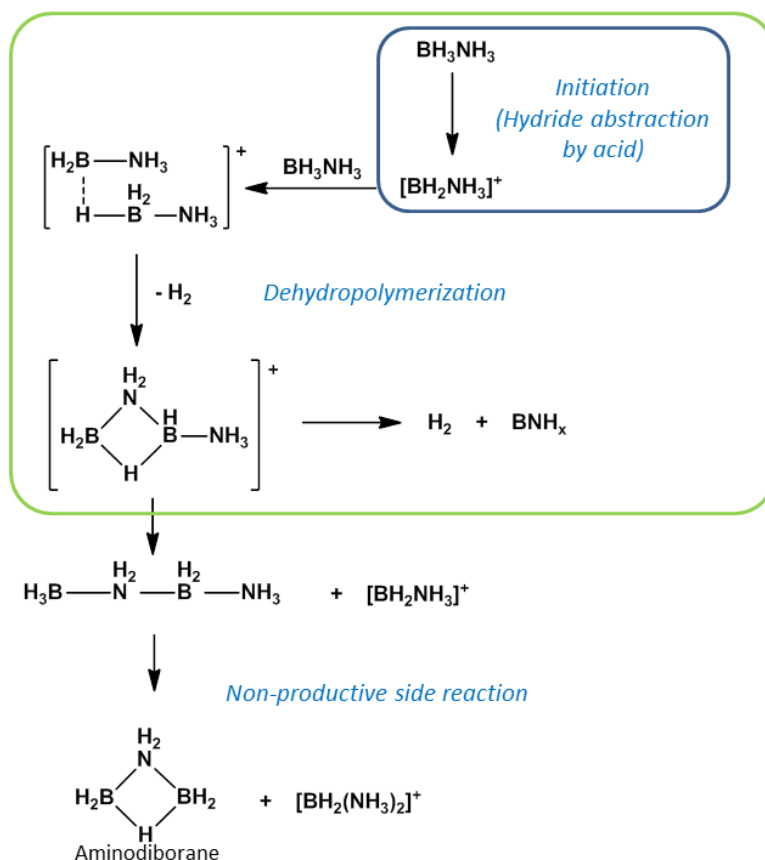
In the course of our investigations Jagirdar et al. published the only other transition metal system that we are aware of for which the formation of a boronium species has been proposed.¹²



However, in this case no experimental evidence was found about the mechanism through which hydrogen is released from this species. Without ruling out an on-metal process, they proposed that BH_2ClNH_3 could react with unreacted ammonia borane in a sequential dehydrogenation to produce oligomeric species and finally yield BNH_x polymer. This mechanistic proposal is based on the findings by Baker et al. about acid initiated ammonia borane dehydrogenation, in which a borenium cation $^+\text{BH}_2\text{NH}_3$ is proposed to be initially formed and initiates the dehydrogenation process without the need of a metal species (Scheme 10).¹³

¹² Kumar, R.; Jagirdar, B.R.; *Inorg. Chem.* **2013**, *52*, 28–36.

¹³ Stephens, F.H.; Baker, R.T.; Matus, H.M.; Grant, D.J.; Dixon, D.A.; *Angew. Chem. Int. Ed.* **2007**, *46*, 746-749.



Scheme 10. Summary of the acid catalysed dehydrogenation of ammonia borane proposed by Baker.

The Lewis acid $\text{B}(\text{C}_6\text{F}_5)_3$ was used in this study, which could catalytically dehydrogenate ammonia borane at high temperatures, but was found to be inactive in the dehydrogenation of DMAB.¹⁴ In contrast, stoichiometric mixtures of the frustrated Lewis pair $\text{B}(\text{C}_6\text{F}_5)_3/\text{P}^t\text{Bu}_3$ were very active in the stoichiometric dehydrogenation of both AB and DMAB at room temperature,¹⁵ indicating that deprotonation from the NH unit might be the limiting step in the acid catalyzed dehydrogenation and probably also in Jagirdar's system. In our platinum system, however, even though the initial step is hydride abstraction from the borane

¹⁴ Jaska, C. A.; Temple, K.; Lough, A. J.; Manners, I.; *J. Am. Chem. Soc.* **2003**, *125*, 9424 – 9434.

¹⁵ Miller, J.M.A.; Bercaw, J.E.; *Chem. Commun.* **2010**, *46*, 1709.

moiety, NH deprotonation to yield H₂ and aminoborane seems to be a much faster process.

As for the fate of the amine borane in these systems, Baker reported that for ammonia borane linear and acyclic branched oligomers were observed as dehydrogenation products in the reaction with B(C₆F₅)₃, with aminodiborane (B₂H₅NR₂) forming as a side product (Scheme 10). The fact that Jagirdar also observed aminodiborane species for reactions with both AB and DMAB indicates that the off-metal process initiated by the boronium cation may also be operating in their system, whereas in our case, no aminodiborane species was observed in the dehydrogenation of DMAB. The fact that NH activation is a metal-mediated step (platinum hydride protonation), along with the key participation of free amine in the initial BH activation, sets our mechanistic proposal apart from these previous examples where the formation of boronium cations had been proposed.

2.8. Dehydrogenation of amine boranes by electron deficient Pt(II) complexes: Reactivity with other metal complexes and amineboranes

2.8.1. Dehydrogenation of other amineboranes with complex **1**

Reaction of complex **1** with ammonia borane (NH₃·BH₃, AB) was found to be akin to the reaction with DMAB for the release of the first equivalent of H₂. The formation of a **1**·AB adduct was initially observed, and as the temperature was raised above 0 °C hydride **30** was formed along with boronium cation [BH₂(NH₃)₂]⁺ **31**·NH₃ that is analogous to **31**·NHMe₂. This species presented a broad triplet in the ¹¹B NMR spectrum at -13.7 ppm with ¹J_{BH} = 104 Hz and was also easily recognized in the ¹H NMR spectra due to its NH₃ signal at 5.15 ppm. Solvent stabilized boronium cation [BH₂(NH₃)(THF)]⁺, independently prepared by reaction of AB with one equivalent of [Ph₃C][B(C₆F₅)₄] in THF, presented a ¹¹B NMR chemical shift of 0.3 ppm and was never observed in the reactions between **1** and AB, as was the case for [BH₂(NHMe₂)(THF)]⁺ in the dehydrogenation of DMAB that has been discussed in a previous section.

As for the dehydrogenation products of ammonia borane observed with this catalyst, in reactions with a small excess of AB (2-3 equivalents) aminodiborane (δ_B -27.3) was formed at the same time as [BH₂(NH₃)₂]⁺ in similar amounts. As the

reaction progressed, aminodiborane was the first intermediate to be consumed followed by the boronium cation, while borazine (δ_B 30.4, d, $^1J_{BH} = 140$ Hz) and polyborazylene (δ_B 27.3, broad) were formed and were the final reaction products along with carbene borane adduct **33**, which is produced from catalyst decomposition. In reactions with a larger excess of AB (e.g. 10 equivalents) other intermediate products could also be identified, such as the cyclic trimer cyclotriborazane (CTB) which presents a broad signal at δ_B -11.5. Other broad signals centered at -5, -12 and -24 ppm (marked with a * in Figure 39) that grew at the same rate were assigned as branched polyaminoborane.¹⁶ Figure 24 shows the ^{11}B NMR monitoring of a catalytic dehydrogenation of AB with complex **1**.

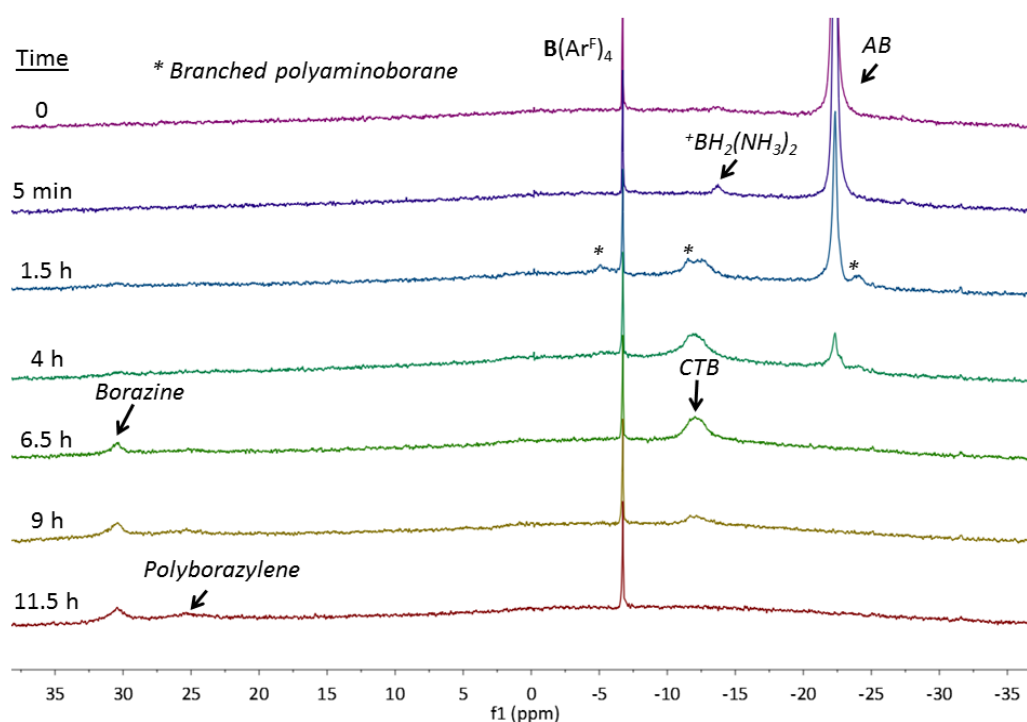


Figure 24. ^{11}B NMR spectra of the catalytic dehydrogenation of a 0.135M THF solution of AB at 25°C with 5 mol% of complex **1**

Unlike reactions with DMAB, aminoborane (BH_2NH_2) was never observed, as it is very reactive and evolves to form the observed cyclic and polymeric products. The

¹⁶ Bluhm, M.E.; Bradley, M.G.; Butterick, R.; Kusari, U.; Sneddon, L.G. *J. Am. Chem. Soc.* **2006**, *128*, 7748.

mechanism by which the next second H₂ is produced from these species in reactions with **1** was not elucidated.

Cationic platinum hydride **32** was the final platinum species in these reactions, and in reactions with only 2-3 equivalents of ammonia borane a platinum by-product that was never detected in reactions with DMAB also formed, constituting around 25% of the final platinum products. This new species presents a hydride signal that resonates in the ¹H NMR at -6.4 ppm and shows two sets of coupling constants to ¹⁹⁵Pt, ¹J_{PtH} = 798 Hz and ²J_{PtH} = 501 Hz, indicative of a terminal hydride that is coupled to two different platinum nuclei (H-Pt-Pt). This species starts forming at the same time as hydride **30**, but unlike that complex, it is not consumed upon reaction completion. Therefore this species must form from an unproductive side reaction that does not lead to AB dehydrogenation. This platinum dimer could not be isolated and so its exact nature could not be ascertained, but integration of some of its ¹H NMR signals that did not overlap with other species led us to conclude that this complex contains two ^tBu ligands per hydride, so it must form from a platinum species that has lost one carbene ligand. Very likely, this unknown complex arises from degradation of complex **1** with BH₃ (leading to ^tBu·BH₃, as mentioned before) and further reactivity the released platinum monocarbene species with ammonia borane.

The complexity of the product distribution of AB dehydrocoupling and catalyst degradation leads us to study the dehydrogenation of other amineboranes.

Complex **1** reacts in a similar fashion with primary amine borane BH₃NH₂^tBu (TBAB). Hydride **30** is initially formed along with boronium cation [BH₂(NH₂^tBu)₂]⁺. As the reaction progresses and H₂ is released, cationic hydride **32** is formed and a dimeric platinum species similar to that formed in reactions with AB appears. In this case, its hydride signal has a chemical shift of -6.13 ppm and again two sets of coupling constants to ¹⁹⁵Pt with values of 506 and 804 Hz are seen (Figure 25). The fact that these dimers present similar signals but not at exactly the same chemical shift may point towards an amine being coordinated to these species. The underlying reasons why a related species is not formed in reactions with DMAB may be due to steric factors, as NHMe₂ is bulkier than NH₃ and NH₂^tBu. Nevertheless, the impossibility of purifying neither of the dinuclear species

obtained in the reactions with both $\text{NH}_3\cdot\text{BH}_3$ and $\text{NH}_2^t\text{Bu}\cdot\text{BH}_3$ makes any attempt to postulate any possible structure too speculative.

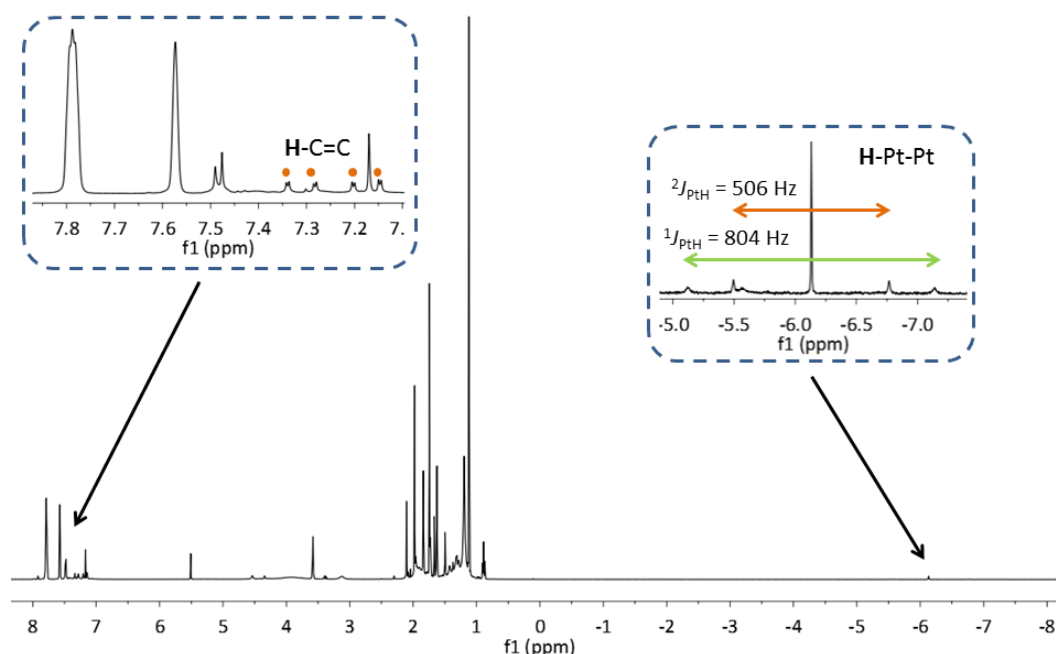


Figure 25. ^1H NMR of a 1:5 mixture of **1** and $\text{BH}_3\text{NH}_2^t\text{Bu}$ in d_8 -THF where the unknown dimeric hydride complex is the major species.

As for the dehydrogenation products of $\text{BH}_3\text{NH}_2^t\text{Bu}$ in these reactions, aminoborane $\text{BH}_2\text{NH}^t\text{Bu}$ (δ_{B} 33.9, $^t\text{}^1J_{\text{BH}} = 128$ Hz) is detected in the ^{11}B spectra in the early stages of the reaction along with $\text{BH}(\text{NH}^t\text{Bu})_2$ (δ_{B} 25.4, $d\text{}^1J_{\text{BH}} = 122$ Hz). Carbene borane adduct **20** is also observed. In reactions with a large excess of $\text{BH}_3\text{NH}_2^t\text{Bu}$, aminodiborane (δ_{B} -26.6, $d\text{}^1J_{\text{BH}} = 127, 31$ Hz) and the two isomers of the cyclic trimer (δ_{B} -9.4, -9.7) are observed. Unfortunately, progressive catalyst decomposition due to formation of the unknown platinum hydride dimer and $^t\text{Bu}\cdot\text{BH}_3$ (**20**) slowed down the reaction and heating to 45 °C was necessary to observe the products of further dehydrogenation. Borazine (δ_{B} 30.6, broad) was also observed at this stage (Figure 26).

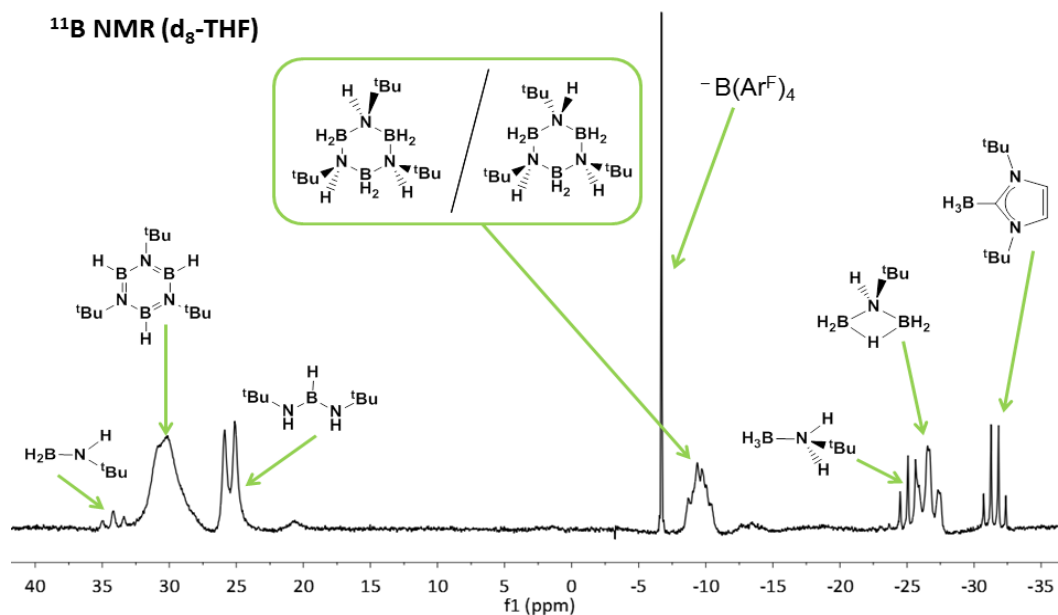


Figure 26. ^{11}B -NMR in d_8 -THF of the catalytic dehydrogenation of t-butylamine borane with 5 mol% **1** after 24h at room temperature (closed system) and heating at 45 °C overnight

We also attempted the dehydrogenation of the bulky secondary amine borane $\text{BH}_3\text{NH}^i\text{Pr}_2$, but as we found out for mixtures of complex **1** and bulkier trimethylamine borane, no interaction could be even observed between the two species and, consequently, no dehydrogenation is produced. Interestingly, if the corresponding borenium cation $[\text{BH}_2\text{NH}^i\text{Pr}_2]^+$ (independently synthesized by reaction of $\text{BH}_3\text{NH}^i\text{Pr}_2$ with $[\text{Ph}_3\text{C}][\text{B}(\text{C}_6\text{F}_5)_4]$) is reacted with hydride **30**, aminoborane $\text{BH}_2\text{N}^i\text{Pr}_2$ (δ_{B} 35.2, t, $^1J_{\text{BH}} = 130$ Hz) was formed along with complex **1** and H_2 . This points towards steric constraints being more decisive for the hydride abstraction step from $\text{BH}_3\cdot\text{NR}_3$, and hydrogen release by neutral platinum hydride being more facile in terms of steric demands once the corresponding THF stabilised boronium cation has been formed.

2.8.2. Dehydrogenation of amineboranes by complex **2b**

When a 1:1 of mixture of complex **2b**, bearing *i*Pr carbenes and DMAB in d_8 -THF was analyzed at room temperature, ^1H NMR signals for both species appeared with the chemical shift of the free products, indicating no interaction. The fact

that complex **1** did show interaction with DMAB under the same conditions indicates that although *tert*-butyl substituted carbenes are typically considered bulkier than IPr, in our system they exert smaller steric hindrance further away from the metal center, where the methyl groups of DMAB lie, allowing coordination to the metal (Figure 27).

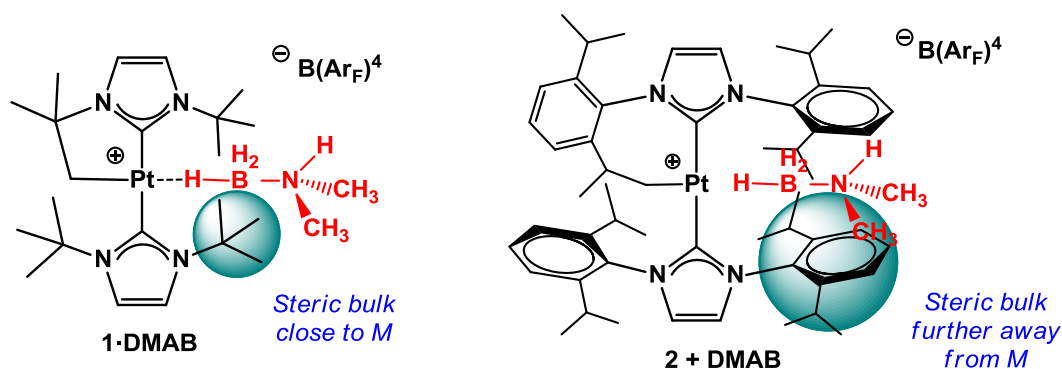
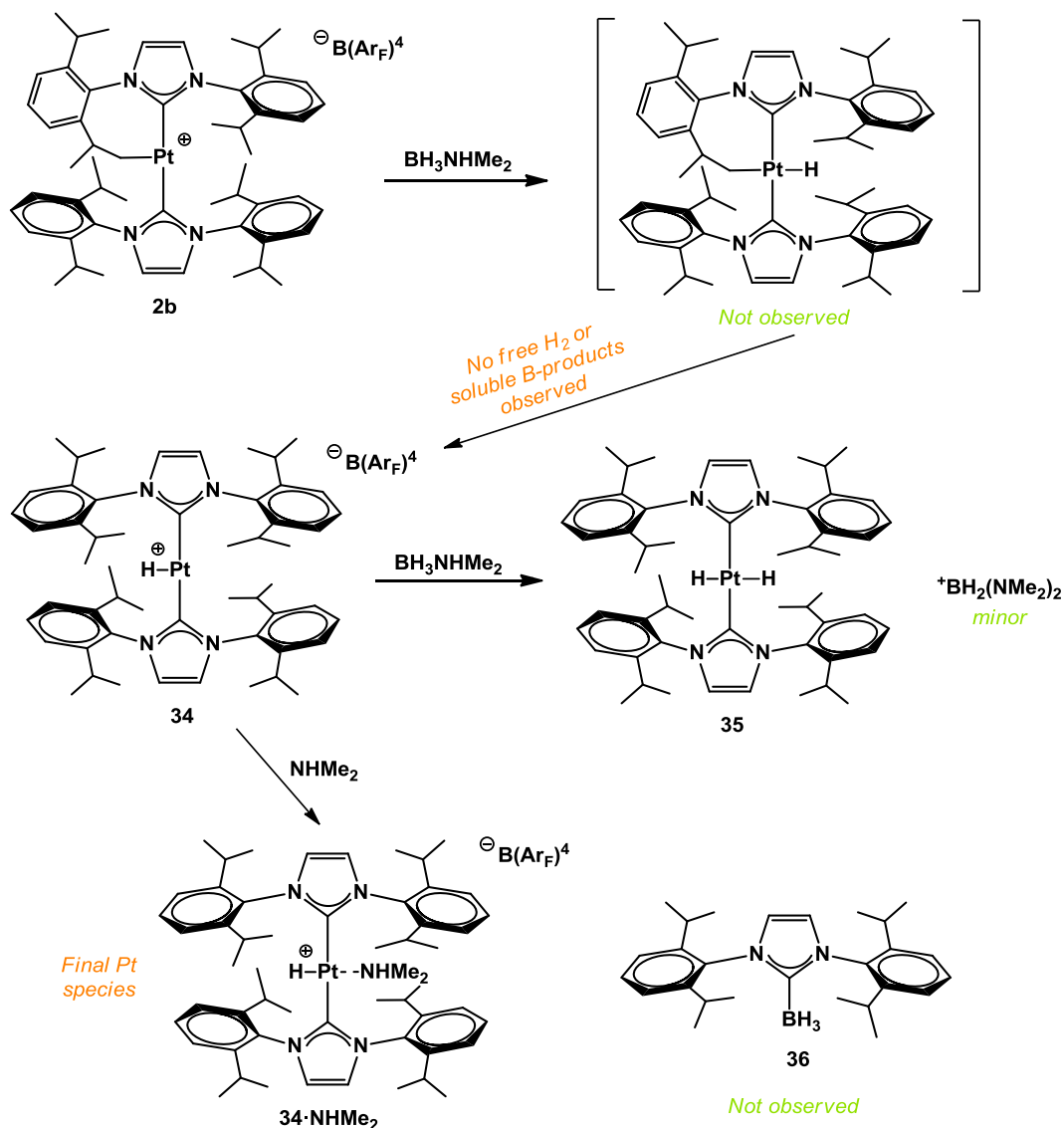


Figure 27. Steric hindrance of carbene ligands affects the region closer to the metal center (*t*Bu) or further away from it (IPr) depending on the nature of the N-substituents.

Therefore interaction of DMAB with **2b** is weaker and only at temperatures below -20°C are signals for coordinated DMAB observed. For example, at -30°C the signal for the coordinated BH_3 protons appears at -0.36 ppm. Even after ^{11}B decoupling, this signal appears quite broad and platinum satellites were barely discernible, with an approximate $^2J_{\text{PtH}}$ value of 90 Hz.

Reaction of **2b** with DMAB is slow even at high catalyst loadings (1:6 mixtures) in closed systems. Only after 6 days at room temperature all DMAB is consumed in these conditions. Monitoring of this reaction showed that no neutral hydride equivalent to **30** was formed, however, cationic hydride **34** ($\delta_{\text{H}} = -36.5$ ppm, broad) and its NHMe_2 adduct ($\delta_{\text{H}} = -20.6$ ppm, $^1J_{\text{PtH}} = 1349$ Hz) could be detected after a couple of hours at room temperature (Scheme 11).



Scheme 11. Products involved in the catalytic dehydrogenation of DMAB with complex **2b**. Note that even though amine adduct **34·NHMe₂** is formed, no carbene borane adduct **36** is detected, indicating that free amine is not forming via catalyst decomposition with BH_3 .

Another platinum hydride appeared roughly at the same time at -14.0 ppm ($^1J_{\text{PtH}} = 1650$ Hz) but we have not been able so far to ascertain its nature. A fourth hydride complex appeared later and was actually the main platinum species after 2 days at room temperature. It resonated at -3.5 ppm ($^1J_{\text{PtH}} = 891$ Hz) and did not have

cyclometallated ligands. It was assigned as neutral *trans*-dihydride species $\text{PtH}_2(\text{IPr})_2$ (**35**) and likely formed by hydride abstraction from DMAB by cationic hydride **34**. The final major platinum species after DMAB consumption was the amine adduct **34**·NHMe₂. Complex **35** was independently prepared by reaction of **34** with NaH in THF. Unlike the independent synthesis of **30**, which was complete in under 30 minutes at room temperature, formation of **35** was slow, even with a large excess of NaH and equilibrium mixtures with cationic hydride **34** appeared to form. Extraction with pentane, however, allowed for the obtention of pure samples of **35**. An interesting feature of the NMR spectra of complex **35** is the observation of coupling to ¹⁹⁵Pt in the signals corresponding to the isopropyl CH and CH₃ carbons. This suggests the presence of anagostic interactions. It must be noted that due to the spatial disposition of the isopropyl substituents, only one of the two sets of CH₃ carbon signals have the appropriate orientation to interact with the platinum center. Similar coupling to platinum is also observed for hydride **30**.

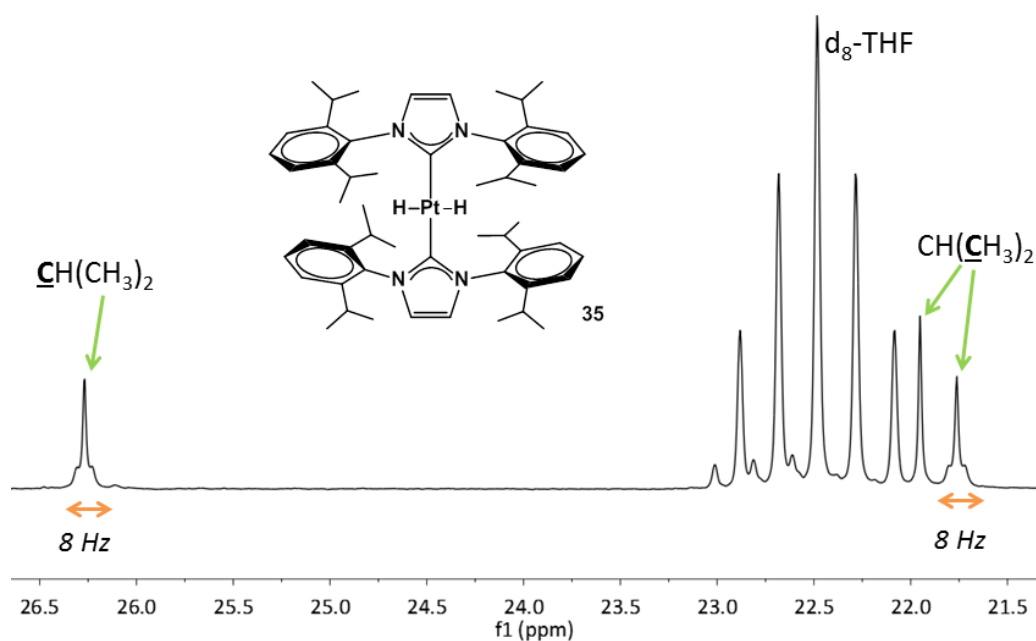
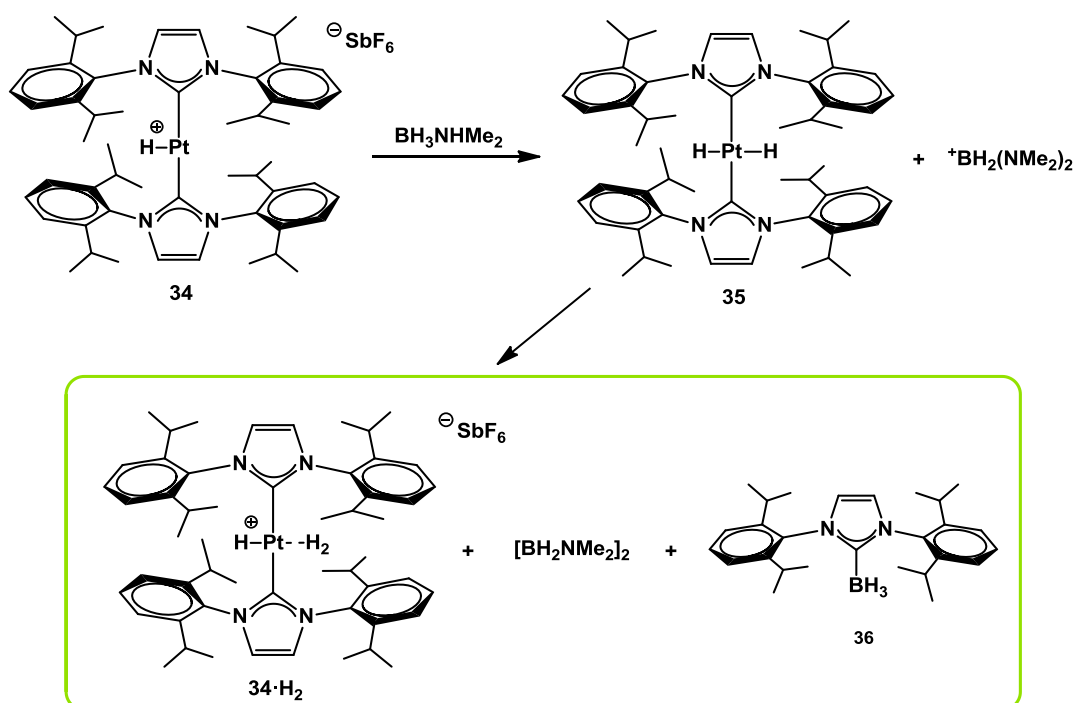


Figure 28. Section of the ¹³C NMR spectrum of complex **35** in d₈-THF

As for the observation of boron containing products in this 1:1 reaction between **2b** and DMAB, at intermediate reaction times, small amounts of boronium cation

31·NHMe₂ were detected, but at variance with reactions using complex **1**, it did not form in the same amounts as the detected neutral dihydride. Interestingly, no other soluble boron containing species were detected upon DMAB consumption and the formation of a white precipitate was observed.

If cationic hydride **34**, which unlike its ^tBu counterpart **32** can be isolated as a solid, is used as the initial catalyst, reaction again is very slow but in this case aminoborane is observed, besides boronium cation **31·NHMe₂**, along with [BH₂NMe₂]₂, which is the final boron containing product. For this reaction **31·NHMe₂** is always present in the same amounts as neutral dihydride **35** and the final platinum species is the dihydrogen adduct of **34**. In this case small amounts of the carbene borane adduct **33**¹⁷ were observed (Scheme 12).



Scheme 12. Reaction products for the catalytic dehydrogenation of DMAB with cationic hydride **34**

¹⁷ Ueng, S.-H.; Makhoulouf Brahmī, M.; Derat, É.; Fensterbank, L.; Lacôte, E.; Malacria, M.; Curran, D. P. *J. Am. Chem. Soc.* **2008**, *130*, 10082.

As for reactions with ammonia borane, when a 1:1 mixture of AB and complex **2b** was monitored by ^1H NMR spectroscopy in d_8 -THF, the initial formation of a **2b**·AB adduct was observed, which as discussed in section 2.3, is due to the steric bulk of the substrate being now smaller. Again no cyclometallated neutral hydride equivalent to **30** is observed even though $[\text{BH}_2(\text{NH}_3)_2]^+$ is detected in the ^{11}B NMR spectrum and is the final boron containing species. However, in this system B–N bond cleavage seemed to be favoured as the ammonia adduct of cationic hydride **34** and carbene borane adduct **36** soon became the major species. The difference in decomposition behavior between reactions with AB or DMAB may again be related to steric hindrance, which renders dehydrogenation very slow for DMAB but also minimizes side reactions such as catalyst decomposition to yield **36**. The tendency towards decomposition for reactions with AB led us to abandon the study of further reactivity in this system.

2.8.3. Dehydrogenation of amineboranes with complexes **15** and **16**

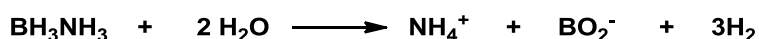
As described in section 2.3, addition of an excess of AB to solutions of **15** leads to the formation of adduct **15**·AB and signals for the excess of AB are seen separately at the chemical shifts of the free species (Figure 13). As the temperature is raised over 0 °C, a neutral hydride is formed with a Pt–H resonance at -5.66 ppm ($^1J_{\text{PtH}} = 818$ Hz) and a Pt–CH₃ at -0.47 ppm ($^2J_{\text{PtH}} = 55$ Hz). This hydride, in all likelihood analogous to **30**, could not be independently prepared by reaction of **15** with NaH, as it appeared to be unstable under analogous reaction conditions and a variety of unidentified species were obtained. The same behavior was observed in the reaction of AB with complex **16**, for which the corresponding neutral hydride appeared at -5.20 ppm with a $^1J_{\text{PtH}}$ of 863 Hz.

In both cases $^+\text{BH}_2(\text{NH}_3)_2$ is initially formed, but the final boron containing dehydrogenation products could not be identified. Significant B–N cleavage seems to take place, as the ammonia adducts of the cationic hydrides derived from **15** and **16** are detected, along with other platinum derived species that could not be identified. Interestingly, hydride signals suggesting the presence of platinum dimers containing both bridging and terminal hydrides are detected in small amounts in both cases. Moreover, for complex **16** a hydride signal similar to that observed for reactions of **1** with AB and TBAB, which was attributed to a platinum dimer with a single terminal hydride, was formed ($\delta_{\text{H}} -10.8$ ppm, $^1J_{\text{PtH}} = 476$ Hz,

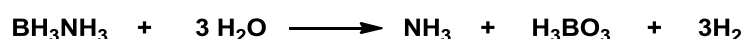
$^2J_{\text{PtH}} = 959$ Hz). Due to the complexity of the mixture of platinum species upon reaction completion it was not possible to isolate and characterize these products.

2.9. Hydrolysis of ammonia borane

Another approach to hydrogen release from amine boranes is metal-mediated B-N dissociation and solvolysis.¹⁸ Even though this reactivity was known, this process was not reported with the specific aim of hydrogen release until 2006 by Xu *et al.*¹⁹ They reported that although ammonia borane water solutions were highly stable, the addition of catalytic amounts of suitable Pt, Pd or Rh species led to rapid evolution of H₂. Given that tertiary amine boranes can be used as the hydrogen source²⁰ it was clear that the BH₃ unit was the source of hydridic hydrogens, whereas protons are provided by the protic solvent. In this manner, up to 3 equivalents of H₂ can be released, as depicted below for a reaction with water:



If an excess of water is present, ammonia is released and boric acid is the final boron containing product²¹:



Complex **1** proved to be very active in the catalytic solvolysis of AB. Reactions carried out under air in THF that had not been previously dried led us to the observation of a much faster reaction than those carried out under anhydrous conditions. ¹¹B NMR spectra of these solutions after hydrogen evolution showed a very broad singlet resonance centered at 18 ppm, indicating that BH₃ hydrolysis had taken place with the formation of B(OH)₃.

¹⁸ Staubitz, A.; Robertson, A.P.M.; Manners, I. *Chem. Rev.* **2010**, *110*, 4079–4124

¹⁹ Chandra, M.; Xu, Q. *J. Power Sources* **2006**, *156*, 190.

²⁰ Couturier, M.; Tucker, J. L.; Andresen, B. M.; Dube', P.; Brenek, S. J.; Negri, J. T. *Tetrahedron Lett.* **2001**, *42*, 2285.

²¹ Liu, C.H.; Wu, Y.C.; Chou, C.C.; Chen, B.H.; Hsueh, C.L.; Ku, J.R.; Tsau, F.; *Int. J. Hydrogen Energy*, **2012**, *37*, 2950-2959.

Addition of water led to an increase in the reaction rate, as depicted in Figure 29. With a large excess of water (e.g. 100 equivalents) release of 3 equivalents of H_2 was completed in under 1 minute with a catalyst loading of 0.5 mol%.

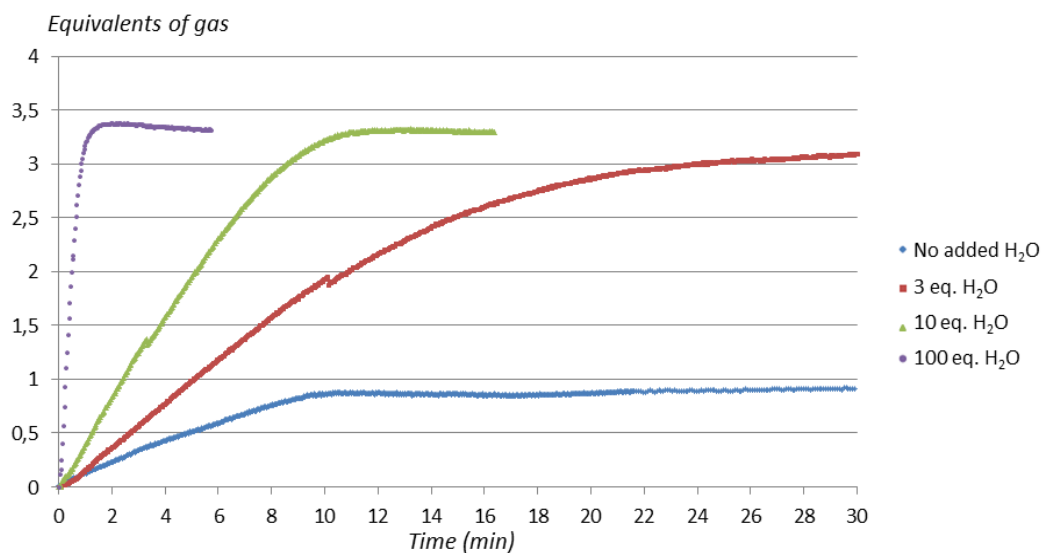


Figure 29. Monitoring of the amount of H_2 released in the catalytic dehydrogenation of a 0.5 M solution of BH_3NH_3 in THF with 0.5 mol% of **1** and different amounts of added water in a closed reaction vessel.

Catalyst loadings as low as 0.15 mol% proved to still give a good performance (Figure 30), with the release of 3 equivalents of H_2 being complete in 5 minutes for reactions with a large excess of water. These results are among the best reported in the literature.²²

²² Umegaki, T.; Yan, J.M.; Zhang, X.B.; Shioyama, H.; Kuriyama, N.; Xu, Q. *Int. J. Hydrogen Energy*, **2009**, *34*, 2303 – 2311

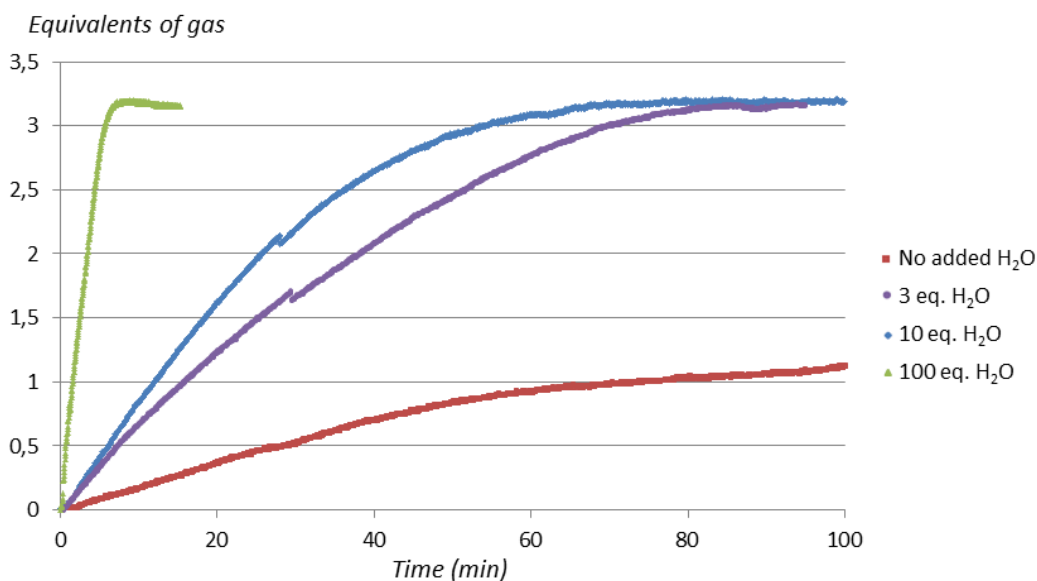


Figure 30. Monitoring of the amount of H₂ released in the catalytic dehydrogenation of a 0.5 M solution of BH₃NH₃ in THF with 0.15 mol% of **1** and different amounts of added water in a closed reaction vessel

Interestingly, both Figure 29 and Figure 30 show the evolution of more than 3 equivalents of gas for the higher water loadings. This is probably due to the contribution of free NH₃ to the pressure in the reaction vessel and some warming due to the reaction being exothermic.

As for the fate of the platinum catalyst, ¹H NMR spectra showed that the ammonia adduct of complex **1**, [Pt(^tBu')(^tBu)(NH₃)[[BAr^F]] was the final species. This species is still catalytically active, as evidenced by the sequential addition of several equivalents of ammonia borane, depicted in Figure 31. Even though the extent of hydrogen release is higher for the first AB batch, the catalyst is still quite active in the following runs.

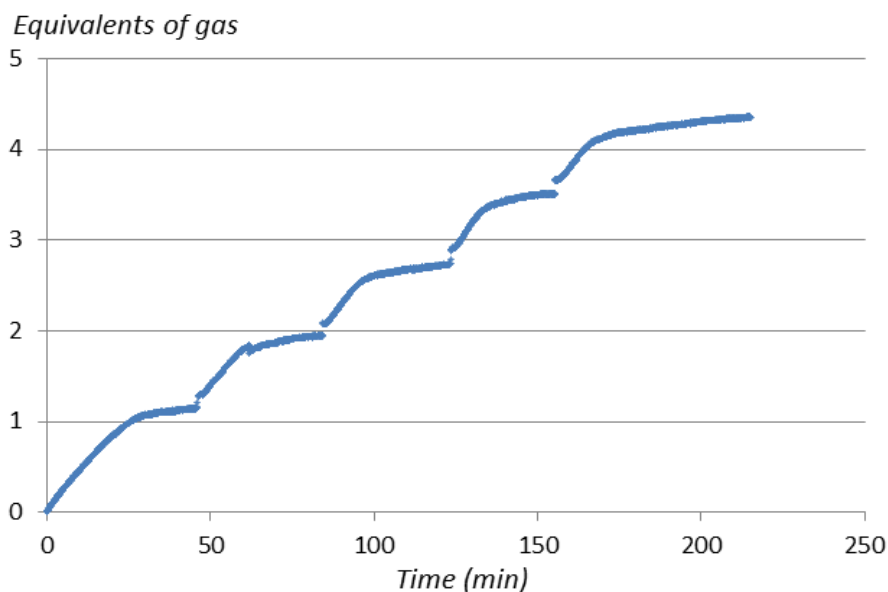


Figure 31. Monitoring of the amount of H₂ released in the catalytic dehydrogenation of a 0.5 M solution of BH₃NH₃ in THF with 0.3 mol% of **1** to which sequential batches of 1 equivalent of BH₃NH₃ were added over time. No added water was present in this test.

2.10. Synthesis of diaminoboranes

As mentioned in previous sections, the study of the products of the catalytic dehydrogenation of DMAB with complex **1** consistently revealed the formation of small amounts of diaminoborane BH(NMe₂)₂ in the reaction crudes. As the role of free amine in the reaction mechanism was disclosed, some reactions with stoichiometric amounts of dimethylamine were carried out. Interestingly, for a 1:1 reaction, not only aminoborane but also BH(NMe₂)₂ were initially observed and in under 15 minutes (with 5 mol% of **1**) all DMAB had been consumed to yield a 1:1 mixture of BH(NMe₂)₂ and cyclic dimer [BH₂NMe₂]₂. Adding a larger excess of amine, namely 5 equivalents, results in exclusive formation of BH(NMe₂)₂, with no aminoborane being detected.

Early reports indicated that diaminoboranes could be prepared by reaction of aminoborane and amine,²³ but in the absence of a catalyst temperatures over 150

²³ a) Burg, A. B.; Randolph, C. L. *J. Am. Chem. Soc.* **1951**, *73*, 953; b) Köster, R.; Bellut, H.; Hattori, S. *Liebigs Ann. Chem.* **1968**, *720*, 1

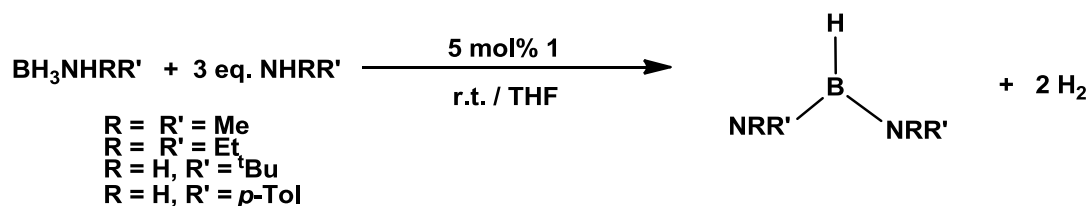
°C were typically needed for the reaction to proceed and even then long reaction times were necessary. Therefore it appeared that the presence of a metal catalyst greatly facilitated this transformation, and encouraged with our preliminary results for DMAB we tested a variety of primary and secondary amineboranes using 5 mol% of complex **1** as a catalyst and 3 equivalents of the corresponding amine.

In these conditions, *p*-tolylamine borane was found to react with *p*-tolylamine the fastest to yield the expected diaminoborane product with concomitant release of dihydrogen, whereas reactions with *t*-butylamine borane and diethylamine borane proceeded in a similar way as DMAB, with reactions being complete in 15-20 minutes at room temperature in quantitative spectroscopic yields without any other by-products (Table 2).

	Reaction time	¹¹ B NMR (ppm)	¹ J _{BH} (Hz)
BH(NMe₂)₂	>15 min	28.7	130
BH(NEt₂)₂	15-20 min	28.5	128
BH₂(<i>p</i>-Tol)	>5 min	26.1	134
BH₂(^tBu)	15-20 min	25.5	125

Table 2. Reaction times at room temperature and ¹¹B NMR data for the prepared diaminoboranes

The color of the solutions during the reaction served as an indicator of the end catalysis, since in the course of the process the solution is colorless and soon after all amine-boranes are consumed the characteristic pale yellow solutions containing complex **1** (probably interacting with excess of amines) is clearly discernible.

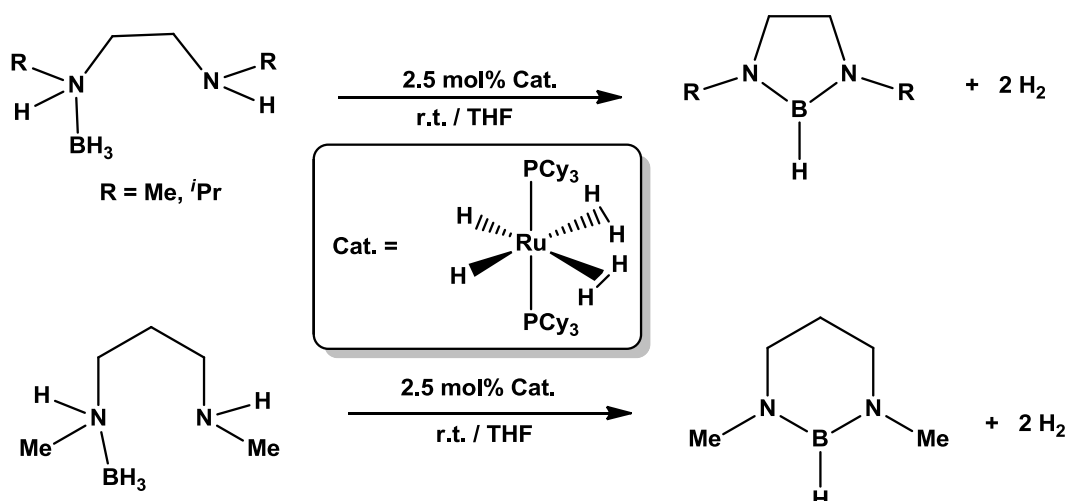


Scheme 13. Synthesis of symmetrical aminoboranes

As mentioned above, reactions with diisopropylamine borane did not proceed at room temperature, probably due to steric reasons. It was found that dehydrogenation could take place with catalyst **1** if the reaction was heated at 60 °C for 15h, resulting in diisopropylaminoborane monomer. Carrying out the reaction in the same conditions, but in the presence of 3 equivalents of diisopropylamine did not lead, however, to the formation of the diaminoborane, as was observed for less bulky amines. In this case the aminoborane remained unreacted.

To the best of our knowledge, there are only two previous examples of metal catalyzed formation of diaminoboranes. The first was reported by Sabo-Etienne²⁴ and involves an intramolecular reaction in which a bis(dihydrogen) ruthenium catalyst produces the cyclization of diamine-monoboranes (Scheme 14).

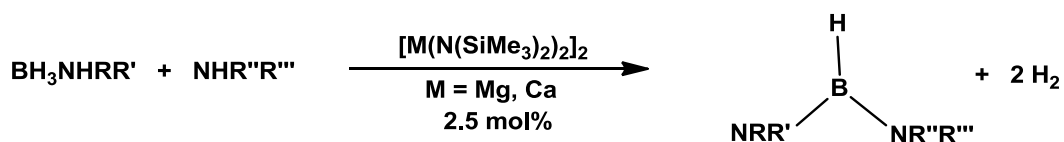
²⁴ Wallis, C. J.; Dyer, H.; Vendier, L.; Alcaraz, G.; Sabo-Etienne, S. *Angew. Chem. Int. Ed.* **2012**, *51*, 3646



Scheme 14. Synthesis of cyclic diaminoboranes, reported by Sabo-Etienne²⁴

This reaction required 3h to reach completion for the methyl substituted diamineborane, but was slower for bulkier amines (e.g. 8h for R = *i*Pr).

Another example, in this case of an intermolecular reaction, was presented by Hill²⁵ and it used group 2 amido complexes to prepare unsymmetrical diaminoboranes with a variety of R groups including methyl, isopropyl, *t*-butyl, ethylene and phenyl (Scheme 15).



Scheme 15. Synthesis of unsymmetrical diaminoboranes²⁵

In this case, the intermolecular reaction was rather slow and typically needed 24h at 70 °C to reach completion.

It appears then that our platinum system is more efficient than these previous reports for the catalytic synthesis of diaminoboranes. Further investigations to test the applicability of the system and to gather mechanistic information are under way.

²⁵ Bellham, P.; Hill, M. S.; Kociok-Köhn, G.; Liptrot, D. J. *Chem. Commun.*, **2013**, 49, 1960

CHAPTER 3

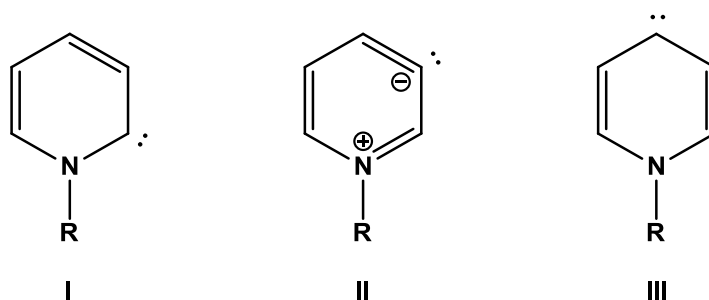
A general route to 2-pyridylidene transition
metal complexes

CHAPTER 3. INTRODUCTION

Pyridylidenes: a family of non-conventional NHCs

III.1. General properties

Pyridylidene carbenes are derived from pyridine rings and can be present in three different isomers, as depicted in Scheme 1, which are usually considered as normal carbenes (**I**), mesoionic carbenes (**II**) or remote carbenes (**III**) according to the location of carbene with respect to the nitrogen atom (**I** and **III**) and to the impossibility to write a structure without introduction of formal charges on the structure (**II**).¹



Scheme 1. 2-, 3- and 4-pyridylidene carbenes.

Although the free carbenes have not been isolated in their free form until present, they have been postulated as intermediates in several occasions. Hammick was one of the firsts to suggest that transient pyridylidenes are formed during

¹ For a review regarding abnormal, mesoionic and remote NHCs see: Crabtree, R. H. *Coord. Chem. Rev.* **2013**, 257, 755.

decarboxylation reactions of 2-picolinic acid, but unequivocal evidence for its transient formation was made in the gas-phase by Schwarz in 1996.²

The stability of 2-pyridylidenes (**I**) is believed to be less than imidazol-2-ylidenes but comparable to imidazolidine-2-ylidenes,³ whereas isomers **II** and **III** are even more unstable.⁴ These carbenes are expected to have better electron donor properties than imidazol-2-ylidenes due to the fact that the carbenic carbon atom is flanked by only one nitrogen atom and carbon nuclei. In addition to the good sigma-donor properties, these pyridine-derived carbenes can also act as good π -acceptors towards transition metals. Bercaw argued that their π -acidity is indeed a feature that sets them apart when compared to structurally analogous pyridyl and pyridine complexes. This was suggested by the structural, spectroscopic and kinetic data of his study of a series of Pt 2-pyridylidene and related complexes.⁵ Later studies by Raubenheimer⁶ and Nechaev⁷ with DFT calculations of model 2-pyridylidene and 2-imidazolylidene carbenes indicated that the HOMO of the former was higher in energy, making them better σ -donors and that their LUMO was lower in energy, indicating they are also better π acceptors than classical carbenes (Figure 1).

² Lavorato, D.; Terlouw, J. K.; Dargel, T. K.; Koch, T.; McGibbon, G. A.; Schwarz, H. *J. Am. Chem. Soc.* **1996**, *118*, 11898.

³ Hollóczy, O.; Nysulaszi, L. *J. Org. Chem.* **2010**, *73*, 4794.

⁴ Lavorato, D.J.; Terlouw, Graham, J.K.; McGibbon, A.; Dargel, T.K.; Koch, W.; Schwarz, H. *Int. J. Mass Spectrom.* **1998**, *179/180*, 7.

⁵ Owen, J.S.; Labinger, J.A.; Bercaw, J.E. *J. Am. Chem. Soc.* **2004**, *126*, 8247

⁶ Raubenheimer, R. G.; Cronje, S. *Dalton Trans.* **2008**, 1265

⁷ Tukov, A. A.; Normand, A. T.; Nechaev, M. S. *Dalton Trans.* **2009**, 7015.

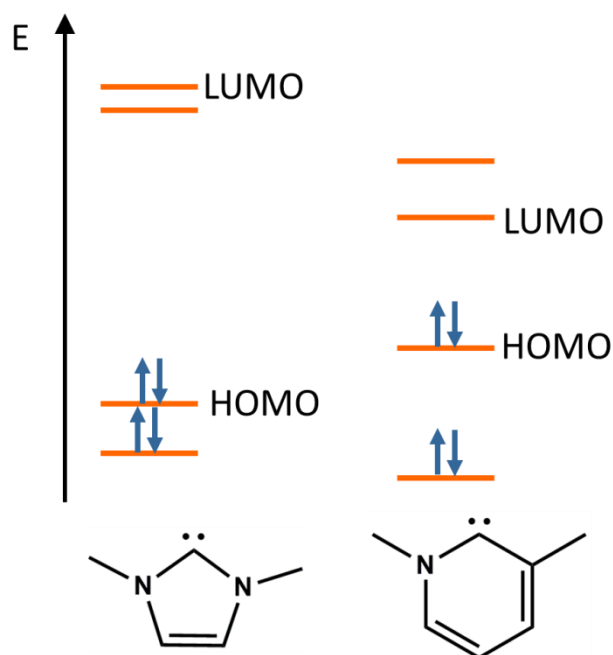


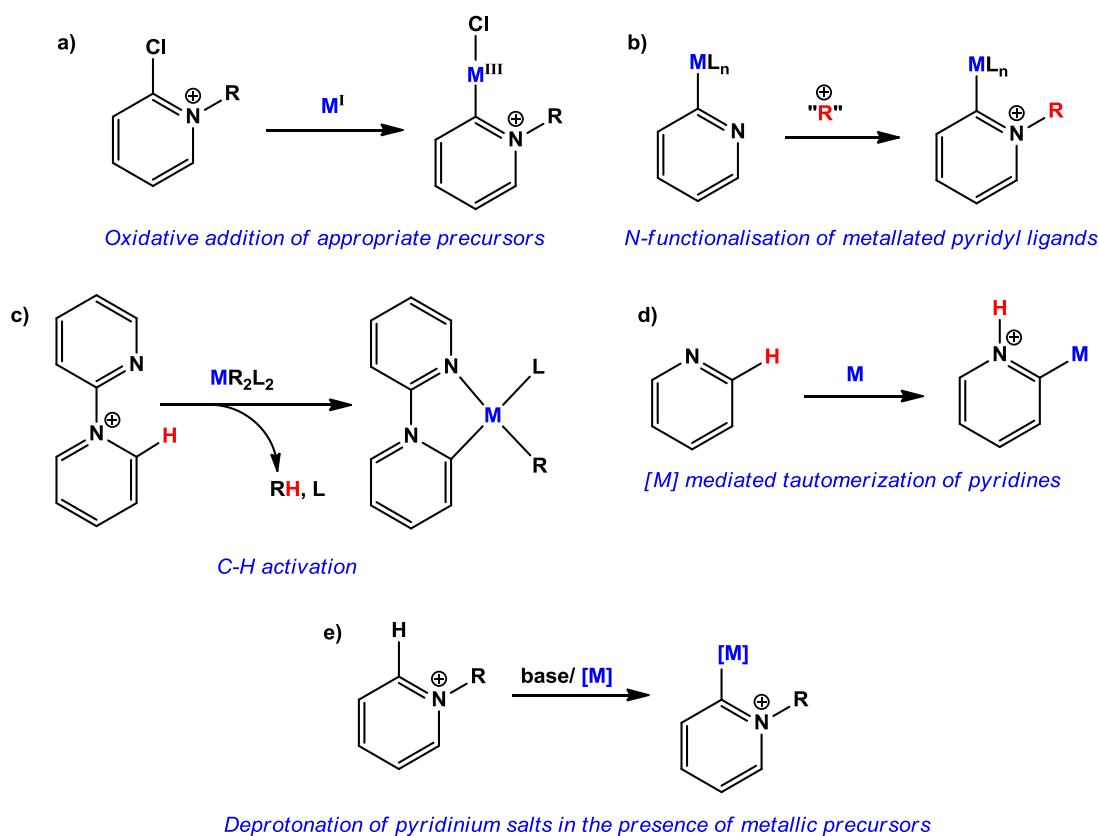
Figure 1. Relative energies of frontier orbitals of 2-imidazolylidene and 2-pyridylidene carbenes. Adapted from Nechaev.⁷

In spite of the lack of methods to prepare free pyridylidenes, their complexes are known since the middle 1970's. The first examples of pyridylidene transition metal complexes were reported by Stone⁸ and used N-methyl-2-chloropyridinium salts and metal carbonyl precursors to generate complexes of a variety of metals.

III.2. Current methods for the preparation of 2-pyridylidene transition metal complexes

As stated before, unlike the ubiquitous 2-imidazolylidenes which can in most cases be isolated as stable free carbenes, free pyridylidenes have only been characterized so far in the gas phase by mass chromatography.² This precludes the use of free carbenes in straightforward synthetic procedures so a variety of alternative routes has been devised to obtain these transition metal complexes, as summarized in Scheme 2.

⁸ a) Fraser, P. J.; Roper, W. R.; Stone, F. G. A. *J. Chem. Soc., Dalton Trans.* **1974**, 760; b) Green, M.; Underbill, M.; Stone, F. G. A. *J. Chem. Soc., Dalton Trans.* **1975**, 939.



Scheme 2. Major previously reported methods for the synthesis of 2-pyridylidene transition metal complexes.

III .2.1. Oxidative addition methods

The first reported 2-pyridylidene complexes mentioned above were prepared using method (a) (Scheme 2) based on the oxidative addition of appropriate precursors to transition metal complexes. Usually transition metal species in a low oxidation state are used and the oxidation state increases +2 in the resulting complex.

The first examples reported by Stone were prepared by oxidative addition of 2-chloropyridinium salts to yield Ir(I), Rh(I), Mn(I), Cr(0), Fe(0) and Os(0) complexes. $[\text{Ir}(\text{CO})_3\text{PPh}_3]^-$, $[\text{Rh}(\text{CO})_2(\text{PPh}_3)_2]^-$, and $[\text{Mn}(\text{CO})_5]^-$ produced cationic 2-pyridylidene derivatives, whereas dianionic $[\text{Cr}(\text{CO})_5]^{2-}$, $[\text{Fe}(\text{CO})_4]^{2-}$ and $[\text{Os}(\text{CO})_4]^{2-}$ resulted in neutral species.^[Error! Marcador no definido.]

As dianionic complexes are scarce, Schubert introduced the use of monoanionic silyl and stannyl complexes of the type $M(ER_3)L_n^-$ ($E = Si, Sn$), as ER_3Cl could be easily eliminated after oxidative addition of the pyridinium salt to yield the desired 2-pyridylidene complex.⁹ This strategy was used for Mn complexes and for the only Rh bis-pyridylidene complex reported so far, by the same group.¹⁰

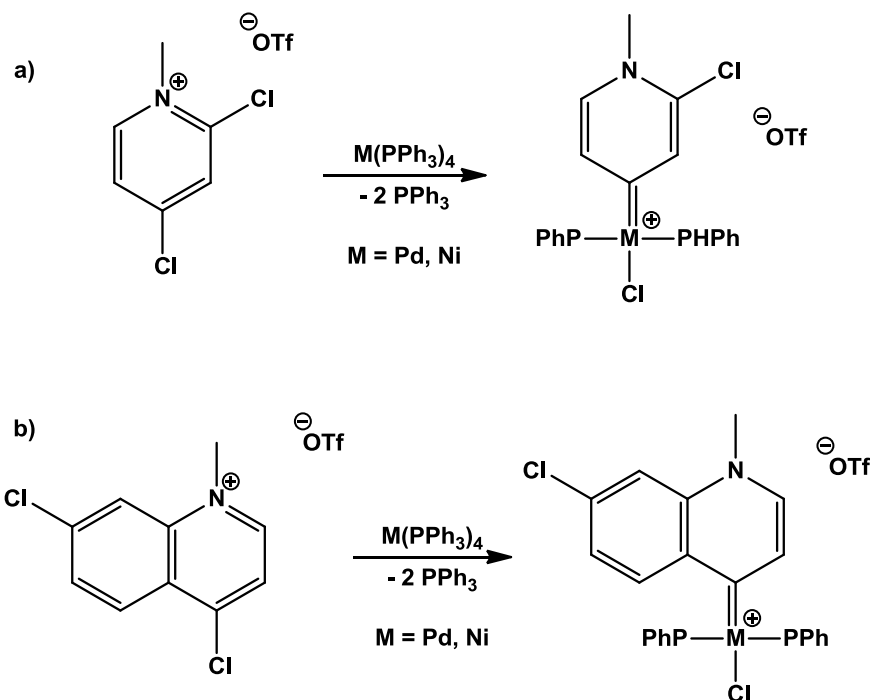
Raubenheimer did a systematic study of the oxidative addition of a variety of halopyridinium salts to Ni, Pd and Pt zerovalent complexes that led not only to 2-pyridinium $M(II)$ complexes but to abnormal and remote 3- and 4-pyridylidene complexes. The same procedure could be extended to quinolinium and acridinium salts to obtain the corresponding group 10 metal carbenes complexes. Some interesting conclusions could be drawn from these studies, most importantly that remote carbenes had the best σ donor properties. This had been determined by DFT calculations but was ascertained by structural analysis of bond distances, which reflect the *trans* influence of the pyridylidene ligands.^{6,11} In fact, calculations indicated that the less stable free carbenes (e.g. 4-pyridylidene vs 2-pyridylidenes) formed the stronger carbene-metal bonds. Moreover, even though oxidative addition of 2-halopyridinium salts was calculated to be more facile than that of their 4-isomers the latter effect won over, as proved by the oxidative addition of a 2,4-dichloropyridinium salt that led exclusively to the 4-pyridylidene carbene having the stronger carbene-metal bond (Scheme 3, a).¹²

⁹ Kirchgaessner, U.; Piana, H.; Schubert, U. *J. Am. Chem. Soc.* **1991**, *113*, 2228.

¹⁰ Schubert, U.; Seebald, S. *J. Organomet. Chem.* **1994**, *472*, C15.

¹¹ a) Schneider, S. K.; Julius, G. R.; Loschen, C.; Raubenheimer, H. G.; Frenking, G.; Herrmann, W. A. *Dalton Trans.* **2006**, 1226; b) Schneider, S. K.; Roembke, P.; Julius, G. R.; Raubenheimer, H. G.; Herrmann, W. A. *Adv. Synth. Catal.* **2006**, *348*, 1862; c) Meyer, W. H.; Deetlefs, M.; Pohlmann, M.; Scholz, R.; Esterhuysen, M. W.; Julius, G. R.; Raubenheimer, H. G. *Dalton Trans.* **2004**, 413.

¹² Stander-Grobler, E.; Schuster, O.; Heydenrych, G.; Cronje, S.; Tosh, E.; Albrecht, M.; Frenking, G.; Raubenheimer, H.G. *Organometallics* **2010**, *29*, 5821.



Scheme 3. Preference of 4-pyridylidene vs 2-pyridylidene formation by oxidative addition (a), preference for oxidative addition at N-containing ring at quinolylidenes (b)¹²

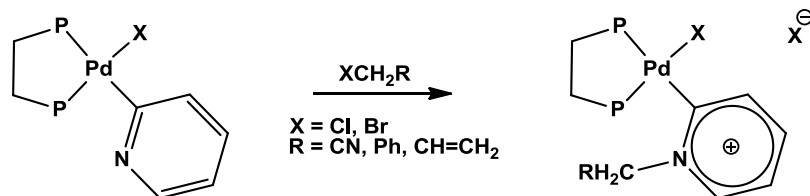
Another competition experiment that used a dichlorinated quinolinium salt showed that oxidative addition took place exclusively at the heterocycle, even though both C–Cl bonds were equally distant from the N atom (Scheme 3, b).¹²

III.2.2. N-functionalisation of metallated pyridyl ligands

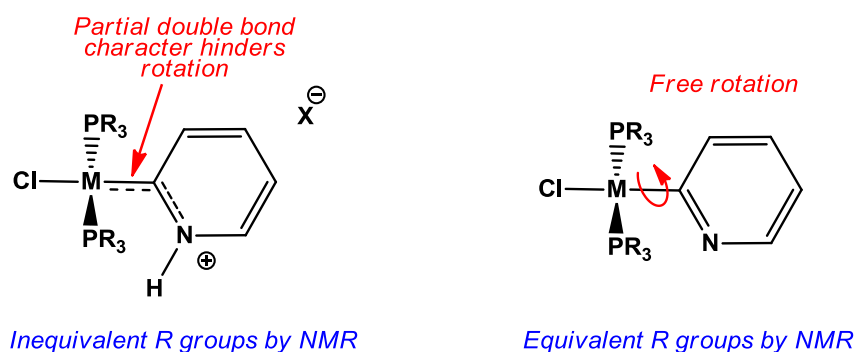
Another method for the preparation of pyridylidene complexes consists on the N-functionalisation of preformed pyridyl complexes. This method was successfully applied by Isobe¹³ and Crociani¹⁴ in the 1980s to prepare Ni, Pd and Pt complexes either by protonation or alkylation of the pyridyl nitrogen atom.

¹³ Isobe, K.; Kai, E.; Nakamura, Y.; Nishimoto, K.; Miwa, T.; Kawaguchi, S.; Kinoshita, K.; Nakatsu, K. *J. Am. Chem. Soc.* **1980**, *102*, 2475.

¹⁴ a) Crociani, B.; Di Bianca, F.; Gioenco, A.; Scriveranti, A. *J. Organomet. Chem.* **1983**, *251*, 393; b) Crociani, B.; Di Bianca, F.; Gioenco, A.; Berton, A. *J. Organomet. Chem.* **1987**, *323*, 123.

Scheme 4. Some examples of pyridylidene complexes reported by Crociani¹⁴

In all cases N-functionalisation led to a downfield shift of the metal bound carbon in the ^{13}C NMR spectra, which was explained by an increased M–C bond order due to the participation of a carbene resonant form. Further experimental evidence to support the participation of this structure is the observed hindered rotation around the M–C bond, which was tested via proton NMR experiments.¹⁴ This effect was not steric, as the analogous pyridyl complex presented fast rotation in the NMR timescale (Scheme 5).

Scheme 5. Pyridylidene complexes have a partial double bond character when compared to their pyridyl counterparts.^{14b}

Protonation of a pyridyl complex has also been used by Raubenheimer to produce gold 2-pyridylidene complexes.¹⁵ His group has also used N-alkylation to prepare group 10 transition metal complexes previously prepared by oxidative addition of halopyridinium salts.^{11c,16} Maitlis prepared the three isomers of rhodium

¹⁵ Raubenheimer, H. G.; Toerien, J. G.; Kruger, G. J.; Otte, R.; van Zyl, W.; Olivier, P. J. *Organomet. Chem.* **1994**, 466, 291.

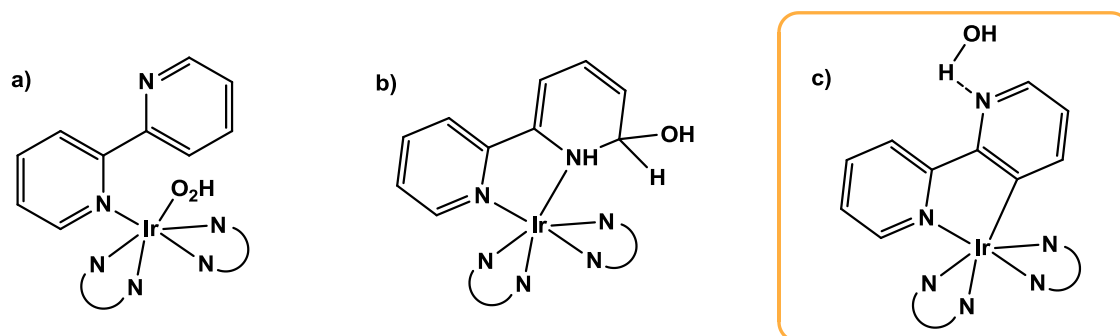
¹⁶ Schuster, O.; Raubenheimer, H.G. *Inorg. Chem.* **2006**, 45, 7997

pyridylidene complexes by the decarbonylative addition of 2-, 3- and 4-pyridine aldehydes to rhodium precursors and subsequent alkylation of the pyridyl rhodium complexes.¹⁷ A similar 4-pyridylidene iridium complex was prepared by a related method.

III.2.3. C–H bond activation with pyridium cations

A third method, related to the oxidative addition of halogenated precursors previously discussed, is the formation of pyridylidene complexes via C–H bond activation of pyridinium ligands, which has the advantage that previous functionalisation (e.g. halogenation) of the pyridinium ring is not necessary provided that the C–H activation step is selective for a particular ring position.

The first example of this procedure was the synthesis of an iridium pyridylidene complex by cyclometallation in an iridium bipy complex, reported by Watts in 1977¹⁸ whose exact nature was controversial until the publication of its X-ray structure¹⁹ (Scheme 6).



Scheme 6. Initial structure for the iridium bipy complex reported by Watts (a), alternative structure proposed with the basis of NMR experiments (b)²⁰ and final pyridylidene structure as confirmed by X-ray diffraction studies (c).

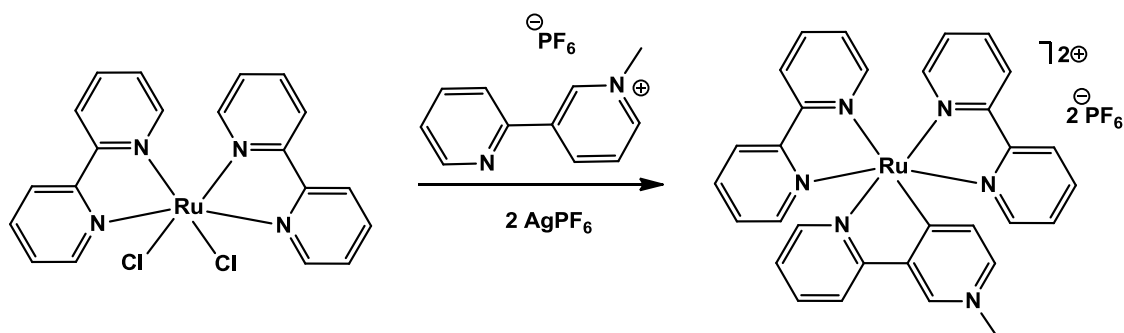
¹⁷ Fanizzi, F. P.; Sunley, G. J.; Wheeler, J. A.; Adams, H.; Bailey, N. A.; Maitlis, P. M. *Organometallics* **1990**, *9*, 131.

¹⁸ Watts, R. J.; Harrington, J. S.; Van Houten, J. *J. Am. Chem. Soc.* **1977**, *99*, 2179.

¹⁹ Wickramasinghe, W. A.; Bird, P. H.; Serpone, N. *J. Chem. Soc., Chem. Commun.* **1981**, 1284.

²⁰ Gillard, R. D.; Lancashire, R. J.; Williams, P. A. *J. Chem. Soc., Dalton Trans.* **1979**, 190.

Wimmer reported the cyclometallation of 2- and 4-pyridyl pyridinium complexes prepared by reaction with $[\text{MCl}_4]^{2-}$ precursors ($\text{M} = \text{Pd}, \text{Pt}$).²¹ Heating up to 200 °C led to the formation of 3-pyridylidene complexes. If cyclometallation proceeds with a 3-pyridyl pyridinium ligand, both 2- and 4-pyridylidene complexes can in principle be obtained. Reaction with a ruthenium precursor led exclusively to the 4-pyridylidene complex (Scheme 7),²² which parallels the results obtained for the oxidative addition synthetic methods described above.



Scheme 7. C–H activation of a 2,3'-bipyridinium salt leads to exclusive formation of the 4-pyridylidene complex.²²

Ruthenium was also the chosen metal to prepare 3- and 4-pyridylidene complexes from terpyridinium derived ligands.²³ The crystal structure of both species showed almost identical distances for the Pt–C bond, but there were great differences in the metal bound carbon chemical shift and in the Ru(II)/Ru(III) oxidation potential. These effects were explained by the increased backdonation in the case of the 4-pyridylidene complex.

Other examples of C–H activation to yield pyridylidene complexes are those reported by Bercaw for the preparation of platinum complexes using both the $[\text{PtMe}_2(\mu\text{-SMe}_2)]_2$ dimer⁵ and $\text{M}(\text{acac})_2$ precursors²⁴ for other group 10 metals. N-(2-pyridyl)pyridinium salts were used in this case.

²¹ Dholakia, S.; Gillard, R. D.; Wimmer, F. L. *Inorg. Chim. Acta* **1983**, *69*, 179.

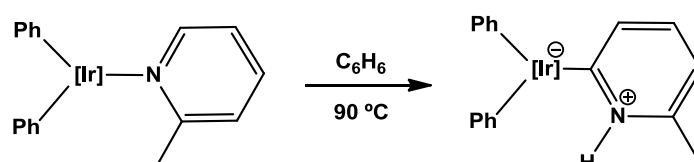
²² Koizumi, T.; Tomon, T.; Tanaka, K. *J. Organomet. Chem.* **2005**, *690*, 1258.

²³ Koizumi, T.; Tomon, T.; Tanaka, K. *Organometallics* **2003**, *22*, 970

²⁴ Piro, N. A.; Owen, J. S.; Bercaw, J. E. *Polyhedron* **2004**, *23*, 2797

III.2.4. Metal mediated tautomerization of pyridines

Pyridylidene complexes have also been obtained by a more specific route in which a pyridine ligand in an iridium complex tautomerizes to the pyridylidene form. This reactivity was first reported by Carmona and Poveda for iridium complexes bearing tris(pyrazolyl)borate (Tp) ligands²⁵, and simultaneously by Esteruelas using osmium complexes.²⁶



Scheme 8. Tautomerization to pyridylidene complex for an iridium pyridine species ($[\text{Ir}] = \text{Tp}^{\text{Me}_2}\text{Ir}$, where $\text{Tp}^{\text{Me}_2} = \text{tris}(3,5\text{-dimethyl})\text{pyrazolyl borate}$).

In the case of the complex with a Tp ligand with 3,5-dimethyl pyrazolyl rings, reaction with 2-picoline at 60 °C leads to the N-coordinated isomer, but higher temperatures (90 °C) lead to a proton shift from the C6 of the pyridine resulting in the pyridylidene isomer. Bulkier substituents at the pyridine C2 position lead similarly to the pyridylidene complex, however unsubstituted pyridine only results in the N coordinated isomer and no tautomerization is observed when heating up to 150 °C. Using a bulkier iridium complex, with 3-mesityl pyrazol rings, two of which cyclometallate to the metal center, the extent of N coordination is reduced and reaction of unsubstituted pyridine at lower temperatures (60 °C) yields a 1:1 mixture of the pyridine and 2-pyridylidene complexes.²⁷ Deuteration experiments indicated that protons of the cyclometallated mesityl substituents are involved in the mechanism of the reaction and partial deuteration at positions 3- and 4- of the pyridine ring indicated that 3- and 4-pyridylidene complexes were also formed but rearrangement to the more stable 2-pyridylidene adduct was observed.

²⁵ Alvarez, E.; Conejero, S.; Paneque, M.; Petronilho, A.; Poveda, M. L.; Serrano, O.; Carmona, E. *J. Am. Chem. Soc.* **2006**, *128*, 13060.

²⁶ Esteruelas, M. A.; Fernández-Alvarez, F. J.; Oñate, E. *J. Am. Chem. Soc.* **2006**, *128*, 13044.

²⁷ Alvarez, E.; Conejero, S.; Lara, P.; Lopez, J. A.; Paneque, M.; Petronilho, A.; Poveda, M. L.; del Rio, D.; Serrano, O.; Carmona, E. *J. Am. Chem. Soc.* **2007**, *129*, 14130.

This tautomerization appears to be more common than previously thought and was also observed for the reaction of quinoline with osmium and ruthenium hydride complexes²⁸ and for the reaction of 2,3'-bipy with $[\text{Ir}(\text{cod})_2][\text{BF}_4]$.²⁹

III.2.5. Deprotonation of pyridinium salts / transmetalation.

A final method, based on deprotonation of the acidic C2-H of pyridinium salts was first reported by Cabeza³⁰ to yield pyridylidene bridged ruthenium clusters. So far this procedure is of limited scope as the reactivity of the pyridylidene remains unclear and only one other example of this synthetic route, in this case using a bulky pyridinium salt and a gold precursor has been reported so far.³¹

III.3. Towards decarboxylation as a useful synthetic procedure for 2-pyridylidene complexes

All the methods discussed above are useful for specific combinations of ligands and metal fragments, but present some drawbacks such as the increase in the oxidation state of the metal, the need to pre-form certain complexes (e.g. pyridyl-M) or to functionalise the starting material (e.g. synthesis of halopyridinium salts). We set about devising a new more widely applicable method for the preparation of 2-pyridylidene transition metal complexes that made use of the decarboxylation of pyridinium carboxylates, a reactivity that had been known for decades. This concept has recently been exploited by Crabtree for the synthesis of classical imidazolylidene transition metal complexes using imidazolium carboxylates as starting materials.³² The major advantage of this procedure is that, in principle, it might be a general method that will not require an increase in the oxidation state of the metal nor special ligands other than good leaving groups.

²⁸ Esteruelas, M. A.; Fernandez-Alvarez, F. J.; Oñate, E. *J. Am. Chem. Soc.* **2006**, *128*, 13044.

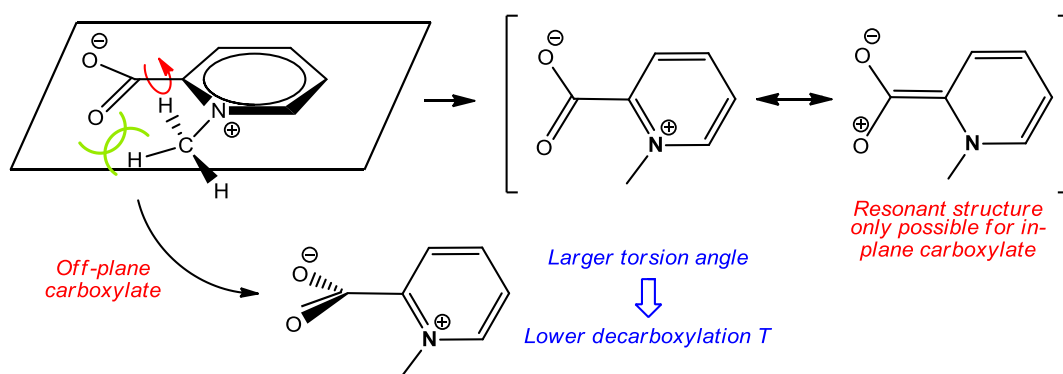
²⁹ Song, G.; Li, Y.; Chen, S.; Li, X. *Chem. Commun.* **2008**, 3558.

³⁰ Cabeza, J. A.; del Río, I.; Pérez-Carreño, E.; Sánchez-Vega, M. G.; Vázquez-García, D. *Angew. Chem. Int. Ed.* **2009**, *48*, 555.

³¹ Hata, K.; Segawa, Y.; Itami, K. *Chem. Commun.*, **2012**, *48*, 6642.

³² Voutchkova, A.M.; Appelhans, L.N.; Chianese, A.R.; Crabtree, R.H. *J. Am. Chem. Soc.* **2005**, *127*, 17624.

The first reports about the decarboxylation of pyridinium carboxylates were published by Hammick over 70 years ago³³ noting that the decarboxylation of pyridine 2-carboxylic acid (commonly known as 2-picolinic acid) took place much more readily than for its 3- and 4-isomers. They assumed that the inductive effect of the adjacent nitrogen atom stabilized the intermediate ylide resonant form. Later reports indicated that N-alkylated 2-pyridinium carboxylates released CO₂ up to 700 times faster than 2-picolinic acid.³⁴ This was caused not only by inductive effects but by the interaction of the N-methyl group with the carboxylate, which hindered its in-plane disposition inhibiting π delocalization and thus weakening the bonding between the carboxylate and the ring (Scheme 9).



Scheme 9. N-substitution pushes the 2-carboxylate group out of the ring plane.

A similar effect has been proposed for imidazolium carboxylates³⁵ for which a clear relationship was found between the NHC-CO₂ torsion angle and the decarboxylation temperature.

The same paper by Haake and Mantecón indicated the decrease in decarboxylation rate for the 3- and 4-isomers of N-methyl-pyridinium-2-carboxylate in a factor close to the attenuation of inductive effects with distance.

The intermediate pyridylidene formed in the decarboxylation of N-alkylated-pyridinium-2-carboxylates can be trapped by electrophiles, as first demonstrated

³³ a) Dyson, P.; Hammick, D.L. *J. Chem. Soc.*, **1937**, 1724; b) Ashworth, M.R.F.; Daffern, R.P.; Hammick, D.L. *J. Chem. Soc.* **1939**, 809.

³⁴ Haake, P.; Mantecón, J. *J. Am. Chem. Soc.* **1964**, *86*, 5230.

³⁵ Van Ausdall, B. R.; Glass, J. L.; Wiggins, K. M.; Aarif, A. M.; Louie, J. *J. Org. Chem.* **2009**, *74*, 7935.

by Frankenfeld.³⁶ Katritzky also used this procedure to prepare pyridinium salts by protonation of the intermediate carbenes in protic solvent³⁷ and to prepare a variety of organic species by trapping the carbenes with electrophiles.³⁸ For example, aldehydes were obtained using alcohols as electrophiles, diazonium ions gave azo compounds, azides yield triazenes and carbon disulphide gives dithioacids.

These precedents in the reactivity of pyridinium-2-carboxylates led us to test their decarboxylation in the presence of transition metal complexes with labile ligands as “trapping agents”. We expected that the intermediate carbenes would displace such ligands and yield 2-pyridylidene transition metal complexes.

³⁶ Quast, H.; Frankenfeld, E. *Angew. Chem., Int. Ed. Engl.* **1965**, *4*, 691.

³⁷ Katritzky, A.R.; Awartani, R.; Patel, R. C. *J. Org. Chem.* **1982**, *47*, 498.

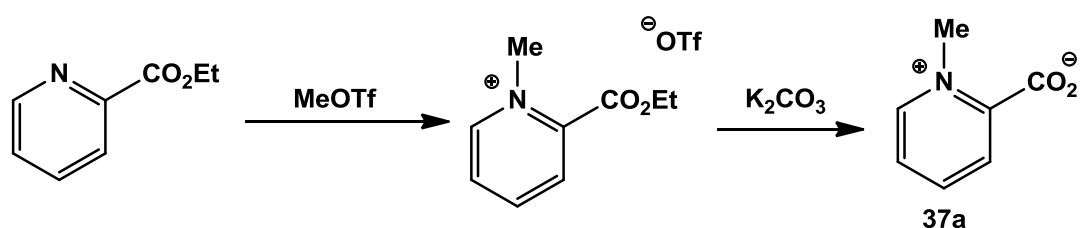
³⁸ Katritzky, A.R.; Faid-Allah, H.M. *Synthesis*, **1983**, 149.

CHAPTER 3. RESULTS AND DISCUSSION

A general route to 2-pyridylidene transition metal complexes

3.1 Preparation of pyridinium carboxylates

The most simple carbene precursor used in our work, N-methyl-2-carboxypyridinium betaine, commonly known as homarine, was prepared by a literature procedure published by Quast and Schmitt¹ that is outlined on Scheme 1. The pyridine nitrogen is first methylated with methyl triflate, in a modification of the original synthetic report, which used iodomethane. Whereas methyl triflate yields the desired product in under an hour, the reaction with iodomethane took one day to reach completion and in our hands it was not so clean. The carboxylic ester is then hydrolyzed to the carboxylate with a base. This is a slow reaction that is carried out in a concentrated aqueous solution at 0 °C. After 3 days the desired product has precipitated out in good yields. Note that the resulting species is zwitterionic, bearing a positive charge on the nitrogen and a negative charge in the carboxylate group.

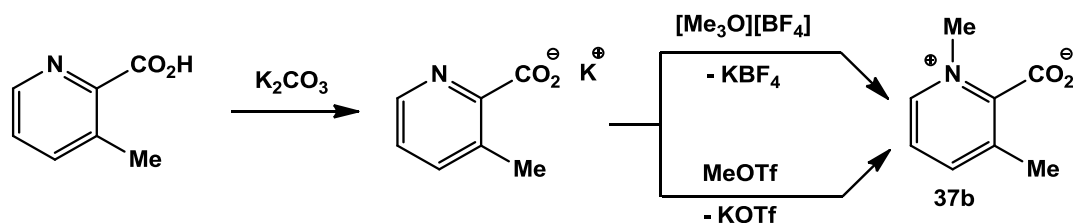


Scheme 1. Synthesis of homarine.

The related species with a methyl group in position 3 had not been described and was prepared from commercial 3-methylpyridine-2-carboxylic acid that was first

¹ Quast, H.; Schmitt, E. *Justus Liebigs Ann. Chem.* **1970**, 732, 64.

deprotonated with potassium carbonate as a base and then methylated at the nitrogen atom with either trimethyloxonium tetrafluoroborate, as depicted in Scheme 2, or with methyl triflate. Similar reaction times (1h) and yields (over 80%) were observed for both methylating agents. The preference for the latter resulted from the ease of separation of the salt by-product.



Scheme 2. Synthesis of 3-methyl homarine.

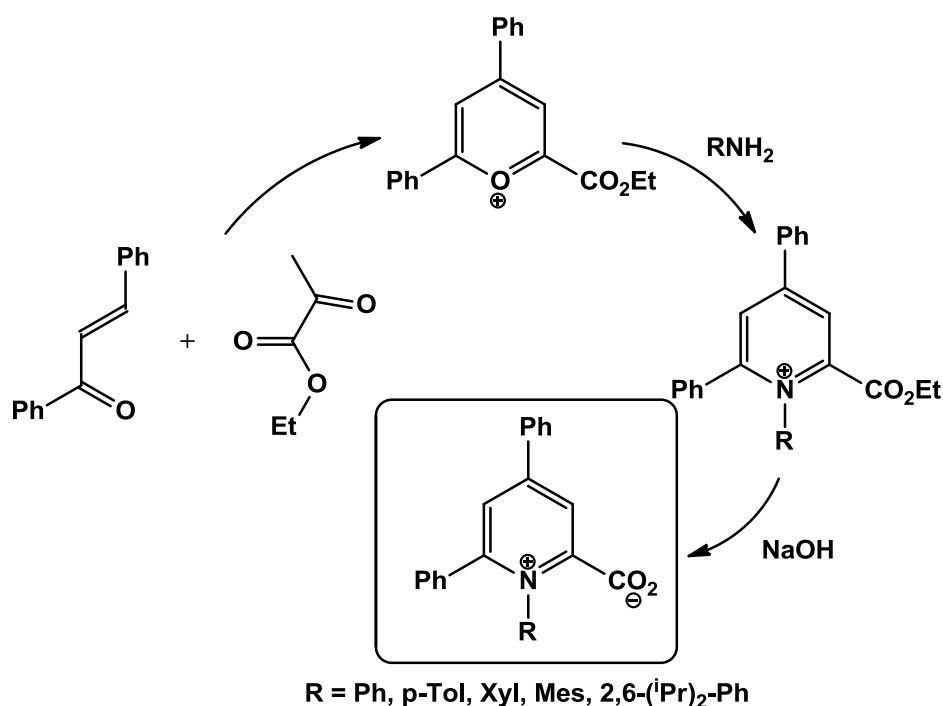
With methyl triflate, potassium triflate was formed as a by-product, which was easier to separate from the resulting betaine than the tetrafluoroborate salt. Still, purification was not straightforward and chromatographic separation was needed.

Betaines **37a** and **37b** are highly hygroscopic white solids that are only soluble in highly polar solvents such as methanol, water or dmsO.

The methods described above to prepare homarine derivatives have as a major drawback that only small alkyl groups (methyl in the precedent examples) can be introduced on the pyridyl unit, Attempts to introduce bulkier groups such as *tert*-butyl or adamantyl failed, as room temperature reactions proved unsuccessful and heating led partly to unwanted decarboxylation and to alkylation exclusively at the carboxylate group. Additionally aryl fragments cannot be incorporated by this procedure. Therefore, to increase the diversity in the pyridine backbone, Katritzky's synthetic procedure for the synthesis of homarine derivatives was employed.² This synthetic route is shown in Scheme 3 and is particularly useful to generate N-arylated pyridinium carboxylates with different steric environments from commercially available reagents. It involves the initial formation of a

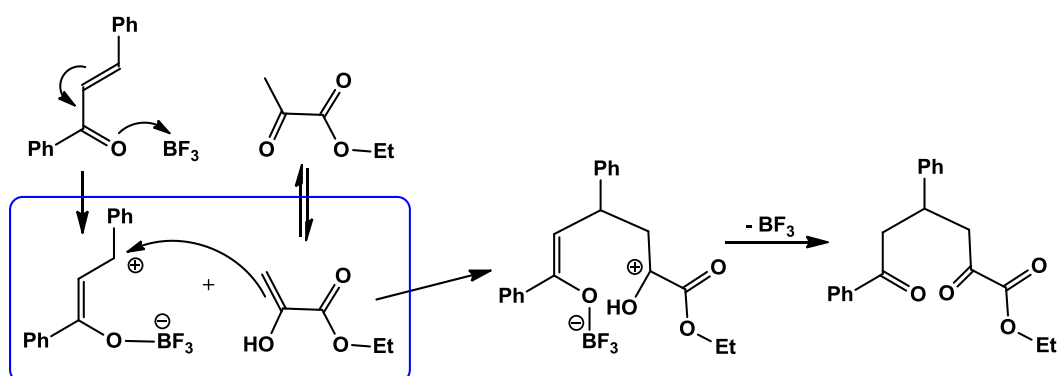
² Katritzky, A. R.; Awartani, R.; Patel, R. C. *J. Org. Chem.* **1982**, *47*, 498.

pyrylium cation that then reacts with a primary amine to produce a pyridinium 2-carboxylic ester which is finally hydrolyzed to the betaine.



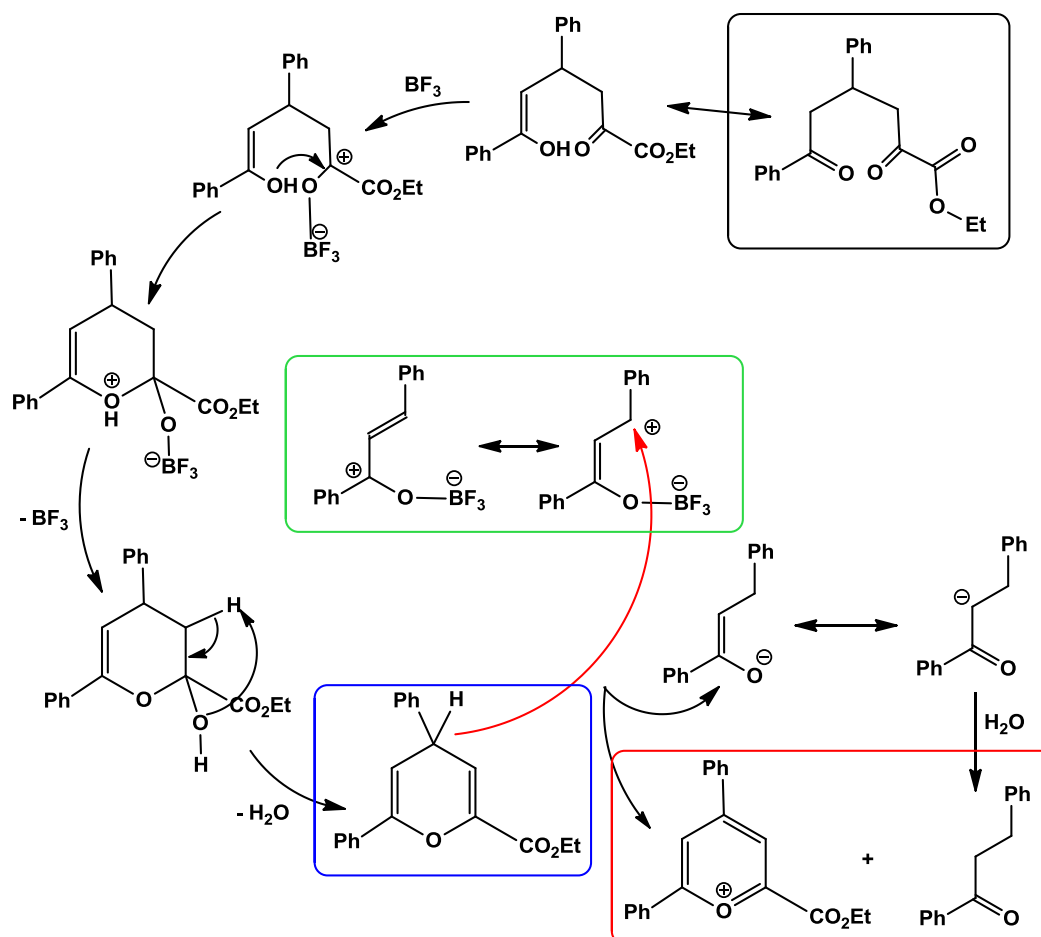
Scheme 3. Katritzky's procedure for the synthesis of betaines.

The first step in the synthesis, outlined in Scheme 4, involves the formation of a cyclic diketone using ethyl pyruvate and 1,3-diphenyl-2-propen-1-one, commonly known as chalcone, in the presence of BF_3 as a Lewis acid. It involves Michael addition of the enol tautomer of ethyl pyruvate to the enone, which has been activated by the Lewis acid (blue box, Scheme 4).



Scheme 4. Lewis acid assisted Michael addition of ethyl pyruvate to chalcone.

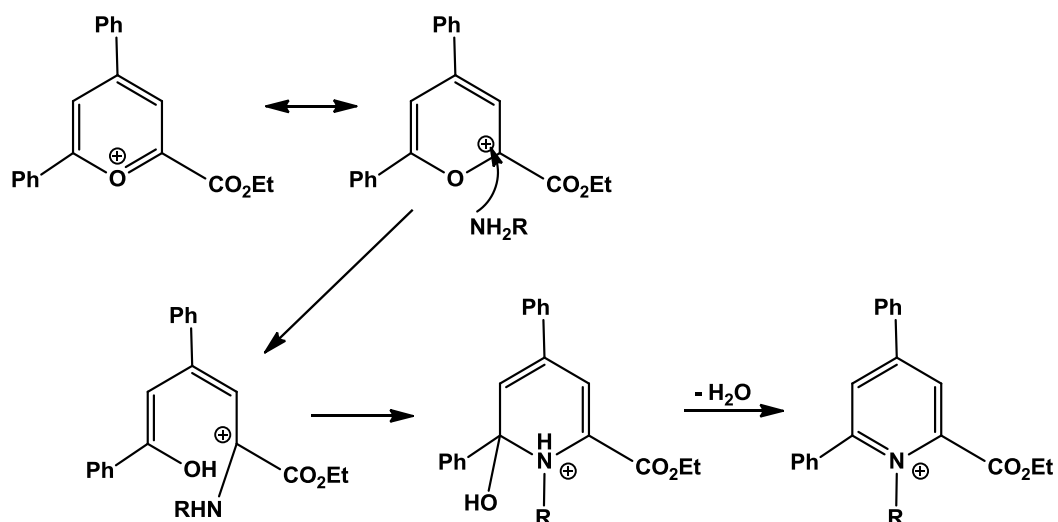
Further rearrangement and BF_3 loss lead to the formation of a 1,5-diketone product. This species is the precursor for the formation of the pyrylium ring, as described in Scheme 5.



Scheme 5. Formation of pyrylium ring from 1,5-diketone.

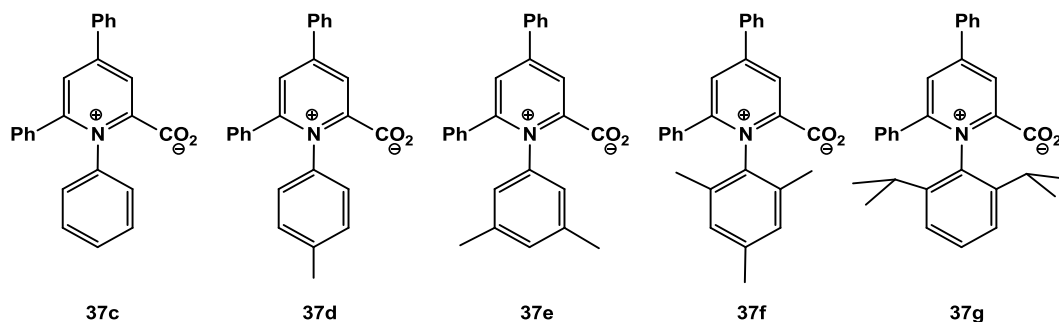
The BF_3 activated enol form of this species can undergo cyclization to yield a neutral product (blue box in Scheme 5). One equivalent of the activated chalcone (green box, Scheme 5) acts as hydride acceptor from this species yielding the desired pyrylium cation and 1,3-diphenyl propanone as a side-product (red box).

The next step is much more straightforward and it involves a condensation reaction of an amine with the pyrylium cation to yield the pyridinium ester (Scheme 6), which is finally hydrolyzed with base resulting in the desired betaine.



Scheme 6. Condensation reaction of the pyrylium cation with an amine to yield a pyridinium cation.

Betaines **37c** and **37d** had already been described by Katritzky and we extended the synthetic procedure to betaines **37e-g** bearing xylyl, mesityl and 2,6-diisopropylphenyl substituents. The spectroscopic data for the new compounds are similar to those reported by Katritzky and do not deserve further comment.

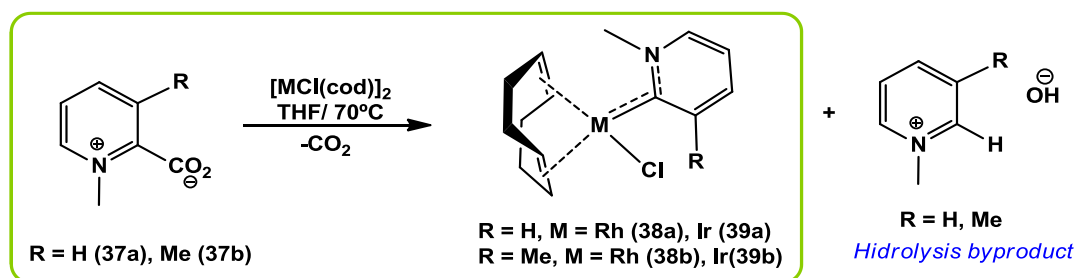


Scheme 7. Betaines synthesized by Katritzky's procedure.

This family of N-aryl substituted betaines proved to be much more soluble in less polar solvents than the smaller **37a** and **37b** and unlike these species they were soluble in dichloromethane and other organic solvents. However, as already noted by Katritzky for **37c** and **37d**, these species appeared to be unstable in organic solvent solution and therefore attempts to crystallize these betaines in a variety of solvents invariably led to decomposition. In any case they could be obtained sufficiently pure as off-white precipitates and were stable enough in THF solution for the purpose of our research.

3.2. Preparation of 2-pyridylidene rhodium and iridium complexes

Betaines **37a** and **37b** were initially tested as precursors for the formation of carbene ligands by carrying out their thermal decomposition in the presence of $[\text{RhCl}(\text{cod})]_2$ and $[\text{IrCl}(\text{cod})]_2$ in THF under strictly anhydrous conditions. Heating at 70 °C produced a clean reaction in which complexes **38** and **39** were formed in good yields (typically 65-85 % isolated yield).



Scheme 8. Synthesis of 2-pyridylidene Rh and Ir complexes by thermal decomposition of betaines.

Small amounts of the corresponding pyridinium salt were formed very likely due to reaction of the transient free carbene with traces of water (Scheme 8). The observation of pyridinium salts indicates that for our system decarboxylation occurs first and then a transient free carbene reacts with the metal precursor. Therefore, traces of water in the reaction media will protonate this carbene intermediate. This is in contrast to the report by Crabtree³ for the synthesis of NHC complexes from imidazolium carboxylates, in which the presence of water did not affect the outcome of the reaction. In Crabtree's system DFT calculations suggested that the imidazolium carboxylate coordinated first to the metal and the NHC was transferred from this species, with no intermediacy of a free carbene.

The most interesting feature of the NMR spectra of these complexes is the chemical shift of the carbene carbon atoms, which appear at 216.6 and 218.2 ppm for rhodium complexes **38a** and **38b**, and at 210.4 and 211.0 ppm for iridium species **39a** and **39b**. Coupling to ¹⁰³Rh is observed in these signals for **38a** and **38b**, with a ¹J_{RhC} of 43 Hz, indicating that the pyridylidene is directly bound to the metal. No signal for -CO₂ is detected in the ¹³C NMR spectra, further proof that decarboxylation has taken place.

³ Voutchkova, A. M.; Feliz, M.; Clot, E.; Eisenstein, O.; Crabtree, R. H. *J. Am. Chem. Soc.* **2007**, *129*, 12834.

Purification of complexes **38** and **39** to remove the small amounts of pyridinium salt was achieved by crystallization in THF/pentane. X-ray quality crystals were obtained for iridium complex **39b**.

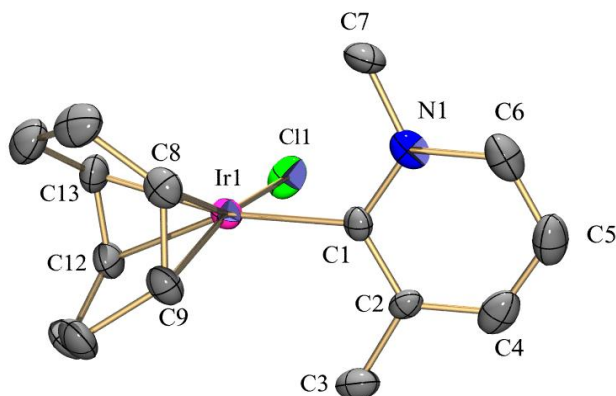


Figure 1. ORTEP diagram of complex **39b**.

The Ir–C1 distance, at 2.050(5) Å, is slightly longer than for other examples of iridium pyridylidene complexes reported by Li (1.999(2) Å and 2.0052(19) Å for bipyridine⁴ and phenanthroline⁵ derived Ir(I) carbenes, respectively) and Carmona⁶ (around 1.98 Å for Ir(III) pyridylidene complexes). Bond lengths within the pyridylidene ring (Table 1) displayed smaller variations than for these examples, suggesting a smaller double bond character for the Ir-carbene bond in **39b**. In any case, the N1–C1 is the longest within the ring, consistent with the examples mentioned above.

Bond	C1–C2	C2–C4	C4–C5	C5–C6	C6–N1	N1–C1
Length (Å)	1.383(8)	1.363(9)	1.364(12)	1.359(12)	1.375(9)	1.398(8)

Table 1. Pyridylidene ring bond distances for complex **39b**

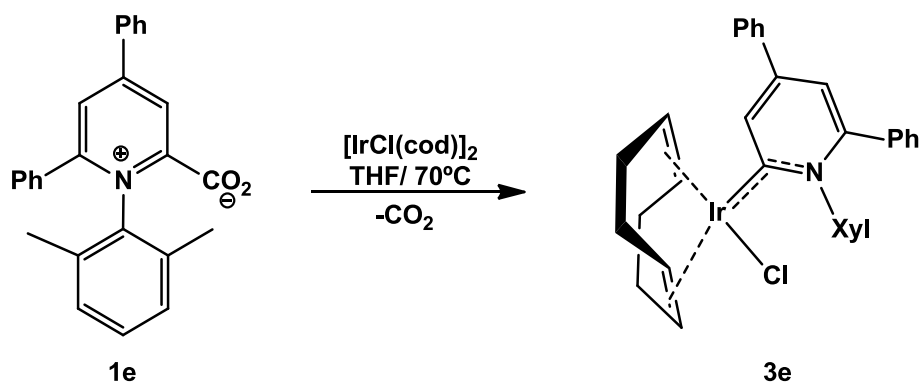
The pyridylidene ring lies almost perpendicular to the iridium coordination plane, at a 89.4° angle.

⁴ Song, G.; Li, Y.; Chen, S.; Li, X. *Chem. Commun.* **2008**, 3558.

⁵ Song, G.; Su, Y.; Periana, R. A.; Crabtree, R. H.; Han, K.; Zhang, H.; Li, X. *Angew. Chem. Int. Ed.* **2010**, *49*, 912.

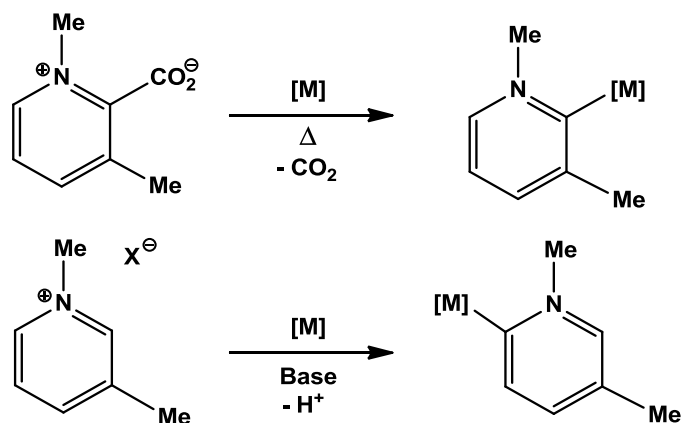
⁶ Álvarez, E.; Conejero, S.; Paneque, M.; Petronilho, A.; Poveda, M. L.; Serrano, O.; Carmona, E. J. *Am. Chem. Soc.* **2006**, *128*, 13060.

Bulkier betaine **37e** was also used in the same reaction conditions with $[\text{IrCl}(\text{cod})]_2$ and resulted in analogous complex **39e**, albeit in a lower yield.



Scheme 9. Synthesis of iridium complex **39e**.

This method offers some advantages with respect to other procedures. A nice illustration comes from decarboxylation of betaine **37b**. In this case, the final product after CO_2 removal is the expected carbene at position 2 of the heterocycle. In comparison, a C–H bond activation or the deprotonation process of the corresponding pyridinium salt shown in Scheme 10 would most likely occur at the less hindered 6-position of the pyridine ring, making selectivity a major drawback.

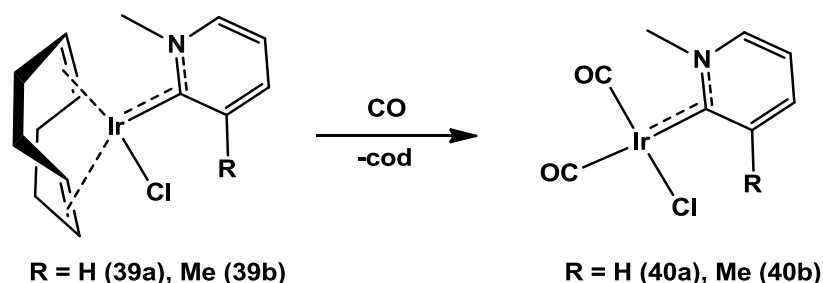


Scheme 10. Selectivity in different methods for the preparation of pyridylidene complexes.

3.3. Synthesis of iridium carbonyl derivatives for the study of the electron donor properties of 2-pyridylidene ligands

We were interested in evaluating the electron donor properties of 2-pyridylidene ligands as compared to classical Arduengo carbenes and other donating ligands such as phosphines. As mentioned in the introduction, theoretical calculations predict slightly better electron sigma donor properties of these kinds of ligands with respect to classical imidazol-2-ylidene derivatives. One way of obtaining this information is the study of the CO stretching bands in the infrared (IR) spectra of complexes of the type $[\text{IrCl}(\text{L})(\text{CO})_2]$, as a large variety of complexes of this sort has been prepared that allows straightforward comparison of IR data.⁷ Within a series of analogous compounds, smaller IR shifts for the CO bands indicate a more donating ligand *trans* to the carbonyl group. This is due to increased back donation from a d orbital of the metal into a π^* orbital of CO, which weakens the C–O bond.

We therefore prepared the biscarbonyl complexes **40a** and **40b** by bubbling CO into a dichloromethane solution of complexes **39a** and **39b** (Scheme 11). Substitution of the cod ligand was facile, with the reaction being complete in under a minute in dichloromethane at room temperature. A color change from orange to yellow was observed and the CO derivatives were obtained quantitatively.



Scheme 11. Synthesis of carbonyl complexes **40a** and **40b**.

⁷ Kelly III, R. A.; Clavier, H.; Giudice, S.; Scott, N. M.; Stevens, E. D.; Bordner, J.; Samardjiev, I.; Hoff, C. D.; Cavallo, L.; Nolan, S. P. *Organometallics* **2008**, *27*, 202.

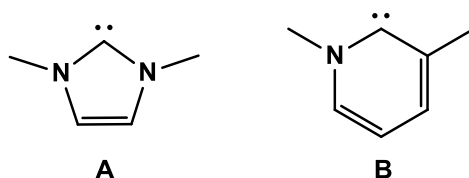
The IR spectra of these species exhibit two stretching bands for the carbonyl groups, which supports a *cis* disposition of these ligands in which they are inequivalent.

	ν (cm ⁻¹)	$\bar{\nu}$ (cm ⁻¹)
40a	2062, 1980	2021
40b	2060, 1977	2018.5

Table 2. Infrared CO stretching frequencies (ν) and average ν for complexes **40a** and **40b**.

The average ν values indicated in Table 2 are smaller than those reported for a variety of bulky imidazolylidene carbenes (in the range of 2022-2024 cm⁻¹),⁷ indicating slightly increased electron donor capabilities for these pyridylidene carbenes. In addition, derivative **40b** is a better sigma donor than **40a**, revealing that subtle changes in the substitution pattern on the pyridylidene moiety have a net effect on its electronic properties.

These experimental data find support in calculations carried out by Nechaev⁸ that indicate that the HOMO of a model 2-pyridylidene carbene **B** is higher in energy than the HOMO of 2-imidazolylidene **A** (Scheme 12), making it a better sigma donor. Moreover, the LUMO of 2-pyridylidene **B** is lower in energy compared to 2-imidazolylidene, making it also a better pi acceptor.



Scheme 12. Model 2-imidazolylidene (**A**) and 2-pyridylidene (**B**) used on molecular orbital calculations by Nechaev.

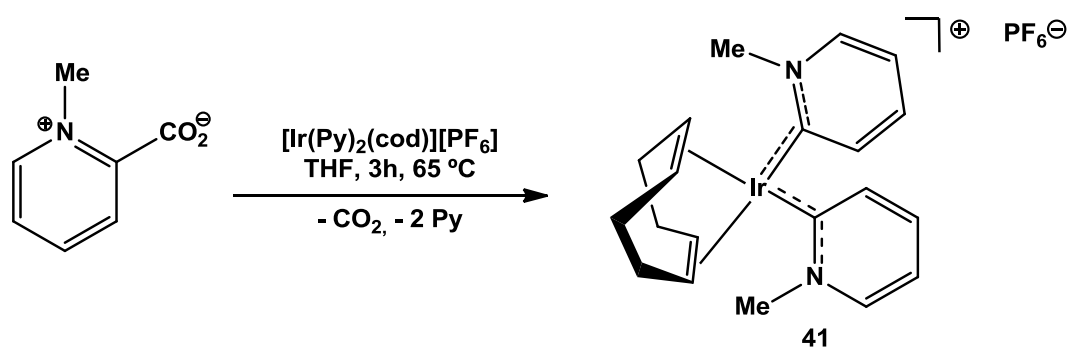
3.4. Synthesis of a bis-pyridylidene transition metal complex

Incorporation of two pyridylidene units into a metal complex is far more difficult than just one. The known methods for the synthesis of pyridine-derived carbenes

⁸ Tukov, A. A.; Normand, A. T.; Nechaev, M. S. *Dalton Trans.* **2009**, 7015.

are not appropriate for this purpose. In fact, only two previous reports exist in the literature of transition metal complexes bearing two 2-pyridylidene ligands. The first example was reported by Raubenheimer⁹ and involves a two-step synthesis in which lithiopyridine is transmetallated to a gold complex and then the nitrogen atoms are methylated. The second example by Shubert and Seebald¹⁰ is prepared via oxidative addition and involves an oxidation change from Rh(I) to Rh(V).

Our methodology seemed suited to produce a bis-carbene complex in one step without change in the oxidation state of the metal and without requiring special precursors as in the above-mentioned case of Raubenheimer. After choosing a suitable iridium (I) precursor with ligands more labile than chloride in complex $[\text{IrCl}(\text{cod})]_2$, namely $[\text{Ir}(\text{Py})_2(\text{cod})][\text{PF}_6]$, reaction with two equivalents of betaine **1a** at 65 °C in dry THF resulted in the substitution of the pyridine ligands by the 2-pyridylidenes (Scheme 13).



Scheme 13. Synthesis of bis-carbene complex **41**.

The optimum conditions for the obtention of a high yield of **41** require a somewhat large excess of homarine (3 equivalents) and prolonged heating (2-3 hours). The protonated pyridinium salt formed after crude work-up can then be removed by simple precipitation in a THF/ether mixture. Shorter reaction times or smaller excess of homarine results in the formation of a considerable amount of

⁹ Raubenheimer, H.G.; Toerien, J.G.; Kruger, G.J.; Otte, R.; van Zyl, W.; Olivier, P. *J. Organomet. Chem.* **1994**, *466*, 291.

¹⁰ Shubert, U., Seebald, S. *J. Organomet. Chem.* **1994**, *472*, C15.

the monocarbene complex Ir(Py)(NHC)(cod), which due to the similarity of its solubility behavior compared to **41** could never be isolated in its pure form.

Complex **41** presented a single set of signals in the ^1H NMR spectrum for both carbene ligands as depicted in Figure 2. This species presented poor solubility in solvents such as dichloromethane and chloroform and was therefore characterized in deuterated acetone. Integration of the NMR signals of the methyl groups on the pyridylidene with respect to those of the cod ligand confirmed the incorporation of two carbene units into the complex.

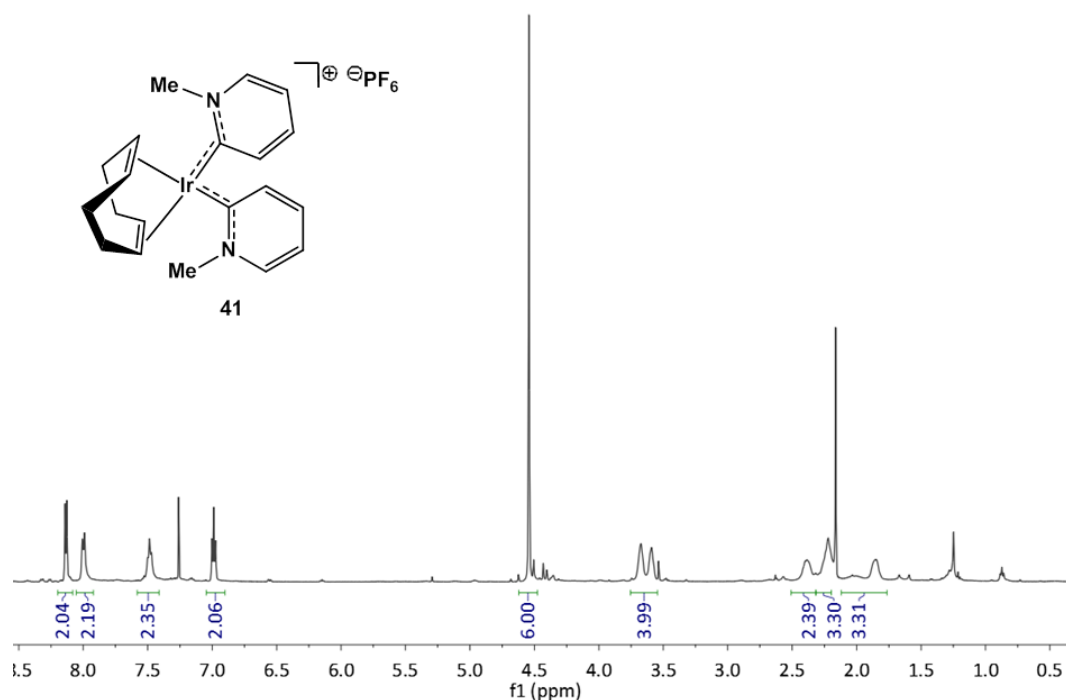
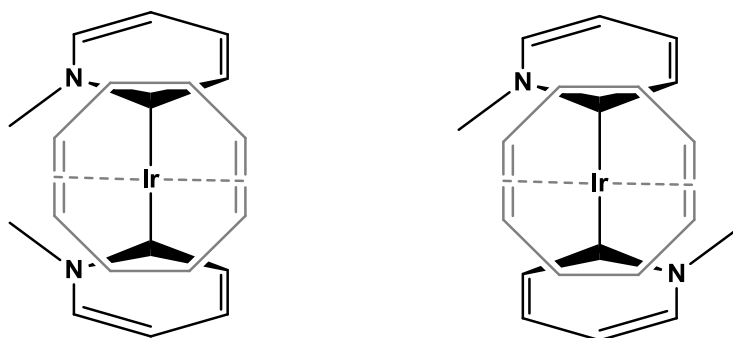


Figure 2. ^1H -NMR in d_6 -acetone of bis-carbene complex **41**.

The carbene carbon atom resonated at 207 ppm, slightly lower than in its monocarbene analogue (210 ppm).

Crystals suitable for X-ray diffraction could be obtained from slow diffusion of ether into THF solutions of **41**. However, due to the high symmetry of the crystal and the molecule, the unequivocal structure of the species could not be determined. As depicted in Scheme 14, there are two orientations of the carbene

ligands, corresponding to two different spatial groups that are compatible with the observed diffraction pattern.



Scheme 14. The two possible orientations of the carbene ligands in complex **41**.

In one of these geometries there is a symmetry plane that makes both carbenes equivalent (Scheme 14, left) and in the other the symmetry arises from a 180° axis (Scheme 14, right). In both cases the solution of the structure indicates a 1:1 mixture of both orientations in the crystal.

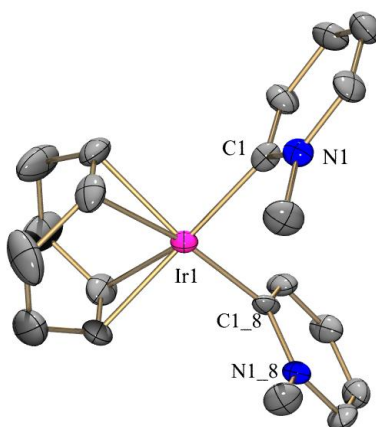


Figure 3. ORTEP diagram of one of the possible orientations for complex **41**.

An ORTEP diagram of one of the possible geometries for **41** is depicted in Figure 3. The length of the iridium-carbene carbon bond is 2.068(8) Å, which is slightly longer than for the more basic carbene in complex **39b** (2.0495(1) Å). Bond lengths within the ring are in this case even more homogeneous, all of them

around 1.39 Å, similar to those on free pyridine. This indicates a markedly single bond character for the carbene-iridium bond in this species.

NOESY experiments indicate that the carbene ligands are most likely rotating around the Ir–C_{carbene} bond in solution, as cross peaks for the methyl substituents are detected with both pyridylidene hydrogens H¹ and H⁴ (Figure 4). If the structure orientation depicted in Figure 3, with both methyl groups at the same side of the molecule, were the only one present in solution, only a cross peak for the methyl groups and H¹ would be detected, at variance with the experimental result.

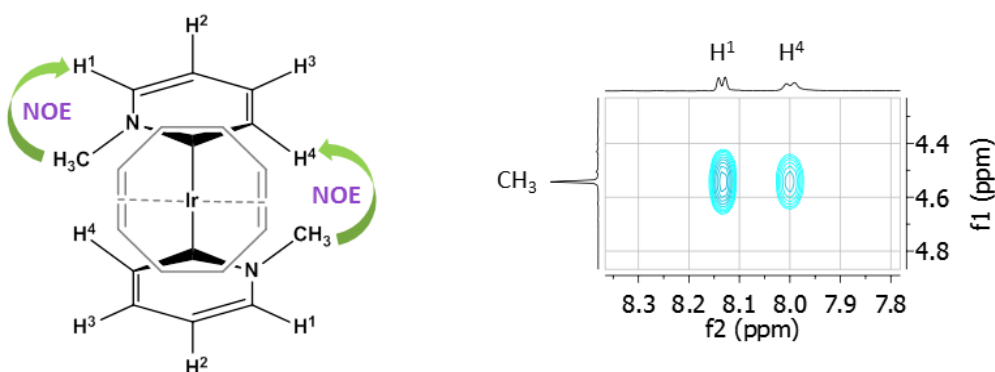
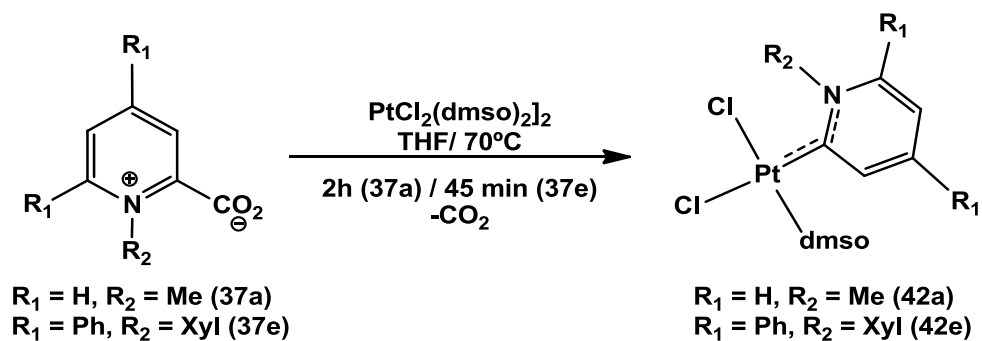


Figure 4. Portion of a NOESY experiment for complex **41**, indicating the interaction of the methyl substituents with the pyridylidene protons.

3.5. Synthesis of platinum and gold 2-pyridylidene complexes

To test the generality of our procedure to synthesize 2-pyridylidene transition metal complexes from thermal decomposition of betaines we tested the reactivity of other metallic precursors in the same conditions than those above mentioned for the synthesis of the iridium complexes.

For example, 2-pyridylidene platinum complexes were obtained using [PtCl₂(dms₂)₂] as starting material. Two representative reactions were carried out, one with homarine (**37a**) and another with one of the bulkier betaines prepared by Katritzky's procedure (**37e**).



Scheme 15. Synthesis of platinum 2-pyridylidene complexes.

The corresponding platinum complexes **42a** and **42e** were obtained (Scheme 15) and they presented similar spectroscopic features, such as their carbene signals appearing at a considerably higher field than for their Rh and Ir counterparts, at 164.9 ppm (**42a**) and 168.6 ppm (**42e**), which was to be expected due to the presence of two chloride ligands (σ - and π -donor) around the metal centre.¹¹ Coordination of the carbenes to the platinum center found further proof in the observation of coupling to ¹⁹⁵Pt for the pyridylidene protons closer to the platinum center, with ³J_{PtH} of 35 and 38 Hz respectively (See Figure 5, inset).

¹¹ a) Newman, C. P.; Clarkson, G. J.; Alcock, N. W.; Rourke, J. P. *Dalton Trans.* **2006**, 3321; b) Nolan, *Organometallics* **2007**, 26, 5880.

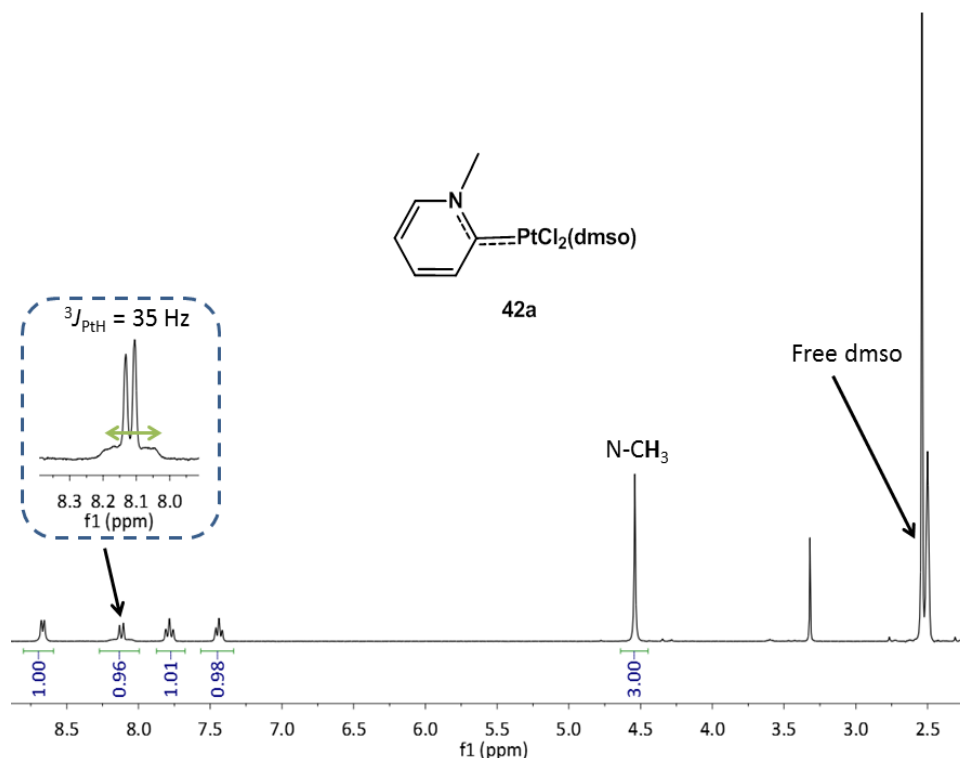
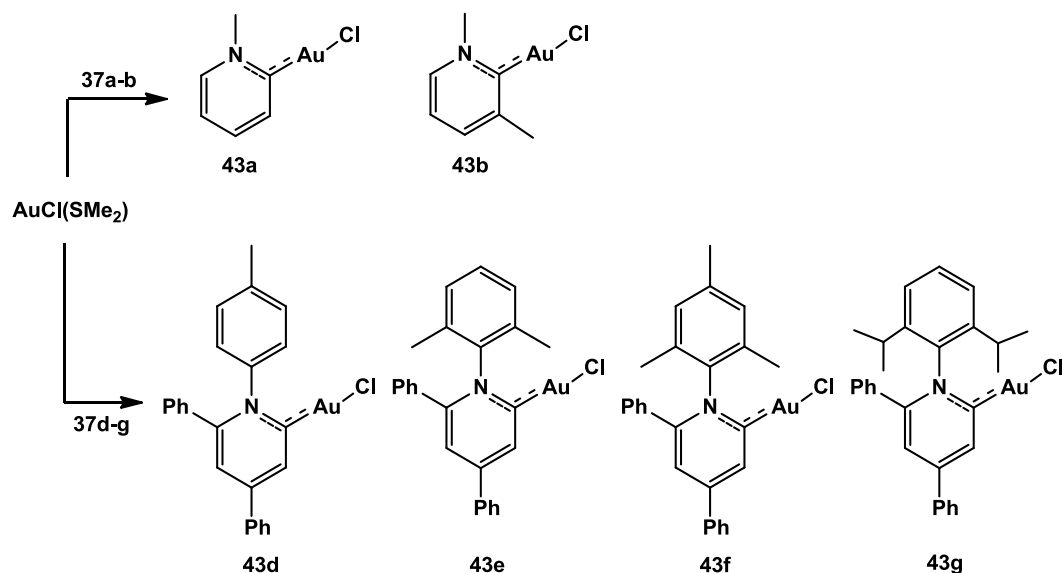


Figure 5. $^1\text{H-NMR}$ in d_6 -dmsol of complex **42a**.

Due to the low solubility of **42a** in other solvents, NMR experiments for this species were carried out in d_6 -dmsol solution. However, in this solvent the Pt-coordinated dmsol experienced exchange with the solvent and therefore spectra displayed a singlet for the displaced dmsol, integrating roughly for 12H, at the chemical shift of the free species (Figure 5). This behavior prevented the observation of the coupling constant to ^{195}Pt for the coordinated dmsol, which was now mainly deuterated.

Complex **42e** was more soluble and could be analysed in CDCl_3 . For this species, coordinated dmsol appeared as a set of two singlets integrating three protons each, as due to the lower symmetry of the complex both methyl groups are inequivalent. Moreover, a $^3J_{\text{PtH}}$ of 22 Hz was observed for both peaks. In this case, a NOESY experiment indicated that the chloride ligands are present in a *cis* disposition, as NOE crosspeaks appeared between the coordinated dmsol and adjacent pyridylidene protons.

Our synthetic method was also tested with gold precursor $[\text{AuCl}(\text{SMe}_2)]$ and the desired gold carbene complexes were obtained for all the betaines described so far. Thus a family of six different $\text{AuCl}(\text{NHC})$ complexes bearing 2-pyridylidene carbenes of different sterics was synthesized in good yields (60-80%) with the ultimate goal of testing these species in catalysis.



Scheme 16. Synthesis of gold 2-pyridylidene complexes.

Gold complexes depicted on Scheme 16 were prepared by dissolving the corresponding betaine and the gold precursor in dry THF and heating at 70 °C for 0.5–1.5 hours. It was found that reactions with betaines **37a-b** needed longer reaction times in comparison with betaines **37d-g**, which reacted in 30-40 minutes at the same temperature. This indicates that decarboxylation is more facile in these N-aryl substituted species, an effect that is very likely related to the easiness of decarboxylation when bulkier substituents are close the carboxylate moiety in the betaine¹² (see below).

All of these complexes presented very similar chemical shifts for the carbene carbon atoms, in the range of 188-191 ppm, suggesting very similar electronic properties.

¹² Van Ausdall, B. R.; Glass, J. L.; Wiggins, K. M.; Aarif, A. M.; Louie, J. J. *Org. Chem.* **2009**, *74*, 7935

X-ray quality crystals were obtained for complexes **43b** and **43g** and both structures show a linear arrangement of the chloride and carbene ligands. The C1–Au–Cl angle is almost 180° for **43b**, at 179.3(2)°, but slightly deviated from linearity for **43g** (175.69°). This is probably due to the compressing effect of the 2,6-diisopropylphenyl fragment at the nitrogen atom forcing the chloride ligand to bend slightly.

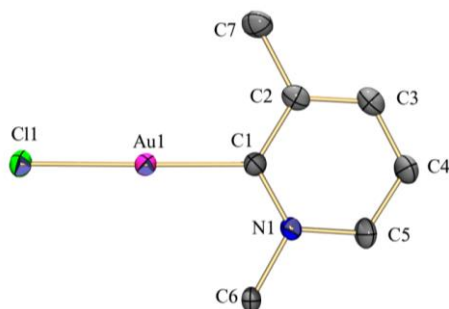


Figure 6. POV-ray view depicting gold complex **43b**.

Bond	C1–C2	C2–C3	C3–C4	C4–C5	C5–N1	N1–C1
Length (Å)	1.41(1)	1.381(9)	1.39(1)	1.38(1)	1.374(9)	1.338(9)

Table 3. Pyridylidene ring bond distances for complex **43b**

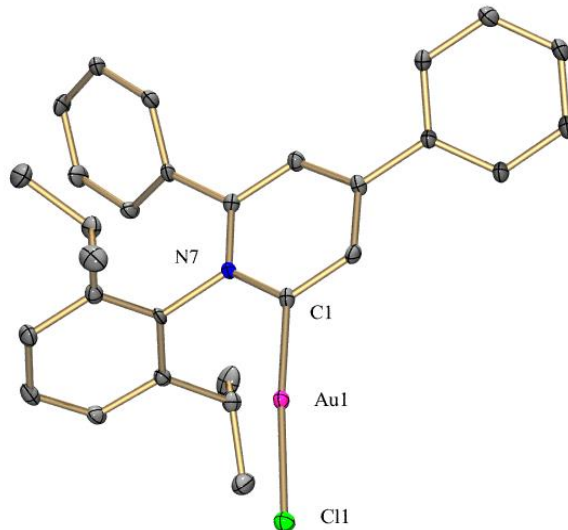
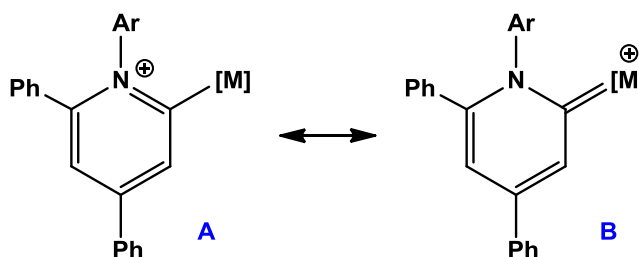


Figure 7. POV-ray view of gold complex **43g**.

Bond	C1–C2	C2–C3	C3–C4	C4–C5	C5–N7	N7–C1
Length (Å)	1.3994	1.3898	1.3895	1.3901	1.374(9)	1.376

Table 4. Pyridylidene ring bond distances for complex **43g**.

The gold-carbene distances are 2.015(7) Å for **43b** and slightly shorter for **43g** at 1.992 Å. In contrast, the nitrogen-carbene distance is shorter for **43b** at 1.338(9) Å than for **43g** (1.3729 Å). This probably indicates that the pyridylidene in **43g** is a better π acceptor, which reflects in a larger double bond character for the gold-carbene bond and consequently a lengthening of the adjacent nitrogen-carbene bond, as reflected in the resonant structure **B** (Scheme 17).

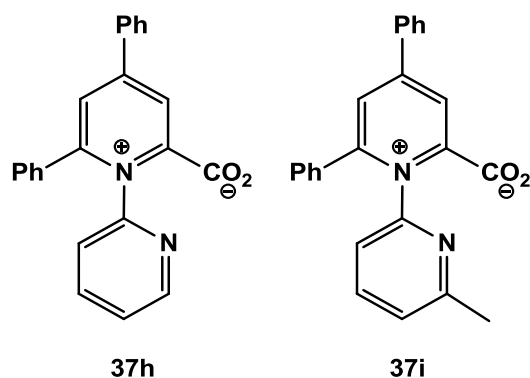


Scheme 17. Resonant structures for a pyridylidene metal complex

3.6. Attempts to prepare transition metal complexes bearing N,C-coordinating bidentate ligands using betaines as precursors

We considered the extension of our general method for the synthesis of 2-pyridylidene complexes to the design of appropriate betaines that upon decarboxylation would not only bind a metal center as carbenes but that would also possess a nitrogen atom in a suitable position to act as bidentate N,C-coordinating ligands.

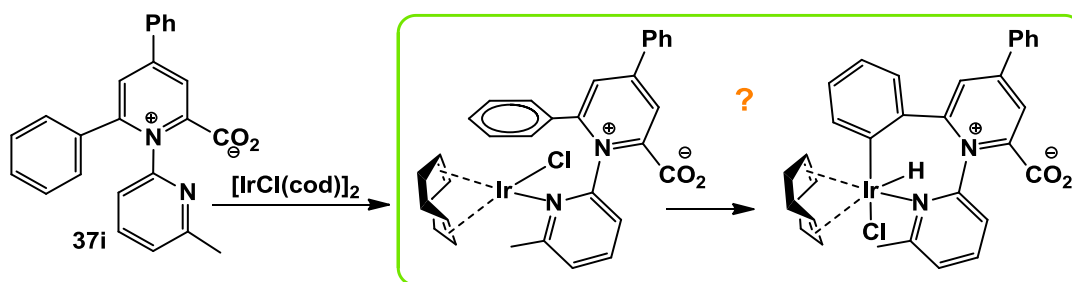
Betaines **37h** and **37j** were considered good candidates that would potentially bind a metal center in a bidentate fashion and were again prepared by an extension of Katritzky's procedure using 2-aminopyridine and 2-amino-6-methylpyridine in the reaction with the previously described pyrilium cation.



Scheme 18. Betaines designed as potential precursors for N,C ligands.

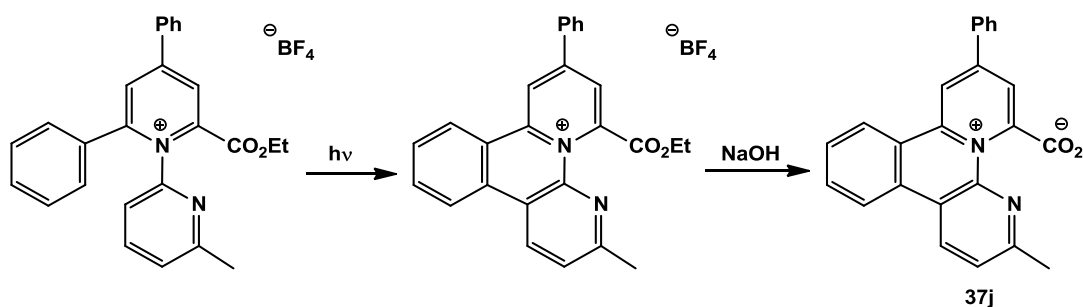
Unlike betaines **37c-37g** that were not soluble in water, which allowed for a straightforward elimination of salts in the final step of the synthesis by simple filtration of the resulting aqueous suspension, betaines **37h** and **37i** are soluble in water. The final reaction step had to be modified and water be removed first, followed by extraction with dichloromethane to separate the betaines from the salt byproduct. Betaine **37i** was used in the following test reactions as the methyl group in the N-pyridyl moiety would make the detection of new products in the NMR spectra easier.

When **37i** was heated in dry THF in the presence of 1 equivalent of $[\text{IrCl}(\text{cod})]_2$ the reaction was not clean as in the previous examples described in the precedent section but rather a complex mixture of products was obtained. The main species was an iridium hydride resonating at -16.8 ppm in the ^1H -NMR spectrum. This species is probably formed from CH bond activation of one of the phenyl rings of the ligand after N coordination (Scheme 19). It was later observed that this species formed even at room temperature, so it is possible that it still contains the carboxylate group.



Scheme 19. Suggested route for the formation of an iridium hydride species by C-H activation of the ligand after N coordination.

To avoid this C–H activation side reaction a modified betaine with a fused aryl backbone was prepared (Scheme 20). This modification should avoid a cyclometallation reaction such as that proposed in Scheme 19 and maintains the pyridyl nitrogen donor atom and C–CO₂[−] unit in the same side of the ligand. Additionally the two pyridyl units would remain coplanar to facilitate coordination of both the nitrogen atom and the generated carbene fragment.



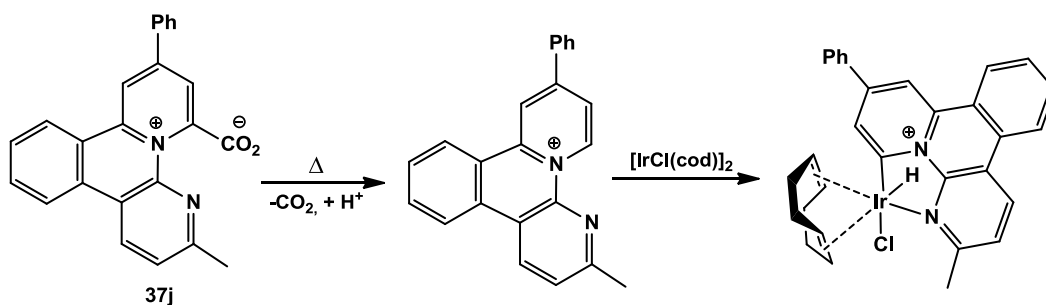
Scheme 20. Preparation of betaine with fused aryl backbone **37j**

Ring fusion was achieved by photochemical irradiation of a solution of the corresponding ester in methanol,¹³ followed by deesterification with base.

Very unfortunately, reaction of betaine **37j** with 1 equivalent of [IrCl(cod)]₂ in dry THF at 70 °C resulted in a complex mixture of unidentified products that could not be separated. It must be noted that even though there was a minority iridium

¹³ Katritzky, A. R.; Zakaria, Z.; Lunt, E. *J. Chem. Soc., Perkin Trans. I* **1980**, 1879.

hydride species in this case, ring fusion of the ligand achieved the desired effect of avoiding the formation of hydrides from C–H activation of the coordinated betaine as a major pathway. A small amount of the cationic organic species resulting from protonation of the free carbene after betaine decarboxylation was detected. This by-product can also coordinate to iridium through its donor N atom and undergo C–H activation at the C2 position of the new generated pyridinium cation which may be the source of the minor iridium hydride species detected in the reaction crudes (Scheme 21).



Scheme 21. Possible undesired reactivity of betaine **37j** with the iridium complex $[\text{IrCl}(\text{cod})]_2$.

The resulting complex from this side reaction would be also a carbene complex formed through an undesired pathway, but in a similar way to the formation of chelating N,C-pyridylidenes reported by Li.¹⁴ In any case, the complex mixture of products formed in the reaction precluded any definite conclusion.

Attempts to use other transition metal precursors, such as $\text{PtCl}_2(\text{dmsO})_2$, also led to mixtures of products so we eventually abandoned the goal of preparing bidentate carbene-nitrogen bound transition metal complexes by betaine decarboxylation.

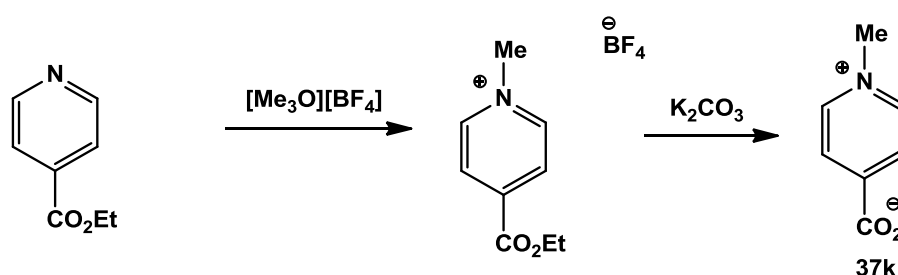
3.7. Attempted preparation of 4-pyridylidene transition metal complexes

Even though early papers already pointed out that decarboxylation of 3- and 4-picolinic acids required higher temperatures than that of their 2-isomer, no

¹⁴ Song, G.; Zhang, Y.; Su, Y.; Deng, W.; Han, K.; Li, X. *Organometallics*, **2008**, *27*, 6193.

studies for the decarboxylation of their N-alkylated derivatives had been carried out to our knowledge. A precedent study for the 2-isomer indicated that decarboxylation of N-alkyl 2-pyridinium carboxylates was up to 700 times faster than for 2-picolinic acid,¹⁵ and this seems to be due, at least partially, to steric effects being decarboxylation favoured with the bulkier N-methylated betaine.

We therefore decided to prepare N-methyl-4-pyridinium carboxylate using the same procedure that was used for the synthesis of the homarine, as summarized in Scheme 22, in an attempt to generate remote 4-carboxylate pyridinium carbenes. Although CO₂ release from this species is less favored, it does occur, although higher temperatures than for 2-pyridinium carboxylates are required.



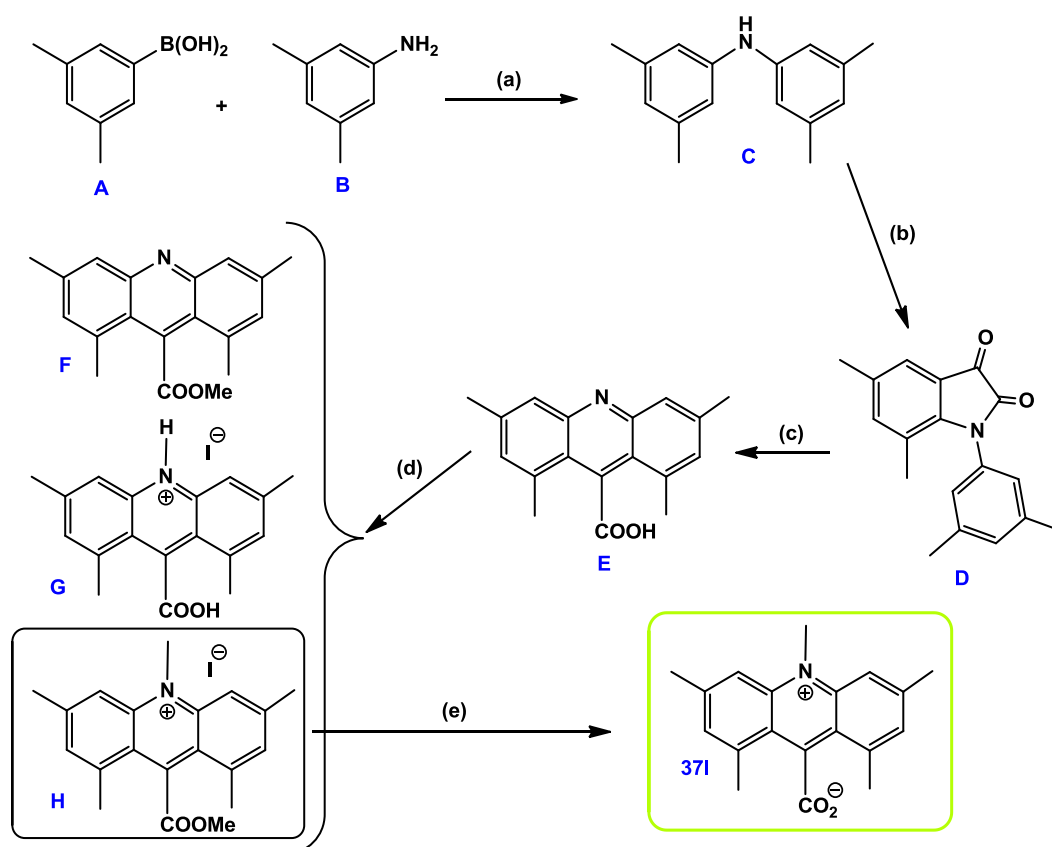
Scheme 22. Synthesis of N-methyl 4-pyridinium carboxylate (**37k**)

We therefore used betaine **37k** in our attempts to produce 4-pyridylidene transition metal complexes due to the simplicity of the system. Initial tests were carried out in the presence of 1 equivalent of [IrCl(cod)]₂ in dry THF at 75 °C. Almost no evolution was observed for short reaction times (approx. 1h) whereas heating overnight led to unreacted betaine along with [IrCl(cod)]₂ decomposition. Higher reaction temperatures of 120 °C and 140 °C in pressure tubes also yielded mainly unreacted betaine and decomposition products. Among the latter, species that appeared to form by C–H activation of the betaine aromatic bonds could be identified in the ¹H-NMR spectra, but could not be isolated.

It appears that the decarboxylation temperature of betaine **37k** in THF solution is over 140 °C and therefore not practical for our desired mild synthesis of 4-pyridylidene transition metal complexes.

¹⁵ Haake, P.; Mantecón, J. *J. Am. Chem. Soc.* **1964**, *86*, 5230.

We considered the preparation of a bulkier 4-pyridinium carboxylate with substituents at both sides of the carboxylic group. Steric hindrance will force this moiety to rotate and lie perpendicular to the pyridinium ring, which stops conjugation of the π electrons in the plane, therefore weakening the Py-CO₂ bond and facilitating decarboxylation.¹² Betaine **37I**, pentamethylacridinium carboxylate, was considered a good candidate for the synthesis of 4-pyridylidene transition metal complexes by our decarboxylation route and a synthetic procedure was devised for its preparation. The complete synthetic procedure for its preparation is shown in Scheme 23.



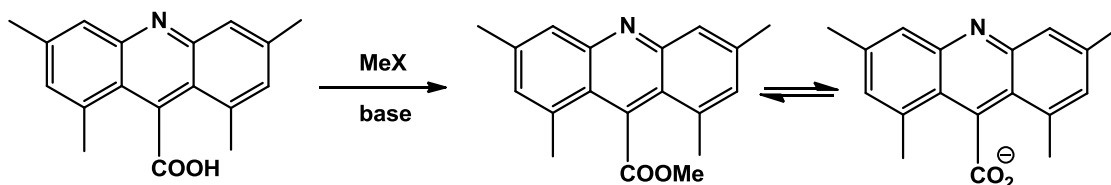
Scheme 23. Synthesis of betaine **37I**. Reaction conditions: (a) 1 eq. 2,6-lutidine, 5 mol% Cu(OAc)₂, 10 mol% decanoic acid in toluene, r.t., 24h;¹⁶ (b) (i) 1.5 eq. oxalyl chloride in CS₂, reflux, 1h, (ii) 4 eq. AlCl₃ in CS₂, reflux, 1.5h;¹⁷ (c) (i) aqueous KOH

¹⁶ Tzschucke, C. C.; Murphy, J. M.; Hartwig, J. F. *Organic letters*, **2007**, *9*, 761

¹⁷ Razavi, Z.; McCapra, F.; *Luminescence*, **2000**, *15*, 245

10%, reflux, 12h, (ii) HCl conc.;¹⁷ (d) (i) MeI neat, reflux, 48h, (ii) Purification (see experimental part); (e) (i) 3 eq. TMSCl + 3 eq. NaI, MeCN, reflux, 12h, (ii) Na₂S₂O₃ aq. 10%.

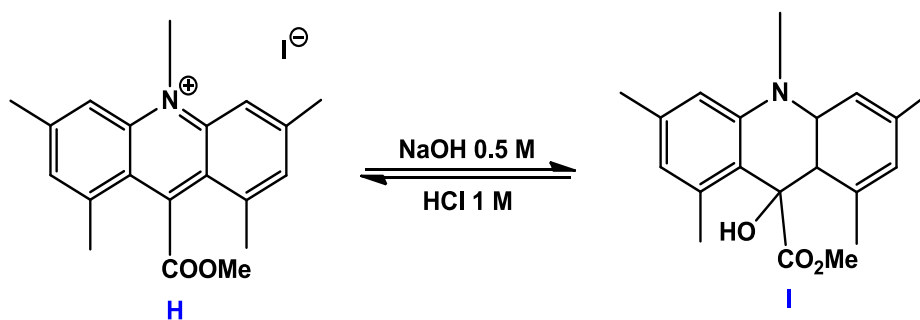
Steps (a), (b) and (c) consisted on previously published preparations, however no literature reports were found for the formation of an alkyl ester such as **F**. It must be noted that Razavi described the preparation of a related phenyl ester in a multi-step procedure with a moderate yield.¹⁷ We decided to devise a simpler reaction and tried a variety of conditions using methylating reagents such as trimethyl oxonium tetrafluoroborate, methyl triflate or iodomethane with and without base. It was observed that the presence of base always led to the presence of carboxylate, even for long reaction times, probably due to the existence of an equilibrium between the starting material and the ester in these conditions (Scheme 24).



Scheme 24. Methylation in the presence of base always led to mixtures of the carboxylic methyl ester and the carboxylate.

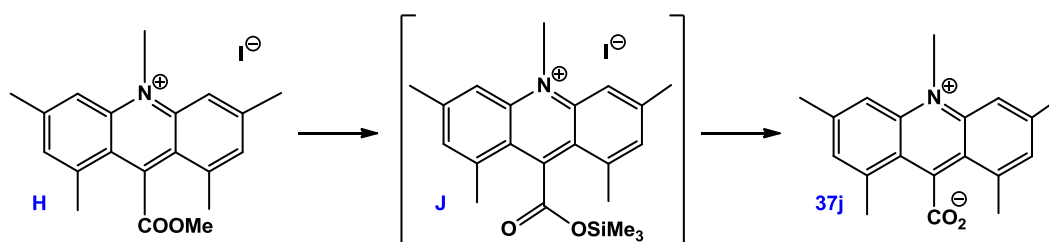
The ester could be isolated from these mixtures by extraction with ether, however further reaction with trimethyl oxonium tetrafluoroborate or methyl triflate did not result in the N-alkylated species **H**. Refluxing **F** in neat iodomethane did result in N-methylation after long reaction times, although complete conversion to **H** was never observed. It was seen that carboxylic acid **E** could be directly refluxed in MeI without added base to produce similar product mixtures. No carboxylic acid is left after refluxing overnight, but around 2 days of heating are needed to obtain a 1:1 mixture of **F** and **H** (Scheme 23, step d). In this reaction it is acridinic acid itself that acts as a base, forming its N-protonated acridinium derivative **G** which is highly insoluble in the reaction media and precipitates out.

The final step in the synthetic route, in which the ester moiety is converted into a carboxylate, does not lead to betaine **37I** if the standard procedure of de-esterification with a base is employed. Instead nucleophilic addition of an hydroxide anion to the electrophilic carbon atom takes place (Scheme 25). This reaction reverts upon addition of acid.



Scheme 25. Treatment of N-methyl carboxylic ester **H** with base does not lead to deesterification.

An alternative procedure was needed to achieve this final de-esterification step and the desired result was obtained by modification of a method published by Olah¹⁸ involving the formation of a silyl ester (Scheme 23, step e). Refluxing an acetonitrile solution of ester **H** with trimethylsilyl chloride and sodium iodide results in the formation of a silyl ester **J** (Scheme 26). Precipitation with ether allows for its separation from other reaction by-products and treatment with an aqueous thiosulfate solution hydrolyses the silyl ester and reduces traces of I₂, leading to betaine **37I** which is an off-white highly insoluble solid.

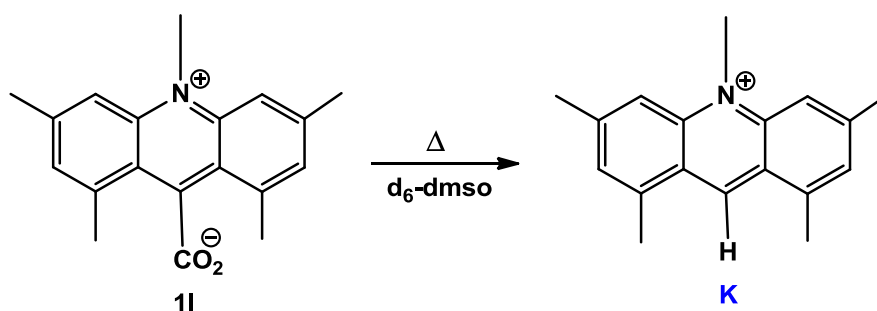


Scheme 26. Products involved in the de-esterification procedure reported by Olah.

¹⁸ Olah, G.A.; Narang, S.C.; Gupta, B.G.B.; Malhotra, R.; *J. Org. Chem.*, **1979**, *44*, 1247

Heating **37l** in dry THF with a variety of metal precursors ($[\text{IrCl}(\text{cod})]_2$, $\text{AuCl}(\text{SMe}_2)_2$, $\text{PtCl}_2(\text{dmsO})_2$) at 95 °C did not lead to the clean formation of the target transition metal complexes, but it was evident that the betaine reacted under these conditions, probably by decarboxylation and protonation, followed by further reaction with the metal precursors to yield complex reaction mixtures.

Heating a d_6 -dmsO solution of **37l** without adding any metallic electrophile at 85 °C leads to the formation of decarboxylated product **K**, which demonstrates that this substituted 4-pyridinium carboxylate is losing CO_2 and then the transient carbene is being protonated by the water present in solution.



Scheme 27. Decarboxylation of **37m** in the absence of a transition metal precursor.

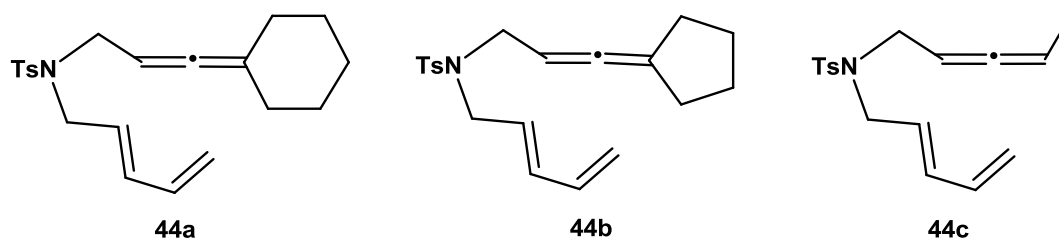
Additionally this experiment confirms that the introduction of two methyl groups in close proximity to the carboxylate lowers the temperature needed for decarboxylation (c.f. betaine **37k** does not decarboxylate at 140 °C).

We can conclude that our inability to observe transition metal complexes bearing this ligand might be due to the large steric hindrance of the two methyl groups at both sides of the carbene position that might hinder the coordination to the metal centre or further reactivity of the generated carbene. This problem may be solved with the synthesis of similar betaines containing only one or none methyl groups in positions 1 and 8 of the acridine, but the fact that those species will probably decarboxylate at higher temperatures must also be taken into account.

3.8. 2-pyridylidene gold complexes as catalysts for the cycloaddition of allenes to dienes

During a short stay in the group of professor José Luis Mascareñas and Fernando López at the University of Santiago de Compostela we tested our family of gold 2-pyridylidene complexes as catalysts for the cycloaddition reaction between allenes and dienes. Cycloaddition reactions, in which acyclic species form new cyclic compounds with the rearrangement of π electrons are a common route to four, five and six-membered rings, with species containing seven membered rings being less common.¹⁹ The use of allyl fragments, which act as 3-center, 2-electron components open new possibilities for the formation of seven membered rings upon [4C+3C] cycloaddition with dienes.²⁰ The group of Mascareñas has ample experience in this reactivity and had done extensive work in both intramolecular²¹ and intermolecular²² versions of this reaction.

We obtained the most interesting results for intramolecular cycloadditions using disubstituted allenediene substrate **44a**. Some reactivity trends were also derived from the cycloaddition of monosubstituted allene diene **44c**.



Scheme 28. Mono- and di-substituted allenediene substrates.

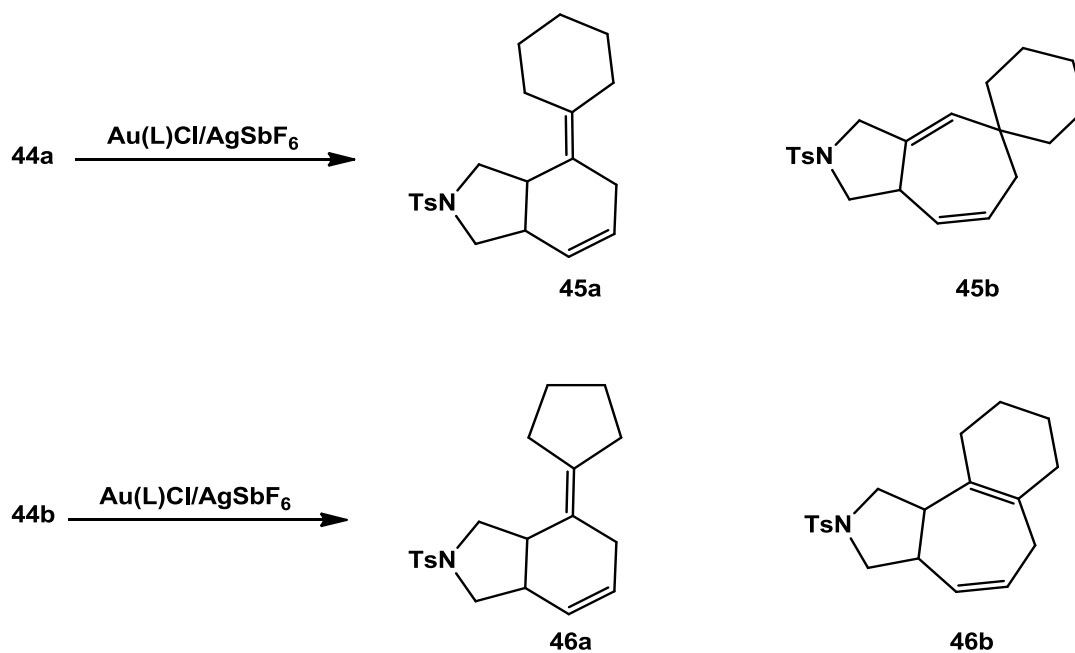
Previous work from the Mascareñas group had shown that catalytic cycloaddition of **44a** and **44b** using 10 mol% of Au(L)Cl/AgSbF₆ could result in two different products for each substrate (Scheme 29) depending on the catalyst used.

¹⁹ Battiste, M. A.; Pelphrey, M. P.; Wright, L. D. *Chem.–Eur. J.* **2006**, *12*, 3438

²⁰ Harmata, M. *Chem. Commun.* **2010**, *46*, 8904.

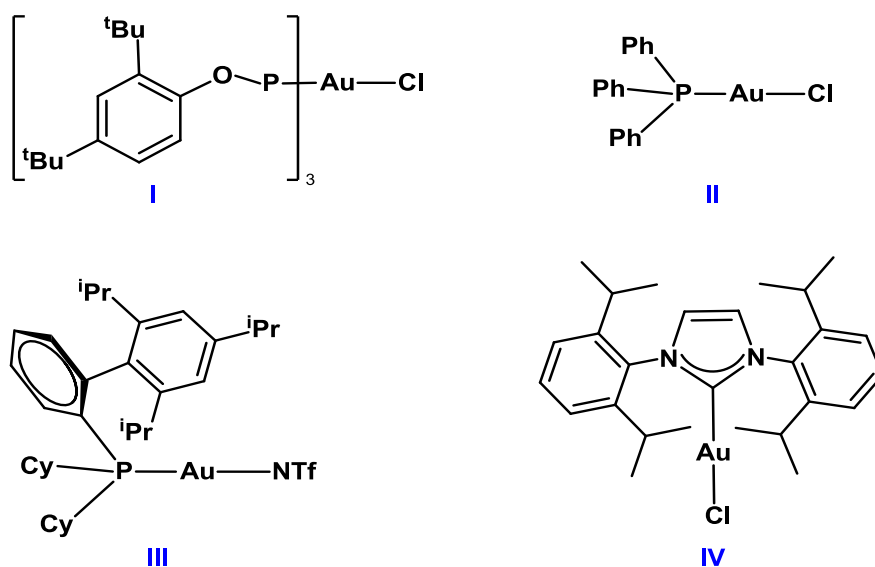
²¹ a) Trillo, B.; López, F.; Gullías, M.; Castedo, L.; Mascareñas, J. L. *Angew. Chem. Int. Ed.* **2008**, *47*, 951; b) Alonso, I.; Trillo, B.; López, F.; Montserrat, S.; Ujaque, G.; Castedo, L.; Lledós, A.; Mascareñas, J. L. *J. Am. Chem. Soc.* **2009**, *131*, 13020; c) Alonso, I.; Faustino, H.; López, F.; Mascareñas, J.L. *Angew. Chem. Int. Ed.* **2011**, *50*, 11496.

²² Faustino, H.; López, F.; Castedo, L.; Mascareñas, J.L. *Chem. Sci.* **2011**, *2*, 633.



Scheme 29. Possible products of the gold catalyzed cycloaddition of disubstituted allenedienes **44a** and **44b**.

45a and **46a** are the [4+2] cycloaddition products and were obtained as the main species when phosphite gold complex **I** (Scheme 30) was used as the catalyst. On the other hand, the [4+3] cycloaddition products **45b** and **46b** are majority when carbene complex **IV** is used. A study on the gold catalyzed cycloaddition of **44b** had previously been reported by the group of Mascareñas, with some results summarized in Table 5. It appeared that increasing the donor ability of the ligand increased the amount of the [4+3] cycloaddition product.^{21b} Compound **46a** was still the major reaction product when triphenyl complex **II** was used but **46b** was the main species for reactions carried out with complexes **III** and **IV**, bearing better electron donor ligands.



Scheme 30. Other gold complexes used for the cycloaddition reactions.

Entry	Cat.*	Time	Temperature	46a:46b
1	I	3h	rt	7:1
2	II	3h	rt	2.5:1
3	III	3h	rt	1:1.4
4	IV	3h	rt	1:3

Table 5. Gold catalyzed cycloaddition reaction of allenediene **44b**^{21b}
(*[Au]/AgSbF₆, 10% mol in CH₂Cl₂).

We therefore expected that our 2-pyridylidene complexes which are better σ -donors would increase the yield of the [4+3] cycloaddition product. Unexpectedly, when complex **43a** was used as a catalyst for the cycloaddition of **44a** product **45a** was obtained as the only species, that is, with the same chemoselectivity than using phosphite complex I (Table 6). This reaction was complete in one hour at room temperature, so it appeared to be slower than the reaction with complex I, which was carried out at 0 °C and was also complete in under an hour. To study the influence of steric factors, bulkier N-xyllyl substituted complex **43e** was then used and it proved to catalyze the cycloaddition reaction much slower than **43a** as 18h were needed to consume all starting material, with compound **45a** being again the only product. The use of bulkier complex **43g** bearing a 2,6-

diisopropylphenyl group made the reaction even slower, but interestingly a small amount of the [4+3] cycloaddition product **45b** was obtained (Table 3, entry 3).

Entry	Cat.*	Time	Temperature	45a:45b
1	7a	1h	rt	1:0
2	7e	18h	rt	1:0
3	7g	- ^a	rt	10:1
4	I	1h	0°C	1:0
5	IV	- ^b	rt	1:2

Table 6. Cycloaddition reactions of allenediene **44a**. (*[Au]/AgSbF₆, 10% mol in CH₂Cl₂; ^a Reaction was stopped after 2 days and had not reached completion; ^b this was a preliminary test to determine the product distribution and no precise reaction time is available).

These experiments suggest that chemoselectivity in the cycloaddition reaction stems from steric factors, with less bulky ligands favouring the [4+2] product. It must be noted that complexes **I-IV**, which were used as examples to stress that the more electron-withdrawing the ligand in the gold catalyst the more favoured the [4+2] product was, also follow the trend of less bulky ligands favouring [4+2] cycloaddition. In fact, even though phosphine and phosphite complexes **I-III** bear bulky substituents, it must be taken into account that in this kind of ligands substituents point away from the metal center, unlike in Arduengo carbenes, where the N-substituents point towards the metal.²³ Therefore, steric hindrance in the proximity of the metal centre is probably much larger for complex **IV** than for complex **I**. In this sense, the 2-pyridylidene ligand in complexes **43a,e,g** induce a reduced steric effect compared to IPr ligand in complex **IV**, as a consequence of having a single substituent flanking the carbene carbon atom.

As for the long reaction times observed with the bulkier 2-pyridylidene complexes, it is likely that this is related to the instability of the catalyst towards decomposition with formation of gold nanoparticles or colloids, as the reaction crude turned purple as time progressed.

We also tested our family of gold catalysts for the cycloaddition of the monosubstituted allenediene **44c**. This case is more complex as four different

²³ Crabtree, R.H. *J. Organomet. Chem.* **2005**, *690*, 5451.

products are observed in the reaction: two isomers arising from [4+3] cycloaddition, a [2+2] cycloaddition product and a product whose exact conformation is undetermined so far. In this case we have no data of the reactivity of **44c** with other gold complexes and the only published results for its cycloaddition reaction involve ruthenium catalysis that results in the preferred formation of the [2+2] product.²⁴

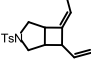
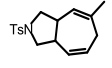
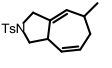
Entry	Catalyst	Unknown	[2+2] 	[4+3] 	[4+3]' 	Conv.	t(h)
1	43a	1	0.48	0.84	0.15	90%	20
2	43b	1	0.34	0.61	0.09	45%	20
3	43d	0.80	0.53	1	0.07	50%	20h
4	43e	0.81	0.61	1	- ^a	50%	46h
5	43f	0.92	0.50	1	- ^a	55%	23h
6	43g	0.24	0.23	1	0.09	43%	20h

Table 7. Gold catalyzed cycloaddition reactions of allenediene **44a**. (^a due to signal overlap, accurate integrals could not be obtained for these reactions, but the amount of [4+3]' product appeared to be less than 10 %).

Although trends are less clear in this case, the [4+3] cycloaddition product is again favoured for the bulkier carbene (entry 6). Complex **43g** also appears to disfavor the formation of the [2+2] product. The influence of sterics on reaction time is not clear for the aryl substituted carbene complexes, but as deduced from entries 1 and 2, the addition of a methyl group at the pyridylidene C6 makes the reaction twice as slow.

As for the fact that [4+2] cycloaddition products are not observed for this monosubstituted allenediene substrate, DFT calculations showed that whereas for disubstituted allenes the energy barriers for the 1,2-hydrogen shift leading to the [4+3] product and for the 1,2-alkyl shift (ring contraction) leading to the [4+2] product are very similar, in the case of monosubstituted allenes the ring

²⁴Gulías, M.; Collado, A.; Trillo, B.; López, F.; Oñate, E.; Esteruelas, M.A.; Mascareñas, J.L. *J. Am. Chem. Soc.* **2011**, *133*, 7660.

contraction is clearly disfavoured.^{21b} A detailed mechanistic study was published in collaboration with the group of Lledós.²⁵

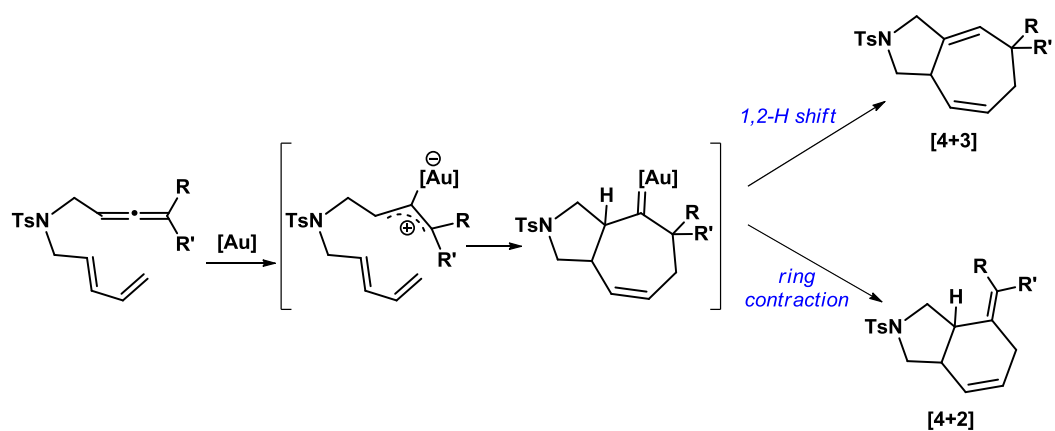


Figure 8. Simplified mechanism for the gold catalyzed cycloaddition reactions of allenedienes.

²⁵ Montserrat, S.; Alonso, I.; López, F.; Mascareñas, J.L.; Lledós, A.; Ujaque, G.; *Dalton Trans.*, **2011**, 40, 11095.

CHAPTER 4

Synthesis of transition metal complexes
bearing bis and tris(imidazole-2-
ylidene)borate ligands

CHAPTER 4. INTRODUCTION

Tris(imidazole-2-ylidene)borate ligands:
An alternative to some common 6 electron
donor ligands with *fac*- coordination

Tris(pyrazolyl)borate ligands (Tp') have been widely applied in chemistry since they were first reported in the 1960s by Trofimenko.¹ The structure of these tripodal ligands as they bind to a metal center was compared by Trofimenko himself to a scorpion holding its prey, as two pyrazolyl units bind the metal as if they were claws, while the third pyrazolyl ring comes from the top as if to "sting" the metal center (Figure 1). This analogy led to these ligands being known as scorpionates.

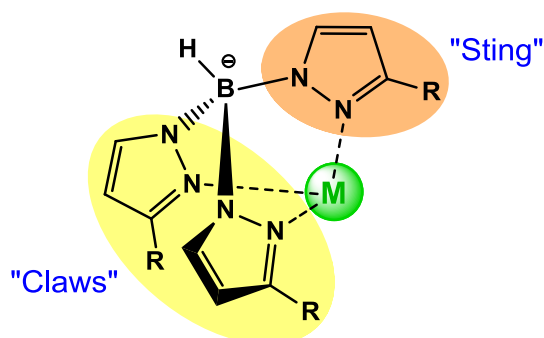


Figure 1. Binding of the classical tri(pyrazolyl)borate ligand to a metal center, leading to the "scorpionate" denomination.

¹ Trofimenko, S.; *Scorpionates: The Coordination Chemistry of Polypyrazolylborate Ligands*. 1999. Imperial College Press, London, UK

The wide applicability of Tp' ligands prompted the development of related anionic tripodal ligands with different donor atoms such as S, O, P or C, with B as the common linker² (Figure 2).

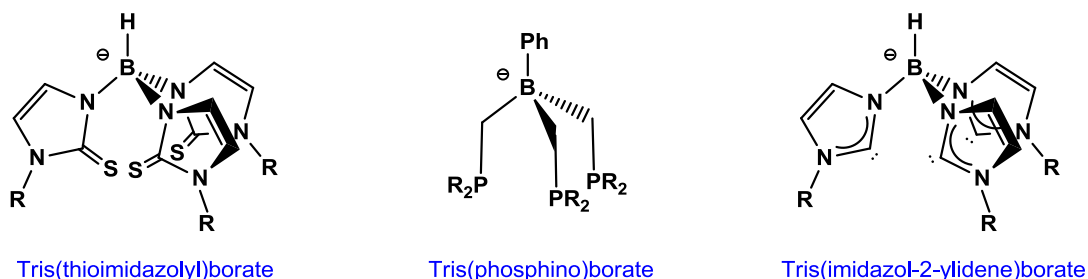
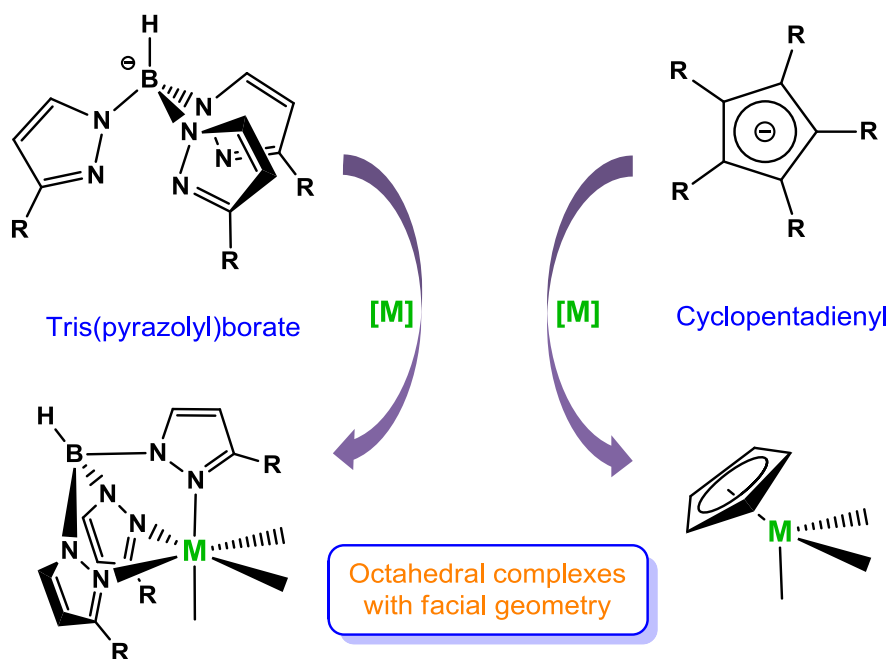


Figure 2. Some anionic scorpionate ligands with S, P and C donor atoms.

Tris(pyrazolyl)borates are often compared with cyclopentadienyl (Cp') ligands, as they are both monoanionic 6-electron donors that give rise to *fac* geometries in octahedral transition metal complexes (Scheme 1). Their steric and electronic properties are however quite different, as Tp' ligands, that coordinate to the metal through N atoms, are hard σ donors, whereas Cp' ligands, which bind through C atoms are π -donors². Incidentally all the scorpionate ligands depicted in Figure 2 are stronger donors than the parent tris(pyrazolyl)borate.

² Smith, J. M. *Comments on Inorganic Chemistry*, **2008**, 29:5, 189



Scheme 1. Tp' and Cp' ligands in octahedral complexes induce *fac* geometries

One of the new classes of scorpionate ligands, tris(imidazole-2-ylidene)borates, are the carbene-based structural analogues of Tp' ligands and were introduced by Fehlhhammer in 1996.³ They are stronger σ donors than Tp' and Cp' ligands,⁴ but at the same time are more similar to Cp' ligands as they both coordinate to metal centers through "soft" carbon atoms. Therefore these triscarbene ligands (Tc) can be considered as having electronic properties between those of Tp' and Cp' ligands. The bidentate version of these ligands, bis(imidazole-2-ylidene)borates (Bc) was also introduced by Fehlhhammer in 2001.⁵

Bis- and tris(imidazole-2-ylidene)borates are just but one type of multidentate carbene ligands. A great variety of chelating ligands with different NHCs and

³ W.P. Fehlhhammer et al., *Angew.Chem. Int. Ed. Engl.*, **1996**, *35*, 310.

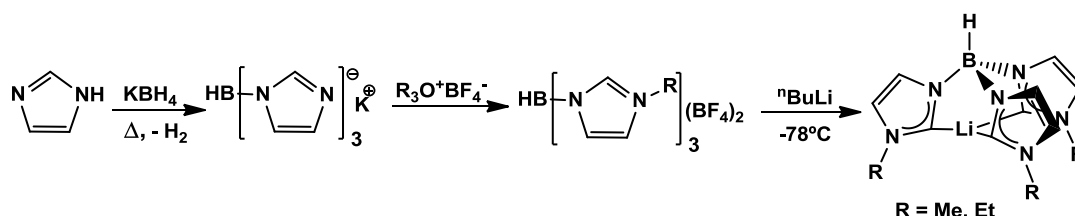
⁴ Muñoz, S. B. III; Foster, W. K.; Lin, H.-J.; Margarit, C. G.; Dickie, D. A.; Smith, J. M. *Inorg. Chem.* **2012**, *51*, 12660.

⁵ W.P. Fehlhhammer et al. *Inorg. Chim. Acta*, **2001**, *312*, 23.

linkers is available⁶ offering an alternative to phosphines arguably the most frequent chelating ligands. A drawback of chelating carbene-based ligands is the irreversibility of the formation of metal-carbene bond, which means that usually the initial kinetic product is obtained as opposed to phosphine ligands where the reversible binding to the metal means that initial binding errors can be corrected to yield the desired chelating product.⁷

IV.1. Preparation of Tc and Bc ligands

The initial synthesis for Tc ligands reported by Fehlhammer was similar to the preparation of Tp' ligands and involved the synthesis of tris(1-imidazolyl)borate from KBH_4 and imidazole. Subsequent alkylation led to the tris(imidazolium) dications, which were deprotonated to yield the tris(carbene)borate ligands (Scheme 2).



Scheme 2. Tc synthesis reported by Fehlhammer.

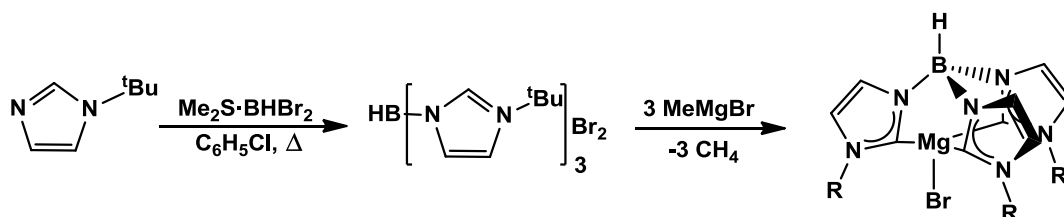
The main drawback of this procedure lied in the alkylation step, which limits the N-substituents that can be introduced in the imidazole ring to the less bulky alkyl groups, such as Me and Et.

This difficulty was overcome by the alternative synthetic route introduced by Smith⁸ in which adequately substituted imidazoles are used as starting materials and $\text{Me}_3\text{N}\cdot\text{BHBr}_2$ or $\text{Me}_2\text{S}\cdot\text{BHBr}_2$ are used as the boron source (Scheme 3). Again deprotonation of the imidazolium salt obtained this way leads to the formation of bulkier tris(carbene)boranes.

⁶ Mata, J. A.; Poyatos, M.; Peris, E. *Coord. Chem. Rev.* **2007**, *251*, 841.

⁷ Crabtree, R. H. *J. Organomet. Chem.* **2005**, *690*, 5451.

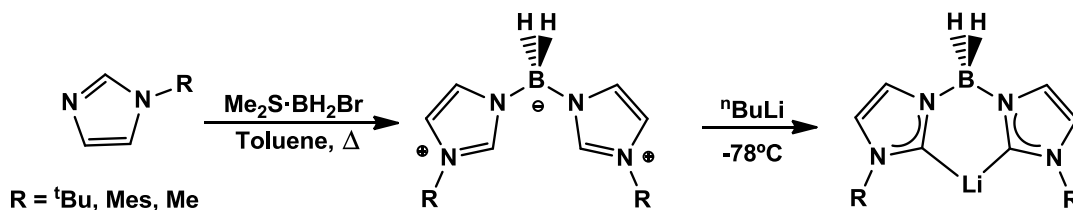
⁸ Smith, J.M. *Chem. Commun.* **2005**, 3811.



Scheme 3. Tc synthesis reported by Smith.

Tc ligands bearing tert-butyl and mesityl substituents have been reported following this procedure, and we have extended the synthetic method to phenyl substituted Tc ligands.

A similar procedure was used for the synthesis of the related bis(carbene)borates, as depicted in Scheme 4. In this case $\text{Me}_2\text{S}\cdot\text{BH}_2\text{Br}$ was used as the boron source.



Scheme 4. Synthesis of bis(carbene)borate ligands (Bc)

With this procedure methyl substituted Bc ligands were reported by Fehlhammer⁵ and tert-butyl and mesityl substituted ones by Smith.⁸

IV.2. Synthesis of transition metal complexes bearing Tc and Bc ligands

Transition metal complexes of manganese,⁹ iron,^{10,11} cobalt,^{10,12} nickel,¹³ copper,¹⁴ silver¹⁵ and gold¹⁵ bearing Tc ligands are so far known. The ligand usually binds in

⁹ Forshaw, A. P.; Bontchev, R. P.; Smith, J. M. *Inorg. Chem.* **2007**, *46*, 3792

¹⁰ Fränkel, R.; Kernbach, U.; Bakola-Christianopoulou, M.; Plaia, U.; Suter, M.; Ponikwar, W.; Nöth, H.; Moinet, C.; Fehlhammer, W. P. *J. Organomet. Chem.* **2001**, *617–618*, 530

¹¹ Nieto, I.; Cervantes-Lee, F.; Smith, J. M. *Chem. Commun.* **2005**, 3811

¹² Cowley, R. E.; Bontchev, R. P.; Duesler, E. N.; Smith, J. M. *Inorg. Chem.* **2006**, *45*, 9771

¹³ Nieto, I.; Bontchev, R. P.; Ozarowski, A.; Smirnov, D.; Krzystek, J.; Telsler, J.; Smith, J. M. *Inorg. Chim. Acta*, **2009**, *362*, 4449

a tridentate κ^3 -C,C,C mode, and in the case of imidazolydene rings with small N-substituents, two Tc ligands can coordinate to the metal in an octahedral environment.¹⁰ Other coordination modes are possible, for example in trimeric copper complex $\{[\text{HB}(\text{MeIm})_3]_2\text{Cu}\}_3[\text{BF}_4]$,¹⁴ where it presents a $\mu^3:\kappa^1:\kappa^1:\kappa^1$ coordination with each copper atom bound to both Tc ligands, as depicted in Figure 3. A similar binding mode is thought to be present in related silver and gold complexes.¹⁵

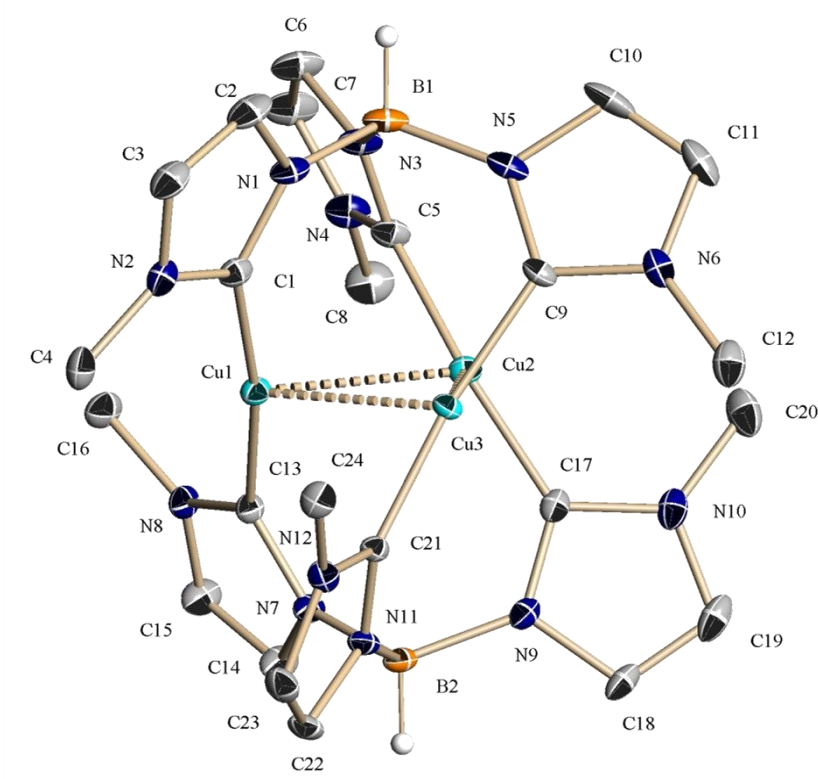
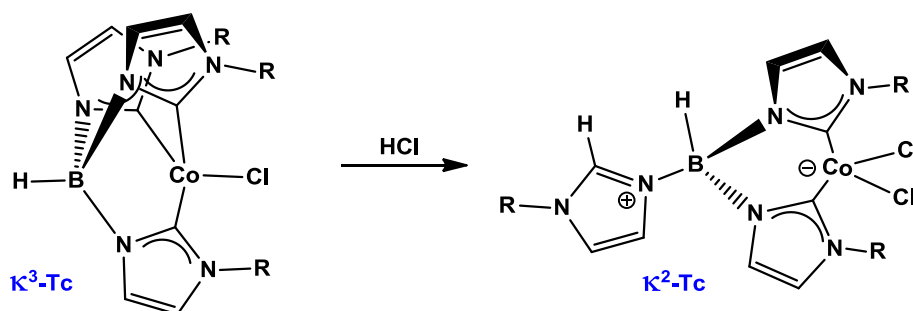


Figure 3. ORTEP representation of copper complex $\{[\text{HB}(\text{MeIm})_3]_2\text{Cu}\}_3[\text{BF}_4]$.¹⁴

In some cases the κ^3 -coordinated species are very sensitive to protonation to yield the κ^2 -coordinated derivative.¹²

¹⁴ A. Biffis, C. Tubaro, E. Scattolin, M. Basato, G. Papini, C. Santini, E. Alvarez, S. Conejero, *Dalton Trans.*, **2009**, 7223

¹⁵ Biffis, A.; Lobbia, G.G.; Papini, G.; Pellei, M.; Santini, C.; Scattolin, E.; Tubaro, C. *J. Organomet. Chem.* **2008**, 693, 3760



Scheme 5. Protonation of a κ^3 -coordinated Tc ligand to yield the κ^2 -coordinated species.

Compared to the rich coordination chemistry of the Tp ligand, for which other binding modes and fluxional behavior between κ^3 and κ^2 coordination are known, the chemistry of the Tc ligand is far too less explored.

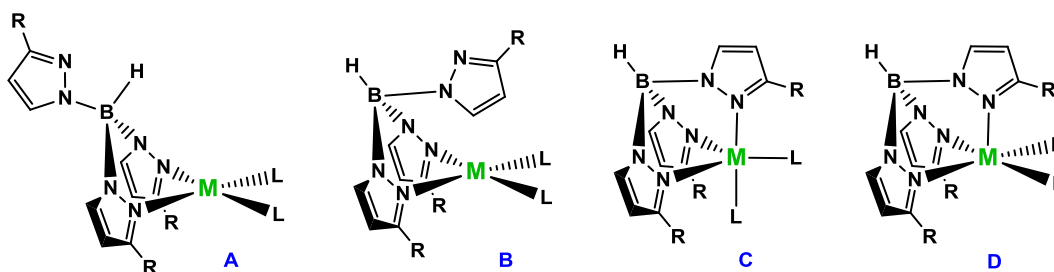


Figure 4. Different coordination modes for $\text{TpM}^{(II)}\text{L}_2$ complexes

As depicted in Figure 4, there are four possible isomers, usually present in equilibrium, for metal complexes of $\text{Tp}'\text{M}^{(II)}\text{L}_2$ (for $\text{M} = \text{Rh}, \text{Ir}$) general type bearing differently substituted Tp ligands. The relative abundance of each isomer depends on the nature of the Tp' ligand, the metal, ligand L and the solvent.¹⁶ Isomers **A** and **B** are 16 electron species with square planar geometry which differ on the orientation of the free pyrazolyl ring. This κ^2 coordination mode is favoured when the Tp' ligand bears bulky substituents. Isomer **B** is favoured when $\text{R} = \text{H}$ or when the bulky substituents are not in position 3 but 5.¹⁷ In contrast, isomers **C** and **D**

¹⁶ Adams, C. J.; Anderson, K. M.; Charmant, J. P. H.; Connelly, N. G.; Field, B. A.; Hallett, A. J.; Horne, M. *Dalton Trans.* **2008**, 2680

¹⁷ Del Ministro, E.; Renn, O.; Regger, H.; Venanzi, L. M.; Burckhardt, U.; Gramlich, V. *Inorg. Chim. Acta* **1995**, *240*, 631

are 18 electron species with a κ^3 coordination mode that display trigonal bipyramid and square pyramid geometries respectively. Calculations showed that isomer **C** was the most stable.¹⁸

Considering that with the exception of silver and gold no 2nd or 3rd row transition metal complexes bearing Tc ligands have so far been reported, we decided to work towards the synthesis of iridium Tc complexes with the objective of studying the differences in stability and reactivity with the well established iridium Tp' chemistry.

¹⁸ Webster, C. E.; Hall, M. B. *Inorg. Chim. Acta* **2002**, 330, 268

CHAPTER 4. RESULTS AND DISCUSSION

Synthesis of transition metal complexes bearing bis and tris(imidazole-2-ylidene)borate ligands

4.1. Preparation of iridium complexes bearing tris(imidazole-2-ylidene)borate ligands

The initial aim of our research was the obtention of iridium complexes of the type $[(\kappa^3\text{-Tc})\text{Ir}(\text{cod})]$, as analogous $[(\text{Tp}')\text{Ir}(\text{cod})]$ species have been reported.¹ Interestingly, the reversible nature of the metal-nitrogen bonding for the Tp' ligands resulted in an observed equilibrium between κ^2 and κ^3 coordination modes, with the former being favored in most cases. We envisioned that the stronger carbene-metal bonds for the Tc ligands would favor the formation of κ^3 -coordinated species.

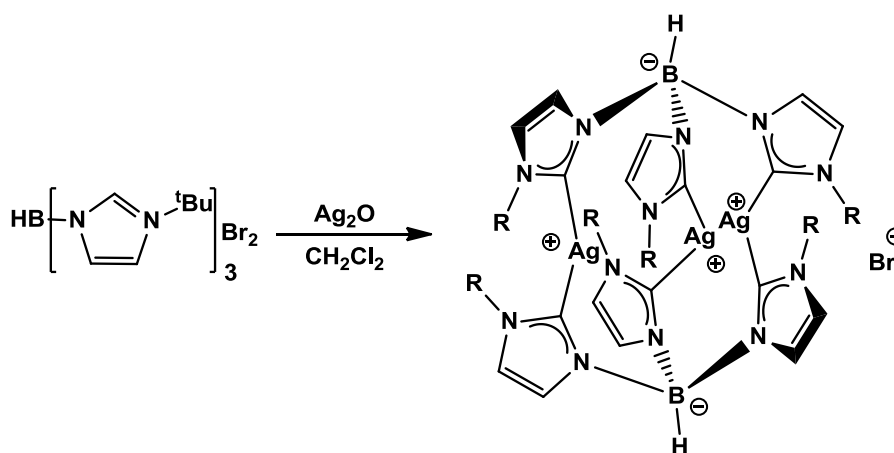
We chose $[\text{IrCl}(\text{cod})]_2$ as the metal precursor for our reactions and different ways of deprotonation of the tris(imidazolium)borate salt and transmetallation to iridium were tested.

Our first attempts involved the use of Ag_2O to form silver Tc complexes. This method for the obtention of silver imidazolylidene complexes from Ag_2O and imidazolium salts was first reported by Wang and Lin² and they showed its applicability to prepare gold and palladium carbene complexes by transmetallation. Crabtree then reported that this methodology could be

¹ Albinati, A.; Bovens, M.; Rügger, H.; Venanzi, L. M. *Inorg. Chem.* **1997**, *36*, 5991.

² Wang, H. M. J.; Lin, I. J. B. *Organometallics* **1998**, *17*, 972.

extended to rhodium and iridium carbene complexes.³ The formation of silver Tc complexes was later reported by Biffis (Scheme 1).⁴



Scheme 1. Preparation of silver Tc complexes reported by Biffis.

However, our attempts to transmetallate the tris(carbene)borate ligand to iridium using silver complexes were not successful.

When MgMeBr was used as a deprotonating agent, as reported by Smith, the corresponding magnesium bromide carbene complexes were obtained in solution for *t*-butyl (Tc^{tBu}) and mesityl (Tc^{Mes}) substituted Tc. However, upon purification to remove residual MgMeBr and MgBr₂ partial protonation of the tris(carbene)borate complex was always observed with the formation of mono- and bi-protonated Tc magnesium species.

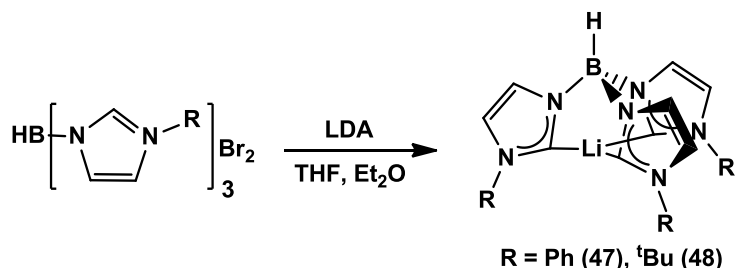
If [IrCl(cod)]₂ was added in situ to the freshly prepared solution of the κ³-Tc^{tBu}MgBr complex, a slow reaction was observed with initial formation of a species bearing a monoprotinated Tc^{tBu} ligand in a κ² coordination mode. After 6h hours however, not all starting magnesium Tc complex had been consumed. Longer reaction times led to evolution to a variety of species with partially protonated ligand. Other iridium precursors were used with these magnesium species, including [IrCl(coe)₂]₂, [IrCl(2,3-dimethylbutadiene)]₂ and [Ir(CO)Cl]_n. Ir(III)

³ Chianese, A. R.; Li, X.; Janzen, M. C.; Faller, J. W.; Crabtree, R. H. *Organometallics* **2003**, *22*, 1663.

⁴ Biffis, A.; Lobbia, G.G.; Papini, G.; Pellei, M.; Santini, C.; Scattolin, E.; Tubaro, C. *J. Organomet. Chem.* **2008**, *693*, 3760

species such as $[\text{IrCl}_3(\text{THT})_3]$ and $[\text{Ir}(\text{acac})_3(\text{Py})]$ were also tested in order to favor κ^3 *fac* coordination. No clean reactions were obtained in any case and no κ^3 -coordinated iridium species were detected in the crudes.

Other deprotonating agents were then tested including ZnMe_2 and $^n\text{BuLi}$, but neither reaction was clean. However, when deprotonation was carried out with freshly prepared lithium diisopropyl amide (LDA) a clean product was obtained for t-butyl (Tc^{tBu}) and phenyl (Tc^{Ph}) substituted carbenes.



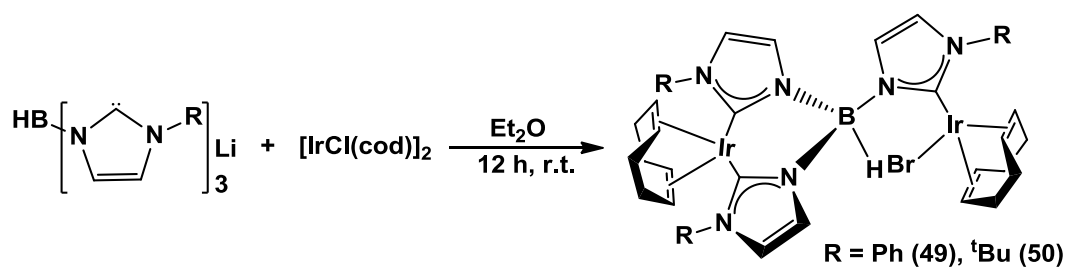
Scheme 2. Deprotonation of tris(imidazolium)borate salts with LDA.

Although the formation of $\text{HB}(\text{tBuIm})_3\text{Li}$ has been previously reported,⁵ no spectroscopic data were previously available, and as for $\text{HB}(\text{PhIm})_3\text{Li}$, this is the first report of the preparation of such a triscarbene species and its use for the synthesis of transition metal complexes bearing the Tc^{Ph} ligand. ^1H NMR spectra of **47** and **48** display two sets of signals for the imidazolyliidene protons at 7.46 and 6.94 ppm and at 7.36 and 6.65 ppm for each of these species respectively. These are considerably shifted up field (c.f. 8.44 and 7.98 ppm for the imidazolium protons of $\text{HB}(\text{PhImH})_3\text{Br}_2$), indicating C2 deprotonation. Moreover, these chemical shifts are in accordance with previously a reported Tc^{Et} lithium complex, for which the imidazolyliidene protons appear at 7.05 and 6.91 ppm.⁵ The ^{13}C NMR spectrum of this complex displayed a characteristic signal for the carbene carbon atom at 191.8 ppm. In our case, the corresponding signal could only be observed for **48**, for which it appeared at 191.2 ppm.

When lithium tris(carbene)borate complex **47** was reacted with $[\text{IrCl}(\text{cod})]_2$ in diethyl ether a single species, that has been identified as the Tc-bridged complex

⁵ Fränkel, R.; Birg, C.; Kernbach, U.; Habereeder, T.; Nöth, H.; Fehlhammer, W. P. *Angew. Chem. Int. Ed.* **2001**, *40*, 1907

49, was obtained. The ^1H NMR of this new derivative is quite complex and reveals the non-symmetric nature of the Tc^{tBu} ligand. All imidazol-2-ylidene moieties appeared as inequivalent according to the ^1H as seen in Figure 1. In addition signals for two different 1,5-cyclooctadiene ligands were observed, suggesting that two iridium atoms are at least present in the molecule. It should be pointed out that the dinuclear species **49** and **50** are formed regardless of the stoichiometry used between the starting iridium complex and the Tc ligand. This is in stark contrast with the observations made in some cases with Tp ligands and the rhodium dimer $[\text{RhCl}(\text{CO})_2]_2$. In this case, if a 1:2 molar ratio (Rh:Tp) is used, a mononuclear rhodium complex exhibiting a κ^2 coordination mode is formed, whereas if a 1:1 molar ratio is utilized the dimeric $[(\text{CO})_2\text{Rh}(\mu:\kappa^2,\kappa^1\text{-TpRhCl}(\text{CO})_2)]$ derivative, analogous to **49** and **50**, is generated.⁶ This different behavior is clearly derived from the excellent coordination properties of the NHCs compared with the pyrazolyl ligand. In other words, a mononuclear tris-carbene complex with a κ^2 -Tc coordination mode is much more reactive towards addition of second equivalent of a metal leading to species such as **49** and **50** than the Tp ligands.



Scheme 3. Formation of iridium dimeric complexes bearing the Tc ligand.

⁶ Criado, R.; Cano, M.; Campo, J. A.; Heras, J. V.; Pinilla, E.; Torres, M. R. *Polyhedron*, **2004**, *23*, 301

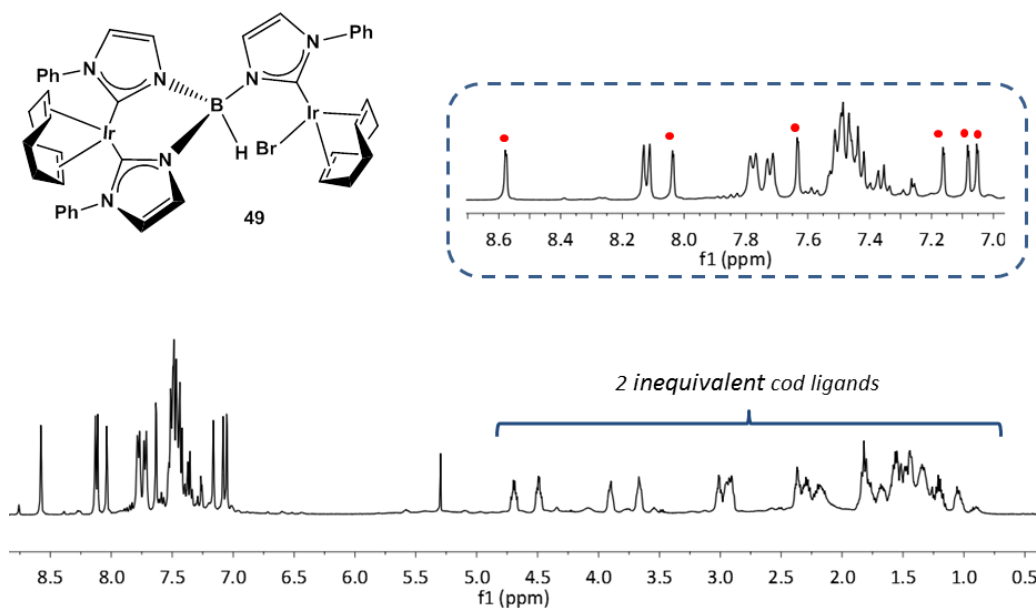


Figure 1. ^1H NMR in CDCl_3 of iridium dimer **49**. Red dots mark the resonances of the 6 inequivalent imidazolium =CHN protons.

On the other hand, reaction of **48** with $[\text{IrCl}(\text{cod})]_2$ resulted in a mixture of two products, none of them presenting protonated imidazolium rings. It was possible to separate the major species **50** upon crystallization in a toluene/pentane solvent mixture. X-ray quality crystals were obtained and their study by diffraction techniques revealed a dimeric iridium complex in which a single Tc^{tBu} ligand acting as a $\mu:\kappa^2,\kappa^1$ is bound to both iridium centers as depicted in Figure 2.

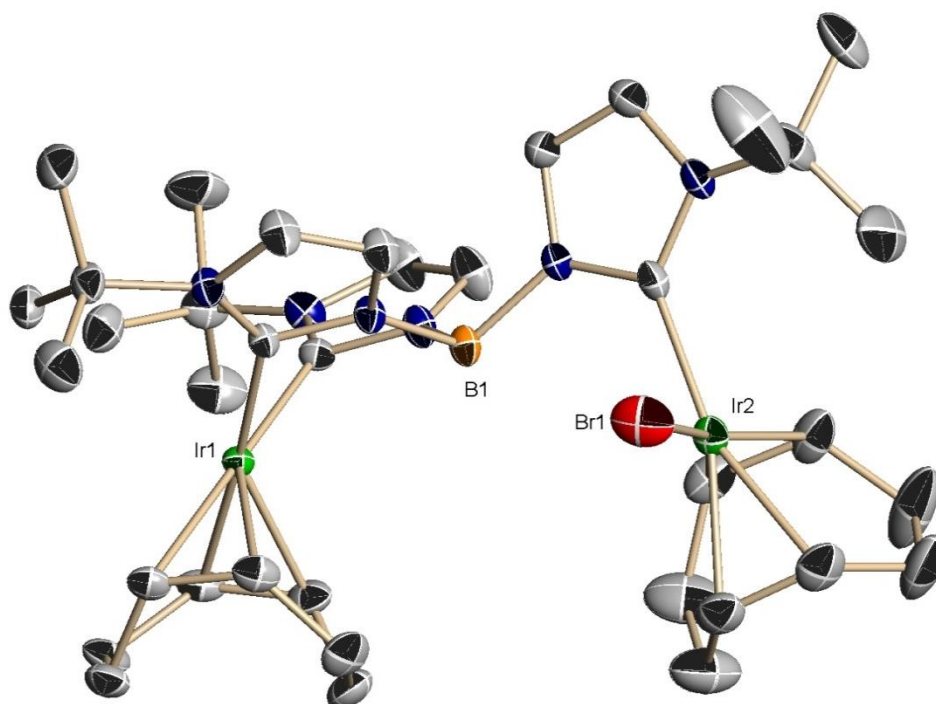


Figure 2. ORTEP diagram of complex **50**

A similar coordination mode has been observed for Tp ligands in the case some rhodium⁶ and a platinum⁷ complexes.

For complex **50** the coordination environment at both iridium atoms is square planar with iridium carbene distances of 2.053(3) Å and 2.047(3) Å for the Ir(NHC)₂(cod) moiety and 2.067(3) Å for the second iridium center, within the range of known iridium imidazolylidene complexes. The iridium atom bearing a single NHC completes its coordination sphere with a bromine atom, originating from chloride/bromine exchange, the latter coming from the anion of the Tc^{tBu} imidazolium ligand. The imidazolylidene rings lie perpendicular to the coordination plane (81.69 Å) in the Ir(NCH)Br(cod) moiety and at a 55.51 Å angle for the Ir(NHC)₂(cod) fragment.

⁷ Reger, D. L.; Baxter, J. C.; Lebioda, L. *Inorg. Chim. Acta* **1989**, *165*, 201

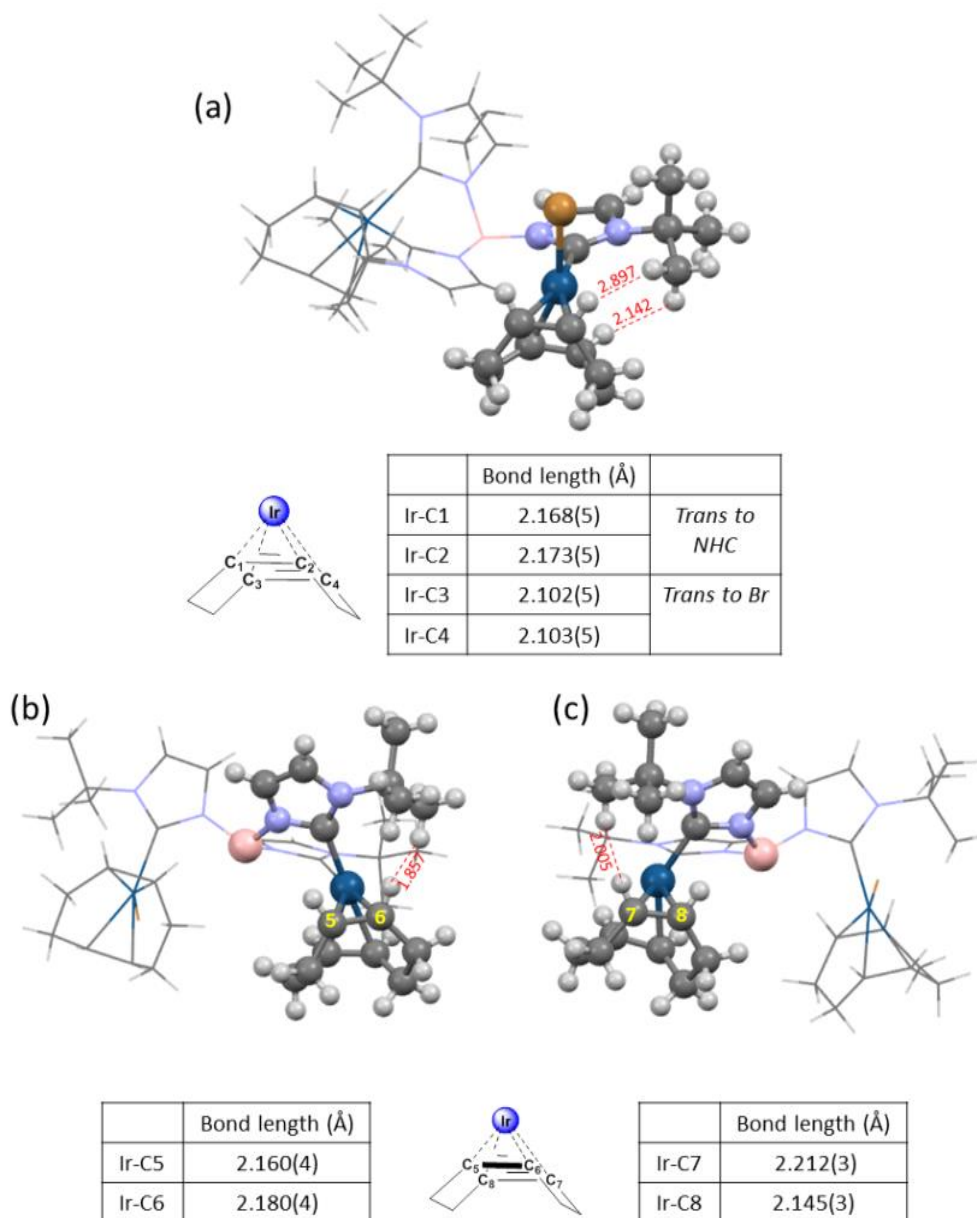


Figure 3. Shortest H–H distances (in Å, red) between the *tert*-butyl NHC substituents and the cyclooctadiene ligand hydrogen atoms (a) for the IrBr(NHC)(cod) part of the dimer, (b) for the Ir(NHC)₂(cod) part of the dimer, (c) for the Ir(NHC)₂(cod) part of the dimer after 180° rotation around the vertical axis. Tables include the iridium-cyclooctadiene bond lengths.

Coordination of iridium to the double bonds of cyclooctadiene is fairly symmetrical at the IrBr(NHC)(cod) moiety of the dimer, as indicated by the similar bond distances to iridium from the double bonds trans to the Br atom and to the NHC (Figure 3, a). For the other iridium center, with two bound NHCs, coordination to the cyclooctadiene ligand is more asymmetric due to steric constraints. As shown in Figure 3 (b, c) the hydrogen atoms from the *tert*-butyl substituents in the carbene ligands are in some cases very close to the hydrogen atoms in cyclooctadiene, with distances around 2 Å or lower. This close contact pushes the cod ligand slightly away from the carbene, making the corresponding bond to iridium (Ir–C6, Ir–C7) longer than that at the other side of the double bonds. This pushes the cod ligand away from the center of the coordination plane (Figure 4).

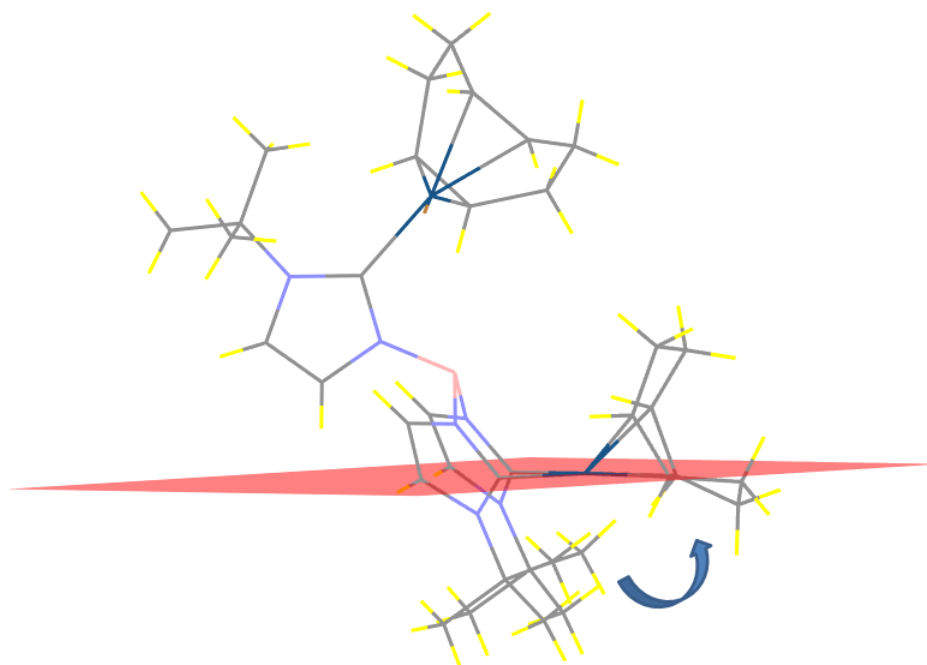


Figure 4. Steric hindrance of ^tBu substituents in complex **50** pushes the cod ligand out of the center of the coordination plane.

The average iridium carbon distance for the double bonds trans to the NHC ligands, at around 2.17 Å is longer than that for some previously reported

TpIr(cod) complexes⁸ (2.12 Å on average), indicating that the NHC has a higher *trans* influence than the pyrazolyl ring.

The ¹H NMR spectrum of complex **50** (Figure 5) presented similar features to that of complex **49**, so in all likelihood complex **49** is the analogous phenyl substituted dimer.

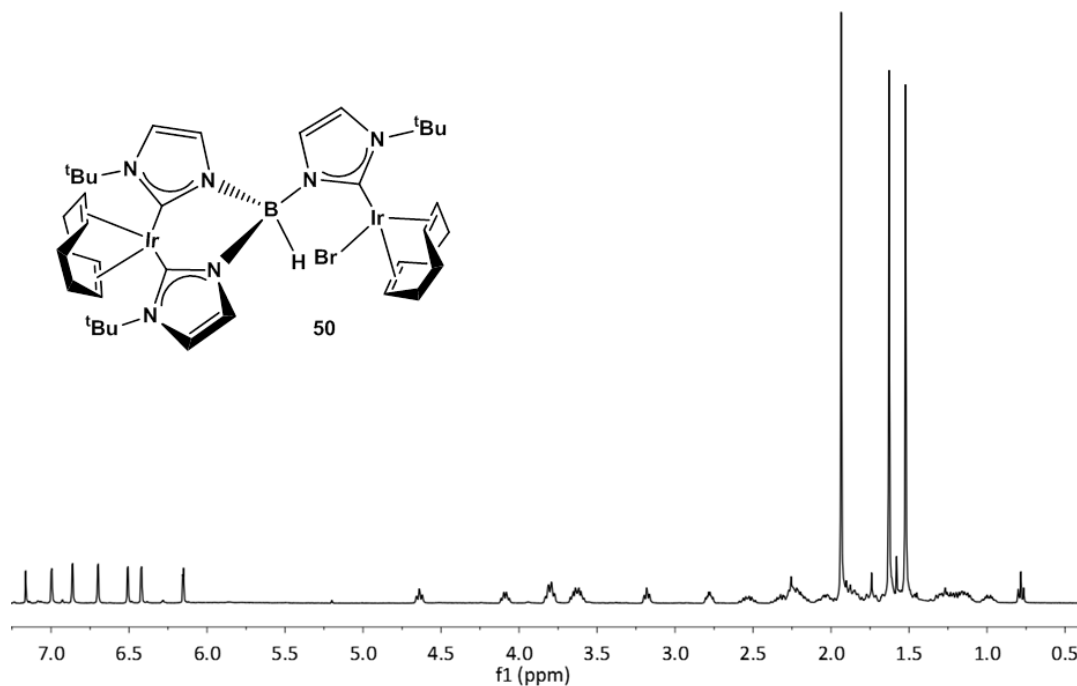


Figure 5. ¹H NMR in CDCl₃ of iridium dimer **50**.

The minor product formed in the reaction of **48** and [IrCl(cod)]₂ was difficult to separate from **50** and only small amounts of sufficiently pure product could be obtained to be characterized via NMR spectroscopy. As can be seen in Figure 6, this minor species also presents inequivalent imidazolyliene rings and two different cod ligands. Interestingly, one of the imidazolyliene protons presents a

⁸ Adams, C. J.; Anderson, K. M.; Charmant, J. P. H.; Connelly, N. G.; Field, B. A.; Hallett, A. J.; Horne, M. *Dalton Trans.*, **2008**, 2680

relatively high chemical shift at 8.60 ppm, at variance with that observed for **49** and **50**.

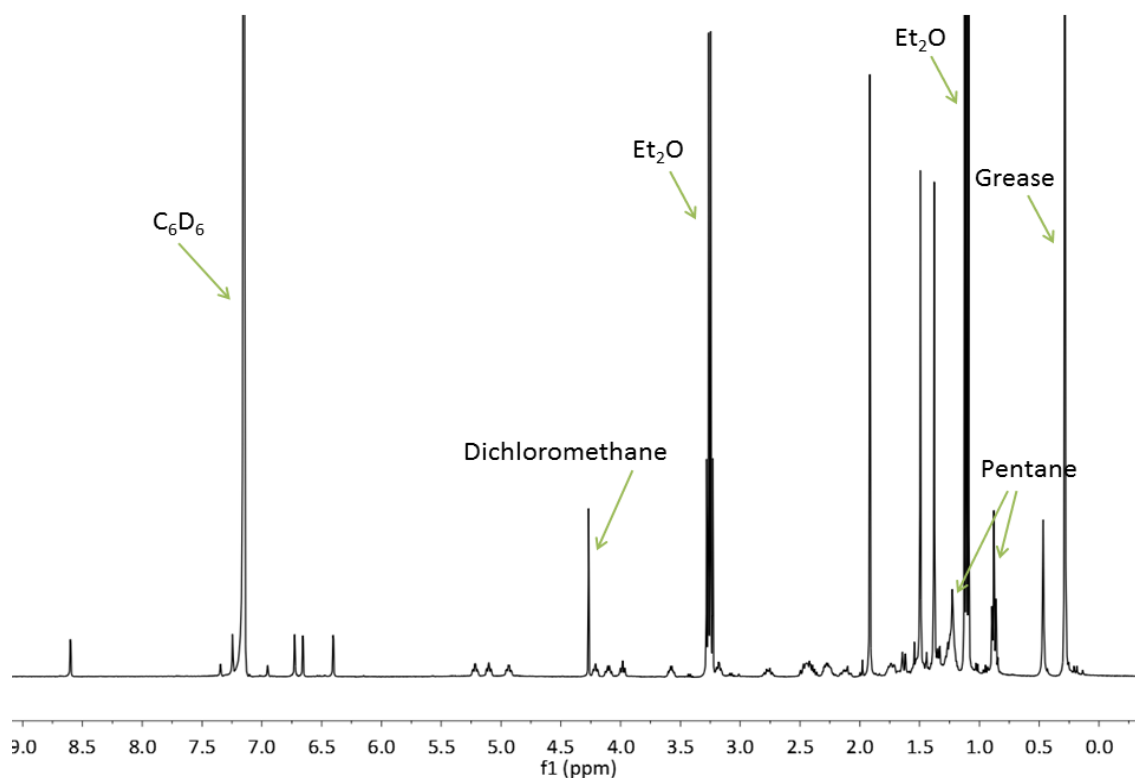


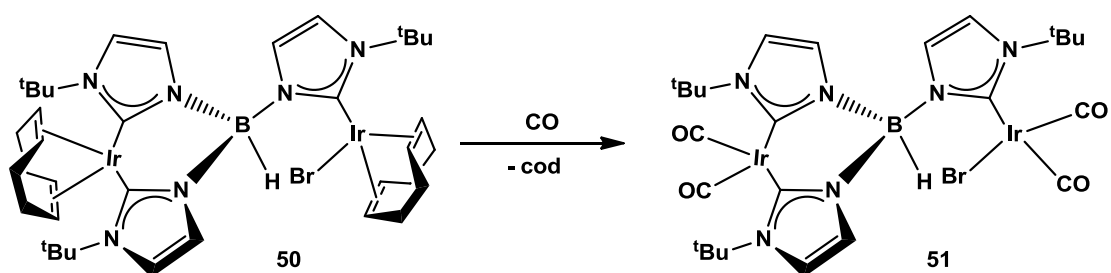
Figure 6. ¹H NMR in C₆D₆ of the minor species formed in the reaction between **48** and [IrCl(cod)]₂. Note that the sixth imidazolium =CH resonance lies under the residual solvent peak, as determined by a H,H-COSY experiment.

It was assumed that this minor species (**50b**) which was present in the ¹H NMR spectra of the crudes as 10-15 % of the products was a different isomer of dimer **50**, quite possibly one in which one of the imidazolylidene rings is acting as an abnormal carbene, that is, binding to the metal via C4. The downfield resonance would correspond to the imidazolylidene proton at C2 that is adjacent to two N atoms. A large chemical shift difference between the protons at C2 and C5, in this case of 2 ppm, with C5-H resonating at 6.66 ppm, appears to be characteristic of abnormally bound imidazolylidenes⁹. However, no crystals could be grown to

⁹ Gründemann, S.; Kovacevic, A.; Albrecht, M.; Faller, J. W.; Crabtree, R. H. *J. Am. Chem. Soc.* **2002**, *124*, 10473

ascertain its exact nature. Moreover, although ^1H NMR data seem to indicate of a C4-imidazolylidene, ^{13}C NMR data does not support this hypothesis, as all three carbene signals appear around 170 ppm, whereas a value close to 140 ppm has been reported for abnormal carbenes.

When a solution of dimer **50** was bubbled with CO, both 1,5-cyclooctadiene ligands were displaced by carbonyl groups (Scheme 4).



Scheme 4. Synthesis of carbonyl iridium dimer **51**

Figure 7 shows the ^1H NMR spectrum of this reaction crude and the resonances for the free 1,5-cyclooctadiene can be seen. Moreover, imidazolylidene protons of complex **51** are more deshielded than those of complex **50**.

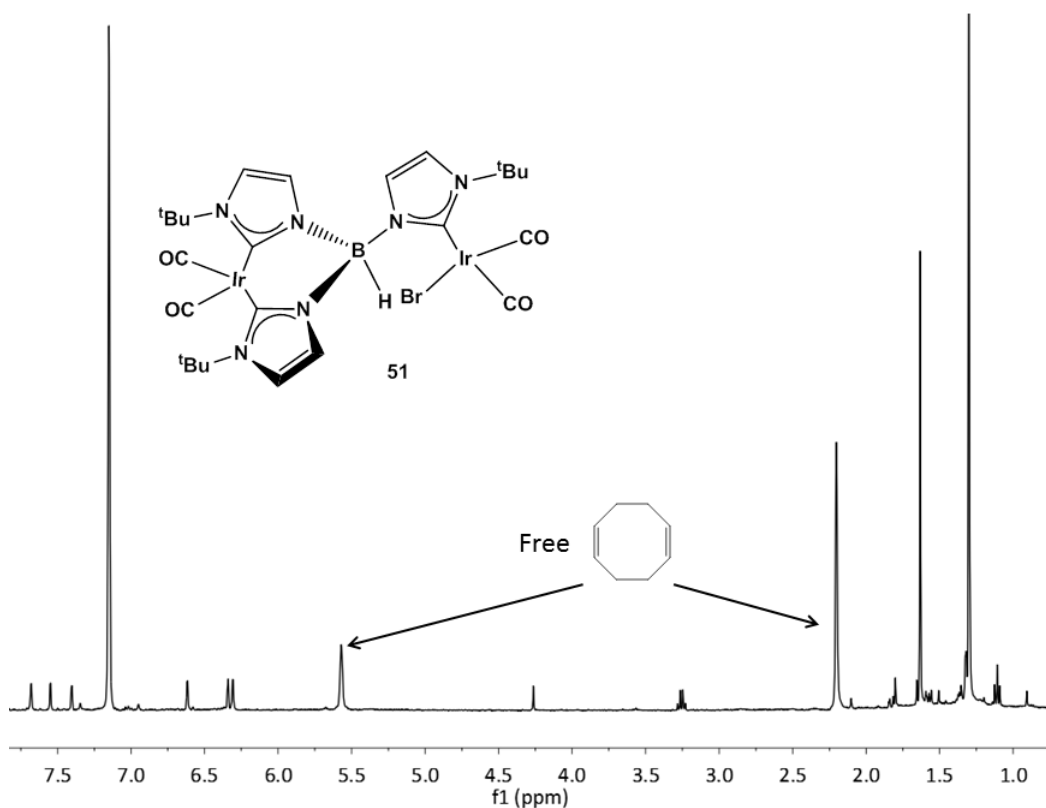
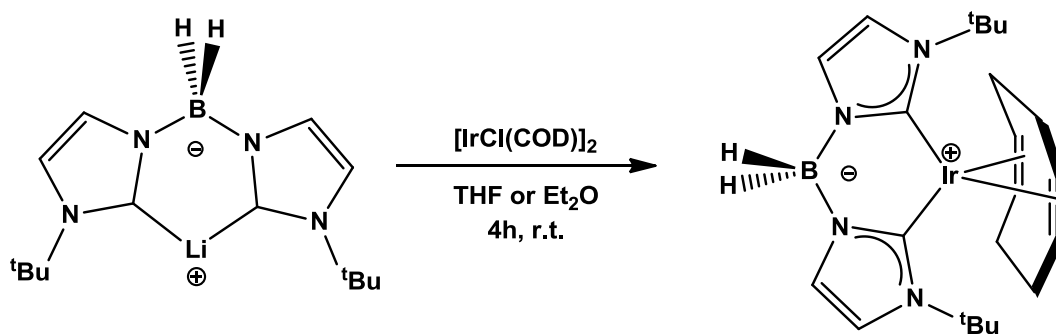


Figure 7. ^1H NMR spectrum in C_6D_6 of the reaction crude resulting in the formation of carbonyl complex **51**.

Therefore, we can conclude from the reactivity of the Tc ligand with iridium precursors so far described that the increased electron donor ability of this ligand compared to Tp prevents the isolation of monomeric κ^3 -coordinated iridium species and that the formation of dimers displaying a $\mu:\kappa^2, \kappa^1$ coordination of the Tc ligand is much more favoured. As mentioned before, coordination of the Tc ligands used in this chapter in a κ^3 coordination mode is not even easy to achieve when Ir(III) precursors were used, in spite of the propensity of the iridium in this oxidation state to form octahedral complexes.

4.2. Preparation of iridium complexes bearing bis(imidazole-2-ylidene)borate ligands

The results obtained with Tc ligands lead us to consider the possibility of using bis(carbene)borates to produce exclusively mononuclear species. Once more, attempts to use Ag_2O to transmetallate the bis(carbene)borate ligands were again not successful, but deprotonation with either $^n\text{BuLi}$ or LDA yielded the desired lithium carbene cleanly. Further reaction with $[\text{IrCl}(\text{cod})]_2$ resulted in the formation of the desired monomeric complex **52**.

Scheme 5. Synthesis of $\text{Bc}(\text{tBu})\text{Ir}(\text{cod})$ (**52**)

However, this species appeared to be unstable in solution and over time traces of adventitious water led to the formation of species with a monoprotonated Bc ligand that could not be isolated.

During the course of our research Chen reported the synthesis of the related $\text{Bc}(\text{tBu})\text{Ir}(\text{CO})_2$ complex and its rhodium analogue,¹⁰ which prompted us to abandon further synthetic efforts in the area of iridium Bc complexes. The same group later reported related Bc rhodium and iridium species bearing phosphine ligands.¹¹

¹⁰ Chen, F.; Sun, J.-F.; Li, T.-Y.; Chen, X.-T.; Xue, Z.-L. *Organometallics*, **2011**, *30*, 2006

¹¹ Chen, F.; Wang, G.-F.; Li, Y.-Z.; Chen, X.-T.; Xue, Z.-L. *J. Organomet. Chem.* **2012**, *710*, 36

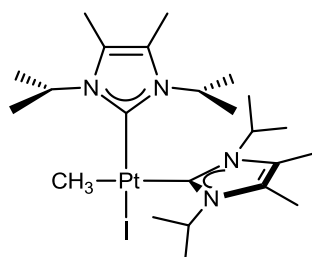
EXPERIMENTAL PART

EXPERIMENTAL PART. CHAPTER 1

Complexes **1**, **2** and **3** had been previously described by our group.¹ Complex **4** was prepared by the procedure reported by Nolan.² Species **7** and **8** have been previously described.³

cis-PtCH₃I(iⁱPr₂Me₂)₂ (**5**) and *trans*-PtCH₃I(iⁱPr₂Me₂)₂ (**6**)

cis-PtCH₃I(iⁱPr₂Me₂)₂ (**5**)



Synthesis:

120 mg (0.20 mmol) of *cis*-PtMe₂(iⁱPr₂Me₂)₂ (**4**) were dissolved in 2 mL of dichloromethane and a large excess of MeI (0.1 mL, 1.60 mmol) was added at room temperature. Gas evolution was observed, and after stirring at room temperature for 10 minutes the solvent was removed *in vacuo* to yield 133 mg (0.19 mmol, 93% yield) of **5**.

Spectroscopic and analytical data

White solid

¹ a) Rivada-Wheelaghan, O.; Donnadiou, B.; Maya, C.; Conejero, S. *Chem. Eur. J.* **2010**, *16*, 10323;
b) Rivada-Wheelaghan, O.; Ortuño, M. A.; Díez, J.; Lledós, A.; Conejero, S. *Angew. Chem. Int. Ed.* **2012**, *51*, 3936.

² Fortman, G.C.; Scott, N.M.; Linden, A.; Stevens, E. D.; Dorta, R.; Nolan, S.P. *Chem. Commun.* **2010**, *46*, 1050.

³ Kuhn, N.; Goehner, M.; Steimann, M. *Z. Naturforschung, B* **2002**, *57*, 631.

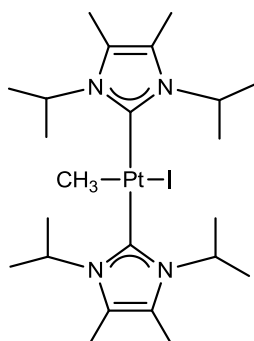
Molecular weight: 697.6

$^1\text{H NMR}$ (500 MHz, CDCl_3 , 25 °C) δ 5.94 (sept, $^3J_{\text{HH}} = 7.1$ Hz, 2H, $\underline{\text{C}}\text{H}(\text{CH}_3)_2$), 5.88 (sept, $^3J_{\text{HH}} = 7.1$ Hz, 2H, $\underline{\text{C}}\text{H}(\text{CH}_3)_2$), 2.18 (s, 6H, $=\text{C}-\underline{\text{C}}\text{H}_3$), 2.16 (s, 6H, $=\text{C}-\underline{\text{C}}\text{H}_3$), 1.55 (d, $^3J_{\text{HH}} = 7.0$ Hz, 6H, $\text{CH}(\underline{\text{C}}\text{H}_3)_2$), 1.42 (d, $^3J_{\text{HH}} = 7.0$ Hz, 6H, $\text{CH}(\underline{\text{C}}\text{H}_3)_2$), 1.19 (d, $^3J_{\text{HH}} = 7.2$ Hz, 12H, $\text{CH}(\underline{\text{C}}\text{H}_3)_2$), 0.48 (s+d, $^2J_{\text{PtH}} = 57$ Hz, 3H, Pt- $\underline{\text{C}}\text{H}_3$).

$^{13}\text{C}\{^1\text{H}\}$ NMR (126 MHz, CDCl_3 , 25 °C) δ 179.6 (C-Pt, *trans* to Me), 161.0 (C-Pt, *trans* to I), 124.5 ($=\underline{\text{C}}-\text{CH}_3$), 123.9 ($=\underline{\text{C}}-\text{CH}_3$), 52.1 ($\underline{\text{C}}\text{H}(\text{CH}_3)_2$), 52.0 ($\underline{\text{C}}\text{H}(\text{CH}_3)_2$), 22.6 ($\text{CH}(\underline{\text{C}}\text{H}_3)_2$), 22.4 ($\text{CH}(\underline{\text{C}}\text{H}_3)_2$), 21.5 ($\text{CH}(\underline{\text{C}}\text{H}_3)_2$), 21.3 ($\text{CH}(\underline{\text{C}}\text{H}_3)_2$), 10.7 ($=\text{C}-\underline{\text{C}}\text{H}_3$), 10.6 ($=\text{C}-\underline{\text{C}}\text{H}_3$), -13.2 (Pt- $\underline{\text{C}}\text{H}_3$).

***trans*-PtCH₃I(IⁱPr₂Me₂)₂ (6)**

Isomerization of **5** (100 mg, 0.143 mmol) to **6** in 3 mL of dichloromethane was complete after stirring overnight at room temperature or in 3 hours under reflux at 60 °C. Quantitative conversion was observed by NMR spectroscopy. The solvent is removed in vacuo and the solid is washed with pentane to yield 86 mg (0.123 mmol, 86% yield) of **6**.



Spectroscopic and analytical data

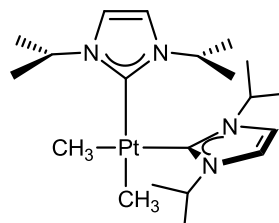
White solid

Molecular weight: 697.6

$^1\text{H NMR}$ (300 MHz, CD_2Cl_2 , 25 °C) δ 5.89 (sept, $^3J_{\text{HH}} = 7.1$ Hz, 4H, $\underline{\text{C}}\text{H}(\text{CH}_3)_2$), 2.14 (s, 12H, $=\text{C}-\underline{\text{C}}\text{H}_3$), 1.41 (d, $^3J_{\text{HH}} = 7.1$ Hz, 12H, $\text{CH}(\underline{\text{C}}\text{H}_3)_2$), 1.14 (d, $^3J_{\text{HH}} = 7.2$ Hz, 12H, $\text{CH}(\underline{\text{C}}\text{H}_3)_2$), -0.12 (s+d, $^2J_{\text{PtH}} = 93$ Hz, 3H, Pt- $\underline{\text{C}}\text{H}_3$).

$^{13}\text{C}\{^1\text{H}\}$ NMR (75 MHz, CD_2Cl_2 , 25 °C) δ 185.4 ($\underline{\text{C}}\text{-Pt}$), 123.8 ($=\underline{\text{C}}\text{-CH}_3$), 51.7 (s+d, $^3J_{\text{PtC}} = 50$ Hz, $\underline{\text{C}}\text{H}(\text{CH}_3)_2$), 23.0 ($\text{CH}(\underline{\text{C}}\text{H}_3)_2$), 21.4 ($\text{CH}(\underline{\text{C}}\text{H}_3)_2$), 10.8 ($=\text{C}-\underline{\text{C}}\text{H}_3$), -9.1 ($\text{Pt}-\underline{\text{C}}\text{H}_3$).

***cis*-Pt(CH₃)₂(ⁱPr)₂ (9)**



Synthesis:

A solution of 250 mg (1.04 mmol) of 1,3-diiisopropyl-imidazolium tetrafluoroborate and 120 mg (1.07 mmol) of potassium *tert*-butoxide in 3 mL of dry THF is stirred at -30 °C for 4 h. Solvent is removed *in vacuo* at 0 °C and the in situ prepared carbene is redissolved in 3 mL of dry benzene. 173 mg (0.52 mmol) of PtMe₂(cod) is added to this suspension and stirred at room temperature for 1 h. The crude is filtered and extracted with benzene (2x1 mL) and the combined filtrate is evaporated to yield 225 mg (0.43 mmol, 80% yield) of **9** as an off-white solid.

Spectroscopic and analytical data

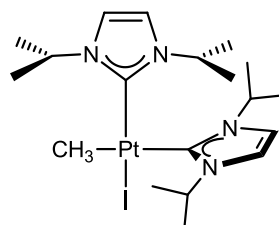
Off-white solid

Molecular weight: 529.6

^1H NMR (400 MHz, CDCl_3 , 25 °C) δ 6.80 (s, 4H, $=\underline{\text{C}}\text{H}$), 5.50 (sept, $^3J_{\text{HH}} = 6.5$ Hz, 4H, $\underline{\text{C}}\text{H}(\text{CH}_3)_2$), 1.38 (d, $^3J_{\text{HH}} = 6.6$ Hz, 12H, $\text{CH}(\underline{\text{C}}\text{H}_3)_2$), 1.06 (d, $^3J_{\text{HH}} = 6.7$ Hz, 12H, $\text{CH}(\underline{\text{C}}\text{H}_3)_2$), 0.13 (s+d, $^2J_{\text{PtH}} = 65$ Hz, 3H, $\text{Pt}-\underline{\text{C}}\text{H}_3$).

$^{13}\text{C}\{^1\text{H}\}$ NMR (101 MHz, CDCl_3 , 25 °C) δ 183.8 (s+d, $^1J_{\text{PtC}} = 851$ Hz, $\text{C}=\text{Pt}$), 115.4 ($=\underline{\text{C}}\text{H}$), 50.3 (s+d, $^3J_{\text{PtC}} = 44$ Hz, $\underline{\text{C}}\text{H}(\text{CH}_3)_2$), 24.5 ($\text{CH}(\underline{\text{C}}\text{H}_3)_2$), 22.9 ($\text{CH}(\underline{\text{C}}\text{H}_3)_2$), -10.1 (s+d, $^2J_{\text{PtC}} = 546$ Hz, $\text{Pt}-\underline{\text{C}}\text{H}_3$).

Elemental analysis: Calculated for $\text{C}_{20}\text{H}_{38}\text{N}_4\text{Pt}$: C 45.36; H 7.23; N 10.58; Found: C 44.9; H 6.8; N 10.6

cis*-PtCH₃I(iⁱPr₂)₂ (**10**) and *trans*-PtCH₃I(iⁱPr₂)₂ (**11**)**cis*-PtCH₃I(iⁱPr₂)₂ (**10**)***Synthesis:*

10 was prepared in an analogous manner to **5**, adding a large excess of iodomethane to a dichloromethane solution of **9**. Quantitative conversion was detected by NMR in only a few minutes at room temperature. For a typical reaction with 100 mg (0.19 mmol) of **9**, 110 mg (0.17 mmol, 91 % yield) of **10** were isolated.

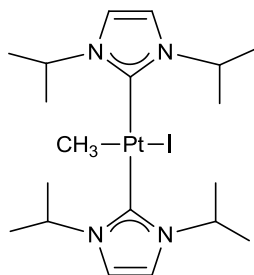
Spectroscopic and analytical data

White solid

Molecular weight: 641.5

¹H NMR (300 MHz, CD₂Cl₂, 25 °C) δ 6.90 (s, 2H, =CH), 6.89 (s, 2H, =CH), 5.41 (m, 4H, CH(CH₃)₂), 1.49 (d, ³J_{HH} = 6.6 Hz, 6H, CH(CH₃)₂), 1.39 (d, ³J_{HH} = 6.8 Hz, 6H, CH(CH₃)₂), 1.21 (d, ³J_{HH} = 6.9 Hz, 6H, CH(CH₃)₂), 1.20 (d, ³J_{HH} = 6.9 Hz, 6H, CH(CH₃)₂), 0.34 (s+d, ²J_{PtH} = 57 Hz, Pt-CH₃).

¹³C{¹H} NMR (126 MHz, CD₂Cl₂, 25 °C) δ 178.6 (C=Pt, *trans* to Me), 160.2 (C=Pt, *trans* to I), 116.8 (=CH), 116.54 (=CH), 51.7 (CH(CH₃)₂), 51.6 (CH(CH₃)₂), 24.5 (CH(CH₃)₂), 24.3 (CH(CH₃)₂), 23.2 (CH(CH₃)₂), 22.9 (CH(CH₃)₂), -13.1 (Pt-CH₃).

***trans*-PtCH₃I(iⁱPr)₂ (**11**)****Synthesis:**

A solution of 120 mg (0.23 mmol) of **9** in 3 mL of dichloromethane and a large excess of MeI (0.3 mL) was heated overnight at 55 °C in a closed system. After solvent removal in vacuo, 136 mg (0.21 mmol, 94 % yield) of **11** are obtained. Crystals can be obtained by slow diffusion of pentane into a concentrated solution of complex **11** in dichloromethane at -20 °C.

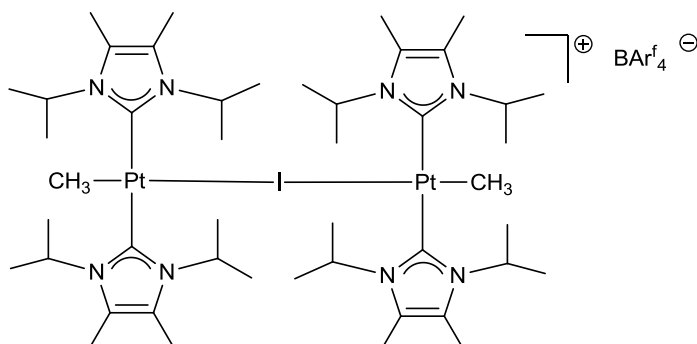
Spectroscopic and analytical data

White solid

Molecular weight: 641.5

¹H NMR (300 MHz, CD₂Cl₂, 25 °C) δ 6.93 (s, 4H, =CH), 5.64 (sept, ³J_{HH} = 6.7 Hz, 4H, CH(CH₃)₂), 1.50 (d, ³J_{HH} = 6.7 Hz, 12H, CH(CH₃)₂), 1.43 (d, ³J_{HH} = 6.7 Hz, 12H, CH(CH₃)₂), 0.20 (s+d, ²J_{PtH} = 93 Hz, 3H, Pt-CH₃).

¹³C{¹H} NMR (126 MHz, CD₂Cl₂, 25 °C) δ 174.1 (C=Pt), 114.0 (=CH), 51.6 (CH(CH₃)₂), 23.4 (CH(CH₃)₂), 23.1 (CH(CH₃)₂).

[Pt₂(μ-I)(CH₃)₂(ⁱPr₂Me₂)₄][B(Ar^F)₄] (12)**Synthesis:**

69 mg (0.08 mmol) of NaB(Ar^F)₄ were added to a solution of 100 mg (0.16 mmol) of *trans*-PtMeI(ⁱPr₂Me₂)₂ (**6**) in 5 mL of dry dichloromethane at – 30 °C. After stirring at low temperature for 20 minutes, the reaction is brought to room temperature and the crude is filtered. The pale yellow solution is evaporated to dryness to yield 123 mg (0.06 mmol, 74% yield) of complex **12**.

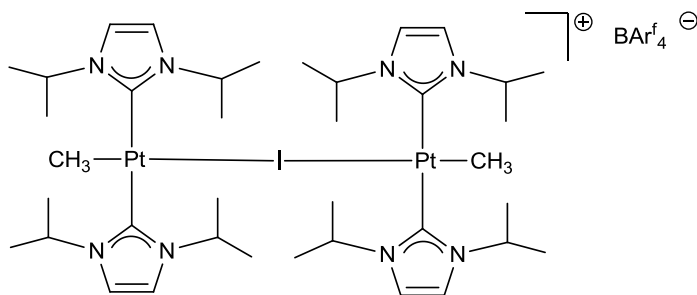
Spectroscopic and analytical data

Pale yellow solid

Molecular weight: 2131.5

¹H NMR (300 MHz, CD₂Cl₂, 25 °C) δ 7.73 (m, 8H, *o*-H (Ar)^F), 7.57 (m, 4H, *p*-H (Ar)^F), 5.94 (sept, ³J_{HH} = 7.0 Hz, 8H, CH(CH₃)₂), 2.14 (s, 24H, =C-CH₃), 1.42 (d, ³J_{HH} = 7.1 Hz, 24H, CH(CH₃)₂), 1.29 (d, ³J_{HH} = 7.1 Hz, 24H, CH(CH₃)₂), 0.28 (s+d, ²J_{PtH} = 98 Hz, 6H, Pt-CH₃).

¹³C{¹H} NMR (75 MHz, CD₂Cl₂, 25 °C) δ 175.5 (C=Pt), 162.0 (q, J_{CB} = 49 Hz, *ipso*-C (Ar)^F), 135.0 (*o*-C (Ar)^F), 129.1 (q, J = 31 Hz, *m*-C (Ar)^F), 124.8 (q, J_{CF} = 273 Hz, CF₃), 124.3 (=C-CH₃), 117.7 (*p*-C (Ar)^F), 52.3 (CH(CH₃)₂), 21.7 (CH(CH₃)₂), 21.1 (CH(CH₃)₂), 10.1 (=C-CH₃), -20.9 (Pt-CH₃).

[Pt₂(μ-I)(CH₃)₂(ⁱPr₂)₄][B(Ar^F)₄] (13)**Synthesis:**

63 mg (0.075 mmol) of NaB(Ar^F)₄ were added to a solution of 100 mg (0.15 mmol) of *trans*-PtMeI(ⁱPr₂)₂ (**11**) in 5 mL of dry dichloromethane at – 30 °C. After stirring at low temperature for 20 minutes, the reaction is brought to room temperature and the crude is filtered. The pale yellow solution is evaporated to yield 122 mg (0.06 mmol, 78% yield) of complex **13**.

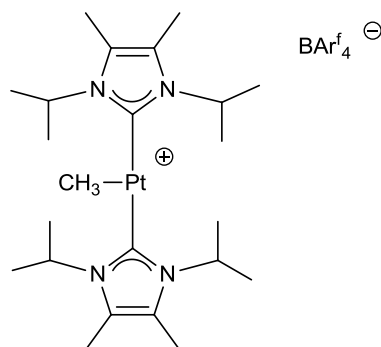
Spectroscopic and analytical data

White solid

Molecular weight: 2019.3

¹H NMR (400 MHz, CD₂Cl₂, 25 °C) δ 7.78 (m, 8H, *o*-H (Ar^F)), 7.61 (m, 4H, *p*-H (Ar^F)), 6.88 (s, 8H, =CH), 5.44 (sept, ³J_{HH} = 6.8 Hz, 8H, CH(CH₃)₂), 1.38 (d, ³J_{HH} = 6.8 Hz, 24H, CH(CH₃)₂), 1.23 (d, ³J_{HH} = 6.8 Hz, 24H, CH(CH₃)₂), 0.29 (s+d, ²J_{PtH} = 96 Hz, 6H, Pt-CH₃).

¹³C{¹H} NMR (101 MHz, CD₂Cl₂, 25 °C) δ 176.2 (C=Pt, ¹J_{PtC} = 1054 Hz), 162.4 (q, J_{CB} = 50 Hz, *ipso*-C (Ar^F)), 135.4 (*o*-C (Ar^F)), 129.5 (q, J_{CF} = 30 Hz, *m*-C (Ar^F)), 125.2 (q, J_{CF} = 272 Hz, CF₃ (Ar^F)), 118.1 (*p*-C (Ar^F)), 116.6 (=CH, ³J_{PtC} = 27 Hz), 51.8 (s+d, ³J_{PtC} = 40 Hz, CH(CH₃)₂), 23.3 (CH(CH₃)₂), 23.2 (CH(CH₃)₂), -20.1 (s+d, ¹J_{PtC} = 793 Hz, Pt-CH₃).

[PtCH₃(ⁱPr₂Me₂)₂][B(Ar^F)₄] (14b)*Synthesis:*

520 mg (0.51 mmol) of [H(OEt₂)₂B(Ar^F)₄] and 300 mg (0.51 mmol) of *cis*-PtMe₂(ⁱPr₂Me₂)₂ were dissolved in 6 mL of dry dichloromethane at -78 °C and the solution is slowly brought to room temperature over the course of 1h. Gas evolution is observed and a dark yellow solution is formed. After stirring for 10 minutes at room temperature, the solvent was concentrated under vacuum to approx. 2 mL and a layer of pentane was added. Slow diffusion at -20 °C leads to the separation of a yellow oil. The solvent is filtered off and the oil dried in vacuo to yield 630 mg (0.44 mmol, 86 % yield) of **14b** as a fluffy yellow solid that is air and moisture sensitive. It must be noted that prolonged time under vacuum leads to partial cyclometallation to form **16** by methane elimination.

Spectroscopic and analytical data

Yellow solid

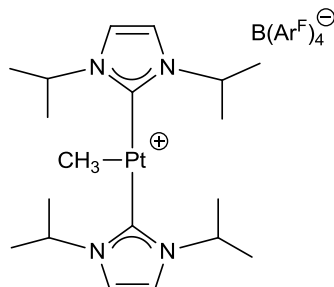
Molecular weight: 1433.9

¹H NMR (300 MHz, CD₂Cl₂, 25 °C) δ 7.73 (m, 8H, *o*-H (Ar)^F), 7.57 (m, 4H, *p*-H (Ar)^F), 5.84 (sept, ³J_{HH} = 6.9 Hz, 4H, CH(CH₃)₂), 2.20 (s, 12H, =C-CH₃), 1.56 (d, ³J_{HH} = 7.2 Hz, 24H, CH(CH₃)₂), 0.68 (s+d, 3H, ²J_{PtH} = 106 Hz, Pt-CH₃).

¹³C{¹H} NMR (75 MHz, CD₂Cl₂, 25 °C) δ 172.2 (br, C=Pt, HMBC) 162.3 (q, J_{CB} = 50 Hz, *ipso*-C (Ar)^F), 135.4 (*o*-C (Ar)^F), 129.4 (q, J_{CF} = 32 Hz, *m*-C (Ar)^F), 126.4 (=C-CH₃), 125.2 (q, J_{CF} = 276 Hz, CF₃ (Ar)^F), 118.1 (*p*-C (Ar)^F), 53.7 (s+d, ³J_{PtC} = 41 Hz, CH(CH₃)₂), 22.3 (CH(CH₃)₂), 10.6 (=C-CH₃), -23.9 (br, Pt-CH₃).

Elemental Analysis: Calculated: C, 46.07; H, 3.87; N, 3.91; Found: C, 45.9; H, 3.7; N, 3.8.

[PtCH₃(IⁱPr₂)₂][B(Ar^F)₄] (15b)



Synthesis:

382 mg (0.38 mmol) of [H(OEt₂)₂B(Ar^F)₄] and 200 mg (0.38 mmol) of PtMe₂(IⁱPr₂)₂ were dissolved in 4 mL of dry dichloromethane at -78 °C. As the reaction was slowly brought to room temperature, gas evolution is observed and a yellow solution is formed. After stirring for 1h at r.t., the solution was concentrated under vacuum to ca. 2 mL and a layer of dry pentane was added. Slow diffusion of at -20 °C results in the precipitation of a yellow oil, which after solvent filtration is dried in vacuo to yield 432 mg (0.31 mmol, 83% yield) of complex **15b** as a yellow solid that is air and moisture sensitive.

Spectroscopic and analytical data

Yellow solid

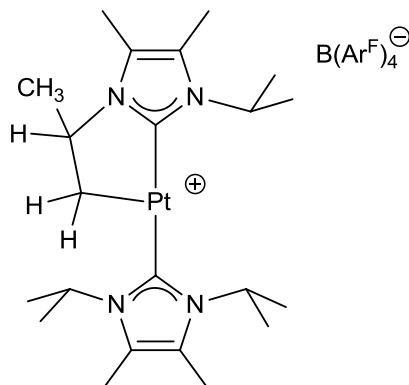
Molecular weight: 1377.8

¹H NMR (400 MHz, CD₂Cl₂, 25 °C) δ 7.74 (m, 8H, *o*-H (Ar^F)), 7.58 (m, 4H, *p*-H (Ar^F)), 7.06 (s, 4H, =CH), 5.45 (sept, ³J_{HH} = 6.7 Hz, 4H, CH(CH₃)₂), 1.48 (d, ³J_{HH} = 6.9 Hz, 24H, CH(CH₃)₂), 0.66 (s+d, br, ²J_{PtH} = 103 Hz, 3H, Pt-CH₃).

¹³C{¹H} NMR (101 MHz, CD₂Cl₂, 25 °C) δ 173.6 (C=Pt, br), 162.4 (q, J_{CB} = 50 Hz, *ipso*-C (Ar^F)), 135.4 (*o*-C (Ar^F)), 129.5 (q, J_{CF} = 32 Hz, *m*-C (Ar^F)), 125.2 (q, J_{CF} = 272 Hz, CF₃ (Ar^F)), 118.1 (*p*-C (Ar^F)), 118.0 (=CH), 53.0 (CH(CH₃)₂), 23.6 (CH(CH₃)₂). Pt-CH₃ not observed.

Elemental Analysis: Calculated: C, 44.46; H, 3.44; N, 4.07; Found: C, 44.1; H, 3.7; N, 3.8.

[Pt(ⁱPr₂Me₂')(ⁱPr₂Me₂)] [B(Ar^F)₄] (16)



Synthesis:

The reaction crude of **14b** is heated overnight at 55 °C. The solution was concentrated in vacuo to *ca.* 2 mL and a layer of pentane was added. After solvent diffusion at -20 °C, **16** precipitated out as a yellow oil. The solvent was filtered off and the oil is dried to produce a fluffy yellow solid. Typical isolated yields range between 72 – 85 %.

Spectroscopic and analytical data

Yellow solid

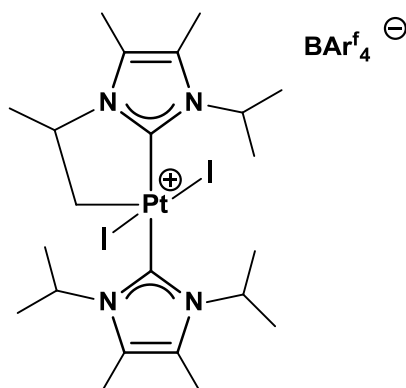
Molecular weight: 1417.87

¹H NMR (500 MHz, CD₂Cl₂, 25 °C) δ 7.73 (m, 8H, *o*-H (Ar)^F), 7.57 (m, 4H, *p*-H (Ar)^F), 5.85 (sept, ³J_{HH} = 7.1 Hz, 2H, CH(CH₃)₂-(ⁱPr₂Me₂)), 4.73 (sept, ³J_{HH} = 7.0 Hz, 1H, CH(CH₃)₂-(ⁱPr₂Me₂')), 3.64 (p, ³J_{HH} = 5.9 Hz, ³J_{PtH} = 144 Hz, 1H, Pt-CH₂CH), 2.84 (dd+d, ³J_{HH} = 10.5, 6.1 Hz, ²J_{PtH} = 115 Hz, 1H, CH₂-Pt), 2.24 (s, 9H, =C-CH₃, (ⁱPr₂Me₂)+(ⁱPr₂Me₂')), 2.14 (s, 3H, =C-CH₃, (ⁱPr₂Me₂')), 1.92 (d+d, ³J_{HH} = 10.5 Hz, ²J_{PtH} = 88 Hz, 1H, CH₂-Pt), 1.54 (d, ³J_{HH} = 7.2 Hz, 6H, CH(CH₃)₂-(ⁱPr₂Me₂')), 1.51 (d, ³J_{HH} = 7.1 Hz, 12H, CH(CH₃)₂-(ⁱPr₂Me₂)), 1.37 (d, ³J_{HH} = 6.3 Hz, 3H, Pt-CH₂CH(CH₃)).

$^{13}\text{C}\{^1\text{H}\}$ NMR (126 MHz, CD_2Cl_2 , 25 °C) δ 172.8 ($\underline{\text{C}}=\text{Pt}$), 166.5($\underline{\text{C}}'=\text{Pt}$), 162.3 (q, $J_{\text{CB}} = 50$ Hz, *ipso*-C (Ar^{F})) 135.4 (*o*-C (Ar^{F})), 129.6 (q, $J_{\text{CF}} = 32$ Hz, *m*-C (Ar^{F})), 126.5 (2 = $\underline{\text{C}}-\text{CH}_3$, ($^i\text{Pr}_2\text{Me}_2$)), 125.2 (q, $J_{\text{CF}} = 272$ Hz, CF_3 (Ar^{F})), 124.5 and 124.3 (= $\underline{\text{C}}-\text{CH}_3$, ($^i\text{Pr}_2\text{Me}_2'$)), 118.1 (*p*-C (Ar^{F})), 58.0 (Pt- CH_2CH), 53.8 (2 $\underline{\text{C}}\text{H}(\text{CH}_3)_2-(^i\text{Pr}_2\text{Me}_2)$), 52.2 ($\underline{\text{C}}\text{H}(\text{CH}_3)_2-(^i\text{Pr}_2\text{Me}_2')$), 25.6 (Pt- $\text{CH}_2\text{CH}(\underline{\text{C}}\text{H}_3)$), 22.6, 22.5 and 22.4 ($\text{CH}(\underline{\text{C}}\text{H}_3)_2$) 11.2 (=C- $\underline{\text{C}}\text{H}_3$, ($^i\text{Pr}_2\text{Me}_2'$)), 10.6 (2 =C- $\underline{\text{C}}\text{H}_3$, ($^i\text{Pr}_2\text{Me}_2$)), 10.0 ($\underline{\text{C}}\text{H}_2\text{-Pt}$, HSQC), 9.6 (=C- $\underline{\text{C}}\text{H}_3$, ($^i\text{Pr}_2\text{Me}_2'$)).

Elemental Analysis: Calculated: C, 45.74; H, 3.63; N, 3.95. Found: C, 45.4; H, 3.8; N, 4.2.

[Pt $_2$ ($^i\text{Pr}_2\text{Me}_2'$)($^i\text{Pr}_2\text{Me}_2$)] $[\text{B}(\text{Ar}^{\text{F}})_4]$ (17**)**



Synthesis:

30 mg (0.021 mmol) of $[\text{Pt}(^i\text{Pr}_2\text{Me}_2')(^i\text{Pr}_2\text{Me}_2)]\text{B}(\text{Ar}^{\text{F}})_4$ (**16**) were dissolved in 0.4 mL of dry CD_2Cl_2 and cooled to -40 °C. Then, 157 μL (5.4 mg, 0.021 mmol) of a solution containing 17 mg of I_2 (0.067 mmol) in 0.5 mL of dry CD_2Cl_2 were added to the cooled solution of **16**, resulting in an immediate color change from yellow to dark red. **17** formed quantitatively and was spectroscopically characterized *in situ* at -40 °C, as it was thermally unstable (e.g. 50 % evolution to Pt(II) species **21** after 2h at 0 °C). Attempts to crystallize **17** at low temperature led to decomposition.

Spectroscopic and analytical data

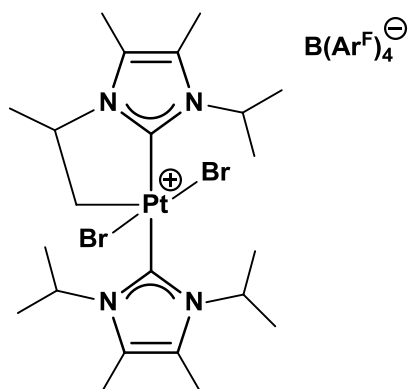
Dark red solid

Molecular weight: 1671.7

$^1\text{H NMR}$ (500 MHz, CD_2Cl_2 , $-40\text{ }^\circ\text{C}$) δ 7.72 (m, 8H, *o*-H (Ar^{F})), 7.55 (m, 4H, *p*-H (Ar^{F})), 5.41 (dd+d, $^3J_{\text{HH}} = 8.4, 4.3\text{ Hz}$, $^2J_{\text{PtH}} = 80\text{ Hz}$, 1H, $\text{CH}_2\text{-Pt}$), 5.08 (t+d, $^3J_{\text{HH}} = 5.1\text{ Hz}$, $^2J_{\text{PtH}} = 80\text{ Hz}$, 1H, $\text{CH}_2\text{-Pt}$), 4.59 (sept, $^3J_{\text{HH}} = 7.1\text{ Hz}$, 1H, $\text{CH}(\text{CH}_3)_2\text{-(iPr}_2\text{Me}_2)$), 4.23 (sext, $^3J_{\text{HH}} = 6.4\text{ Hz}$, 1H, Pt- CH_2CH), 4.10 (sept, $^3J_{\text{HH}} = 7.3\text{ Hz}$, 1H, $\text{CH}(\text{CH}_3)_2\text{-(iPr}_2\text{Me}_2')$), 3.24 (sept, $^3J_{\text{HH}} = 6.8\text{ Hz}$, 1H, $\text{CH}(\text{CH}_3)_2\text{-(iPr}_2\text{Me}_2)$), 2.33, 2.30, 2.25 and 2.22 (s, 3H each, =C- CH_3), 1.66 – 1.38 (m, 21H, $\text{CH}(\text{CH}_3)_2$).

$^{13}\text{C}\{^1\text{H}\}$ NMR (126 MHz, CD_2Cl_2 , $-40\text{ }^\circ\text{C}$) δ 161.7 (q, $J_{\text{CB}} = 50\text{ Hz}$, *ipso*-C (Ar^{F})), 154.1 (C=Pt, $\text{-(iPr}_2\text{Me}_2)$), 148.4 (C=Pt, $\text{-(iPr}_2\text{Me}_2')$), 135.4 (*o*-C (Ar^{F})), 129.0 (=C- CH_3), 128.6 (q, $J_{\text{CF}} = 31\text{ Hz}$, *m*-C (Ar^{F})), 128.5, 127.6 and 126.9 (=C- CH_3), 124.4 (q, $J_{\text{CF}} = 272\text{ Hz}$, CF_3 (Ar^{F})), 117.5 (*p*-C (Ar^{F})), 61.4 (Pt- CH_2CH), 55.4, 52.9 and 52.6 ($\text{CH}(\text{CH}_3)_2$), 44.5 ($\text{CH}_2\text{-Pt}$), 21.3, 21.1, 20.8, 20.4, 20.3 and 17.0 ($\text{CH}(\text{CH}_3)_2$ in a 1:2:1:1:1:1 ratio), 10.6, 10.5 and 9.6 (=C- CH_3 in a 2:1:1 ratio).

[PtBr₂(iPr₂Me₂')(iPr₂Me₂)](B(Ar^F)₄) (18)



Synthesis:

30 mg (0.021 mmol) of $[\text{Pt}(\text{iPr}_2\text{Me}_2)'\text{(iPr}_2\text{Me}_2)]\text{B}(\text{Ar}^{\text{F}})_4$ (**16**) were dissolved in 0.4 mL of dry CD_2Cl_2 and cooled to $-40\text{ }^\circ\text{C}$. Then, 55 μL (0.021 mmol) of a solution containing 10 μL (31 mg, 0.195 mmol) of Br_2 in 0.5 mL of dry CD_2Cl_2 were added to the cooled solution of **16**, resulting in an immediate color change from yellow to dark red. Complex **18** formed quantitatively and was spectroscopically characterized *in situ* at $-40\text{ }^\circ\text{C}$, as it was thermally unstable (decomposition to a

mixture of unidentified species over 0° C). Attempts to crystallize **18** at low temperature led to decomposition.

Spectroscopic and analytical data

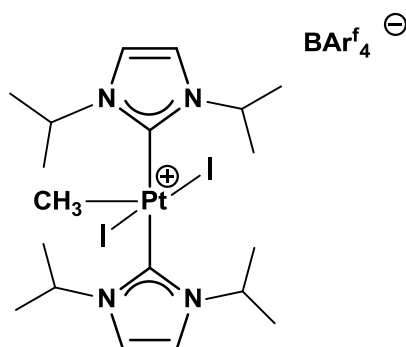
Dark red solid

Molecular weight: 1577.7

$^1\text{H NMR}$ (500 MHz, CD_2Cl_2 , 0 °C) δ 7.73 (m, 8H, *o*-H (Ar^{F})), 7.57 (m, 4H, *p*-H (Ar^{F})), 5.36 (dd+d, $J_{\text{HH}} = 6.8, 4.1\text{Hz}$, $^2J_{\text{PtH}} = 86\text{ Hz}$, 1H, $\text{CH}_2\text{-Pt}$), 5.11 (dd+d, $J_{\text{HH}} = 6.8, 4.1\text{Hz}$, $^2J_{\text{PtH}} = 86\text{ Hz}$, 1H, $\text{CH}_2\text{-Pt}$), 4.71 (sept, $J = 6.8\text{ Hz}$, 1H, $\text{CH}(\text{CH}_3)_2\text{-}(\text{i}^{\text{Pr}}_2\text{Me}_2')$), 4.37 (sept, $J = 7.2\text{ Hz}$, 1H, $\text{CH}(\text{CH}_3)_2\text{-}(\text{i}^{\text{Pr}}_2\text{Me}_2)$), 4.10 (m, 1H, $\text{CH}(\text{CH}_2)(\text{CH}_3)$), 4.01 (m, 1H, $\text{CH}(\text{CH}_3)_2\text{-}(\text{i}^{\text{Pr}}_2\text{Me}_2)$), 2.36, 2.33, 2.30 and 2.26 (s, 3H each, =C- CH_3) 1.70 (d, $^3J_{\text{HH}} = 6.8\text{ Hz}$, 3H, $\text{CH}(\text{CH}_3)_2\text{-}(\text{i}^{\text{Pr}}_2\text{Me}_2')$), 1.67 (d, $^3J_{\text{HH}} = 7.0\text{ Hz}$, 3H, $\text{CH}(\text{CH}_3)_2\text{-}(\text{i}^{\text{Pr}}_2\text{Me}_2')$), 1.60 (m, 15H, $\text{CH}(\text{CH}_3)_2$).

$^{13}\text{C}\{^1\text{H}\}$ NMR (126 MHz, CD_2Cl_2 , 0 °C) δ 162.1 (q, $J_{\text{CB}} = 50\text{ Hz}$, *ipso*-C (Ar^{F})), 158.3 (C=Pt, $-(\text{i}^{\text{Pr}}_2\text{Me}_2)$), 150.8 (C=Pt, $-(\text{i}^{\text{Pr}}_2\text{Me}_2')$), 135.2 (*o*-C (Ar^{F})), 130.5 and 130.3 (=C- CH_3), 129.2 (q, $J_{\text{CF}} = 32\text{ Hz}$, *m*-C (Ar^{F})), 124.9 (q, $J_{\text{CF}} = 273\text{ Hz}$, CF_3 (Ar^{F})), 117.9 (*p*-C (Ar^{F})), 60.4 (Pt- CH_2CH), 57.5, 52.9 and 52.8 ($\text{CH}(\text{CH}_3)_2$), 49.3 (s+d, $^1J_{\text{PtC}} = 483\text{ Hz}$, $\text{CH}_2\text{-Pt}$), 23.2, 23.0, 22.8, 21.9, 21.8 and 21.5 ($\text{CH}(\text{CH}_3)_2$), 18.7 ($^3J_{\text{PtC}} = 36\text{ Hz}$, Pt- $\text{CH}_2\text{CH}(\text{CH}_3)$), 11.0, 10.9, 10.4 and 9.9 (=C- CH_3).

$[\text{PtMeI}_2(\text{i}^{\text{Pr}}_2\text{N})_2][\text{B}(\text{Ar}^{\text{F}})_4] \text{ (19)}$



Synthesis:

35 mg (0.025 mmol) of $[\text{PtCH}_3(\text{iPr}_2)]\text{B}(\text{Ar}^{\text{F}})_4$ (**15**) were dissolved in 0.4 mL of dry CD_2Cl_2 and cooled to $-40\text{ }^\circ\text{C}$. Then, 145 μL (6.4 mg, 0.025 mmol) of a solution containing 22 mg of I_2 in 0.5 mL of dry CD_2Cl_2 were added to the cooled solution of **15**, resulting in an immediate color change from yellow to dark red. Complex **19** formed quantitatively and was spectroscopically characterized *in situ* at $-40\text{ }^\circ\text{C}$, as it was thermally unstable (decomposition through initial iodomethane loss over $0\text{ }^\circ\text{C}$ to a mixture of unidentified species). Attempts to crystallize **19** at low temperature led to decomposition.

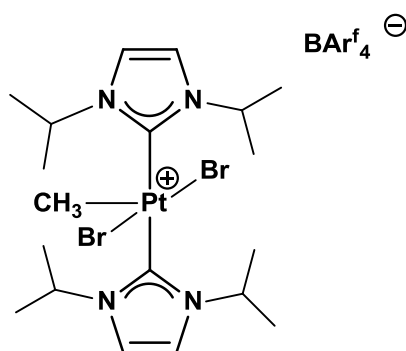
Spectroscopic and analytical data

Dark red solid

Molecular weight: 1631.6

^1H NMR (400 MHz, CD_2Cl_2 , $-30\text{ }^\circ\text{C}$) δ 7.72 (m, 8H, *o*-H (Ar^{F})), 7.56 (m, 4H, *p*-H (Ar^{F})), 7.11 (s, 4H, = CH), 5.28 (sept, $^3J_{\text{HH}} = 6.8\text{ Hz}$, 4H, $\text{CH}(\text{CH}_3)_2$), 2.09 (s+d, $^2J_{\text{PtH}} = 30\text{ Hz}$, 3H, Pt- CH_3), 1.54 (d, $^3J_{\text{HH}} = 6.8\text{ Hz}$, 12H, $\text{CH}(\text{CH}_3)_2$), 1.48 (d, $^3J_{\text{HH}} = 6.8\text{ Hz}$, 12H, $\text{CH}(\text{CH}_3)_2$).

$^{13}\text{C}\{^1\text{H}\}$ NMR (101 MHz, CD_2Cl_2 , $-30\text{ }^\circ\text{C}$) δ 162.3 (q, $J_{\text{CB}} = 50\text{ Hz}$, *ipso*-C (Ar^{F})), 154.4 ($\text{C}=\text{Pt}$), 135.4 (*o*-C (Ar^{F})), 129.5 (q, $J_{\text{CF}} = 32\text{ Hz}$, *m*-C (Ar^{F})), 125.2 (q, $J_{\text{CF}} = 273\text{ Hz}$, CF_3 (Ar^{F})), 119.2 (=CH), 118.0 (*p*-C (Ar^{F})), 53.3 ($\text{CH}(\text{CH}_3)_2$), 23.3 ($\text{CH}(\text{CH}_3)_2$), 23.1 ($\text{CH}(\text{CH}_3)_2$), -7.9 (Pt- CH_3).

 $[\text{PtMeBr}_2(\text{iPr}_2)]\text{B}(\text{Ar}^{\text{F}})_4$ (**20**)

Synthesis:

35 mg (0.025 mmol) of $[\text{PtCH}_3(\text{iPr}_2)_2]\text{B}(\text{Ar}^{\text{F}})_4$ (**15**) were dissolved in 0.4 mL of dry CD_2Cl_2 and cooled to $-40\text{ }^\circ\text{C}$. Then, 65 μL (0.025 mmol) of a solution containing 10 μL (31 mg, 0.195 mmol) of Br_2 in 0.5 mL of dry CD_2Cl_2 were added to the cooled solution of **15**, resulting in an immediate color change from yellow to dark red. **20** formed quantitatively and was spectroscopically characterized *in situ* at $-30\text{ }^\circ\text{C}$, as it was thermally unstable (decomposition through initial bromomethane loss over $0\text{ }^\circ\text{C}$ to a mixture of unidentified species). Attempts to crystallize **20** at low temperature led to decomposition.

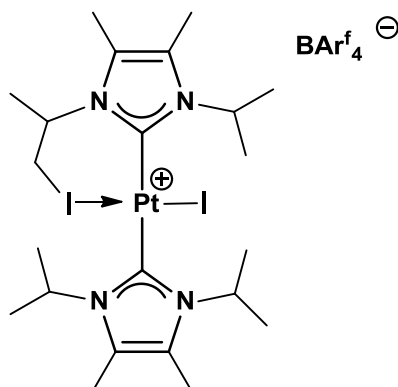
Spectroscopic and analytical data

Dark red solid

Molecular weight: 1535.6

$^1\text{H NMR}$ (400 MHz, CD_2Cl_2 , $-30\text{ }^\circ\text{C}$) δ 7.71 (m, 8H, *o*-H (Ar^{F})), 7.55 (m, 4H, *p*-H (Ar^{F})), 7.08 (s, 4H = $\underline{\text{C}}\text{H}$), 5.36 (m, 4H, $\underline{\text{C}}\text{H}(\text{CH}_3)_2$), 2.61 (s+d, $^2J_{\text{PtH}} = 32\text{ Hz}$, 3H, Pt- $\underline{\text{C}}\text{H}_3$), 1.50 (d, $^3J_{\text{HH}} = 6.8\text{ Hz}$, 12H, $\text{CH}(\underline{\text{C}}\text{H}_3)_2$), 1.47 (d, $^3J_{\text{HH}} = 7.0\text{ Hz}$, 12H, $\text{CH}(\underline{\text{C}}\text{H}_3)_2$).

$^{13}\text{C}\{^1\text{H}\}$ NMR (101 MHz, CD_2Cl_2 , $-30\text{ }^\circ\text{C}$) δ 161.7 (q, $J_{\text{CB}} = 50\text{ Hz}$, *ipso*-C (Ar^{F})), 155.9 ($\underline{\text{C}}=\text{Pt}$), 134.7 (*o*-C (Ar^{F})), 128.6 (q, $J_{\text{CF}} = 32\text{ Hz}$, *m*-C (Ar^{F})), 124.5 (q, $J_{\text{CF}} = 273\text{ Hz}$, CF_3 (Ar^{F})), 118.3 (= $\underline{\text{C}}\text{H}$), 117.6 (*p*-C (Ar^{F})), 52.7 ($\underline{\text{C}}\text{H}(\text{CH}_3)_2$), 23.1 ($\text{CH}(\underline{\text{C}}\text{H}_3)_2$), 23.0 ($\text{CH}(\underline{\text{C}}\text{H}_3)_2$), -8.4 (Pt- $\underline{\text{C}}\text{H}_3$).

 $[\text{Pt}(\text{iPr}_2\text{Me}_2\text{-I})(\text{iPr}_2\text{Me}_2)]\text{B}(\text{Ar}^{\text{F}})_4$ (21**)**

Synthesis:

A sample of **17** in dry CD₂Cl₂, prepared as described above, was left to evolve at room temperature for 5h. The dark red color faded over time to yield a yellow solution. **21** formed as the main product, along with 10 – 15% of other unidentified species. Attempts at further purification led to decomposition, so no elemental analysis data could be obtained.

Spectroscopic and analytical data

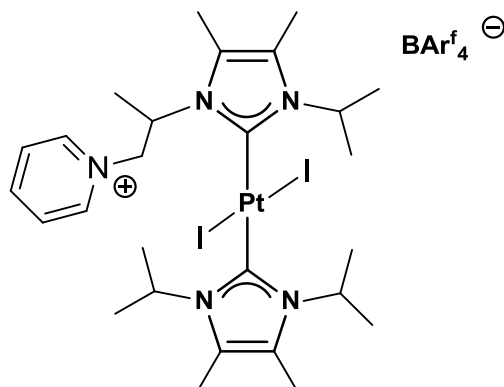
Yellow solid

Molecular weight: 1671.7

¹H NMR (400 MHz, CD₂Cl₂, 25 °C) δ 7.72 (m, 8H, *o*-H (Ar)^F), 7.57 (m, 4H, *p*-H (Ar)^F), 6.07, 5.66 and 5.60 (sept, ³J_{HH} = 7.1 Hz, 1H each, CH(CH₃)₂), 4.51 (m, 1H, Pt-ICH₂CH), 3.72 (dd, ³J_{HH} = 10.0, ²J_{HH} = 2.0 Hz, 1H, CH₂l), 3.43 (dd, ³J_{HH} = 9.9, ²J_{HH} = 3.4 Hz, 1H, CH₂l), 2.29, 2.28, 2.24 and 2.18 (s, 3H each, =C-CH₃), 2.14 (d, ³J_{HH} = 6.7 Hz, 3H, Pt-ICH₂CH(CH₃)), 1.65 – 1.56 (m, 12H, CH(CH₃)₂), 1.49 and 1.45 (d, ³J_{HH} = 7.2 Hz, 3H each, CH(CH₃)₂).

¹³C{¹H} NMR (101 MHz, CD₂Cl₂, 25 °C) δ 162.3 (q, J_{CB} = 50 Hz, *ipso*-C (Ar)^F), 153.8 (C=Pt, -(ⁱPr₂Me₂)), 149.6 (C=Pt, -(ⁱPr₂Me₂')), 135.4 (*o*-C (Ar)^F), 129.4 (q, ²J_{CF} = 31 Hz, *m*-C (Ar)^F), 128.1, 127.2, 127.1 and 126.4 (=C-CH₃), 125.2 (q, J_{CF} = 272 Hz, CF₃ (Ar)^F), 118.0 (sept, ³J_{CF} = 4 Hz, *p*-C (Ar)^F), 56.6 and 54.0 (CH(CH₃)₂ in a 1:2 ratio), 52.6 (Pt-ICH₂CH), 24.1 (CH₂l), 22.3 (Pt-ICH₂CH(CH₃)), 21.6 (CH(CH₃)₂ x5), 21.2 (CH(CH₃)₂), 11.4, 10.8, 10.6 and 9.4 (=C-CH₃).

$[\text{Pt}_2(\text{i}^i\text{Pr}_2\text{Me}_2\text{-Py})(\text{i}^i\text{Pr}_2\text{Me}_2)]\text{B}(\text{Ar}^{\text{F}})_4$ (**22**)



Synthesis:

2 μL (0.025) of dry pyridine were added to a sample of freshly prepared **17** (0.025 mmol) in dry CD_2Cl_2 at $-40\text{ }^\circ\text{C}$. As the sample was brought to room temperature, the dark red color faded to yield a yellow solution of **22**, which formed quantitatively and was spectroscopically characterized *in situ*. Crystallization attempts led to the precipitation of an oil from which trace impurities could not be separated, so no elemental analysis data could be obtained.

Spectroscopic and analytical data

Yellow solid

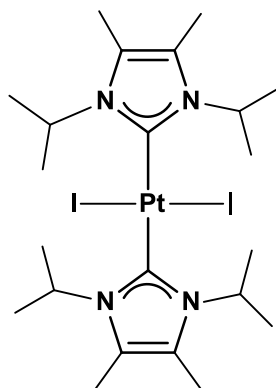
Molecular weight: 1623.9

$^1\text{H NMR}$ (500 MHz, CD_2Cl_2 , $25\text{ }^\circ\text{C}$) δ 8.87 (d, $^3J_{\text{HH}} = 6.0$ Hz, 2H, 2- CH_{Py}), 8.54 (t, $^3J_{\text{HH}} = 7.9$ Hz, 1H, 4- CH_{Py}), 8.05 (t, $^3J_{\text{HH}} = 7.1$ Hz, 2H, 3- CH_{Py}), 7.73 (m, 8H, *o*-H (Ar^{F})), 7.57 (m, 4H, *p*-H (Ar^{F})), 6.38 (p, 1H, $\underline{\text{C}}\text{H}(\text{CH}_3)_2$), 6.08 (sept, $^3J_{\text{HH}} = 7.2$ Hz, 1H, $\underline{\text{C}}\text{H}(\text{CH}_3)_2$), 5.92 (br, 1H, $\underline{\text{C}}\text{H}(\text{CH}_3)(\text{CH}_2\text{Py})$), 5.80 (p, $^3J_{\text{HH}} = 7.2$ Hz, 1H, $\underline{\text{C}}\text{H}(\text{CH}_3)_2$), 5.74 (br, 1H, $\underline{\text{C}}\text{H}_2\text{Py}$), 4.78 (dd, $^3J_{\text{HH}} = 13, 7$ Hz, 1H, $\underline{\text{C}}\text{H}_2\text{Py}$), 2.32 – 2.18 (m, 12H, = $\underline{\text{C}}\text{-CH}_3$), 2.02 – 1.88 (m, 3H, $\text{CH}(\underline{\text{C}}\text{H}_3)(\text{CH}_2\text{Py})$), 1.65 – 1.50 (m, 18H, $\text{CH}(\underline{\text{C}}\text{H}_3)_2$).

$^{13}\text{C}\{^1\text{H}\}$ NMR (101 MHz, CD_2Cl_2 , $25\text{ }^\circ\text{C}$) δ 164.6($\underline{\text{C}}=\text{Pt}$), 161.7 (q, $J_{\text{CB}} = 50$ Hz, *ipso*-C (Ar^{F}), 157.5 ($\underline{\text{C}}'=\text{Pt}$), 147.1 (4- CH_{Py}), 144.2 (2- CH_{Py}), 134.8 (*o*- $\underline{\text{C}}$ (Ar^{F})), 129.3 (3- CH_{Py}), 128.9 (qq, $^2J_{\text{CF}} = 31$ Hz, $^4J_{\text{CF}} = 3$ Hz, *m*-C (Ar^{F})), 125.6 and 125.0 (= $\underline{\text{C}}\text{-CH}_3$), 124.6 (q, $J_{\text{CF}} = 272$ Hz, CF_3 (Ar^{F})), 124.1 (= $\underline{\text{C}}\text{-CH}_3$, x2), 117.5 (sept, $^3J_{\text{CF}} = 4$ Hz, *p*-C

(Ar)^F, 64.1 (CH₂Py), 55.9 (CH(CH₃)(CH₂Py)), 53.8, 52.7 and 52.5 (CH(CH₃)₂), 21.0, 20.8, 20.6, 20.4 and 20.3 (CH(CH₃)₂ in a 1:1:2:1:1 ratio), 18.0 (CH(CH₃)(CH₂Py)), 10.3, 10.2, 10.1 and 9.8 (=C-CH₃).

trans-PtI₂(IⁱPr₂Me₂)₂ (23)



Synthesis:

A solution of 19 mg (0.072 mmol) of I₂ in 0.5 mL of dichloromethane was added to a solution of 50 mg (0.072 mmol) of *trans*-PtMeI(IⁱPr₂Me₂)₂ (**6**) in 2 mL of dichloromethane at room temperature. After stirring at room temperature for 15 minutes, solvent is removed *in vacuo* and the resulting pale yellow solid is washed with 2 mL of pentane at 0 °C to yield 45 mg (0.056 mmol, 78% yield) of **23**.

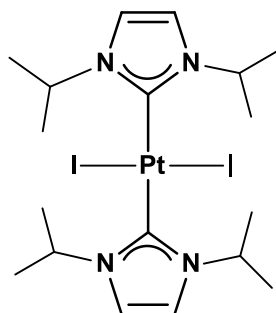
Spectroscopic and analytical data

Pale yellow solid

Molecular weight: 809.5

¹H NMR (400 MHz, d₈-THF, 25 °C) δ 6.17 (sept, ³J_{HH} = 7.2 Hz, 4H, CH(CH₃)₂), 2.24 (s, 12H, =C-CH₃), 1.55 (d, ³J_{HH} = 7.1 Hz, 24H, CH(CH₃)₂).

¹³C{¹H} NMR (101 MHz, d₈-THF, 25 °C) δ 163.5 (C=Pt), 125.5 (=C-CH₃), 53.3 (CH(CH₃)₂), 21.4 (CH(CH₃)₂), 10.5 (=C-CH₃).

trans-PtI₂(i^tPr₂)₂ (24)*Synthesis:*

A solution of 20 mg (0.078 mmol) of I₂ in 0.5 mL of dichloromethane was added to a solution of 50 mg (0.078 mmol) of *trans*-PtMeI(i^tPr₂)₂ (**11**) in 2 mL of dichloromethane at room temperature. After stirring at room temperature for 15 minutes, solvent is removed *in vacuo* and the resulting pale yellow solid is washed with 2 mL of pentane at 0 °C to yield 48 mg (0.064 mmol, 83% yield) of **24**.

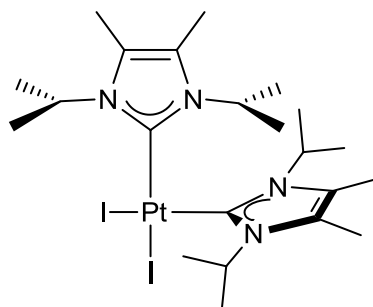
Spectroscopic and analytical data

Pale yellow solid

Molecular weight: 753.4

¹H NMR (400 MHz, CD₂Cl₂, 25 °C) δ 6.97 (s, 4H, =CH), 5.63 (sept, ³J_{HH} = 6.8 Hz, 4H, CH(CH₃)₂), 1.49 (d, ³J_{HH} = 6.9 Hz, 24H, CH(CH₃)₂).

¹³C{¹H} NMR (101 MHz, CD₂Cl₂, 25 °C) δ 163.1 (s+d, ¹J_{PtC} = 893 Hz, C=Pt), 116.9 (s+d, ³J_{PtC} = 22 Hz, =CH), 52.0 (s+d, ³J_{PtC} = 26 Hz, CH(CH₃)₂), 23.0 (CH(CH₃)₂).

***cis*-PtI₂(ⁱPr₂Me₂)₂ (**25**)****Synthesis:**

43 mg (0.07 mmol) of *cis*-PtMe₂(ⁱPr₂Me₂)₂ were added to a solution of 19 mg (0.07 mmol) of I₂ in 2 mL of methanol at room temperature. The red solution turns immediately to pale yellow. After stirring for 15 minutes the solvent is removed *in vacuo* to yield 51 mg (0.06 mmol, 90 % yield) of **25** as a pale yellow solid.

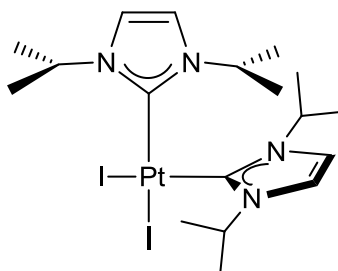
Spectroscopic and analytical data

Pale yellow solid

Molecular weight: 809.5

¹H NMR (400 MHz, CD₂Cl₂, 25 °C) δ 5.82 (sept, ³J_{HH} = 7.1 Hz, 4H, CH(CH₃)₂), 2.22 (s, 12H, =C-CH₃), 1.56 (d, ³J_{HH} = 7.0 Hz, 12H, CH(CH₃)₂), 1.25 (d, ³J_{HH} = 7.2 Hz, 12H, CH(CH₃)₂).

¹³C{¹H} NMR (101 MHz, CD₂Cl₂, 25 °C) δ 148.1 (s+d, ¹J_{PtC} = 1525 Hz, C=Pt), 126.1 (s+d, ³J_{PtC} = 34 Hz, =C-CH₃), 53.2 (s+d, ³J_{PtC} = 46 Hz, CH(CH₃)₂), 22.1 (CH(CH₃)₂), 21.4 (CH(CH₃)₂), 11.0 (=C-CH₃).

***cis*-PtI₂(ⁱPr₂)₂ (**26**)****Synthesis:**

50 mg (0.09 mmol) of *cis*-PtMe₂(ⁱPr₂Me₂)₂ were added to a solution of 23 mg (0.09 mmol) of I₂ in 2 mL of methanol at room temperature. The red solution turns immediately to pale yellow. After stirring for 15 minutes the solvent is removed *in vacuo* to yield 62 mg (0.08 mmol, 88% yield) of **26** as a pale yellow solid.

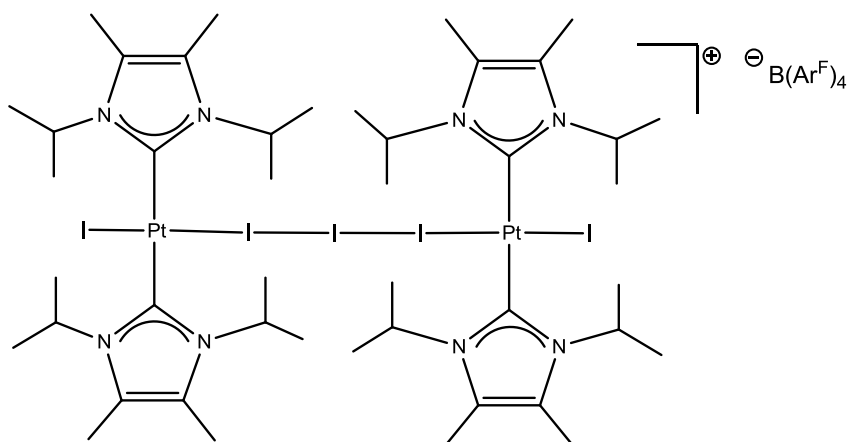
Spectroscopic and analytical data

Pale yellow solid

Molecular weight: 753.4

¹H NMR (400 MHz, CD₂Cl₂, 25 °C) δ 6.98 (s, 4H, =CH), 5.44 (sept, ³J_{HH} = 6.7 Hz, 4H, CH(CH₃)₂), 1.55 (d, ³J_{HH} = 6.6 Hz, 12H, CH(CH₃)₂), 1.28 (d, ³J_{HH} = 6.8 Hz, 12H, CH(CH₃)₂).

¹³C{¹H} NMR (101 MHz, CD₂Cl₂, 25 °C) δ 148.9 (s+d, ¹J_{PtC} = 1463 Hz, C=Pt), 117.9 (s+d, ³J_{PtC} = 40 Hz, =CH), 52.4 (s+d, ³J_{PtC} = 40 Hz, CH(CH₃)₂), 24.2 (CH(CH₃)₂), 23.2 (CH(CH₃)₂).

[Pt₂(μ-I₃)(I)₂(ⁱPr₂)₄]B(Ar^F)₄ (27**)****Synthesis:**

22 mg (0.025 mmol) of NaB(Ar^F)₄ were added to a solution of 40 mg (0.050 mmol) of *trans*-PtI₂(ⁱPr₂Me₂)₂ (**23**) in 2 mL of dry dichloromethane. Then, 158 μL (6.3 mg, 0.025 mmol) of a solution containing 20 mg of I₂ in 0.5 mL of dichloromethane were added to the previous mixture and a color change from pale yellow to bright red was observed. The crude was filtered and the residue washed with 2 mL of dichloromethane. The combined filtrate was evaporated *in vacuo* to yield 52 mg (0.020 mmol, 81% yield) of **27**. Crystals suitable for X-ray diffraction were grown by slow diffusion of pentane into a concentrated dichloromethane solution of **27**.

Spectroscopic and analytical data

Red solid

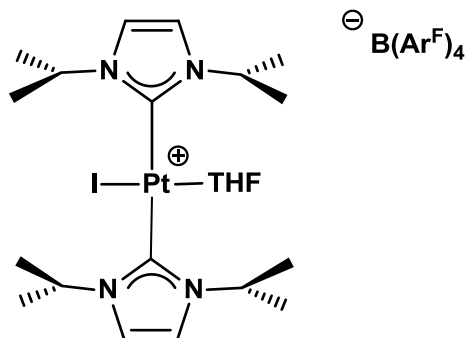
Molecular weight: 2609.1

¹H NMR (400 MHz, CD₂Cl₂, 25 °C) δ 7.72 (m, 8H, *o*-H (Ar^F)), 7.57 (m, 4H, *p*-H (Ar^F)), 5.80 (sept, ³J_{HH} = 7.1 Hz, 8H, CH(CH₃)₂), 2.21 (s, 24H, =C-CH₃), 1.56 (d, ³J_{HH} = 7.2 Hz, 48H, CH(CH₃)₂).

¹³C{¹H} NMR (101 MHz, CD₂Cl₂, 25 °C) δ 162.3 (q, J_{CB} = 50 Hz, *ipso*-C (Ar^F)), 157.8 (C=Pt), 135.4 (*o*-C (Ar^F)), 129.4 (qq, ²J_{CF} = 31 Hz, ⁴J_{CF} = 3 Hz, *m*-C (Ar^F)), 127.2 (=C-

$\underline{\text{C}}\text{H}_3$), 125.2 (q, $^1J_{\text{CF}} = 272$ Hz, CF_3 (Ar^{F}), 118.1 (sept, $^3J_{\text{CF}} = 4$ Hz, $p\text{-C}$ (Ar^{F}), 53.7 ($\underline{\text{C}}\text{H}(\text{CH}_3)_2$), 21.6 ($\text{C}\underline{\text{H}}(\text{CH}_3)_2$), 10.6 ($=\text{C}\text{-}\underline{\text{C}}\text{H}_3$).

***trans*-PtI(THF)(*i*Pr₂)₂ (**28**)**



Synthesis:

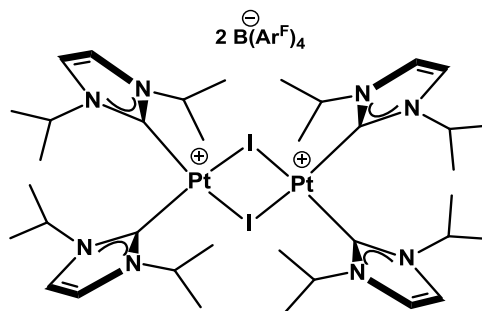
35 mg (0.040 mmol) of $\text{NaB}(\text{Ar}^{\text{F}})_4^4$ were added to a solution of 30 mg (0.040 mmol) of *cis*- $\text{PtI}_2(\text{iPr}_2)_2$ (**26**) in 0.5 mL of dry CD_2Cl_2 at room temperature. **28** formed quantitatively and was spectroscopically characterized *in situ*. Rapid dimerization (less than 1h at room temperature) precluded isolation and only the ^1H NMR is given below.

Spectroscopic data

Molecular weight: 698.6

^1H NMR (400 MHz, CD_2Cl_2 , 25 °C) δ 7.73 (m, 8H, *o*-H (Ar^{F})), 7.57 (m, 4H, *p*-H (Ar^{F})), 7.02 (s, 4H, $=\underline{\text{C}}\text{H}$), 5.28 (sept, $^3J_{\text{HH}} = 6.8$ Hz, 4H, $\underline{\text{C}}\text{H}(\text{CH}_3)_2$), 3.74 (m, 2H, THF), 1.88 (m, 2H, THF), 1.51 (d, $^3J_{\text{HH}} = 6.5$ Hz, 12H, $\text{C}\underline{\text{H}}(\text{CH}_3)_2$), 1.27 (d, $^3J_{\text{HH}} = 6.8$ Hz, 12H, $\text{C}\underline{\text{H}}_3$).

⁴ The $\text{NaB}(\text{Ar}^{\text{F}})_4$ batch we used contained THF and it was found to be crucial to stabilize this monomeric species.

[Pt(μ -I)(i Pr₂)₂]₂ (30**)***Synthesis:*

The crude of the preparation of **28** (0.040 mmol) was left to evolve at room temperature overnight. The solution was filtered and the residue was washed with 2x1 mL of dichloromethane. The combined filtrate is concentrated and a layer of pentane was added. After solvent diffusion at -20 °C, 101 mg (0.034 mmol, 85% yield) of **28** were obtained as pale yellow crystals.

Spectroscopic and analytical data

Pale yellow solid

Molecular weight: 2979.3

¹H NMR (400 MHz, CD₂Cl₂, 25 °C) δ 7.72 (m, 16H, *o*-H (Ar)^F), 7.56 (m, 8H, *o*-H (Ar)^F), 7.02 (s, 8H, =CH), 5.34 (m, 8H, CH(CH₃)₂), 1.44 (d, ³J_{HH} = 6.6 Hz, 24H, CH(CH₃)₂), 1.28 (d, ³J_{HH} = 6.8 Hz, 24H, CH(CH₃)₂)

¹³C{¹H} NMR (101 MHz, CD₂Cl₂, 25 °C) δ 162.3 (q, J_{CB} = 50 Hz, *ipso*-C (Ar)^F), 139.9 (C=Pt), 135.4 (*o*-C (Ar)^F), 129.4 (qq, ²J_{CF} = 31 Hz, ⁴J_{CF} = 3 Hz, *m*-C (Ar)^F), 125.2 (q, ¹J_{CF} = 272 Hz, CF₃ (Ar)^F), 119.5 (=CH), 118.1 (*p*-C (Ar)^F), 53.6 (CH(CH₃)₂), 24.75 (CH(CH₃)₂), 22.80 (CH(CH₃)₂).

EXPERIMENTAL PART. CHAPTER 2

Hydride complexes **32**, **34** and **34·H₂** had been previously described by our group.¹

- Catalytic reactions monitoring

A typical catalytic reaction between DMAB and complex **1** was carried out as follows:

A solution of 4.8 mg (0.003 mmol, 5%) of **1** was dissolved in 0.3 mL of dry d₈-THF, cooled to 0 °C and added to a solution of 4 mg (0.068 mmol) of dimethylamine borane in 0.2 mL of dry d₈-THF at 0 °C in an NMR tube under argon. At this temperature dehydrogenation does not take place. The sample is brought to the spectrometer, the tube stopper is removed and single scan ¹¹B{¹H} NMR experiments were recorded every 15 seconds. Plotting the decreasing DMAB integral (δ_B -13.6 ppm) over time allows for the obtention of kinetic data.

Alternatively the reaction is carried out in a Man on the moon series X102 kit.² The solution of DMAB in THF is placed in the reaction vessel, the pressure/temperature monitoring is started and the catalyst **1** solution in THF is rapidly injected through the stopper, for a total solvent volume of 0.5 mL. The pressure/temperature data is converted into number of mols of gas released using the Ideal Gas Law, $P \cdot V = n \cdot R \cdot T$, where P and T are the pressure and temperature of the reactor (as provided by the sensor), V is the volume of the gas (volume of the reactor minus the volume of the solution, 34.2 mL), n is the number of moles of gas and R is the ideal gas constant (0.082 atm·L/K·mol).

¹ "Síntesis de complejos coordinativamente insaturados de Pt(II) estabilizados por ligandos carbeno N-heterocíclicos. Activación y funcionalización de enlaces C-H". Rivada-Wheelaghan, O.; Tesis Doctoral, 2013.

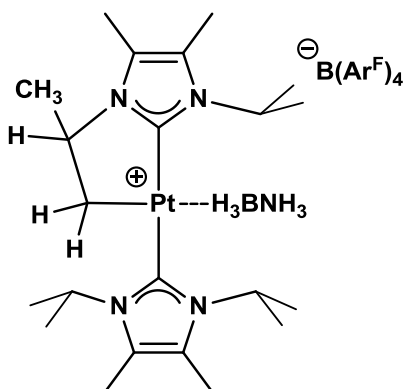
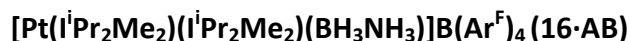
² www.manonthemoontech.com

- Amineborane adducts

Standard synthetic procedure for amineborane adducts exemplified for 1·DMAB:

A mixture of 25 mg (0.017 mmol) of $[\text{Pt}(\text{tBu})(\text{tBu})][\text{B}(\text{Ar}^{\text{F}})_4]$ and 1 mg (0.017 mmol) of BH_3NHMe_2 is dissolved in 0.5 mL of d_8 -THF cooled to $-30\text{ }^\circ\text{C}$. The sample is brought to the spectrometer and characterized by multinuclear NMR at $0\text{ }^\circ\text{C}$.

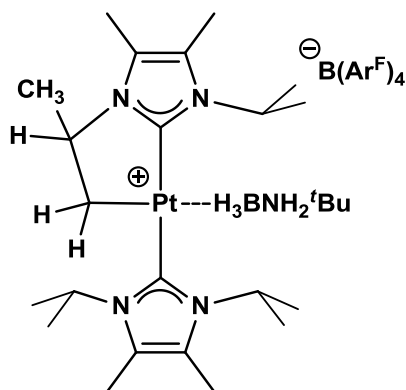
Amineborane adducts of complex 16



^1H NMR (400 MHz, CD_2Cl_2 , $0\text{ }^\circ\text{C}$) δ 7.72 (m, 8H, o -H (Ar^{F}), 7.56 (m, 4H, p -H (Ar^{F}), 6.01 and 5.62 (m, 1H each, $\text{CH}(\text{CH}_3)_2$), 4.75 (p, $^3J_{\text{HH}} = 7.1\text{ Hz}$, 1H, $\text{CH}(\text{CH}_3)_2$), 4.10 (q+d, $^3J_{\text{HH}} = 6.2\text{ Hz}$, $^2J_{\text{PtH}} = 100\text{ Hz}$, 1H, Pt- CH_2CH), 3.33 (br s, 3H, NH_3), 2.43 (dd+d, $J_{\text{HH}} = 11, 7\text{ Hz}$, $^2J_{\text{PtH}} = 98\text{ Hz}$, 1H, CH_2 -Pt), 2.22, 2.20, 2.19 and 2.14 (s, 3H each, =C- CH_3), 1.68 (d+d, $^3J_{\text{HH}} = 11\text{ Hz}$, $^3J_{\text{PtH}} = 77\text{ Hz}$, 1H, CH_2 -Pt), 1.53 (m, 6H, CH(CH_3) $_2$), 1.50, 1.48, 1.43 and 1.42 (d, $^3J_{\text{HH}} \sim 7\text{ Hz}$, 3H each, CH(CH_3) $_2$), 1.29 (d, $^3J_{\text{HH}} = 6.2\text{ Hz}$, 3H, Pt- $\text{CH}_2\text{CH}(\text{CH}_3)$), 0.29 (br s, 3H, BH_3).

$^{11}\text{B}\{^1\text{H}\}$ NMR (128 MHz, CD_2Cl_2 , $0\text{ }^\circ\text{C}$) δ -6.7 ($\text{B}(\text{Ar}^{\text{F}})_4$), -23.9 (BH_3)

$[\text{Pt}(\text{i}^i\text{Pr}_2\text{Me}_2)'(\text{i}^i\text{Pr}_2\text{Me}_2)(\text{BH}_3\text{NH}_2^t\text{Bu})][\text{B}(\text{Ar}^F)_4]$ (16·TBAB)

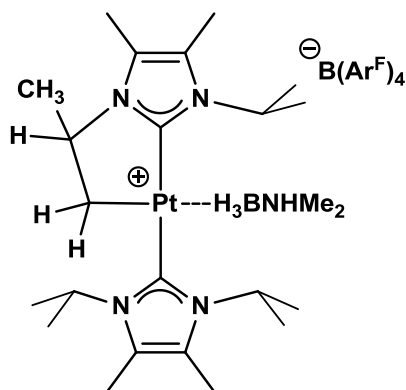


^1H NMR (500 MHz, CD_2Cl_2 , 0°C) δ 7.73 (m, 8H, *o*-H (Ar^F)), 7.57 (s, 4H, *p*-H (Ar^F)), 5.94, 5.60 and 4.84 (sept, $^3J_{\text{HH}} \sim 7$ Hz, 1H, $\text{CH}(\text{CH}_3)_2$), 4.05 (q+d, $^3J_{\text{HH}} = 6.3$ Hz, $^3J_{\text{PtH}} = 102$ Hz, 1H, Pt- CH_2CH), 3.17 (br s, 1H, NH), 3.07 (br s, 1H, NH), 2.43 (dd, $^3J_{\text{HH}} = 11.4$, 6.6 Hz, $^3J_{\text{PtH}} = 99$ Hz, 1H, CH_2 -Pt), 2.23, 2.20, 2.19 and 2.13 (s, 3H each, =C- CH_3), 1.68 (d+d, $^3J_{\text{HH}} = 11.3$ Hz, $^3J_{\text{PtH}} = 78$ Hz, 1H, CH_2 -Pt), 1.53, 1.50, 1.49, 1.44, 1.43 and 1.36 (d, $^3J_{\text{HH}} \sim 7$ Hz, 3H each, $\text{CH}(\text{CH}_3)_2$), 1.28 (d, $^3J_{\text{HH}} = 6.5$ Hz, 3H, Pt- $\text{CH}_2\text{CH}(\text{CH}_3)$), 1.17 (s, 9H, $\text{NH}_2\text{C}(\text{CH}_3)$), -0.16 (br s, 3H, BH_3).

$^{11}\text{B}\{^1\text{H}\}$ NMR (128 MHz, CD_2Cl_2 , 0°C) δ -6.7 ($\text{B}(\text{Ar}^F)_4$), -22.8 (BH_3)

$^{13}\text{C}\{^1\text{H}\}$ NMR (126 MHz, CD_2Cl_2 , 0°C) δ 172.2 ($\underline{\text{C}}=\text{Pt}$, $-(\text{i}^i\text{Pr}_2\text{Me}_2)$), 171.1 ($\underline{\text{C}}=\text{Pt}$, $-(\text{i}^i\text{Pr}_2\text{Me}_2')$), 162.1 (q, $J_{\text{CB}} = 49.8$ Hz, *ipso*-C (Ar^F)), 135.1 (*o*-C (Ar^F)), 129.2 (q, $J_{\text{CF}} = 32.2$ Hz, *m*-C (Ar^F)), 126.4 and 126.1 ($=\underline{\text{C}}-\text{CH}_3$), 124.9 (q, $J_{\text{CF}} = 272.2$ Hz, CF_3 (Ar^F)), 124.0 and 123.4 ($=\underline{\text{C}}-\text{CH}_3$), 117.9 (*p*-C (Ar^F)), 57.9 (Pt- $\text{CH}_2\underline{\text{C}}\text{H}$), 56.0 ($\text{NH}_2\underline{\text{C}}(\text{CH}_3)$), 53.6 and 53.0 ($\underline{\text{C}}\text{H}(\text{CH}_3)_2$ in a 2:1 ratio), 28.1 ($\text{NH}_2\underline{\text{C}}(\text{CH}_3)$), 25.6 (Pt- $\text{CH}_2\text{CH}(\underline{\text{C}}\text{H}_3)$), 22.5, 22.2 and 22.0 ($\text{CH}(\underline{\text{C}}\text{H}_3)_2$, 2:2:2 ratio) 14.2 ($\underline{\text{C}}\text{H}_2$ -Pt), 11.0, 10.6, 10.5 and 9.7 ($=\text{C}-\underline{\text{C}}\text{H}_3$).

[Pt(ⁱPr₂Me₂)'(ⁱPr₂Me₂)(BH₃NHMe₂)] [B(Ar^F)₄] (16-DMAB)

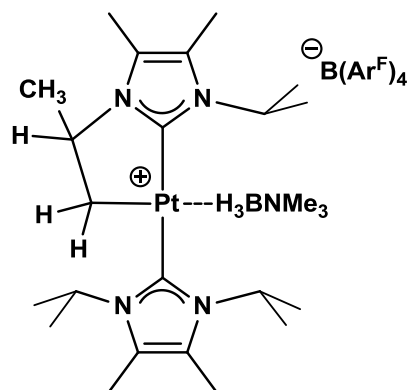


¹H NMR (500 MHz, CD₂Cl₂, 0 °C) δ 7.71 (m, 8H, *o*-H (Ar)^F), 7.56 (m, 4H, *p*-H (Ar)^F), 5.95, 5.65 and 4.82 (sept, ³J_{HH} ~ 7 Hz, 1H each, CH(CH₃)₂), 4.05 (q+d, ³J_{HH} = 6.3 Hz, ³J_{PtH} = 101 Hz, 1H, Pt-CH₂CH), 2.96 (s, 1H, NH), 2.52 (m, 6H, NH(CH₃)₂), 2.38 (m, 1H, CH₂-Pt), 2.20, 2.19, 2.17 and 2.12 (s, 3H, =C-CH₃), 1.57 (d, ³J_{HH} = 11.5 Hz, 1H, CH₂-Pt), 1.48 (d, ³J_{HH} = 7.2 Hz, 6H, CH(CH₃)₂), 1.46 (d, ³J_{HH} = 7.3 Hz, 3H, CH(CH₃)₂), 1.42 (d, ³J_{HH} = 7.0 Hz, 6H, CH(CH₃)₂), 1.35 (d, ³J_{HH} = 7.0 Hz, 3H, CH(CH₃)₂), 1.27 (d, ³J_{HH} = 6.3 Hz, 3H, Pt-CH₂CH(CH₃)), 0.13 (s, 1H, BH₃).

¹¹B{¹H} NMR (128 MHz, CD₂Cl₂, 0°C) δ -6.7 (B(Ar^F)₄), -15.8 (BH₃)

¹³C{¹H} NMR (126 MHz, CD₂Cl₂, 0°C) δ 170.9 (C=Pt, -(ⁱPr₂Me₂')), 170.0 (C=Pt, (ⁱPr₂Me₂)'), 162.1 (q, J_{CB} = 49.6 Hz, ipso-C (Ar)^F), 135.1 (*o*-C (Ar)^F), 129.2 (q, J_{CF} = 32.2 Hz, *m*-C (Ar)^F), 126.6, 126.5 and 126.4 (=C-CH₃), 124.9 (q, J_{CF} = 272.2 Hz, CF₃ (Ar)^F), 123.5 (=C-CH₃), 117.9 (*p*-C (Ar)^F), 57.8 (Pt-CH₂CH), 53.5, 53.4 and 52.8 (CH(CH₃)₂), 44.6 (NH(CH₃)₂), 25.6 (Pt-CH₂CH(CH₃)), 22.4, 22.3, 22.2, 22.1, 22.0 and 21.9 (CH(CH₃)₂), 14.6 (CH₂-Pt), 11.0, 10.7, 10.6 and 9.7 (=C-CH₃).

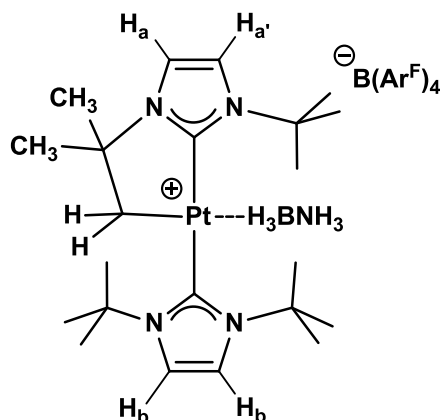
$[\text{Pt}(\text{i}^i\text{Pr}_2\text{Me}_2)'\text{(i}^i\text{Pr}_2\text{Me}_2)(\text{BH}_3\text{NMe}_3)]\text{B}(\text{Ar}^{\text{F}})_4$ (16·TMAB)



^1H NMR (500 MHz, CD_2Cl_2 , 0°C) δ 7.75 (s, 8H, *o*-H (Ar^{F}), 7.58 (s, 4H, *p*-H (Ar^{F}), 5.99, 5.64 and 5.25 (sept, $^3J_{\text{HH}} \sim 7$ Hz, 1H, $\underline{\text{CH}}(\text{CH}_3)_2$), 3.99 (q+d, $^3J_{\text{HH}} = 6.4$ Hz, $^3J_{\text{PtH}} = 106$ Hz, 1H, Pt- $\underline{\text{CH}_2\text{CH}}$), 2.52 (s, 9H, N($\underline{\text{CH}_3}$)₃), 2.44 (m, $^2J_{\text{PtH}} = 93$ Hz, 1H, $\underline{\text{CH}_2}$ -Pt), 2.20 (s, 6H, =C- $\underline{\text{CH}_3}$), 2.15 and 2.12 (s, 3H each, =C- $\underline{\text{CH}_3}$), 1.63 (d+d, $^3J_{\text{HH}} = 11.2$ Hz, $^2J_{\text{PtH}} = 78$ Hz, 1H, $\underline{\text{CH}_2}$ -Pt), 1.55, 1.50, 1.49, 1.46, 1.43 and 1.37 (d, $^3J_{\text{HH}} \sim 7.1$ Hz, 3H, CH($\underline{\text{CH}_3}$)₂), 1.32 (d, $^3J_{\text{HH}} = 6.3$ Hz, 3H, Pt- $\underline{\text{CH}_2\text{CH}}(\underline{\text{CH}_3}$)), -0.10 (s, 3H, $\underline{\text{BH}_3}$).

$^{11}\text{B}\{^1\text{H}\}$ NMR (128 MHz, CD_2Cl_2 , 0°C) δ -6.7 ($\text{B}(\text{Ar}^{\text{F}})_4$), -8.8 (BH_3).

$^{13}\text{C}\{^1\text{H}\}$ NMR (75 MHz, CD_2Cl_2 , 0°C) δ 172.9 ($\underline{\text{C}}=\text{Pt}$, -($\text{i}^i\text{Pr}_2\text{Me}_2$), 171.54 ($\underline{\text{C}}=\text{Pt}$, -($\text{i}^i\text{Pr}_2\text{Me}_2'$), 162.1 (q, $J_{\text{CB}} = 50$ Hz, *ipso*-C (Ar^{F}), 135.1 (*o*-C (Ar^{F}), 129.0 (q, $J_{\text{CF}} = 31.5$ Hz, *m*-C (Ar^{F}), 125.6 (=C- $\underline{\text{CH}_3}$, x2), 124.9 (q, $J_{\text{CF}} = 272.4$ Hz, CF_3 (Ar^{F}), 123.9 (=C- $\underline{\text{CH}_3}$), 123.1 (=C- $\underline{\text{CH}_3}$), 57.8 (s+d, $^3J_{\text{Cpt}} = 45.6$ Hz, Pt- $\underline{\text{CH}_2\text{CH}}$), 54.0 (N($\underline{\text{CH}_3}$)₃), 53.1, 52.9 and 52.8 ($\underline{\text{CH}}(\text{CH}_3)_2$), 25.4 (s+d, $^4J_{\text{Cpt}} = 21.3$ Hz, Pt- $\underline{\text{CH}_2\text{CH}}(\underline{\text{CH}_3}$)), 22.6, 22.5, 22.3, 22.1, 21.9 and 21.6 (CH($\underline{\text{CH}_3}$)₂), 13.4 ($\underline{\text{CH}_2}$ -Pt), 10.8, 10.3, 10.2 and 9.4 (=C- $\underline{\text{CH}_3}$).

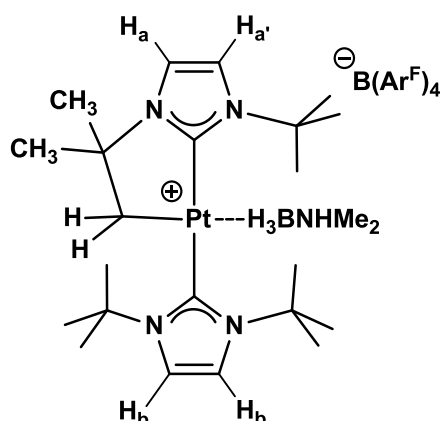
Amineborane adducts of complex **1****[Pt(BH₃NH₃)(I^tBu')(I^tBu)][B(Ar^F)₄] (1·AB)**

¹H NMR (500 MHz, CD₂Cl₂, 0 °C) δ 7.72 (m, 8H, *o*-H (Ar)^F), 7.56 (m, 4H, *p*-H (Ar)^F), 7.25 (s, 2H, =CH_b), 7.13 (d, ³J_{HH} = 2.3 Hz, 1H, =CH_a), 6.90 (d, ³J_{HH} = 2.3 Hz, 1H, =CH_{a'}), 3.39 (br s, 3H, NH₃), 2.55 (s, ²J_{PtH} = 97 Hz, 2H, CH₂-Pt), 1.93 (s, 18H, C(CH₃)₃, I^tBu), 1.68 (s, 9H, C(CH₃)₃, I^tBu'), 1.46 (s, 6H, C(CH₂)(CH₃)₂), 0.58 (br s, 3H, BH₃).

¹¹B{¹H} NMR (128 MHz, CD₂Cl₂, 0 °C) δ -6.7 (B(Ar^F)₄), -19.2 (br)

¹³C{¹H} NMR (101 MHz, CD₂Cl₂, 0 °C) δ 172.8 (C=Pt, I^tBu), 166.8 (C=Pt, I^tBu'), 162.1 (q, J_{CB} = 50 Hz, *ipso*-C (Ar)^F), 135.12 (*o*-C (Ar)^F), 129.14 (q, J_{CF} = 32 Hz, *m*-C (Ar)^F), 124.9 (q, J_{CF} = 272 Hz, CF₃ (Ar)^F), 119.2 (2 =CH_b), 118.26 (=CH_a), 117.9 (*p*-C (Ar)^F), 114.7 (=CH_{a'}), 64.6 (C(CH₂)(CH₃)₂), 59.9 (2 C(CH₃)₃, I^tBu), 57.9 (C(CH₃)₃, I^tBu'), 32.3 (C(CH₂)(CH₃)₂), 31.0 (C(CH₃)₃, I^tBu), 30.7 (C(CH₃)₃, I^tBu'), 21.0 (CH₂-Pt).

[Pt(BH₃NHMe₂)(^tBu')(^tBu)][B(Ar^F)₄] (1·DMAB)



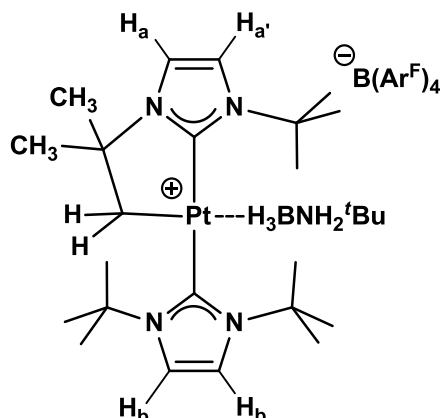
For 1:1 mixtures of **1** and DMAB in CD₂Cl₂, signals corresponding to DMAB were so broad they could not be discerned for temperatures in the range of -10 to 25 °C. This behavior was not observed in d₈-THF, which was then chosen as the solvent for the characterization of this adduct.

¹H{¹¹B} NMR (400 MHz, d₈-THF, -10 °C) δ 7.82 (m, 8H, *o*-H (Ar^F)), 7.62 (m, 4H, *p*-H (Ar^F)), 7.56 (s, 2H, =CH_b), 7.44 (s, 1H, =CH_a), 7.25 (s, 1H, =CH_{a'}), 5.04 (s, 1H, NH(CH₃)₂), 2.49 (d, ³J_{HH} = 5.5 Hz, 6H, NH(CH₃)₂), 2.38 (s+d, ²J_{PtH} = 93 Hz, 2H, CH₂-Pt), 1.98 (s, 18H, C(CH₃)₃, ^tBu), 1.75 (s, 9H, C(CH₃)₃, ^tBu'), 1.48 (s, 6H, C(CH₂)(CH₃)₂), 0.03 (s, 3H, BH₃).

¹¹B{¹H} NMR (128 MHz, d₈-THF, -10 °C) δ -6.7 (B(Ar^F)₄), -10.6 (br).

¹³C{¹H} NMR (101 MHz, d₈-THF, 0 °C) δ 173.4 (C=Pt, ^tBu), 167.7 (C=Pt, ^tBu'), 163.0 (q, J_{CB} = 50 Hz, *ipso*-C (Ar^F)), 135.7 (*o*-C (Ar^F)), 130.1 (q, J_{CF} = 32 Hz, *m*-C (Ar^F)), 125.6 (q, J_{CF} = 272 Hz, CF₃ (Ar^F)), 120.2 (2 =C_{Hb}), 119.5 (=C_{Ha}), 118.4 (*p*-C (Ar^F)), 116.1 (=C_{Ha'}), 65.8 (C(CH₂)(CH₃)₂), 60.1 (C(CH₃)₃, ^tBu), 58.7 (C(CH₃)₃, ^tBu'), 44.6 (NH(C_H)₂), 32.8 (C(C_H)₃, ^tBu), 31.5 (C(C_H)₃, ^tBu'), 30.4 (C(CH₂)(C_H)₂), 19.2 (C_H-Pt).

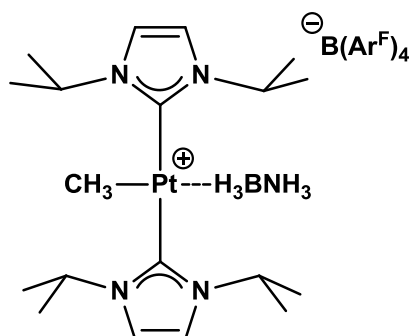
[Pt(BH₃NH₂^tBu)(^tBu')(^tBu)][B(Ar^F)₄] (1·TBAB)



¹H NMR (500 MHz, CD₂Cl₂, 0 °C) δ 7.72 (m, 8H, *o*-H (Ar)^F), 7.56 (m, 4H, *p*-H (Ar)^F), 7.29 (s, 2H, =CH_b), 7.11 (d, ³J_{HH} = 2.3 Hz, 1H, =CH_{a'}), 6.88 (d, ³J_{HH} = 2.3 Hz, 1H, =CH_a), 3.10 (br s, 2H, NH₂^tBu), 2.37 (s+d, ³J_{PtH} = 90 Hz, 2H, CH₂-Pt), 1.93 (s, 18H, C(CH₃)₃, ^tBu), 1.67 (s, 9H, (CH₃)₃, ^tBu'), 1.45 (s, 6H, C(CH₂)(CH₃)₂), 1.19 (s, 9H, NH₂C(CH₃)₃), 0.12 (br s, 3H, BH₃).

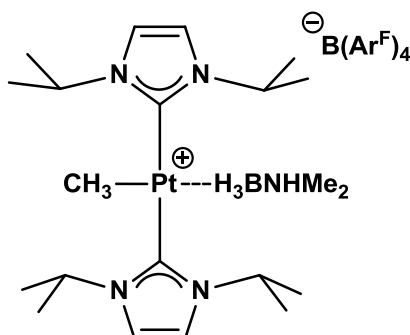
¹¹B{¹H} NMR (128 MHz, CD₂Cl₂, 0°C) δ -6.7 (B(Ar^F)₄), -18.2 (br).

¹³C{¹H} NMR (126 MHz, CD₂Cl₂, 0°C) δ 173.8 (C=Pt, ^tBu), 167.5 (C=Pt, ^tBu'), 162.1 (q, J_{CB} = 49.5 Hz, *ipso*-C (Ar)^F), 135.1 (*o*-C (Ar)^F), 129.1 (q, J_{CF} = 36.8, 32.4 Hz, *m*-C (Ar)^F), 124.9 (q, J_{CF} = 272.5 Hz, CF₃ (Ar)^F), 119.6 (=CH_b, x2), 118.3 (=CH_{a'}), 117.9 (*p*-C (Ar)^F), 114.7 (=CH_a), 64.7 (C(CH₂)(CH₃)₂), 60.2 (C(CH₃)₃, ^tBu), 58.1 (C(CH₃)₃, ^tBu'), 55.1 (NH₂C(CH₃)₃), 32.3 (C(CH₃)₃, ^tBu), 31.1 (C(CH₃)₃, ^tBu'), 30.6 (C(CH₂)(CH₃)₂), 28.2 (NH₂C(CH₃)₃), 20.7 (CH₂-Pt).

Amineborane adducts of complex **15****[PtCH₃(BH₃NH₃)(*i*Pr₂)₂][B(Ar^F)₄] (15·AB)**

¹H{¹¹B} NMR (400 MHz, d₈-THF, 0 °C) δ 7.81 (m, 8H, *o*-H (Ar^F)), 7.60 (m, 4H, *o*-H (Ar^F)), 7.37 (s, 4H, =CH), 5.51 (sept, ³J_{HH} = 6.8 Hz, 4H, CH(CH₃)₂), 4.61 (br s, 3H, NH₃), 1.48 (d, ³J_{HH} = 7.5 Hz, 12H, CH(CH₃)₂), 1.46 (d, ³J_{HH} = 7.5 Hz, 12H, CH(CH₃)₂), 0.20 (s+d, ²J_{PtH} = 90 Hz, 3H, CH₃-Pt), -0.09 (s+d, ²J_{PtH} = 117 Hz, 3H, BH₃).

¹¹B{¹H} NMR (128 MHz, d₈-THF, 0 °C) δ -6.7 (B(Ar^F)₄), -22.4 (br).

[PtCH₃(BH₃NHMe₂)(*i*Pr₂)₂][B(Ar^F)₄] (15·DMAB)

A mixture of 20 mg (0.014 mmol) of [Pt(CH₃)(*i*Pr₂)₂][B(Ar^F)₄] and 0.8 mg (0.014 mmol) of BH₃NHMe₂ is dissolved in 0.5 mL of d₈-THF cooled to -30 °C. NMR spectra was recorded at 0 °C. This product is unstable at higher temperatures evolving to unidentified species together with hydrogen.

¹H{¹¹B} NMR (400 MHz, d₈-THF, 0 °C) δ 7.81 (m, 8H, *o*-H (Ar^F)), 7.60 (m, 4H, *p*-H (Ar^F)), 7.38 (s, 4H, =CH), 5.99 (s, 1H, NH(CH₃)₂), 5.50 (sept, ³J_{HH} = 6.7 Hz, 4H,

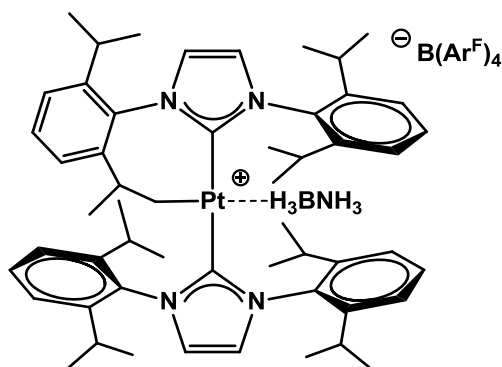
$\underline{\text{C}}\text{H}(\text{CH}_3)_2$, 2.22 (d, $^3J_{\text{HH}} = 5.5$ Hz, 6H, $\text{NH}(\underline{\text{C}}\text{H}_3)_2$), 1.51 and 1.46 (d, $^3J_{\text{HH}} = 6.8$ Hz, 12H each, $\text{CH}(\underline{\text{C}}\text{H}_3)_2$), 0.29 (s+d, $^2J_{\text{PtH}} = 90$ Hz, 3H, $\text{Pt}-\underline{\text{C}}\text{H}_3$), -0.37 (s+d, $^2J_{\text{PtH}} = 107$ Hz, 3H, $\text{B}\underline{\text{H}}_3$).

$^{11}\text{B}\{^1\text{H}\}$ NMR (128 MHz, d_8 -THF, 0 °C) δ -6.7 ($\text{B}(\text{Ar}^{\text{F}})_4$), -15.3 (br).

$^{13}\text{C}\{^1\text{H}\}$ NMR (101 MHz, d_8 -THF, 0 °C) δ 173.5 (Pt=C), 163.0 (q, $J_{\text{CB}} = 50$ Hz, *ipso*-C (Ar^{F}), 135.7 (*o*-C (Ar^{F}), 130.1 (q, $J_{\text{CF}} = 32$ Hz, *m*-C (Ar^{F}), 125.6 (q, $J_{\text{CF}} = 272$ Hz, CF_3 (Ar^{F}), 118.4 (*p*-C (Ar^{F}), 118.2 (=CH), 52.9 ($^3J_{\text{PtH}} = 42$ Hz, $\underline{\text{C}}\text{H}(\text{CH}_3)_2$), 43.9 ($\text{NH}(\underline{\text{C}}\text{H}_3)_2$), 23.6 and 23.0 ($\text{CH}(\underline{\text{C}}\text{H}_3)_2$), -22.5 (Pt- $\underline{\text{C}}\text{H}_3$).

Amineborane adducts of complex 2b

[Pt(BH₃NH₃)(IPr')(IPr)][B(Ar^F)₄] (2b-AB)



Due to the complexity of the system and extensive signal overlap, not all signals could be assigned.

^1H NMR (400 MHz, d_8 -THF, -10 °C) δ 7.82 (m, 8H, *o*-H (Ar^{F}), 7.62 (m, 4H, *p*-H (Ar^{F}), 7.57-7.26 (m, 12H, 8H Ph + 4 =CH), 7.12 (m, 2H, Ph), 6.84 (d, $^3J_{\text{HH}} = 7.7$ Hz, 1H, Ph), 6.37 (d, $^3J_{\text{HH}} = 7.4$ Hz, 1H, Ph), 4.31 (s, br, 3H, NH_3), 3.09 (m, 2H, $\underline{\text{C}}\text{H}(\text{CH}_3)_2$), 2.91 (sept, $^3J_{\text{HH}} = 6.9$ Hz, 1H, $\underline{\text{C}}\text{H}(\text{CH}_3)_2$), 2.78 (m, 1H, $\underline{\text{C}}\text{H}(\text{CH}_3)_2$), 2.68 (m, 1H, $\underline{\text{C}}\text{H}(\text{CH}_3)_2$), 2.23 (sept, $^3J_{\text{HH}} = 6.5$ Hz, 1H, $\underline{\text{C}}\text{H}(\text{CH}_3)_2$), 2.03 (sept, $^3J_{\text{HH}} = 6.9$ Hz, 1H, $\underline{\text{C}}\text{H}(\text{CH}_3)_2$), 1.92 (m, 1H, $\underline{\text{C}}\text{HCH}_2\text{-Pt}$), 1.70 (m, 2H, $\text{CH}_2\text{-Pt}$), 1.40, 1.37, 1.29, 1.22, 1.13, 1.03, 0.97, 0.93, 0.86, 0.79 and 0.67 (d, $^3J_{\text{HH}} \sim 6.5$ Hz, $\text{CH}(\underline{\text{C}}\text{H}_3)_2$ in a 3:3:6:3:6:3:3:3:6:6 ratio), -0.45 (s, 3H, BH_3).

$^{13}\text{C}\{^1\text{H}\}$ NMR (400 MHz, d_8 -THF, $-10\text{ }^\circ\text{C}$) δ 175.3 (Pt=C), 174.5 (Pt=C'), 163.0 (q, $J_{CB} = 50\text{ Hz}$, *ipso*-C (Ar)^F), 147.2, 147.1, 146.7, 146.2, 145.7, 145.5, 145.1, 141.9, 137.5, 137.3, 136.1 and 136.0 (12 C_q Ph), 135.7 (*o*-C (Ar)^F), 130.1 (q, $J_{CF} = 32\text{ Hz}$, *m*-C (Ar)^F), 131.0–129.5, 127.1 and 126.0–124.4 (16 CH, Ph + =CH), 125.6 (q, $J_{CF} = 272\text{ Hz}$, CF₃ (Ar)^F), 118.4 (*p*-C (Ar)^F), 39.5 (CHCH₂–Pt), 31.0, 29.7, 29.6, 29.5, 29.2 and 28.9, 28.7 (7 CH(CH₃)₂), 27.4, 27.0, 26.9, 26.6, 26.3, 26.0, 25.9, 25.8, 25.6, 24.1, 23.6, 23.3, 23.2, 23.1 and 22.7 (15 CH(CH₃)₂), 18.09 (CH₂–Pt).

Amineborane adducts of complex **3b**

[Pt(BH₃NH₃)(IMes*')(IMes*')][B(Ar^F)₄] (3b**·AB)**

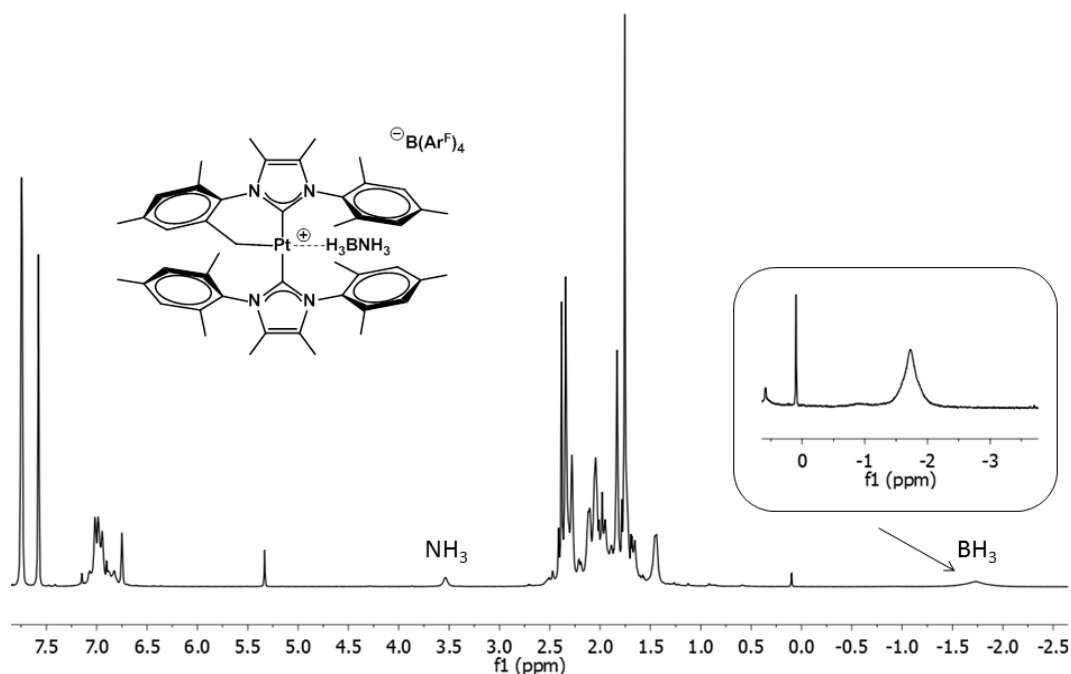
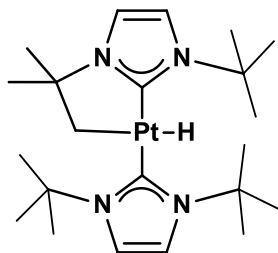


Figure 1. $^1\text{H}\{^{11}\text{B}\}$ NMR in CD_2Cl_2 of $[\text{Pt}(\text{BH}_3\text{NH}_3)(\text{IMes}^{\ast\prime})(\text{IMes}^{\ast\prime})][\text{B}(\text{Ar}^{\text{F}})_4]$. Due to signal overlap and rapid evolution to the reaction products, it was very difficult to assign individual peaks for **3b**·AB. However, the coordinated BH_3 signal was clearly seen, as marked in the figure inset

- Neutral hydrides

[PtH(^tBu')(^tBu)] (30)



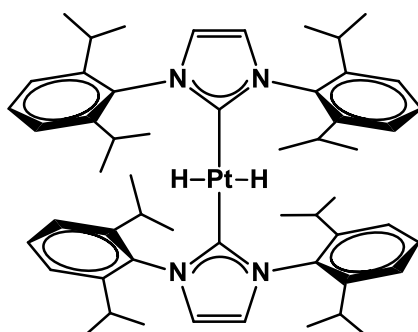
A mixture of 100 mg (0.070 mmol) of [Pt(^tBu')(^tBu)][B(Ar^F)₄] and 5 mg (0.208 mmol) of NaH was dissolved in 2 mL of dry THF at r.t.. After stirring for 30 min at room temperature, the initially yellow solution turned colorless. Solvent is removed in vacuo and the solid is extracted with pentane (3 x 2 mL). Evaporation of the pentane solution yields 36 mg (0.065 mmol, 93% yield) of a white solid.

¹H NMR (400 MHz, C₆D₆, 25 °C) δ 6.73 (s, ⁴J_{PtH} = 9.4 Hz, 2H, =CH), 6.61 (d, ³J_{HH} = 2.1 Hz, 1H, =CH), 6.48 (d, ³J_{HH} = 2.1 Hz, 1H, =CH), 2.12 (d, ³J_{HH} = 2.8 Hz, ²J_{PtH} = 49.6 Hz, 2H, Pt-CH₂), 1.93 (s, 9H, C(CH₃)₃, ^tBu'), 1.92 (s, 18H, C(CH₃)₃, ^tBu), 1.60 (s, 6H, C(CH₂)(CH₃)₂), -4.89 (t, ³J_{HH} = 2.8 Hz, ¹J_{PtH} = 894 Hz, 1H, Pt-H).

¹³C{¹H} NMR (101 MHz, C₆D₆, 25 °C) δ 179.2 (C=Pt (^tBu), ¹J_{PtC} = 1020 Hz), 172.5 (C=Pt (^tBu'), ¹J_{PtC} = 1036 Hz), 116.1 (³J_{PtC} = 30 Hz, =CH (^tBu')), 115.4 (³J_{PtC} = 39 Hz, =CH (^tBu)), 115.0 (³J_{PtC} = 47 Hz, C=H (^tBu')), 65.4 (²J_{PtC} = 17 Hz, C(CH₃)₂CH₂), 58.3 (²J_{PtC} = 12 Hz, C(CH₃)₃), 58.2 (C(CH₃)₃), 36.3 (¹J_{PtC} = 451 Hz, Pt-CH₂), 33.6 (³J_{PtC} = 18 Hz, C(CH₃)₂CH₂), 31.0 (³J_{PtC} = 18 Hz, C(CH₃)₃, (^tBu)), 30.9 (³J_{PtC} = 22 Hz, C(CH₃)₃, (^tBu')).

IR (Nujol): ν(Pt-H) 1925 cm⁻¹.

Elemental analysis: Found: C 47.4, H 7.2, N 10.0; Calculated: C 47.55, H 7.26, N 10.08

PtH₂(IPr)₂ (35)**Synthesis:**

30 mg (0.025 mmol) of [PtH(IPr)₂][SbF₆] were dissolved in 2 mL of dry THF and 6 mg (0.250 mmol) of NaH were added at room temperature. The solution is heated at 50 °C for 3 hours and a 1:1 equilibrium mixture of the starting material and the desired dihydride is formed. Further heating or addition of more NaH do not alter this ratio. The solvent is removed in vacuo and the residue is extracted with pentane (3x2mL) to yield 11 mg (0.011 mmol, 45% yield) of **35**.

Spectroscopic and analytical data

White solid

Molecular weight: 974.3

¹H NMR (400 MHz, d₈-THF) δ 7.20 (t, ³J_{HH} = 7.7 Hz, 4H, *p*-H Ph), 6.96 (d, ³J_{HH} = 7.7 Hz, 8H, *m*-H Ph), 6.83 (s+d, ³J_{PtH} = 6 Hz, 4H, =CH), 2.76 (sept, ³J_{HH} = 7.0 Hz, 4H, CH(CH₃)₂), 0.94 (d, ³J_{HH} = 6.9 Hz, 24H, CH(CH₃)₂), 0.88 (d, ³J_{HH} = 6.8 Hz, 24H, CH(CH₃)₂), -3.53 (s+d, ¹J_{PtH} = 887 Hz, 1H, Pt-H).

¹³C{¹H} NMR (101 MHz, d₈-THF) δ 184.9 (s+d, ¹J_{PtC} = 1023 Hz, C=Pt), 147.0 (*o*-CH Ph), 139.3 (C_{ipso} Ph), 129.2 (*p*-CH Ph), 124.1 (*m*-CH Ph), 123.2 (s+d, ³J_{PtC} = 34 Hz, =CH), 29.3 (s+d, J_{PtC} = 8 Hz, CH(CH₃)₂), 25.0 (CH(CH₃)₂), 24.8 (s+d, J_{PtC} = 8 Hz, CH(CH₃)₂).

HRMS: Calculated: 973.5561; Found: 973.5563

- Boronium cations

[BH₂(NHMe₂)₂][B(Ar^F)₄] (31·NHMe₂)

40 mg of BH₂(NHMe₂)₂Cl³ (0.288 mmol) and 256 mg of NaBAr^F (0.288 mmol) are dissolved in 3 mL of dry THF. After stirring at room temperature for 10 minutes, a white precipitate formed. The solution is filtered to remove the NaCl and THF is removed in vacuo to yield 225 mg (0.233 mmol, 81% yield) of a white solid.

¹H{¹¹B} NMR (400 MHz, d₈-THF) δ 7.79 (m, 8H, *o*-H (Ar^F)), 7.58 (m, 4H, *p*-H (Ar^F)), 6.44 (br s, 2H, NHMe₂), 2.57 (s, 12H, NHMe₂), 1.87 (s, 2H, BH₂).

¹¹B NMR (128 MHz, d₈-THF) δ -2.8 (t, ¹J_{BH} = 113 Hz, BH₂), -6.7 (s, BA^F).

¹³C{¹H} NMR (101 MHz, d₈-THF) δ 163.1 (q, J_{CB} = 50 Hz, *ipso*-C (Ar^F)), 135.8 (*o*-C (Ar^F)), 130.2 (q, J_{CF} = 32 Hz, *m*-C (Ar^F)), 125.7 (q, J_{CF} = 272 Hz, CF₃ (Ar^F)), 118.3 (*p*-C (Ar^F)), 41.3 (NHMe₂).

HRMS: Calculated: 103.1407; Found: 103.1406.

Other boronium cations:

Synthesis:

Standard procedure exemplified by the synthesis of [BH₂NH₃(THF)][B(C₆F₅)₄]: a solid mixture of 1 mg (0.032 mmol) of BH₃NH₃ and 30 mg (0.032 mmol) of [Ph₃C][B(C₆F₅)₄] are placed in an NMR tube under argon and 0.5 mL of dry d₈-THF are added at 0 °C. The initial yellow solution turns to colorless as it is brought to

³ BH₂(NHMe₂)₂Cl was prepared as described by Kodama (Kodama, G., Inoue, M.; *Inorg. Chem.* **1968**, *7*, 430) from reaction of BH₃NHMe₂ with HCl in diethyl ether and then further reaction with another equivalent of amine, which results in the precipitation of BH₂(NHMe₂)₂Cl as white solid that is washed with ether and dried under vacuum.

BH₂(NHMe₂)₂Cl: ¹H{¹¹B} NMR (400 MHz, CD₂Cl₂) δ 7.75 (s, 2H, NHMe₂), 2.58 (d, ³J_{HH} = 5.4 Hz, 12H, NHMe₂), 1.91 (s, 2H, BH₂); ¹¹B NMR (85.5 MHz, CD₂Cl₂) δ -1.11 (t, ¹J_{BH} = 109.1 Hz).

room temperature. The THF stabilized boronium cation is formed in quantitative yields, but attempts to isolate it led to decomposition.

${}^+BH_2(NH_3)_2$ had been previously prepared⁴ by a different method to that we used for the synthesis of $[BH_2(NHMe_2)_2][B(Ar^F)_4]$ so we did not try to isolate it. In our hands, it always formed in significant amounts when excess AB was present in reactions with $[Ph_3C][B(C_6F_5)_4]$ and hydride (**30**).

${}^+BH_2(NH_3)(THF)$: ${}^1H\{{}^{11}B\}$ NMR (400 MHz, d_8 -THF) δ 5.68 (NH₃), 2.68 (BH₃); ${}^{11}B$ NMR (128 MHz, d_8 -THF) δ 0.3 (t, ${}^1J_{BH} = 120$ Hz).

${}^+BH_2(NH_3)_2$: ${}^1H\{{}^{11}B\}$ NMR (400 MHz, d_8 -THF) δ 5.14 (NH₃), 2.17 (BH₃); ${}^{11}B$ NMR (128 MHz, d_8 -THF) δ -13.6 (t, ${}^1J_{BH} = 108$ Hz).

${}^+BH_2(NHMe_2)(THF)$: ${}^1H\{{}^{11}B\}$ NMR (400 MHz, d_8 -THF) δ 6.53 (s, 2H, NHMe₂), 2.58 (d, ${}^3J_{HH} = 5.4$ Hz, 6H, NHMe₂), 2.37 (s, 2H, BH₂); ${}^{11}B$ NMR (128 MHz, d_8 -THF) δ 4.62 (t, ${}^1J_{BH} = 123$ Hz).

${}^+BH_2(NH^iPr_2)(THF)$: ${}^1H\{{}^{11}B\}$ NMR (400 MHz, d_8 -THF) δ 5.11 (s, 1H, NH), 3.50 (m, 2H, CH(CH₃)₂), 2.76 (BH₃), 1.36 (d, ${}^3J_{HH} = 6.7$ Hz, 6H, CH(CH₃)₂), 1.29 (d, ${}^3J_{HH} = 6.7$ Hz, 6H, CH(CH₃)₂); ${}^{11}B$ NMR (128 MHz, d_8 -THF) δ 2.5 (t, br).

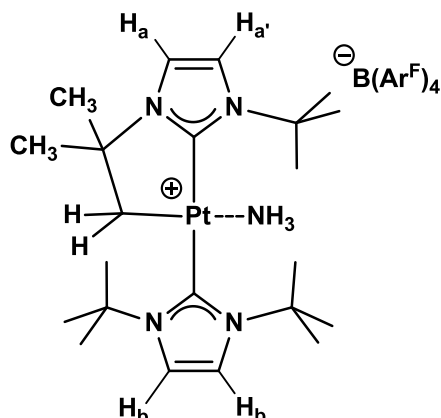
- Amine adducts:

Synthesis:

These species were prepared from the corresponding unsaturated complexes **1**, and **32** by addition of amine to the THF solutions of the metal complexes. NH₃ was bubbled in (**1**·NH₃ and **32**·NH₃) or NHMe₂ was added as a 2.0 M solution in THF (**32**·NHMe₂). Solvent removal resulted in amine evaporation, yielding the starting species. Therefore these species were characterized *in situ*.

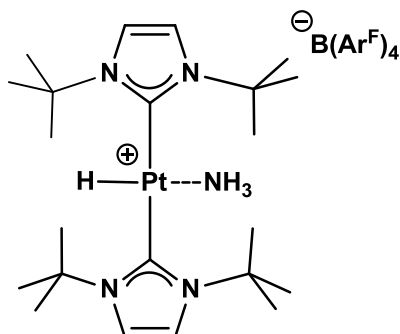
⁴ a) Preparation: Kodama, G.; Parry, R. W. *J. Am. Chem. Soc.* **1960**, *82*, 6250; b) NMR data: Heitsch, C. W. *Inorg. Chem.* **1965**, *4*, 1019.

[Pt(NH₃)(^tBu')(^tBu)][B(Ar^F)₄] (1·NH₃)

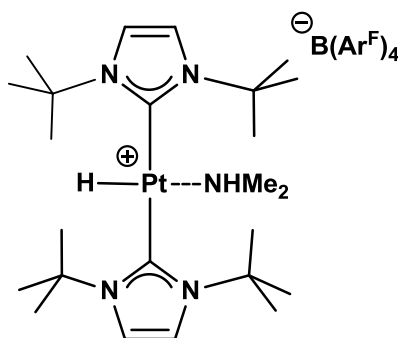


¹H NMR (300 MHz, d₈-THF) δ 7.78 (m, 8H, *o*-H (Ar^F)), 7.56 (m, 4H, *p*-H (Ar^F)), 7.51 (s, 2H, =CH_b), 7.32 (d, ³J_{HH} = 2.3 Hz, 1H, =CH_a), 7.14 (d, ³J_{HH} = 2.2 Hz, 1H, =CH_{a'}), 2.75 (s, br, 3H, NH₃), 1.95 (s, 18H, C(CH₃)₃, ^tBu), 1.87 (s, 2H, CH₂-Pt), 1.73 (s, 9H, C(CH₃)₃, ^tBu'), 1.47 (s, 6H, C(CH₂)(CH₃)₂).

[PtH(NH₃)(^tBu)₂][B(Ar^F)₄] (19·NH₃)



¹H NMR (300 MHz, d₈-THF) δ 7.78 (m, 8H, *o*-H (Ar^F)), 7.57 (m, 4H, *p*-H (Ar^F)), 7.43 (s, 4H, =CH), 2.56 (s, br, 3H, NH₃), 2.00 (s, 36H, C(CH₃)₃), -20.25 (s+d, ¹J_{PtH} = 1408 Hz, 1H, Pt-H).

[Pt(NHMe₂)(^tBu)₂][B(Ar^F)₄] (19· NHMe₂)

¹H NMR (400 MHz, CD₂Cl₂) δ 7.72 (m, 8H, *o*-H (Ar^F)), 7.56 (m, 4H, *p*-H (Ar^F)), 7.22 (s, 4H, =CH), 2.36 (br s, 6H, NH(CH₃)₂), 1.96 (s, 36H, C(CH₃)₃), -21.03 (s+d, ¹J_{PtH} = 1497 Hz, 1H, Pt-H). NH(CH₃)₂ not observed.

¹³C NMR (101 MHz, CD₂Cl₂) δ 164.2 (C=Pt), 162.3 (q, J_{CB} = 49.5 Hz, *ipso*-C (Ar^F)), 135.37 (*o*-C (Ar^F)), 129.5 (q, J_{CF} = 32.2 Hz, *m*-C (Ar^F)), 125.2 (q, J_{CF} = 272.5 Hz, CF₃ (Ar^F)), 118.3 (=CH), 118.0 (*o*-C (Ar^F)), 59.6 (C(CH₃)₃), 31.93 (C(CH₃)₃).

Synthesis of diaminoboranes:

In a typical procedure 20 mg (0.014 mmol) of complex **1** was dissolved in 2 mL of dry THF and 3 equivalents of amine (0.042 mmol) were added. 1 equivalent (0.014 mmol) of the corresponding amineborane BH₃·NHRR' was dissolved in 0.5 mL of dry THF and added to the solution of the catalyst. The reaction was stirred at room temperature until gas evolution had ceased and the color of the solution had turned to pale yellow, indicating amineborane consumption (reaction times fluctuate between a few seconds for amineborane BH₃·NH(*p*-tol)₂ to 15 min for amineborane BH₃·NHEt₂). Spectroscopic yields are in all cases quantitative. Due to the low boiling point of most diaminoboranes their isolation required first trap-to-trap (cooled with liquid nitrogen) evaporation of the volatiles (THF, diaminoborane and excess of amine) followed by THF and amine evaporation at -30 °C. Under these conditions most of the diaminoborane remained as a colourless liquid in the trap.

BH(NMe₂)₂: ¹¹B NMR (128 MHz, d₈-THF) δ 28.7 (d, ¹J_{BH} = 130 Hz).

BH(NEt₂)₂: ¹¹B NMR (96 MHz, d₈-THF) δ 28.5 (d, ¹J_{BH} = 128 Hz).

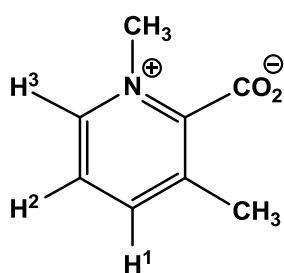
BH(NH(*p*-Tol))₂: ¹¹B NMR (96 MHz, d₈-THF) δ 26.1 (d, ¹J_{BH} = 134 Hz).

BH(NH^tBu)₂: ¹¹B NMR (96 MHz, d₈-THF) δ 25.5 (d, ¹J_{BH} = 125 Hz).

EXPERIMENTAL PART. CHAPTER 3

Betaine **37a** prepared as reported by Quast and Schmitt.¹ Betaines **37c** and **37d** have been previously reported by Katritzky² along with betaine **37h**.³ Preparation of betaines **37k** and **37l** was reported by Haake and Mantecón.⁴ Later reports include spectroscopic data for **37k**⁵ and **37l**.¹ In this case, both betaines were prepared by the procedure reported by Quast and Schmitt. In the multi-step synthesis of betaine **37m**, the first step to prepare bis(3,5-dimethyl)phenyl amine followed the report by Hartwig⁶ and subsequent steps up to 1,3,6,8-tetramethylacridine-9-carboxylic acid have been reported by Razavi.⁷ Preparation of betaines not previously reported is detailed below.

1,3-dimethyl-2-carboxypyridine (37b)



Synthesis

400 mg (3.6 mmol) of Na₂CO₃ are added to a solution of 1g (7.3 mmol) of 3-methylpyridine-2-carboxylic acid in 5 mL of methanol. The mixture is stirred at room temperature for 1.5 hours to yield a colorless solution that is then cooled to

¹ Quast, H.; Schmitt, E. *Justus Liebigs Ann. Chem.*, **1970**, 732, 64

² Katritzky, A. R.; Awartani, R.; Patel, R. C.; *J. Org. Chem.*, **1982**, 47, 498

³ Katritzky, A. R.; Faid-Allah, H. M. *Synthesis*, **1983**, 2, 149

⁴ Haake, P.; Mantecón, J. *J. Am. Chem. Soc.*, **1964**, 86, 5230

⁵ Jahn, T.; König, G. M.; Wright, A. D. *Tetrahedron Lett.*, **1997**, 38, 3883

⁶ Tzschucke, C. C.; Murphy, J. M.; Hartwig, J. F. *Organic Letters*, **2007**, 9, 761

⁷ Razavi, Z.; McCapra, F.; *Luminescence*, **2000**, 15, 245

-60 °C and treated with 880 μ L (7.3 mmol) of methyl triflate. After 30 minutes the solution is brought to room temperature and the solvent is removed *in vacuo*. The resulting white solid, which contains sodium triflate, is charged on a 10x2 cm silica gel column, the salt being eluted with acetone (100 mL) and the carboxypyridine **1b** with a CH_2Cl_2 /methanol 1:1 mixture. Solvent is removed *in vacuo* to yield 930 mg (84% yield) of a white highly hygroscopic solid. This compound is dissolved in the minimum amount of methanol and dried with activated molecular sieves for a period of two days to remove all traces of water. The solvent is then removed *in vacuo* and the white solid stored in a glove-box.

Spectroscopic and analytical data

White solid

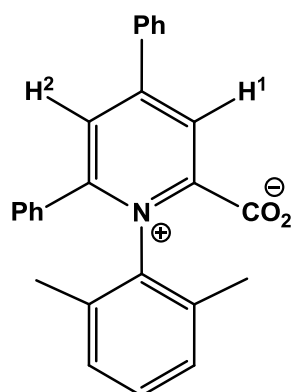
Molecular weight: 151.2

IR (nujol): ν (CO_2) 1640 cm^{-1} .

^1H NMR (400 MHz, d_6 -dmsO, 25 °C): δ 8.55 (d, 1H, $^3J_{\text{HH}} = 6.2$ Hz, H^3), 8.28 (d, 1H, $^3J_{\text{HH}} = 7.7$ Hz, H^1), 7.72 (dd, 1H, $^3J_{\text{HH}} = 7.7$ and 6.2 Hz, H^2), 4.16 (s, 3H, N- CH_3), 2.37 (s, 3H, C- CH_3).

$^{13}\text{C}\{^1\text{H}\}$ NMR (100 MHz, d_6 -dmsO, 25 °C): δ 161.5 (CO_2), 155.9 (CO_2 - $\underline{\text{C}}$), 145.5 (CH^2), 141.1 (CH^3), 132.7 (CH^1), 123.6 ($\underline{\text{C}}$ - CH_3), 45.5 (N- CH_3), 17.6 (C- $\underline{\text{C}}$ H_3).

Anal. Calcd. for $\text{C}_8\text{H}_9\text{NO}_2$: C, 63.56; H, 6.00; N, 9.27. **Found:** C, 63.2; H, 5.9; N, 9.3.

N-xylol-4,6-diphenyl-pyridinium-2-carboxylate (37e)*Synthesis:*

N-xylol-2-ethoxycarbonyl-4,6-diphenyl-pyridinium tetrafluoroborate is prepared *in situ* from a solution of 500 mg (1.27 mmol) of 2-ethoxycarbonyl-4,6-diphenyl-pyridinium tetrafluoroborate in 15 mL of dichloromethane to which 173 μ L of 2,6-dimethylaniline are added dropwise. After stirring at room temperature for 4h the yellow solution is concentrated, cooled to $-60\text{ }^{\circ}\text{C}$ and dropwise addition of 20 mL of diethyl ether leads to the precipitation of a pale yellow solid. The solvent is filtered off, the solid is dried *in vacuo* and then suspended in 3.8 mL (1.9 mmol) of a 0.5M NaOH aqueous solution. After stirring at room temperature overnight an off-white suspension is formed. The water is filtered off and the resulting white solid is washed with water (2x5 mL) and ether (2x3 mL) and dried to yield 360 mg (0.95 mmol, 73% yield) of **37e**.

Spectroscopic data

Off-white solid

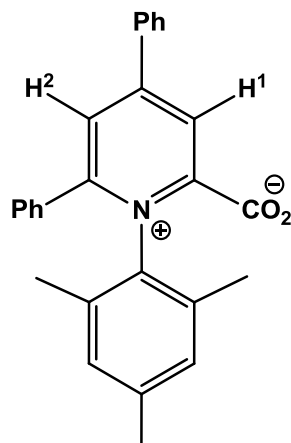
Molecular weight: 379.4

IR (nujol): ν 1656, 1616 cm^{-1} (CO_2)

^1H NMR (500 MHz, CDCl_3 , $25\text{ }^{\circ}\text{C}$) δ 8.38 (d, $^4J_{\text{HH}} = 2.4\text{ Hz}$, 1H, H^1), 7.98 (d, $^4J_{\text{HH}} = 2.4\text{ Hz}$, 1H, H^2), 7.91 (d, $^3J_{\text{HH}} = 7.1\text{ Hz}$, 2H, Ph), 7.63 (m, 3H, Ph), 7.42 (t, $^3J_{\text{HH}} = 7.5\text{ Hz}$, 1H, Ph), 7.32 (t, $^3J_{\text{HH}} = 7.6\text{ Hz}$, 2H, Ph), 7.22 (d, $^3J_{\text{HH}} = 7.6\text{ Hz}$, 2H, Ph), 7.18 (d, $^3J_{\text{HH}} = 7.6\text{ Hz}$, 1H, *p*-H, Xyl), 7.02 (d, $^3J_{\text{HH}} = 7.5\text{ Hz}$, 2H, *m*-H, Xyl), 2.18 (s, 6H, CH_3).

$^{13}\text{C}\{^1\text{H}\}$ NMR (101 MHz, CDCl_3 , 25 °C) δ 162.0 ($\text{C}-\text{CO}_2^-$), 159.4 ($\text{C}-\text{CO}_2^-$), 157.2 (C_q -pyr), 153.2 (C_q -pyr), 138.1 (N-C-Xyl), 134.5 (CH-Ph), 134.1 (C_q -Xyl), 131.9 (C_q -Ph), 130.9 (CH-Ph), 130.6 (*p*-CH-Xyl), 130.0 (CH-Ph), 129.2 (C_q -Ph), 128.8 (*m*-CH-Xyl), 128.6 (CH-Ph, x2), 127.8 (CH-Ph), 123.79 (CH^2), 121.86 (CH^1), 18.64 (CH_3 , Xyl).

N-mesityl-4,6-diphenyl-pyridinium-2-carboxylate (**37f**)



Synthesis:

Preparation of **37f** is analogous to **37e**. 2,4,6-trimethyl aniline was used to prepare the corresponding pyridinium cation. For 1 g (2.55 mmol) of pyridinium cation, 782 mg (1.99 mmol, 78% yield) of **37f** were obtained.

Spectroscopic data

Off-white solid

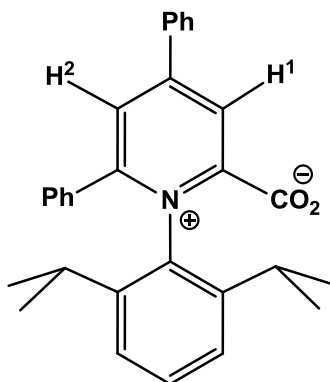
Molecular weight: 393.2

IR (nujol): ν 1652, 1615 cm^{-1} (CO_2)

^1H NMR (400 MHz, CDCl_3 , 25 °C) δ 8.28 (d, $^4J_{\text{HH}} = 2.3$ Hz, 1H, H^1), 7.88 (d, $^4J_{\text{HH}} = 2.3$ Hz, 1H, H^2), 7.86 (m, 2H, Ph), 7.62 (m, 3H, Ph), 7.42 (t, $^3J_{\text{HH}} = 7.4$ Hz, 1H, Ph), 7.33 (m, 2H, Ph), 7.25 – 7.19 (m, 2H, Ph), 6.82 (s, 2H, *m*-H, Mes), 2.22 (s, 3H, *p*- CH_3), 2.14 (s, 6H, *o*- CH_3).

$^{13}\text{C}\{^1\text{H}\}$ NMR (125 MHz, CDCl_3 , 25 °C) δ 162.1 ($\text{C}-\text{CO}_2^-$), 159.7 ($\text{C}-\text{CO}_2^-$), 157.0 (C_q -pyr), 153.4 (C_q -pyr), 140.6 (C_q -Mes), 135.6 (N-C-Mes), 134.2 (C_{ipso} -Ph), 134.1 (C_o -Mes), 132.3 (CH-Ph), 132.1 (C_{ipso} -Ph), 130.9 (CH-Ph), 130.0 (CH-Ph), 129.6 (CH-Mes), 128.7 (CH-Ph), 128.6 (CH-Ph), 127.8 (CH-Ph), 123.7 (CH^2), 121.8 (CH^1), 21.2 (p - CH_3 , Mes), 18.6 (o - CH_3 , Mes).

N-(2,6'-diisopropylphenyl)-4,6-diphenyl-pyridinium-2-carboxylate (37g)



Synthesis:

Preparation of **37g** is analogous to **37e**. 2,6-diisopropyl aniline was used to prepare the corresponding pyridinium cation. Reaction times were longer in this case: 12h for the preparation of the etoxycarbonyl derivative and two days for the decarboxylation step. For 1 g (2.55 mmol) of pyrilium cation, 677 mg (1.55 mmol, 61% yield) of **37g** were obtained.

Spectroscopic data

Off-white solid

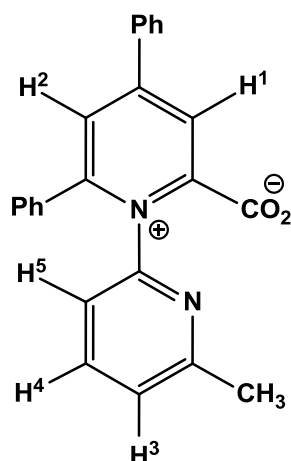
Molecular weight: 435.5

IR (nujol): ν 1652, 1615 cm^{-1} (CO_2)

^1H NMR (500 MHz, CDCl_3 , 25 °C) δ 8.57 (s, 1H, H^1), 8.01 (s, 1H, H^2), 7.95 (d, $^3J_{\text{HH}} = 6.7$ Hz, 2H, Ph), 7.66 (m, 3H, Ph), 7.47 (m, 1H, p -H, diip), 7.33 (m, 3H, Ph), 7.21 (d, $^3J_{\text{HH}} = 7.7$ Hz, 2H, o -H, diip), 7.14 (d, $^3J_{\text{HH}} = 7.9$ Hz, 2H, Ph), 2.46 (sept, $^3J_{\text{HH}} = 6.7$ Hz, 2H), 1.40 (d, $^3J_{\text{HH}} = 6.5$ Hz, 6H), 0.79 (d, $^3J_{\text{HH}} = 6.6$ Hz, 6H)

$^{13}\text{C}\{^1\text{H}\}$ NMR (101 MHz, CDCl_3 , 25 °C) δ 161.1 ($\text{C}-\underline{\text{C}}\text{O}_2^-$), 160.1 ($\underline{\text{C}}-\text{CO}_2^-$), 156.8 (C_q -pyr), 154.0 (C_q -pyr), 144.2 (C_o -diip), 135.5 (N-C-diip), 132.5 (CH, Ph), 131.6 (CH_p diip), 131.2 (C_q -Ph), 130.4, 129.8 and 129.4 (CH, Ph in a 2:2:1 ratio), 128.9 (C_q -Ph), 128.6 and 127.7 (CH, Ph in a 2:2 ratio), 124.9 (CH_m diip), 124.3 (CH^2), 123.3 (CH_1), 29.3 ($\underline{\text{C}}\text{H}(\text{CH}_3)_2$), 24.6 and 23.6 ($\text{CH}(\underline{\text{C}}\text{H}_3)_2$).

6'-methyl-4,6-diphenyl-[1,2'-bipyridinium]-2-carboxylate (37i)



Synthesis:

Preparation of **37i** is analogous to **37e**. 2-amino-6-methyl pyridine was used to prepare the corresponding pyridinium cation. The decarboxylation step in this case was complete in 5h. This product was partly soluble in water, so after decarboxylation the aqueous solution was evaporated and the crude extracted in dichloromethane. For 800 mg (2.04 mmol) of pyridinium cation, 677 mg (1.23 mmol, 60% yield) of **37i** were obtained.

Spectroscopic data

Off-white solid

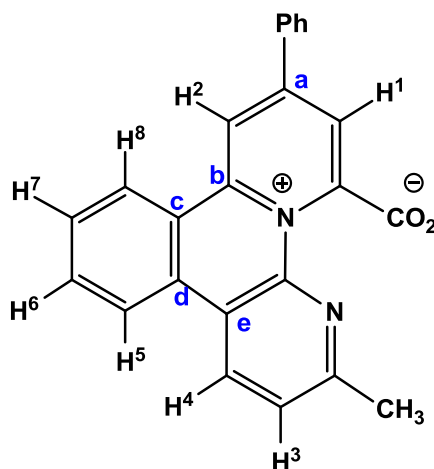
Molecular weight: 366.4

^1H NMR (500 MHz, CDCl_3 , 25 °C) δ 8.42 (d, $^4J_{\text{HH}} = 1.6$ Hz, 1H, H^1), 7.86 (d, $^4J_{\text{HH}} = 1.6$ Hz, 1H, H^2), 7.83 (d, $^3J_{\text{HH}} = 7.6$ Hz, 2H, Ph), 7.63 – 7.55 (m, 4H, Ph + H^4), 7.36 (m,

1H, Ph), 7.30 (t, $^3J_{\text{HH}} = 7.6$ Hz, 2H, Ph), 7.27 (d, $^3J_{\text{HH}} = 8.6$ Hz, 1H, H³), 7.21 (d, $^3J_{\text{HH}} = 7.1$ Hz, 2H, Ph), 7.12 (d, $^3J_{\text{HH}} = 7.7$ Hz, 1H, H⁵), 2.42 (s, 3H, CH₃).

$^{13}\text{C}\{^1\text{H}\}$ NMR (101 MHz, CDCl₃, 25 °C) δ 162.0 (CO₂⁻), 159.1 (NCN), 158.3 (C-CO₂⁻), 157.5 (C_q, pyr), 153.3 (C_q, pyr), 151.3 (C-CH₃), 138.7 (CH⁴), 134.4 (C_q, Ph), 132.9 (C_q, Ph), 132.4, 130.4, 130.0, 129.3, 128.7 and 127.9 (CH, Ph in a 1:1:2:2:2:2 ratio), 125.0 (CH⁵), 123.8 (CH²), 122.7 (CH¹), 119.1 (CH³), 24.0 (CH₃).

2-methyl-10-phenylbenzo[c]pyrido[1,2-a][1,8]naphthyridin-13-ium-12-carboxylate (37j)



Synthesis:

6'-methyl-2-ethoxycarbonyl-4,6-diphenyl-[1,2'-bipyridinium] tetrafluoroborate was prepared by an extension of Katritzky's methodology from 2-ethoxycarbonyl-4,6-diphenyl-pyridinium tetrafluoroborate and 2-amino-6-methylpyridine that were stirred at room temperature in dichloromethane for 2 hours (77% yield). Then 1.1 g (2.28 mmol) of this species were dissolved in 300 mL of methanol and irradiated with a 400 W lamp for 14h. Precipitation with diethyl ether yielded 650 mg (1.35 mmol, 60% yield) of the cyclization product. 230 mg (0.48 mmol) of the polycyclic ester were suspended in 2 mL of a 0.5 M NaOH aqueous solution and stirred at room temperature for 24h. The resulting yellow suspension was filtered off and washed with ether (2x2 mL) to yield 71 mg (0.19 mmol, 41% yield) of betaine **37j**

Spectroscopic data

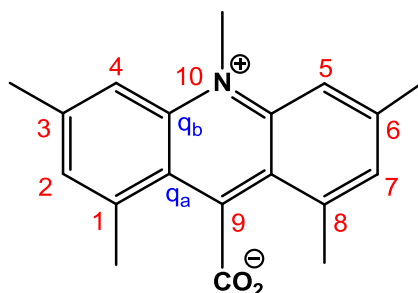
Pale yellow solid

Molecular weight: 364.4

$^1\text{H NMR}$ (400 MHz, CDCl_3 , 25 °C) δ 9.27 (d, $^5J_{\text{HH}} = 2.1$ Hz, 1H, H^2), 9.01 (d, $^3J_{\text{HH}} = 8.3$ Hz, 1H, H^8), 8.97 (d, $^3J_{\text{HH}} = 8.3$ Hz, 1H, H^4), 8.64 (d, $^3J_{\text{HH}} = 8.2$ Hz, 1H, H^5), 8.34 (d, $^5J_{\text{HH}} = 2.0$ Hz, 1H, H^1), 8.16 (m, 2H, Ph), 7.97 (t, $^3J_{\text{HH}} = 7.6$ Hz, 1H, H^6), 7.84 (t, $^3J_{\text{HH}} = 7.7$ Hz, 1H, H^7), 7.77 (d, $^3J_{\text{HH}} = 8.3$ Hz, 1H, H^3), 7.66 (m, 3H, Ph), 2.82 (s, 3H, CH_3).

$^{13}\text{C}\{^1\text{H}\}$ NMR (101 MHz, CDCl_3 , 25 °C) δ 168.8 (CO_2^-), 161.0 (NCN), 155.8 (Cq_a), 151.4 ($\underline{\text{C}}-\text{CO}_2^-$), 146.5 (Cq_b), 142.2 ($\underline{\text{C}}-\text{CH}_3$), 135.5 (C_{ipso} Ph), 135.3 (CH^4), 134.8 (CH^6), 133.5 (CH^7), 131.5 (Ph), 131.0 (Ph, x2), 130.4 (Cq_d), 129.5 (Ph, x2), 128.1 (CH^8), 127.8 (CH^3), 124.5 (Cq_c), 124.4 (CH^5), 122.6 (CH^1), 118.9 (CH^2), 118.7 (Cq_e), 23.4 (CH_3)

1,3,6,8,10-pentamethylacridin-10-ium-9-carboxylate (37m)



Synthesis:

Previously reported 1,3,6,8-tetramethylacridine-9-carboxylic acid (E) was reacted in neat iodomethane by heating at 60 °C for 2 days to yield an equilibrium mixture from which 9-(methoxycarbonyl)-1,3,6,8,10-pentamethylacridinium iodide (H) was extracted with dichloromethane.⁸ 9-(methoxycarbonyl)-1,3,6,8-tetramethylacridinium iodide (F) is also present in this dichloromethane extract and could be separated by extraction with diethyl ether and reused in subsequent methylation reactions with iodomethane. Deesterification was carried out using

⁸ After MeI evaporation, the part of the crude that is not soluble in DCM is the N-protonated carboxylic acid. This species can be heated with an excess of tetramethylpiperidine and MeI overnight leading to the formation of F and tetramethylpiperidinium. Again, extraction with ether allows for the separation of F, which can be reused in the preparation of H.

the procedure described by Olah.⁹ 9-(methoxycarbonyl)-1,3,6,8,10-pentamethylacridinium iodide was refluxed in acetonitrile with 3 equivalents of trimethylsilyl chloride and sodium iodide. After 24h, diethyl ether is added to precipitate out an off-white solid which was not isolated but was in all likelihood 1,3,6,8,10-pentamethyl-9-(((trimethylsilyl)oxy)carbonyl)acridinium iodide (J). This solid was suspended in water and after addition of 1 equivalent of sodium thiosulfate **37m** was formed as yellow precipitate that was filtered off and washed with a small amount of methanol.

¹H NMR data of some intermediates:

F: ¹H NMR (300 MHz, d₄-methanol, 25 °C) δ 7.75 (s, 2H), 7.27 (s, 2H), 4.10 (s, 3H), 2.65 (s, 6H), 2.51 (s, 6H)

H: ¹H NMR (500 MHz, CDCl₃, 25 °C) δ 8.50 (2H), 7.53 (2H), 5.12 (3H), 4.20 (3H), 2.79 (12H)

J: ¹H NMR (300 MHz, d₄-methanol, 25 °C) δ 8.36 (s, 2H), 7.71 (s, 2H), 4.83 (s, 3H), 3.00 (s, 6H), 2.76 (s, 6H), 1.30 (s, 9H)

Spectroscopic and analytical data

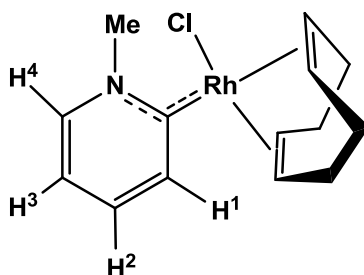
Yellow solid

Molecular weight: 293.3

¹H NMR (500 MHz, d₆-dmsO, 25 °C) δ 8.31 (s, 2H, H⁴+H⁵), 7.61 (s, 2H, H²+H⁷), 4.66 (s, 3H, N-CH₃), 2.98 (s, 6H, C¹-CH₃ + C⁸-CH₃), 2.66 (s, 6H, C³-CH₃ + C⁶-CH₃).

¹³C{¹H} NMR (126 MHz, d₆-dmsO, 25 °C) δ 170.35 (CO₂), 148.88 (Cq_b), 142.83 (Cq_a), 138.59 (C³), 132.83 (C²H), 132.37 (C⁹), 119.45 (C¹), 116.34 (C⁴H), 40.69 (N-CH₃), 22.29 (C³-CH₃), 21.59 (C¹-CH₃).

⁹ Olah, G.A.; Narang, S.C.; Gupta, B.G.B.; Malhotra, R.; *J. Org. Chem.*, **1979**, *44*, 1247

RhCl[2-(N-methyl)pyridylidene](cod) (38a)

A suspension of 40 mg (0.29 mmol) of N-methyl-2-carboxypyridine, **37a**, and 72 mg (0.15 mmol) of $[\text{RhCl}(\text{cod})]_2$ in 2 mL of dry THF is heated at 65°C for 2 hours under inert atmosphere. The dark red solution is filtered *via* cannula and addition of 5 mL of pentane to the resulting solution yields a yellow precipitate that is further washed with 2 mL of pentane. The solid is dried *in vacuo* to yield 69 mg of **38a** (70% yield).

Spectroscopic and analytical data

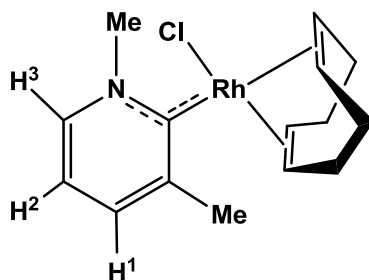
Yellow solid

Molecular weight: 339.7

^1H NMR (500 MHz, CDCl_3 , 25 °C): δ 8.15 (d, 1H, $^3J_{\text{HH}} = 8.4$ Hz, H^1), 8.00 (d, 1H, $^3J_{\text{HH}} = 6.4$ Hz, H^4), 7.22 (dd, 1H, $^3J_{\text{HH}} = 8.4$ and 6.4 Hz, H^2), 6.91 (m, 1H, H^3), 5.00 (m, 2H, =CH, cod), 4.80 (s, 3H, N-Me), 3.24 (m, 1H, =CH, cod), 3.11 (m, 1H, =CH, cod), 2.52-2.22 (m, 4H, CH_2 , cod), 2.05-1.84 (m, 4H, CH_2 , cod).

$^{13}\text{C}\{^1\text{H}\}$ NMR (125 MHz, CDCl_3 , 25 °C): δ 216.6 (d, $^1J_{\text{RhC}} = 43$ Hz, Rh-C), 142.2 (CH^4), 139.0 (CH^1), 131.6 (CH^2), 118.5 (CH^3), 99.5, 99.4 (d, $^1J_{\text{RhC}} = 5$ Hz, =CH, cod), 71.4, 66.05 (d, $^1J_{\text{RhC}} = 15$ Hz, =CH, cod), 52.9 (N-Me), 33.4, 32.3, 29.0, 28.4 (CH_2 , cod).

Anal. Calcd for $\text{C}_{14}\text{H}_{19}\text{ClNRh}$: C, 49.50; H, 5.64; N, 4.12. **Found:** C, 4.8; H, 6.0; N, 4.0.

RhCl[2-(N,6-dimethyl)pyridylidene](cod) (38b)

A suspension of 40 mg (0.26 mmol) of 1,3-dimethyl-2-carboxypyridine and 65 mg (0.13 mmol) of $[\text{RhCl}(\text{cod})]_2$ in 2 mL of dry THF is heated to 70° C for 2 hours. The solvent is removed *in vacuo* and the crude solid is extracted with toluene (2x2 mL). 5 mL of dry pentane are added to the toluene, the solution is filtered and the solvent is removed *in vacuo* to yield a dark yellow solid which is further purified by crystallization in CH_2Cl_2 /pentane, resulting in 59 mg of **38b** (65% yield).

Spectroscopic and analytical data

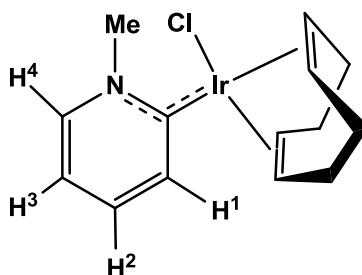
Yellow solid

Molecular weight: 383.8

$^1\text{H NMR}$ (500 MHz, CDCl_3 , 25 °C): δ 7.86 (d, 1H, $^3J_{\text{HH}} = 6.4$ Hz, H^3), 7.16 (d, 1H, $^3J_{\text{HH}} = 7.3$ Hz, H^1), 6.85 (dd, 1H, $^3J_{\text{HH}} = 6.4$ and 7.3 Hz, H^2), 5.01 (m, 1H, = CH_{cod}), 4.97 (m, 1H, = CH_{cod}), 4.88 (s, 3H, N-Me), 3.12 (s, 3H, C-Me), 3.05 (m, 2H, = CH_{cod}), 2.54-2.39 (m, 3H, CH_2), 2.32 (m, 1H, CH_2), 2.06-1.85 (m, 4H, CH_2).

$^{13}\text{C}\{^1\text{H}\}$ NMR (125 , MHz, CDCl_3 , 25 °C): δ 218.2 (d, $^1J_{\text{RhC}} = 43$ Hz, Rh-C), 147.7 (C_{q} -Me), 139.1 (CH^3), 131.6 (CH^1), 118.8 (CH^2), 98.6, 98.3 (d, $^1J_{\text{RhC}} = 6$ Hz, =CH), 68.6, 67.8 (d, $^1J_{\text{RhC}} = 13$ Hz, =CH), 52.3 (N-Me), 33.2, 32.0, 29.1, 28.4 (CH_2), 24.7 (Me).

Anal. Calcd for $\text{C}_{15}\text{H}_{21}\text{ClNRh}$: C, 50,94; H, 5,98; N, 3,96. **Found:** C, 50.7; H, 5.7; N, 3.5.

IrCl[2-(N-methyl)pyridylidene](cod) (39a)

A suspension of 40 mg (0.29 mmol) of N-methyl-2-carboxypyridine and 98 mg (0.15 mmol) of $[\text{IrCl}(\text{cod})]_2$ in 2 mL of dry THF is heated at 65 °C for 2 hours under inert atmosphere. The dark red solution is filtered *via* cannula and addition of 5 mL of pentane to the resulting solution yields a yellow precipitate that is further washed with 2 mL of pentane. The solid is dried *in vacuo* to yield 105 mg of **39a** (0.24 mmol, 84% yield).

Spectroscopic and analytical data

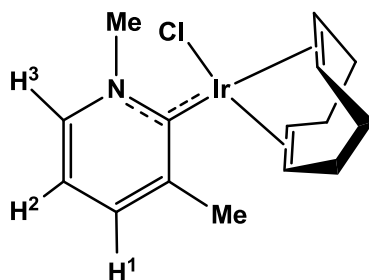
Red solid

Molecular weight: 459.0

$^1\text{H NMR}$ (500 MHz, CDCl_3 , 25 °C): δ = 8.01 (d, 1H, $^3J_{\text{HH}} = 8.4$ Hz, H^4), 7.98 (d, 1H, $^3J_{\text{HH}} = 7.3$ Hz, H^1), 7.37 (dd, 1H, $^3J_{\text{HH}} = 8.4$ and 7.3 Hz, H^2), 6.90 (dd, 1H, $^3J_{\text{HH}} = 8.4$ and 7.3 Hz, H^3), 4.63 (m, 1H, =CH, cod), 4.59 (m, 1H, =CH, cod), 4.58 (s, 3H, N-Me), 2.88 (m, 1H, =CH, cod), 2.78 (m, 1H, =CH, cod), 3.32 (m, 2H, CH_2 , cod), 2.19 (m, 2H, CH_2 , cod), 1.86 (m, 1H, CH_2 , cod), 1.76-1.67 (m, 3H, CH_2 , cod).

$^{13}\text{C}\{^1\text{H}\}$ NMR (125 MHz, CDCl_3 , 25 °C): δ = 210.4 (Ir-C), 142.5 (CH^4), 139.4 (CH^1), 133.3 (CH^2), 118.1 (CH^3), 85.1, 84.9 (=CH, cod), 55.9 (=CH, cod), 52.4 (N-Me), 50.3 (=CH), 34.0, 33.2, 29.5, 29.4 (CH_2 , cod).

Anal. Calcd for $\text{C}_{14}\text{H}_{19}\text{ClIrN}$: C, 39.20; H, 4.46; N, 3.27. **Found:** C, 39.4; H, 4.4; N, 3.4.

IrCl[2-(N,6-dimethyl)pyridylidene](cod) (39b)

A suspension of 40 mg (0.26 mmol) of N-methyl-2-carboxypyridine and 89 mg (0.13 mmol) of $[\text{IrCl}(\text{cod})]_2$ in 2 mL of dry THF is heated to 65°C for 2 hours under inert atmosphere. The dark red solution is evaporated and the crude solid extracted with toluene (3x 2mL). 5 mL of dry pentane are added to the toluene, the solution is filtered and the solvent is removed *in vacuo* to yield a dark yellow solid which is crystallized in CH_2Cl_2 /pentane mixture (1:1) to yield 84 mg of **39b** (73 % yield).

Spectroscopic and analytical data

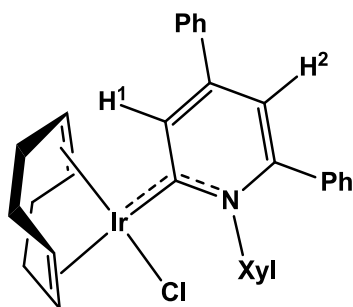
Dark yellow solid

Molecular weight: 473.1

$^1\text{H NMR}$ (500 MHz, CDCl_3 , 25 °C): δ 8.87 (d, 1H, $^3J_{\text{HH}} = 6.4$ Hz, H^3), 7.28 (d, 1H, $^3J_{\text{HH}} = 7.4$ Hz, H^1), 6.85 (dd, 1H, $^3J_{\text{HH}} = 6.4$ and 7.4 Hz, H^2), 4.64 (s, 3H, N-Me), 4.62 (m, 1H, $=\text{CH}_{\text{cod}}$), 4.54 (m, 1H, $=\text{CH}_{\text{cod}}$), 2.95 (s, 3H, C-Me), 2.71 (m, 2H, $=\text{CH}_{\text{cod}}$), 2.37-2.14 (m, 4H, CH_2), 1.83 (m, 1H, CH_2), 1.74-1.62 (m, 2H, CH_2), 1.58, (m, 1H, CH_2).

$^{13}\text{C}\{^1\text{H}\}$ NMR (125 , MHz, CDCl_3 , 25 °C): δ 211.0 (Ir-C), 148.1 (C_q -Me), 139.4 (CH^3), 133.6 (CH^1), 118.4 (CH^2), 83.7, 83.3, 52.7, 51.8 ($=\text{CH}$), 51.7 (N-Me), 33.8, 32.6, 29.7, 29.1 (CH_2), 24.4 (Me).

Anal. Calcd for $\text{C}_{15}\text{H}_{21}\text{ClIrN}$: C, 40.67; H, 4.78; N, 3.16. **Found:** C, 41.0; H, 5.1; N, 3.5.

IrCl[2-(N-xyllyl,4,6-diphenyl)pyridylidene](cod) (39e)*Synthesis:*

A solution of 40 mg (0.11 mmol) of 1-*m*-xyllyl-4,6-diphenyl-2-carboxypyridine and 35 mg (0.05 mmol) of [IrCl(cod)]₂ in 2 mL of dry THF is heated to 65°C for 2 hours under inert atmosphere. Solvent is removed in vacuo and the crude solid is crystallized in a toluene/pentane mixture (1:1) to yield 40 mg of a dark yellow solid, **39e** (54% yield).

Spectroscopic and analytical data

Dark yellow solid

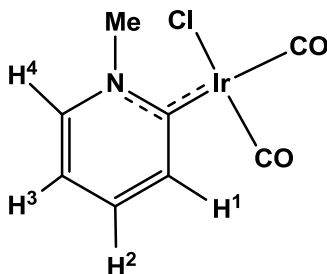
Molecular weight: 671.3

¹H NMR (500 MHz, CDCl₃, 25 °C): δ 8.53 (d, 1H, ⁴J_{HH} = 2.3, H¹), 7.82 (m, 2H, Ph), 7.51 (m, 3H, Ph), 7.28 (m, 1H, Ph), 7.22 (m, 4H, Ph), 7.19 (d, 1H, ⁴J_{HH} = 2.3, H²), 7.17 (m, 2H, H⁴ and H⁵), 6.84 (m, 1H, H³), 4.55 (m, 1H, =CH_{cod}), 4.29 (m, 1H, =CH, cod), 3.45 (m, 1H, =CH, cod), 2.59 (s, 3H, Me), 2.39 (m, 1H, CH₂), 2.26 (m, 1H, =CH, cod), 2.10-1.91 (m, 2H, CH₂, cod), 1.82-1.72 (m, 2H, CH₂, cod) 1.69 (s, 3H, Me), 1.29-1.19 (m, 2H, CH₂, cod), 1.00 (m, 1H, CH₂, cod).

¹³C{¹H} NMR (125 , MHz, CDCl₃, 25 °C): δ 213.0 (Ir-C), 154.9 (C_{q-Ph-N}), 144.5 (C_q), 144.3 (C_{q-Xyl-N}), 136.5 (C_q), 136.3 (C_{q-Xyl}), 135.7 (CH¹), 134.9 (C_q), 132.9 (C_{q-Xyl}), 130.1, 129.4, 129.1 (CH_{Ph}), 129.0, 128.9 (CH⁴, CH⁵), 128.4, 127.9, 127.7 (CH_{Ph}), 127.2 (CH³), 119.7 (CH²) 84.6, 81.4, 56.3, 48.8 (=CH, cod), 36.5, 31.5, 30.7, 26.4 (CH₂, cod), 21.5 (Me), 18.8 (Me).

Anal. Calcd for C₃₃H₃₃IrClN: C, 59.04; H, 4.95; N, 2.09; **Found:** C, 59.4; H, 4.9; N, 1.8.

IrCl[2-(N-methyl)pyridylidene](CO)₂ (40a)



20 mg (0.047 mmol) of **39a** are dissolved in 2 mL of CH₂Cl₂ and CO is bubbled into the solution, which turns from orange to yellow. Solvent is removed *in vacuo* and the solid is washed with pentane (3x2mL) to produce **40a** quantitatively.

Spectroscopic and analytical data

Dark yellow solid

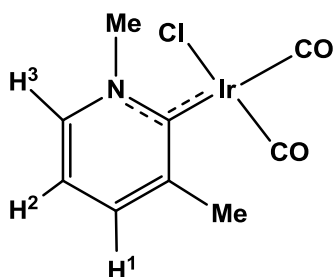
Molecular weight: 378.8

IR (nujol): ν (CO) 2062, 1980 cm⁻¹.

¹H NMR (500 MHz, CDCl₃, 25 °C): δ 8.21 (d, 1H, ³J_{HH} = 6.2 Hz, H⁴), 8.14 (d, 1H, ³J_{HH} = 8.0 Hz, H¹), 7.74 (t, 1H, ³J_{HH} = 7.7 Hz, H²), 7.32 (dd, 1H, ³J_{HH} = 6.2, 8.0 Hz, H³), 4.54 (s, 3H, Me).

¹³C{¹H} NMR (125 MHz, CDCl₃, 25 °C): δ 197.4 (C–Ir), 181.8 (CO), 169.5 (CO), 143.0 (CH⁴), 140.3 (CH¹), 136.4 (CH²), 121.5 (CH¹), 53.8 (N-Me), 28.0 (Me).

Anal. Calcd for C₈H₇ClIrNO₂: C, 25.36; H, 2.39; N, 3.70. **Found:** C, 25.2; H, 2.1; N, 3.4.

IrCl[2-(N,6-dimethyl)pyridylidene](CO)₂ (40b)*Synthesis:*

20 mg (0.045 mmol) of **39b** are dissolved in 2 mL of CH₂Cl₂ and CO is bubbled into the solution, which turns from orange to yellow. Solvent is removed *in vacuo* and the solid is washed with pentane (3x2mL) to produce **40b** quantitatively.

Spectroscopic and analytical data

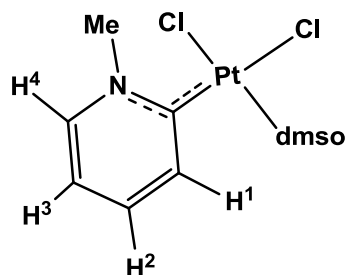
Dark yellow solid

Molecular weight: 393.8

IR (nujol): ν (CO) 2060, 1977 cm⁻¹.

¹H NMR (500 MHz, CDCl₃, 25 °C): δ 8.08 (d, 1H, ³J_{HH} = 5.9 Hz, H³), 7.63 (d, 1H, ³J_{HH} = 7.8 Hz, H¹), 7.25 (dd, 1H, ³J_{HH} = 5.9 and 7.8 Hz, H²), 4.55 (s, 3H, N-Me), 2.83 (s, 3H, C-Me). **¹³C{¹H} NMR** (125 , MHz, CDCl₃, 25 °C): δ 197.4 (Ir-C), 182.3, 169.0 (Ir-CO), 149.3 (C_q), 140.4 (CH³), 137.2 (CH¹), 121.6 (CH²), 53.6 (N-Me), 25.3 (Me).

HRMS (EI) Calcd for C₉H₉NO₂ClIr requires 390.9951, Found 390.9968

PtCl₂[2-(N-methyl)pyridylidene](dmsO) (42a)*Synthesis:*

A suspension of 40 mg (0.29 mmol) of N-methyl-2-carboxypyridine and 109 mg (0.29 mmol) of [PtCl₂(dmsO)₂] in 2 mL of dry THF is heated to 70°C for 2 hours under inert atmosphere. Solvent is removed *in vacuo* and the resulting solid is washed with methanol (2x2 mL) to yield 93 mg of **6a** (60 % yield) as an off-white product.

Spectroscopic and analytical data

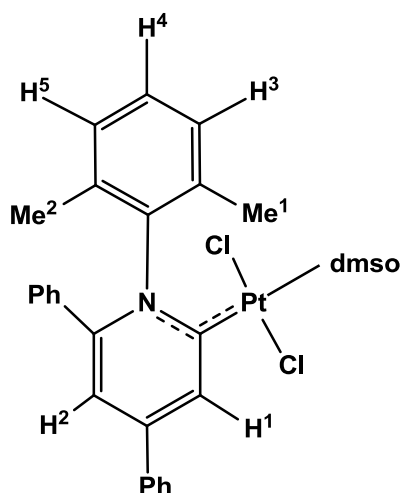
Off-white solid

Molecular weight: 437.2

¹H NMR (500 MHz, CDCl₃, 25 °C): δ 8.67 (d, 1H, ³J_{HH} = 6.2 Hz, H⁴), 8.12 (d, 1H, ³J_{HH} = 7.3 Hz, ³J_{HPT} ~ 35 Hz, H¹), 7.78 (dd, 1H, ³J_{HH} = 6.2, 7.3 Hz, H²), 7.44 (dd, 1H, ³J_{HH} = 6.2, 7.3 Hz, H³), 4.54 (s, 3H, Me), 2.54 (s, 6H, dissociated dmsO).

¹³C{¹H} NMR (100 MHz, CDCl₃, 25 °C): δ 164.9 (Pt–C), 144.1 (CH⁴), 138.2 (CH²), 138.0 (CH¹), 121.4 (CH³), 52.0 (N-Me), 40.5 (dissociated dmsO).

Anal. Calcd for C₈H₁₃Cl₂NOPtS: C, 21.98; H, 3.00; N, 3.20. **Found:** C, 22.1; H, 2.7; N, 3.3.

PtCl₂[2-(N-xylyl,4,6-diphenyl)pyridylidene](dmsO) (42e)*Synthesis:*

A suspension of 30 mg (0.079 mmol) of 1-*m*-xylyl-4,6-dipheyl-2-carboxypyridine and 33 mg (0.079 mmol) of [PtCl₂(dmsO)₂] in 2 mL of dry THF is heated at 70 °C for 45 minutes. 3 mL of diethyl ether are added to the resulting dark red solution to precipitate an off-white solid that is further washed with ether and crystallized in CH₂Cl₂/ether to yield 25 mg (0.037 mmol, 46% yield) of **42e**.

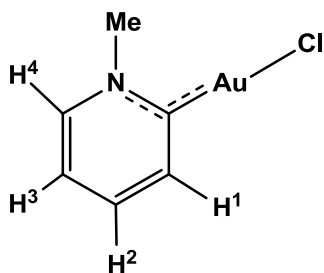
Spectroscopic data

Off-white solid

Molecular weight: 679.3

¹H NMR (500 MHz, CDCl₃, 25 °C): δ = 8.62 (d, 1H, ⁴J_{HH} = 2.1, ³J_{PtH} = 38 Hz, H¹), 7.82 (m, 2H, Ph), 7.84 (d, 1H, ⁴J_{HH} = 2.1, H²), 7.53 (m, 3H, Ph), 7.30 (m, 1H, H⁴), 7.26 (m, 1H, H⁵), 7.21 (m, 5H, Ph), 6.88 (d, 1H, ³J_{HH} = 7.3, H³), 3.46 (s, 3H, ³J_{PtH} = 23 Hz, dmsO), 2.67 (s, 3H, Me²), 2.63 (s, 3H, ³J_{PtH} = 22 Hz, dmsO), 1.76 (s, 3H, Me¹)

¹³C{¹H} NMR (125 MHz, CDCl₃, 25 °C): δ = 168.6 (Pt-C), 155.3 (C_{q-Ph}), 149.5 (C_{q-Ph}), 143.7 (C_{q-Xyl-N}), 136.9 (CH¹), 136.8 (C_{q-Xyl}), 134.9 (C_{q-Ph}), 134.7 (C_{q-Xyl}), 134.4 (C_{q-Ph}), 131.6 (CH_{Ph}), 130.0 (CH⁴), 129.7 (CH⁵), 129.6 (CH_{Ph}), 129.4 (CH_{Ph}), 128.6 (CH_{Ph}), 128.3 (CH_{Ph}), 128.1 (CH³), 127.8 (CH_{Ph}), 121.8 (CH²), 47.3 (dmsO), 43.5 (dmsO), 22.0 (Me²), 19.8 (Me¹)

AuCl[2-(N-methyl)pyridylidene] (43a)

A suspension of 30 mg (0.22 mmol) of N-methyl-2-carboxypyridine and 64 mg (0.22 mmol) of [AuCl(SMe₂)] in 2 mL of dry THF is heated to 70°C for 1.5 hours under inert atmosphere. Solvent is removed *in vacuo* and the resulting solid is extracted with dry CH₂Cl₂ (5 mL). A yellow solid precipitates upon addition of 10 mL of pentane. The solution is filtered off and the yellow solid dried *in vacuo* to yield 43 mg of **43a** (59 % yield).

Spectroscopic and analytical data

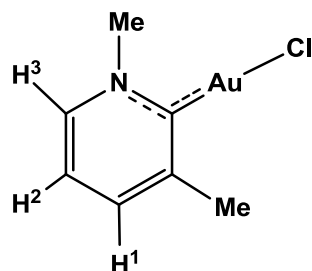
Off-white solid

Molecular weight: 325.5

¹H NMR (500 MHz, CDCl₃, 25 °C): δ 8.26 (d, 1H, ³J_{HH} = 6.4 Hz, H⁴), 7.98 (d, 1H, ³J_{HH} = 8.2 Hz, H¹), 7.80 (dd, 1H, ³J_{HH} = 8.2 and 7.8 Hz, H²), 7.40 (dd, 1H, ³J_{HH} = 6.4 and 7.8 Hz, H³), 4.46 (s, 3H, Me).

¹³C{¹H} NMR (125 , MHz, CDCl₃, 25 °C): δ 187.6 (Au–C), 142.2 (CH⁴), 140.3 (CH¹), 137.8 (CH²), 121.9 (CH³), 54.7 (N-Me).

Anal. Calcd for C₆H₇AuClN: C, 22.14; H, 2.17; N, 4.30. **Found:** C, 22.5; H, 2.3; N, 4.2.

AuCl[2-(N,6-dimethyl)pyridylidene] (43b)*Synthesis:*

A suspension of 40 mg (0.26 mmol) of 1,3-dimethyl-2-carboxypyridine and 76 mg (0.26 mmol) of [AuCl(SMe₂)] in 2 mL of dry THF is heated to 70°C for 1.5 hours under inert atmosphere. Solvent is removed *in vacuo* and the resulting solid is extracted with dry CH₂Cl₂ (5 mL). A white solid precipitates upon addition of 10 mL of pentane. The solution is filtered off and the white solid dried *in vacuo* to yield 62 mg of **43b** (70 % yield).

Spectroscopic and analytical data

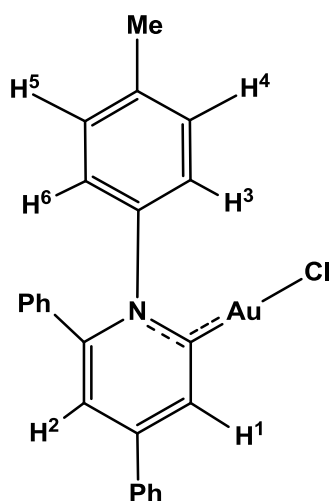
White solid

Molecular weight: 339.6

¹H NMR (500 MHz, CDCl₃, 25 °C): δ 8.18 (d, 1H, ³J_{HH} = 6.4 Hz, H³), 7.78 (d, 1H, ³J_{HH} = 7.8 Hz, H¹), 7.32 (dd, 1H, ³J_{HH} = 6.4 and 7.8 Hz, H²), 4.47 (s, 3H, N-Me), 2.69 (s, 3H, Me).

¹³C{¹H} NMR (125 , MHz, CDCl₃, 25 °C): δ 188.7(Au–C), 148.1 (C_q), 139.4 (CH³), 137.1 (CH¹), 121.5 (CH²), 54.2 (N-Me), 25.2 (Me).

Anal. Calcd for C₇H₉AuClN: C, 24.76; H, 2.67; N, 4.12. **Found:** C, 24.7; H, 2.6; N, 4.1.

AuCl[2-(N-*p*-tolyl,4,6-diphenyl)pyridylidene] (43d)*Synthesis:*

A solution of 192 mg (0.651 mmol) of [AuCl(SMe₂)] in 10 mL of dry THF is added to 250 mg (0.684 mmol) of 1-*p*-tolyl-4,6-diphenyl-2-carboxypyridine and the solution is heated at 60 °C for 30 minutes. The THF solution is filtered through celite and addition of 20 mL of pentane solvent yields 288 mg (0.520 mmol, 80% yield) of **43d** as a light yellow solid.

Spectroscopic and analytical data

Pale yellow solid

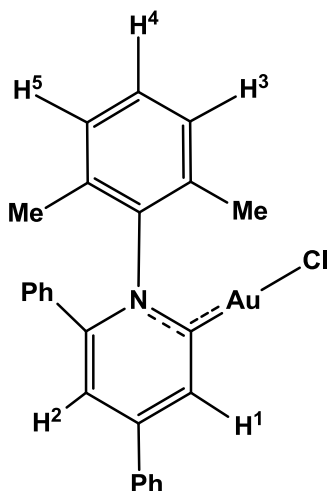
Molecular weight: 553.8

¹H NMR (500 MHz, CDCl₃, 25 °C) δ 8.23 (d, ⁵J_{HH} = 2.3 Hz, 1H, H¹), 7.78 (m, 2H, Ph), 7.59 (d, ⁵J_{HH} = 2.3 Hz, 1H, H²), 7.57 (m, 3H, Ph), 7.37 – 7.25 (m, 3H, Ph), 7.22 – 7.15 (m, 4H, Ph + *o*-H, *p*-tol), 7.07 (d, ³J_{HH} = 7.9 Hz, 2H, *m*-H, *p*-tol), 2.28 (s, 3H, CH₃).

¹³C NMR{¹H} (125 MHz, CDCl₃, 25 °C) δ 189.7 (C–Au), 154.9 (C–N, pyr), 150.4 (C_{ipso} Ph), 144.9 (C–N, *p*-tol), 139.4 (C–CH₃, *p*-tol), 135.5 (Cq), 135.1 (CH¹), 135.0 (Cq), 131.2, 129.8, 129.7, 129.6, 129.3, 128.6, 127.7 and 127.4 (CH Ph+*p*-tol in a 1:2:2:1:2:2:2:2 ratio), 121.8 (CH¹), 21.3 (CH₃).

Anal. Calcd for $C_{24}H_{19}AuClN$: C, 52,05; H, 3,46; N, 2,41; Found: C, 52.1; H, 3.7; N, 2.7

AuCl[2-(N-xylyl,4,6-diphenyl)pyridylidene] (43e)



Spectroscopic and analytical data

Pale yellow solid

Molecular weight: 567.9

A suspension of 200 mg (0.527 mmol) of 1-(2,6-dimethylphenyl)-4,6-diphenyl-2-carboxypyridine and 160 mg (0.527 mmol) of $[AuCl(SMe_2)]$ in 5 mL of dry THF is heated at 70 °C for 40 minutes. The THF solution was filtered and solvent was removed in vacuo to yield 240 mg (0.423 mmol, 81% yield) of **43e** as a light yellow solid. (If impurities are present in the THF solution, the product is crystallized in THF/ether).

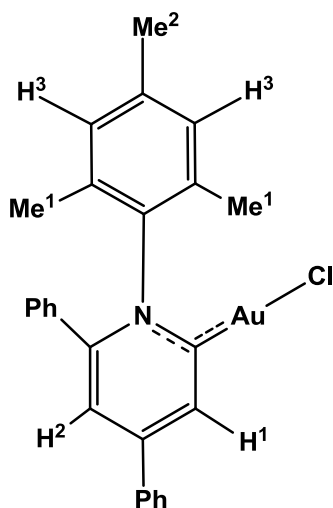
1H NMR (500 MHz, $CDCl_3$, 25 °C): δ 8.32 (d, 1H, $^4J_{HH} = 2.2$ Hz, H^1), 7.81 (m, 2H, Ph), 7.64 (d, 1H, $^4J_{HH} = 2.2$ Hz, H^2), 7.58 (m, 3H, Ph), 7.35 (t, 1H, $^3J_{HH} = 7.4$ Hz, Ph), 7.27 (t, 2H, $^3J_{HH} = 7.4$ Hz, Ph), 7.18 (t, 1H, $^3J_{HH} = 7.6$, H^4), 7.16 (d, 2H, $^3J_{HH} = 7.6$ Hz, Ph), 6.92 (d, 2H, $^3J_{HH} = 7.6$ Hz, H^3 y H^5), 2.046 (s, 6H, Me);

^{13}C NMR{ 1H } (125 MHz, $CDCl_3$, 25 °C): δ 189.8 (Au–C), 154.9 (C_q , pyr), 150.6 (C_q , Ph), 145.0 (N- C_q Xyl), 135.6 (CH^1), 135.4 (C_q , pyr), 133.9 (C_q , Ph), 133.2 (C_q , Xyl),

131.4 (CH, Ph), 130.3 (CH, Ph), 129.9 (C_q, Ph), 129.8 (CH⁴), 129.0 (CH^{5/3}), 128.5 (CH, Ph), 128.4 (CH, Ph), 127.8 (CH, Ph), 122.3 (CH²), 18.7 (Me)

Anal. Calcd for C₂₅H₂₁AuClN: C, 52,88; H, 3,73; N, 2,47; **Found:** C, 52.9; H, 3.9; N, 2.5

AuCl[2-(N-mesityl,4,6-diphenyl)pyridylidene] (43f)



Spectroscopic and analytical data

Pale yellow solid

Molecular weight: 581.9

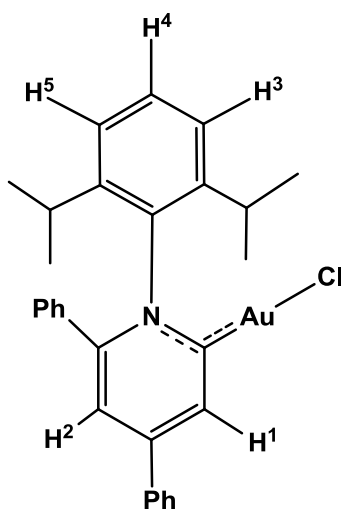
A suspension of 200 mg (0.51 mmol) of 1-(2,4,6-trimethylphenyl)-4,6-diphenyl-2-carboxypyridine and 150 mg (0.51 mmol) of [AuCl(SMe₂)] in 5 mL of dry THF is heated at 70 °C for 30 minutes. The THF solution was filtered and solvent was removed in vacuo to yield 200 mg (0.34 mmol, 68% yield) of **43f** as a light yellow solid. (If impurities are present in the THF solution, the product is crystallized in THF/ether).

¹H NMR (500 MHz, CDCl₃, 25 °C): δ 8.26 (d, 1H, ⁴J_{HH} = 2.1 Hz, H¹), 7.82 (m, 2H, Ph), 7.79 (m, 2H, Ph), 7.62 (d, 1H, ⁴J_{HH} = 2.1 Hz, H²), 7.56 (m, 3H, Ph), 7.33 (t, 1H, ³J_{HH} = 7.4 Hz, Ph), 7.26 (t, 2H, ³J_{HH} = 7.6 Hz, Ph), 7.14 (d, 2H, ³J_{HH} = 7.6 Hz, Ph), 6.78 (s, 2H, *m*-H-Mes), 2.19 (s, 3H, Me²), 1.97 (s, 6H, Me¹)

^{13}C NMR{ ^1H } (125 MHz, CDCl_3 , 25 °C): δ 189.6 (Au–C), 154.9 ($\text{C}_{\text{q-Ph}}$), 150.4 ($\text{C}_{\text{q-Ph}}$), 142.6 (N- C_{q} , Mes), 139.4 ($\sigma\text{-C}$, Mes), 135.4 ($\text{C}_{\text{q-Ph}}$), 135.3 (CH^1), 133.8 (C_{q} , Ph), 132.6 ($\rho\text{-C}$, Mes), 131.2 (CH, Ph), 130.1 (CH, Ph), 129.6 (CH, Ph), 129.5 (CH, Mes), 128.4 (CH, Ph), 128.3 (CH, Ph), 127.7 (CH, Ph), 121.8 (CH^2), 21.1 (Me^2), 18.5 (Me^1)

Anal. Calcd for $\text{C}_{26}\text{H}_{23}\text{AuClN}$: C, 53,67; H, 3,98; N, 2,41; **Found:** C, 53.8; H, 4.0; N, 2.7

AuCl[2-(N-(2,6-diisopropyl)-4,6-diphenyl)pyridylidene] (43g)



Spectroscopic and analytical data

Pale yellow solid

Molecular weight: 623.9

A suspension of 200 mg (0.459 mmol) of 1-(2,6-diisopropylphenyl)-4,6-diphenyl-2-carboxypyridine and 135 mg (0.459 mmol) of $[\text{AuCl}(\text{SMe}_2)]$ in 5 mL of dry THF is heated at 70 °C for 40 minutes. The THF solution was filtered and solvent was removed in vacuo to yield 237 mg (0.381 mmol, 83% yield) of **43g** as a light yellow solid. (If impurities are present in the THF solution, the product is crystallized in THF/ether).

^1H NMR (500 MHz, CDCl_3 , 25 °C) δ 8.29 (d, $^4J_{\text{HH}} = 1.6$ Hz, 1H, H^1), 7.82 (m, 2H, Ph), 7.68 (d, $^4J_{\text{HH}} = 1.6$ Hz, 1H, H^2), 7.57 (m, 3H, Ph), 7.40 (t, $^3J_{\text{HH}} = 7.7$ Hz, 1H, H^4), 7.32 (t, $^3J_{\text{HH}} = 7.2$ Hz, 1H, Ph), 7.24 (t, $^3J_{\text{HH}} = 7.4$ Hz, 2H, Ph), 7.13 (d, $^3J_{\text{HH}} = 7.8$ Hz, 2H, H^3+H^5), 7.10 (d, $^3J_{\text{HH}} = 7.8$ Hz, 2H, Ph), 2.25 (sept, $^3J_{\text{HH}} = 16.6$ Hz, 2H, $\underline{\text{C}}\text{H}(\text{CH}_3)_2$), 1.42 (d, $^3J_{\text{HH}} = 6.6$ Hz, 6H, $\text{CH}(\underline{\text{C}}\text{H}_3)_2$), 0.89 (d, $^3J_{\text{HH}} = 6.7$ Hz, 6H, $\text{CH}(\underline{\text{C}}\text{H}_3)_2$).

$^{13}\text{C}\{^1\text{H}\}$ NMR (125 MHz, CDCl_3 , 25 °C) δ 190.8 (Au–C), 155.3 (C_q pyr), 150.4 (C_q pyr), 143.5 (N–C, Diip), 142.0 (C_q , Diip, x2), 135.4 (C_q Ph), 134.8 (CH^1), 134.1 (C_q Ph), 131.3 (CH Ph, x1), 130.8 (CH^4), 130.21, 129.8, 129.7, 128.4 and 127.8 (CH Ph in a 2:2:2:2 ratio), 124.8 (CH^3+CH^5), 122.0 (CH^2), 28.8 $\underline{\text{C}}\text{H}(\text{CH}_3)_2$, 25.7 ($\text{CH}(\underline{\text{C}}\text{H}_3)_2$), 23.0 ($\text{CH}(\underline{\text{C}}\text{H}_3)_2$).

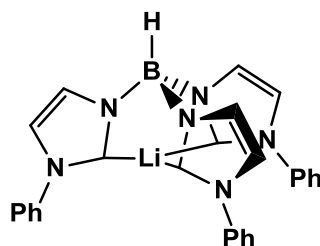
Anal. Calcd for $\text{C}_{29}\text{H}_{29}\text{AuClN}$: C, 55.82; H, 4.68; N, 2.24; **Found:** C, 55.8; H, 5.0; N, 2.4

EXPERIMENTAL PART. CHAPTER 4

Imidazolium salt $\text{HB}^{\text{tBu}}\text{ImH}_3\text{Br}_2$ ($\text{Tc}^{\text{tBu}}\cdot 3\text{HBr}_2$) was prepared according to the reported literature procedure¹ and novel $\text{HB}^{\text{Ph}}\text{ImH}_3\text{Br}_2$ was synthesized in a similar way. It was obtained as a highly insoluble white solid in 50% yield. (¹H NMR (500 MHz, $\text{dms}\text{-d}_6$, 25 °C) δ 9.70 (s, 3H, NCHN), 8.44 (s, 3H, =CH), 7.98 (s, 3H, =CH), 7.88 (d, ³J_{HH} = 8.0 Hz, 6H, H_o-Ph), 7.73 – 7.63 (t, ³J_{HH} = 8.0 Hz, 6H, H_m-Ph), 7.58 (t, ³J_{HH} = 7.4 Hz, 3H, H_p-Ph), 4.67 (s, 1H, B-H). ¹³C NMR (126 MHz, $\text{dms}\text{-d}_6$, 25 °C) δ 138.0 (NCHN), 134.9 (C_{ipso}-Ph), 130.0 (C_m-Ph), 129.5 (C_p-Ph), 124.6 (=CH), 122.1 (=CH), 122.0 (C_o-Ph), IR (Nujol) 2466.8 cm⁻¹ (B-H).

Imidazolium salt $\text{H}_2\text{B}^{\text{tBu}}\text{ImH}_2\text{Br}$ ($\text{Bc}^{\text{tBu}}\cdot 2\text{HBr}$) was prepared according to the reported literature procedure.²

$\text{HB}^{\text{Ph}}\text{Im}_3\text{Li}$ (47)



Synthesis:

A fresh solution of lithium diisopropylamide (LDA) was prepared by adding 200 μL of ⁿBuLi 1.6M in hexanes (0.324 mmol) to a solution of 45 μL (0.324 mmol) of diisopropylamine in 1.5 mL of dry THF cooled to -20 °C. After stirring at -20 °C for 15 minutes and at room temperature for another 15 minutes, this LDA solution was cooled to -50 °C and transferred to 50 mg (0.083 mmol) of $\text{HB}^{\text{Ph}}\text{Im}_3\text{Br}_2$. The white suspension was stirred for 10 minutes at low temperature and then allowed

¹ Nieto, I.; Cervantes-Lee, F.; Smith, J. M. *Chem. Commun.*, **2005**, 3811

² Nieto, I.; Bontchev, R. P.; Smith, J. M. *Eur. J. Inorg. Chem.* **2008**, 2476

to reach room temperature for 30 minutes, yielding a pale yellow solution of $\text{HB}(\text{PhIm})_3\text{Li}$.

Due to its instability towards protonation, this species was never isolated and was always prepared and used in situ. Therefore, no yield values are available. Nevertheless, spectroscopic data were obtained by THF evaporation and dissolving the resulting pale yellow oil in C_6D_6 .

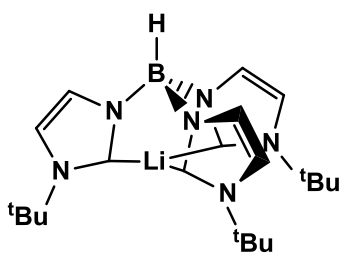
Spectroscopic and analytical data

Pale yellow oil.

Molecular weight: 448.3

^1H NMR (400 MHz, C_6D_6 , 25°C) δ 7.92 (d, $^3J_{\text{HH}} = 8.4$ Hz, 6H, $\underline{\text{H}}_o\text{-Ph}$), 7.46 (s, 3H, $=\underline{\text{C}}\text{H}$), 7.13 (t, $^3J_{\text{HH}} = 9.3$ Hz, 6H, $\underline{\text{H}}_m\text{-Ph}$), 6.94 (s, 3H, $=\underline{\text{C}}\text{H}$), 6.89 (t, $^3J_{\text{HH}} = 7.6$ Hz, 3H, $\underline{\text{H}}_p\text{-Ph}$).

$\text{HB}(\text{tBuIm})_3\text{Li}$ (**48**)



Synthesis:

48 was prepared in an analogous manner to **47**. Again, in this case attempts of isolation led to formation of protonated imidazolium salt $\text{HB}(\text{tBuImH})_3^{2+}$, which precipitates out of solution during the manipulation process.

Spectroscopic and analytical data

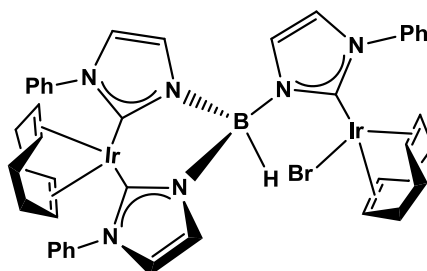
Pale yellow oil

Molecular weight: 388.3

^1H NMR (400 MHz, C_6D_6 , 25°C) δ 7.36 (s, 3H, =CH), 6.65 (s, 3H, =CH), 5.21 (br, 1H, BH), 1.39 (s, 27H, C(CH₃)₃).

$^{13}\text{C}\{^1\text{H}\}$ NMR (101 MHz, C_6D_6 , 25°C) δ 191.2 (C-Li), 125.5 (=CH), 115.2 (=CH), 55.7 (C(CH₃)₃), 31.7 (C(CH₃)₃).

IrBr(cod)[μ - κ_1 : κ_2 -HB(^{Ph}Im)₃]Ir(cod)] (49)



Synthesis:

A solution of ligand **47** is prepared as discussed above using 50 mg (0.083 mmol) of HB(^tBuImH)₃Br₂. Solvent is removed in vacuo to remove the isopropylamine by-product. The resulting yellow oil is redissolved in 2 mL of dry diethyl ether and cooled to -40 °C. 56 mg (0.083 mmol) of [IrCl(cod)]₂ are added to this pale yellow solution and the temperature is kept at -40°C for 20 minutes. The reaction is allowed to reach room temperature over the course of 1 hour, resulting in a dark red solution where lithium salts precipitate out. Solvent is removed in vacuo and the reaction crude is extracted with dry dichloromethane (2x2mL) to afford a dark red solution. After solvent evaporation, 64 mg (0.057 mmol, 69% yield) of a dark red solid are obtained.

Spectroscopic and analytical data

Dark red solid

Molecular weight: 1122.0

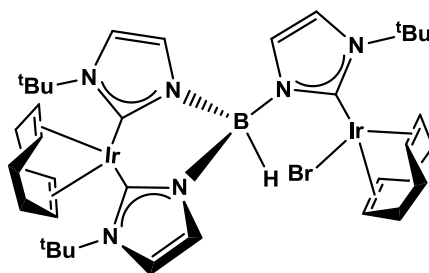
^1H NMR (400 MHz, CDCl_3 , 25 °C) δ 8.58 (d, $^3J_{\text{HH}} = 1.9$ Hz, 1H, =CH), 8.12 (d, $^3J_{\text{HH}} = 7.8$ Hz, 2H, H_o-Ph), 8.04 (d, $^3J_{\text{HH}} = 1.8$ Hz, 1H, =CH), 7.78 (d, $^3J_{\text{HH}} = 7.4$ Hz, 2H, H_o-Ph), 7.72 (d, $^3J_{\text{HH}} = 7.4$ Hz, 2H, H_o-Ph), 7.63 (d, $^3J_{\text{HH}} = 1.8$ Hz, 1H, =CH), 7.56 – 7.32 (m, 9H, Ph), 7.16 (d, $^3J_{\text{HH}} = 1.7$ Hz, 1H, =CH), 7.08 (d, $^3J_{\text{HH}} = 1.9$ Hz, 1H, =CH), 7.05

(d, $^3J_{\text{HH}} = 1.7$ Hz, 1H, =CH), 4.69 (td, $J_{\text{HH}} = 7.8, 4.0$ Hz, 1H, CH-cod), 4.49 (td, $J_{\text{HH}} = 7.7, 3.6$ Hz, 1H, CH-cod), 3.98 – 3.85 (m, 1H, CH-cod), 3.66 (m, 1H, CH-cod), 3.01 (m, 1H, CH-cod), 2.93 (m, 2H, CH-cod), 2.37 (m, 1H, CH-cod), 2.30 (m, 2H, CH₂-cod), 2.25 – 2.05 (m, 1H, CH₂-cod), 1.89 – 1.14 (m, 11H, CH₂-cod), 1.05 (m, 1H, CH₂-cod).

$^{13}\text{C}\{^1\text{H}\}$ NMR (101 MHz, CDCl₃, 25 °C) δ 182.6 (C-Ir), 177.3 (C-Ir), 175.8 (C-Ir), 141.7 (C_{ipso}-Ph), 141.1 (C_{ipso}-Ph), 141.0 (C_{ipso}-Ph), 129.0 (Ph), 128.9 (Ph), 128.2 (Ph), 128.0 (Ph), 127.9 (Ph), 127.7 (=CH), 127.0 (=CH), 126.9 (Ph), 126.0 (CH_o-Ph), 125.5 (CH_o-Ph), 125.2 (CH_o-Ph), 125.1, 121.0, 120.9 and 119.7 (=CH in a 1:1:1:1 ratio), 80.4, 76.0, 74.5, 74.3, 73.4, 52.6 and 50.7 (CH-cod), 33.4, 33.0, 31.0, 30.7, 30.4, 30.2 and 29.3 (CH₂-cod, in a 1:1:1:1:2:1:1).

Elemental analysis calculated for C₄₃H₄₆BBIr₂N₆: C 46.44; H 4.58; N 7.66; **experimental**: C 46.0; H 4.1; N 7.5.

Ir(Br)(cod)[μ - κ_1 : κ_2 -HB(^tBuIm)₃]Ir(cod)] (50)



Synthesis:

A solution of ligand **48** is prepared as discussed above with 50 mg (0.092 mmol) of HB(^tBuImH)₃. Solvent is removed in vacuo to remove the isopropylamine by-product. The resulting yellow oil is redissolved in 2 mL of dry diethyl ether and cooled to -40 °C. 62 mg (0.092 mmol) of [IrCl(cod)]₂ are added to this pale yellow solution and the temperature is kept at -40 °C for 20 minutes. The reaction is allowed to reach room temperature over the course of 1 hour, resulting in a bright red solution where lithium salts precipitate out. Solvent is removed in vacuo and the reaction crude is extracted with dry dichloromethane (2x2 mL) to afford a bright red solution. After solvent evaporation, 88 mg (0.083 mmol, 90% yield) of a dark red solid are obtained.

Spectroscopic data

Bright red solid.

Molecular weight: 1062.04

$^1\text{H NMR}$ (400 MHz, CDCl_3 , 25 °C) δ 7.10 (d, $^3J_{\text{HH}} = 2.0$ Hz, 1H, =CH), 6.96 (d, $^3J_{\text{HH}} = 1.9$ Hz, 1H, =CH), 6.80 (d, $^3J_{\text{HH}} = 1.9$ Hz, 1H, =CH), 6.61 (d, $^3J_{\text{HH}} = 1.9$ Hz, 1H, =CH), 6.52 (d, $^3J_{\text{HH}} = 2.0$ Hz, 1H, =CH), 6.25 (d, $^3J_{\text{HH}} = 1.9$ Hz, 1H, =CH), 4.74 (t, $^3J_{\text{HH}} = 7.0$ Hz, 1H, CH-cod), 4.19 (q, $J = 7.5$ Hz, 1H, CH-cod), 3.90 (q, $J = 8.6, 8.2$ Hz, 2H, CH-cod), 3.73 (tt, $J = 13.5, 6.3$ Hz, 2H, CH-cod), 3.28 (t, $J = 6.7$ Hz, 1H, CH-cod), 2.88 (td, $J = 7.9, 4.0$ Hz, 1H, CH-cod), 2.74 – 2.53 (m, 1H, CH_2 -cod), 2.50-2.22 (m, 5H, CH_2 -cod), 2.20-1.24 (m, 16H, CH_2 -cod), 2.03 (s, 9H, ^tBu), 1.73 (s, 9H, ^tBu), 1.62 (s, 9H, ^tBu), 1.09 (dt, $J = 8.7, 4.2$ Hz, 2H, CH_2 -cod).

$^{13}\text{C}\{^1\text{H}\}$ NMR (101 MHz, CDCl_3 , 25 °C) δ 185.2 (C-Ir), 177.8 (C-Ir), 175.5 (C-Ir), 123.1, 121.4, 118.7, 116.6 and 116.0 (=CH, in a 2:1:1:1:1 ratio), 77.5, 76.2, 73.5, 72.2, 66.9 and 66.4 (CH-cod in a 1:1:1:1:1:1 ratio), 58.0, 56.1 and 55.6 (C(CH_3)₃ in a 1:1:1 ratio), 54.7 and 48.7 (CH-cod in a 1:1 ratio), 35.1 and 34.2 (CH_2 -cod in a 1:1 ratio), 32.9 (C(CH₃)₃), 32.6 (CH_2 -cod), 32.5 (C(CH₃)₃), 32.2 (C(CH₃)₃), 30.8, 29.1, 28.8, 27.6 (CH_2 -cod in a 1:1:1:1 ratio).

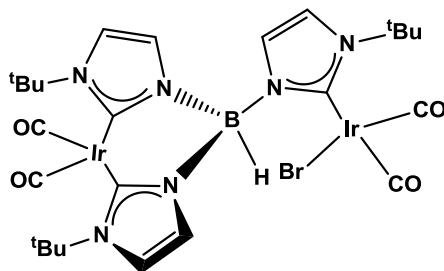
50b

This species was formed in aprox. 10% in the synthesis of **50** and was slightly more soluble. It could be partially separated in the filtrate of Et_2O /pentane crystallizations of **50**. These solutions still contained traces of **50** in most cases.

$^1\text{H NMR}$ (400 MHz, C_6D_6 , 25 °C) δ 8.61 (d, $^3J_{\text{HH}} = 1.9$ Hz, 1H, =CH), 7.25 (d, $^3J_{\text{HH}} = 1.9$ Hz, 1H, =CH), 7.16 (d, $^3J_{\text{HH}} = 1.9$ Hz, =CH), 6.73 (d, $^3J_{\text{HH}} = 1.9$ Hz, 1H, =CH), 6.67 (d, $^3J_{\text{HH}} = 1.9$ Hz, 1H, =CH), 6.41 (d, $^3J_{\text{HH}} = 1.8$ Hz, 1H, =CH), 5.23 (td, $J_{\text{HH}} = 7.7, 3.1$ Hz, 1H, cod), 5.11 (m, 1H, cod), 4.94 (td, $J_{\text{HH}} = 8.0, 3.1$ Hz, 1H, cod), 4.22 (m, 1H, cod), 4.11 (m, 1H, cod), 3.99 (t, $^3J_{\text{HH}} = 7.3$ Hz, 1H, cod), 3.59 (td, $J_{\text{HH}} = 8.3, 4.5$ Hz, 1H, cod), 3.19 (td, $J_{\text{HH}} = 7.5, 3.2$ Hz, 1H, cod), 2.77 (m, 1H, cod), 2.52 – 2.36 (m, 3H, cod), 2.33 – 2.22 (m, 2H, cod), 2.20 – 2.07 (m, 1H, cod), 1.93 (s, 9H, C(CH₃)₃), 1.75 (m, 2H, cod), 1.71 – 1.58 (m, 2H, cod), 1.58 – 1.43 (m, 2H, cod), 1.50 (s, 9H, C(CH₃)₃), 1.39 (s, 9H, C(CH₃)₃), 1.35 (m, 2H, cod), 1.31 – 1.18 (m, 1H, cod).

$^{13}\text{C}\{^1\text{H}\}$ NMR (101 MHz, C_6D_6 , 25 °C) δ 180.9 ($\underline{\text{C}}\text{-Ir}$), 179.5 ($\underline{\text{C}}\text{-Ir}$), 176.3 ($\underline{\text{C}}\text{-Ir}$), 130.0, 126.1, 124.4, 117.8, 117.5 and 116.2 ($=\underline{\text{C}}\text{H}$ in a 1:1:1:1:1:1 ratio), 78.7, 77.6, 76.6, 70.0, 69.4 and 69.3 (CH-cod in a 1:1:1:1:1:1 ratio), 58.0, 56.4 and 56.1 ($\underline{\text{C}}(\text{CH}_3)_3$ in a 1:1:1 ratio), 52.0 (CH-cod), 50.4 (CH-cod), 34.6 ($\text{CH}_2\text{-cod}$), 34.4 ($\text{CH}_2\text{-cod}$), 33.6 ($\text{C}(\underline{\text{C}}\text{H}_3)_3$), 33.0 ($\text{C}(\underline{\text{C}}\text{H}_3)_3$), 32.5 ($\text{CH}_2\text{-cod}$), 32.5 ($\text{C}(\underline{\text{C}}\text{H}_3)_3$), 32.0, 31.1, 29.4, 28.9 and 28.7 ($\text{CH}_2\text{-cod}$ in a 1:1:1:1:1:1 ratio).

$\text{Ir}(\text{Br})(\text{CO})_2[\mu\text{-}\kappa_1:\kappa_2\text{-HB}(\text{t}^{\text{Bu}}\text{Im})_3]\text{Ir}(\text{CO})_2$ (51)



Synthesis:

CO is bubbled into a solution of 30 mg (0.028 mmol) of $\text{Ir}(\text{Br})(\text{cod})[\mu\text{-}\kappa_1:\kappa_2\text{-HB}(\text{t}^{\text{Bu}}\text{Im})_3]\text{Ir}(\text{cod})$ in dry dichloromethane for one minute at room temperature. Solvent removal results in the obtention of 24 mg (0.025 mmol, 89% yield) of a bright red solid.

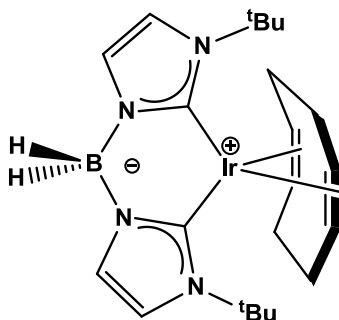
Spectroscopic data

Bright red solid.

Molecular weight: 961.7

^1H NMR (500 MHz, C_6D_6 , 25 °C) δ 7.69 (d, $^3J_{\text{HH}} = 1.8$ Hz, 1H, $=\underline{\text{C}}\text{H}$), 7.56 (d, $^3J_{\text{HH}} = 1.8$ Hz, 1H, $=\underline{\text{C}}\text{H}$), 7.41 (d, $^3J_{\text{HH}} = 2.0$ Hz, 1H, $=\underline{\text{C}}\text{H}$), 6.63 (d, $^3J_{\text{HH}} = 2.0$ Hz, 1H, $=\underline{\text{C}}\text{H}$), 6.35 (d, $^3J_{\text{HH}} = 1.8$ Hz, 1H, $=\underline{\text{C}}\text{H}$), 6.32 (d, $^3J_{\text{HH}} = 1.9$ Hz, 1H, $=\underline{\text{C}}\text{H}$), 1.64 (s, 9H, $\text{C}(\underline{\text{C}}\text{H}_3)_3$), 1.31 (s, 18H, $\text{C}(\underline{\text{C}}\text{H}_3)_3 \times 2$).

$^{13}\text{C}\{^1\text{H}\}$ NMR (126 MHz, C_6D_6 , 25 °C) δ 182.9 ($\underline{\text{C}}\text{O}$, x3), 182.7 ($\underline{\text{C}}\text{O}$), 174.4 ($\underline{\text{C}}\text{-Ir}$), 169.8 ($\underline{\text{C}}\text{-Ir}$), 169.5 ($\underline{\text{C}}\text{-Ir}$), 128.0, 127.31, 123.4, 118.3, 117.8 and 117.7 ($=\underline{\text{C}}\text{H}$ in a 1:1:1:1:1:1 ratio), 58.0 ($\underline{\text{C}}(\text{CH}_3)_3$), 57.2 ($\underline{\text{C}}(\text{CH}_3)_3$ in a 1:1 ratio), 32.6 ($\text{C}(\underline{\text{C}}\text{H}_3)_3$), 31.8 ($\text{C}(\underline{\text{C}}\text{H}_3)_3$), 31.7 ($\text{C}(\underline{\text{C}}\text{H}_3)_3$).

κ_2 -[H₂B(^tBuIm)₂]Ir(cod) (**52**)*Synthesis:*

140 μ L of a 2.5 M solution of ⁿBuLi in hexanes was added to a suspension of 50 mg (0.15 mmol) of H₂B(^tBuImH)₂Br in 5 mL of dry diethyl ether cooled at -50 °C. After 1h, the pale yellow solution is brought to room temperature, stirred for 10 minutes and then it is added to 49 mg (0.07 mmol) of [IrCl(cod)]₂. After stirring the red suspension overnight, the solvent is removed *in vacuo* and the resulting solid is extracted with pentane (3x5 mL) to yield 61 mg (0.11 mmol, 73 % yield) of **52** after solvent evaporation.

Spectroscopic and analytical data

Orange solid

Molecular weight: 560.3

¹H NMR (300 MHz, C₆D₆, 25 °C) δ 7.19 (d, ³J_{HH} = 2.2 Hz, 2H, =CH), 6.43 (d, ³J_{HH} = 1.7 Hz, 2H, =CH), 4.19 – 4.06 (m, 2H, cod), 4.04 – 3.92 (m, 2H, cod), 2.40 – 2.26 (m, 3H, cod), 1.95 (qd, ³J_{HH} = 7.3, 2.0 Hz, 2H, cod), 1.50 (d, ³J_{HH} = 5.1 Hz, 1H, cod), 1.46 – 1.44 (m, 2H, cod), 1.41(s, 18H, C(CH₃)₃).

¹³C{¹H} NMR (75 MHz, C₆D₆, 25 °C) δ 176.03 (C-Ir), 124.54 (=CH), 115.26 (=CH), 71.85 (cod), 64.49 (cod), 54.77 (C(CH₃)₃), 31.74 (cod), 31.31 (cod), 30.08 (C(CH₃)₃).

CONCLUSIONS

In the course of this PhD thesis we have studied the synthesis and reactivity of a series of transition metal complexes bearing 5- and 6-membered ring N-heterocyclic carbenes. Their significant sigma donor properties and their ease of functionalisation make them suitable alternatives to other common ligands such as phosphines. However, to increase the practical applications of NHCs the synthesis of new organometallic complexes bearing NHC ligands with varying steric and electronic properties is necessary. In this sense, we have studied complexes containing classical NHCs, based on imidazole rings, and also other non conventional carbenes based on pyridine rings which present better sigma donor and pi acceptor properties.

1. In the first part of our work, we centered our efforts on the synthesis of coordinatively unsaturated T-shaped cationic platinum (II) species bearing classical NHCs. Besides the complexes bearing carbenes with *tert*-butyl, mesityl and diisopropylphenyl substituents at the nitrogen atoms already prepared by the group, we synthesised derivatives with less bulky ligands, namely the NHCs substituted with isopropyl groups with and without methyl groups in positions 3 and 4 of the imidazol ring. The smaller size of the NHCs used in these studies indicates that under certain conditions, it is not possible to prepare low electron count Pt(II) compounds, due to the formation of dinuclear species. The reactivity of these new platinum complexes towards halogens (Br_2 , I_2) was tested and compared to that of their bulkier counterparts. It has been proved that similar coordinatively unsaturated platinum (IV) species were formed when the 14-electron platinum (II) derivatives were treated with one equivalent of halogen. Nevertheless, their stability is intermediate between that observed with complexes bearing NHCs substituted with *tert*-butyl groups and bulky aryl groups. In addition, no paramagnetic Pt(III) species were detected when the same synthetic procedure used for obtention of a previously described

Pt(III) IPr derivative was employed. In this case the formation of Pt(II) dimers was favored.

2. Our family of unsaturated Pt(II) complexes was tested as catalysts for the dehydrogenation of ammonia borane and other amine boranes. It has been shown that some of these complexes dehydrogenate very efficiently the amine boranes, and that the rate of the dehydrocoupling depends on the nature of the NHCs in the platinum complex and on the amine borane utilized, being more favored for non-bulky secondary amine boranes and slower for ammonia borane and bulkier secondary amine boranes. Mechanistic studies allowed the observation of a first step in which the amine borane forms a sigma B–H complex with the platinum atom. In addition, a novel mechanism that involves hydride abstraction by the platinum atom, assisted by an external amine, to yield a platinum-hydride complex with concomitant formation of the boronium cation $[(\text{NHMe}_2)_2\text{BH}_2]^+$ was unveiled. This latter species is very likely in equilibrium with the THF stabilized borenium cation $[(\text{NHMe}_2)(\text{THF})\text{BH}_2]^+$, bearing an acidic NH group that is able to protonate the platinum hydride, releasing H_2 and the amino borane $\text{H}_2\text{B-NMe}_2$, regenerating the catalytic $[\text{Pt}]^+$ species. DFT calculations supported this mechanistic proposal. In addition, the same catalyst proved very active for the formation of diaminoboranes $(\text{NR}_2)_2\text{BH}$ for a variety of differently substituted amines.
3. A new method for the synthesis of 2-pyridylidene transition metal complexes based on the decarboxylation of 2-carboxypyridine derivatives was devised. Heating these species in the presence of appropriate metal precursors resulted in the generation of iridium, rhodium, platinum and gold 2-pyridylidene complexes. Moreover, an iridium complex bearing two 2-pyridylidene ligands was prepared, with no change of oxidation state. The electron donor properties of these ligands were studied through the analysis of the IR spectra of the iridium carbonyl derivatives and they were found to be slightly better donors than classical NHCs. Steric diversity was introduced in the ligands by the preparation of betaine precursors using Katritzky's synthetic procedure. With all of these carboxylates, a family of

gold complexes with different steric environments was prepared. These species were tested as catalysts for the cycloaddition of allenedienes and preliminary results suggest a larger influence of steric rather than electronic factors in the selectivity of the products of this reaction.

4. The coordination properties of tridentate ligands tris(imidazol-2-ylidene)borate ligands, which are based on classical NHCs and are isostructural to the well known tris(pyrazolyl)borate ligands have been explored. It has been found that these kinds of ligands have a strong propensity to act as a $\mu:\kappa^2, \kappa^1$ ligand leading to dinuclear species. When reacted with iridium precursors. Their bidentate counterpart, bis(imidazole-2-ylidene)borates, were also tested in the formation of iridium complexes and in this case a monomeric species could be obtained that nonetheless proved to be very sensitive to protonation of one imidazolylidene ring.